LABORATORY AND FIELD-BASED INVESTIGATIONS OF SUBSURFACE GEOCHEMICAL PROCESSES IN SEAFLOOR HYDROTHERMAL SYSTEMS

By

Eoghan Reeves

B.Sc., University of Wales, Bangor, 2002
M.Sc., University of Leeds, 2004

Submitted in partial fulfillment of the requirements for the degree of

Doctor of Philosophy

at the

MASSACHUSETTS INSTITUTE OF TECHNOLOGY

and the

WOODS HOLE OCEANOGRAPHIC INSTITUTION

June 2010

Signature of Author

4/2/2010

Joint Program in Oceanography/Applied Ocean Science and Engineering
Massachusetts Institute of Technology
and Woods Hole Oceanographic Institution
April 2nd, 2010

Certified by

4/2/2010

Dr. Jeffrey S. Seewald
Thesis Supervisor

Accepted by

4/2/2010

Prof. Roger Summons
Chair, Joint Committee for Chemical Oceanography
Massachusetts Institute of Technology

LABORATORY AND FIELD-BASED INVESTIGATIONS OF SUBSURFACE GEOCHEMICAL PROCESSES IN SEAFLOOR HYDROTHERMAL SYSTEMS

by

Eoghan Reeves

Submitted on April 2nd, 2010, to the MIT/WHOI Joint Program in Oceanography and Applied Ocean Science and Engineering in partial fulfillment of the requirements for the degree of Doctor of Philosophy in the field of Chemical Oceanography

THESIS ABSTRACT

This thesis presents the results of four discrete investigations into processes governing the organic and inorganic chemical composition of seafloor hydrothermal fluids in a variety of geologic settings. Though Chapters 2 through 5 of this thesis are disparate in focus, each represents a novel investigation aimed at furthering our understanding of subsurface geochemical processes affecting hydrothermal fluid compositions. Chapters 2 and 3 concern the abiotic (non-biological) formation of organic compounds in high temperature vent fluids, a process which has direct implications for the emergence of life in early Earth settings and sustainment of present day microbial populations in hydrothermal environments. Chapter 2 represents an experimental investigation of methane (CH_4) formation under hydrothermal conditions. The overall reduction of carbon dioxide (CO_2) to CH_4, previously assumed to be kinetically inhibited in the absence of mineral catalysts, is shown to proceed on timescales pertinent to crustal residence times of hydrothermal fluids. In Chapter 3, the abundance of methanethiol (CH_3SH), considered to be a crucial precursor for the emergence of primitive chemoautotrophic life, is characterized in vent fluids from ultramafic-, basalt- and sediment-hosted hydrothermal systems. Previous assumptions that CH_3SH forms by reduction of CO_2 are not supported by the observed distribution in natural systems. Chapter 4 investigates factors regulating the hydrogen isotope composition of hydrocarbons under hydrothermal conditions. Isotopic exchange between low molecular weight *n*-alkanes and water is shown to be facilitated by metastable equilibrium reactions between alkanes and their corresponding alkenes, which are feasible in natural systems. In Chapter 5, the controls on vent fluid composition in a backarc hydrothermal system are investigated. A comprehensive survey of the inorganic geochemistry of fluids from sites of hydrothermal activity in the eastern Manus Basin indicates that fluids there are influenced by input of acidic magmatic solutions at depth, and subsequently modified by variable extents of seawater entrainment and mixing-related secondary acidity production.

Thesis Supervisor: Dr. Jeffrey S. Seewald
Title: Senior Scientist, Woods Hole Oceanographic Institution

ACKNOWLEDGEMENTS

First and foremost, I would like to thank my advisor, Jeff Seewald, for the past 5+ years of guidance throughout my graduate education and research. Jeff's limitless optimism and scientific imagination have been inspirational and I have thoroughly enjoyed and benefited from being part of his lab group. His infectious positive attitude and constant disbelief at my occasional worries have left an indelible mark on my professional and personal attitudes. I would also like to express my sincerest thanks to Meg Tivey, for her continual support, guidance and advice on all aspects of my life in the Joint Program. My committee members Tom McCollom and Phil Gschwend have been an integral part of making this thesis what it is and I thank them for their feedback, questions and genuine interest in my research.

My research would not have been successful without many persons at WHOI and elsewhere who provided invaluable assistance. Firstly, I would like to thank Sean Sylva (and Sebastion the Dog) for unfailingly answering my countless technical questions or pointing me in the direction of answers (or in the case of Sebastion just staring blankly at me until I figured it out), and for conducting isotopic analyses in several of the chapters in this thesis. My research and life here have also benefited greatly from help and conversations with Giora Proskurowski, for which thanks are due. Numerous others were of assistance on the various cruises for which data was collected: A.L. Reysenbach, W.E. Seyfried, N. Pester, M. Rough, S. Sievert, P. Saccocia, E. Walsh, M. Wert and T. Nielson. Collaborators who kindly provided some of the data included in Chapter 5 include Wolfgang Bach, Paul Craddock, Wayne C. Shanks, Thomas Pichler and Martin Rosner. Thanks are also due to Alex Sessions for assistance with water isotope analysis for Chapter 4. Many thanks are also due to the Academic Programs Office staff members who constantly endeavor to keep the Joint Program running smoothly – Marsha Gomes, Julia Westwater, Christine Charette, Jim Yoder and Jim Price. Thanks also to Ronni Schwartz and Mary Elliff at MIT. Sheila Clifford, Donna Mortimer and the MC&G administrative staff have always provided help and service when needed with a smile and are greatly appreciated.

I must express my deepest thanks and love for my family, especially my mother Margaret Reeves, as well as my little sister Clare, my brothers Tadhg and Niall, and my grandmother 'Lil' who sadly did not live to see me defend my thesis. To my mum, thank you for always believing in me and supporting me unconditionally, right from the start, even though you never fully understood this unusual road I chose to take many years ago. You and Lil always stated that each generation of a family should have even richer opportunities than the last, and your hard work and sacrifice have shown that and helped me to get where I am today. I will never forget that.

My life in the Joint Program, in addition to being professionally fulfilling, has been enriched by the many great friendships I have made here since I started. To my many past and present housemates who double as great friends, Joanna Gyory, Frieder Klein, Christian Miller, Tyler Goepfert, Emily Peacock, Nick Drenzek, Louisa Morrison, Casey Saenger and Mike Brosnahan, thanks for the laughs, dinners, parties and happy times. To my incredibly supportive friends who helped through to the end of this with style: Laura Hmelo, Taylor Crockford, Emilia DeForce, Michelle Bringer, Justin Ossolinski, Louie Wurch, John Ahern, Frieder & Joanna, J.B.: thank you for so many things. I would also like to thank the many others who have been a part of my life here over the years: Stephanie Owens, Breea Govenar, Erin Bertrand, Carly Buchwald, Caitlin Frame, Alysia Cox, Jeff Kaeli, Maya Yamato, Erin Banning and Travis Poole.

The thesis research presented here was funded by the National Science Foundation through grants OCE-0327448, OCE-0136954, MCB-0702677, OCE-0549829, and by the Department of Energy grant DE-FG02-97ER14746. Funding was also provided by the WHOI Deep Ocean Exploration Institute Graduate Fellowship, as well by the WHOI Academic Programs Office.

TABLE OF CONTENTS

ABSTRACT 3
ACKNOWLEDGEMENTS 5
TABLE OF CONTENTS 7
LIST OF TABLES 10
LIST OF FIGURES 11

CHAPTER 1. INTRODUCTION 13

CHAPTER 2. EXPERIMENTAL INVESTIGATION OF CO_2 REDUCTION TO CH_4 UNDER HYDROTHERMAL CONDITIONS 23
1. Introduction 25
2. Methods 29
2.1. Experimental Apparatus and Design 29
2.2. Analysis of Dissolved Species 31
3. Results 33
3.1. CO_2 and H_2 33
3.2. CH_4 and CH_3OH formation 34
3.3. Other C species 35
3.4. S-bearing species 35
4. Discussion 37
4.1. Thermodynamic constraints on metastable equilibrium 39
4.2. The relative roles of CH_3OH and CH_3SH in abiotic synthesis of CH_4 41
4.3. Implications for hydrothermal systems 41
4.3.1 CH_3OH and CH_4 formation 41
4.3.2 CH_3SH formation 44
5. Conclusions 45

CHAPTER 3. INSIGHTS INTO THE ORIGIN OF METHANETHIOL IN SEAFLOOR HYDROTHERMAL FLUIDS 67
1. Introduction 68
2. Methods 70
3. Results 72
5. Discussion 73
4. Conclusions 79

CHAPTER 4. RAPID HYDROGEN ISOTOPE ($^2H/^1H$) EXCHANGE BETWEEN AQUEOUS *N*-ALKANES AND WATER UNDER HYDROTHERMAL CONDITIONS: IMPLICATIONS FOR THE ISOTOPIC COMPOSITION OF ABIOGENIC AND THERMOGENIC HYDROCARBONS 93
1. Introduction 95
2. Materials and Methods 98
2.1 Experimental Approach and Setup 98

2.2 Analytical Methods 101
3. Results 105
3.1 $^{2}H/^{1}H$ ratios 105
3.2 Dissolved species concentrations 106
3.2.1 H_2 and H_2S concentrations 106
3.2.2 Dissolved hydrocarbon concentrations 106
3.2.3 ΣCO_2 and organic acid concentrations 107
4. Discussion 109
4.1 Alkane-alkene equilibria 109
4.2 Reversible $^{2}H/^{1}H$ exchange and isotopic equilibrium 110
4.2.1 Alkane-alkene equilibrium and $^{2}H/^{1}H$ exchange 110
4.2.2 Isotopic equilibrium and alkane $\delta^{2}H$ trends 113
4.2.3 Variations in $\delta^{2}H_{meth}$ 115
4.3 Implications for natural systems 116
4.3.1 ^{2}H / ^{1}H ratios and abiogenesis in igneous environments 116
4.3.2 $^{2}H/^{1}H$ signatures in thermogenic hydrocarbons 121
5. Conclusions 126

CHAPTER 5. GEOCHEMISTRY OF HYDROTHERMAL FLUIDS FROM THE PACMANUS, NORTHEAST PUAL AND VIENNA WOODS VENT FIELDS, MANUS BASIN, PAPUA NEW GUINEA 151
1. Introduction 154
2. Geological Setting 157
2.1 Hydrothermal Vent Fields 158
2.1.1 Vienna Woods 158
2.1.2 PACMANUS and Northeast Pual 158
3. Methods 161
3.1 Sample collection 161
3.2 Analytical methods 162
3.3 Calculation of endmember compositions 164
4. Results 167
4.1 Temperature 167
4.2 Mg and SO_4 168
4.3 pH 169
4.4 H_2, H_2S, CH_4, CO and CO_2 169
4.5 Cl, Br and F 171
4.6 $\delta^{18}O_{H2O}$ and δD_{H2O} 172
4.7 Alkalis, alkaline earths and B 172
4.8 Fe, Mn, Al and SiO_2 174
5. Discussion 175
5.1 Influence of water/rock reaction and substrate composition on fluid compositions 176
5.1.1 Fluid-mineral equilibria 176
5.1.2 Alkalis and B 179
5.1.3 Quartz-fluid equilibrium and dissolved SiO_2 181
5.1.4 pH and metal mobility 182
5.2 Phase separation and Cl variability 184

5.3 Magmatic fluid input at Pual Ridge 187
5.3.1 Isotopic evidence for magmatic H_2O 187
5.3.2 Magmatic CO_2, F, and Cl 191
5.3.3 Magmatic SO_2 input and disproportionation 194
5.3.4 Spatial variability of magmatic fluid inputs 197
5.4 Subsurface seawater entrainment 198
5.4.1 Secondary Acidity 202
6. Summary 205

CHAPTER 6. COMMENTS AND FUTURE RESEARCH DIRECTIONS 271

LIST OF TABLES

CHAPTER 2.

2.1. Concentrations of aqueous species measured during heating of HCOOH at 325-300°C and 35MPa 47

2.2. Predicted concentrations of methanol in equilibrium with measured CO_2 and H_2 for two representative fluids from high temperature ultramafic-hosted hydrothermal systems 48

CHAPTER 3.

3.1. Measured concentrations of Mg and dissolved gases in vent fluids 81

3.2. Endmember concentrations of CH_3SH, H_2, H_2S, ΣCO_2, CO and CH_4 82

CHAPTER 4.

4.1. Concentrations of aqueous species during heating of C1 to C5 *n* -alkane mixtures at 323°C and 35MPa with a pyrite-pyrrhotite-magnetite (PPM) mineral assemblage 129

4.2. Hydrogen isotope compositions of dissolved C1 to C5 *n* -alkanes and corresponding solutions during heating with a pyrite-pyrrhotite-magnetite (PPM) mineral assemblage 130

CHAPTER 5.

5.1. Measured compositions of vent fluid samples from the Vienna Woods, PACMANUS and NE Pual vent fields, Manus Basin 208

5.2. Summary of vent fluid compositions extrapolated to zero Mg concentration from the Vienna Woods, PACMANUS and NE Pual vent fields, Manus Basin 210

5.3. Selected elemental ratios at zero Mg concentration from the Vienna Woods, PACMANUS and NE Pual vent fields, Manus Basin 211

LIST OF FIGURES

CHAPTER 2.

2.1. Model for the sequential aqueous reduction of CO_2 to CH_4 by H_2 *via* a series of intermediate oxidation state single carbon compounds 49

2.2. Temperature dependence of the equilibrium constants (K_{eq}) for CH_3OH, CH_3SH and CH_4 formation by overall CO_2 reduction 50

2.3. Schematic of the SEYFRIED (1987) design of flexible-cell hydrothermal reactor and pressure containment vessel 51

2.4. Measured concentrations of dissolved species as a function of time during the 325°C and 300°C phases of the experiment 52

2.5. Mass spectrum of normal ^{13}C abundance CH_3OH, CH_3SH and CH_4 standards compared with ^{13}C-labeled forms in experimental samples 53

2.6. Thermodynamic affinities for the production of CH_3OH ($A_{Methanol}$) and CH_4 ($A_{Methane}$) by the overall reactions shown in Figure 2.2 during the experiment 54

2.7. Equilibrium abundances of aqueous species as a function of pH at 35MPa for model solutions 56

CHAPTER 3.

3.1. Equilibrium constants (Log K_{eq}) for the formation of CH_3SH from either CO_2 (reduction) or CH_4 (oxidation) as a function of temperature at 300 bar 83

3.2. Predicted concentration (open symbols) of CH_3SH according to reaction (1) and reaction (2) as a function of measured H_2 concentrations 85

CHAPTER 4.

4.1. Activity diagram showing the phase relations in the system Fe-S-O-H at 325°C and 35MPa 131

4.2. C_1 to C_5 *n*-alkane δ^2H values from Experiment 1 and Experiment 2 as a function of time at 323°C and 35MPa 132

4.3. Concentrations of C_1 to C_5 *n*-alkanes and ΣCO_2 from Experiment 1 and Experiment 2 as a function of time at 323°C and 35MPa 133

4.4. Concentrations of C_2, C_3 and C_5 *n*-alkenes in Experiment 1 and Experiment 2 as a function of time at 323°C and 35MPa 134

4.5. Chemical affinities for oxidation of C_2, C_3 and C_5 *n*-alkanes to their corresponding terminal *n*-alkenes as a function of time at 323°C and 35MPa in Experiment 1 and Experiment 2 135

4.6. Proposed mechanism for the reversible equilibration of *n*-pentane with individual pentene isomers allowing exchange of all H atoms at each carbon position (*) throughout the molecule 136

4.7. Equilibrium constants (K_{eq}) for reactions between C_2 to C_5 *n*-alkenes and their corresponding terminal *n*-alkenes as a function of temperature 137

4.8. Isotopograms showing the δ^2H values of *n*-alkanes as a function of chain length for the Kidd Creek Mine abiogenic gases, thermogenic gases from Southwest Ontario gas fields, Lost City vent fluidsand alkanes produced by experiment aqueous Fischer-Tropsch-type (FTT) synthesis at 400°C 138

4.9. Plot of theoretical alkane-water equilibrium fractionation factors for ethane ($\alpha_{ethane/w}$), propane ($\alpha_{propane/w}$), *n*-butane ($\alpha_{butane/w}$) and *n*-pentane ($\alpha_{pentane/w}$) H calculated as a function of temperature 139

CHAPTER 5.

5.1. Regional map showing the Manus Basin (eastern Bismarck Sea) and SeaBeam map of bathymetric map of Pual Ridge and nearby Marmin Knolls neovolcanic edifices 213

5.2. SM2000 bathymetry of the Vienna Woods hydrothermal field and the northern and southern portions of the PACMANUS hydrothermal field 215

5.3. Plot of vent pressures and maximum temperatures (T_{max}) for all moderate- to high-temperature fluids sampled at Vienna Woods and PACMANUS 217

5.4. Measured SO_4 concentrations *vs.* measured Mg for all vent fluid samples from the Vienna Woods, PACMANUS and NE Pual fields 219

5.5. Endmember H_2, ΣCO_2, H_2S and CH_4 concentrations *vs.* endmember Cl concentrations for all PACMANUS, NE Pual and Vienna Woods fluids 221

5.6. Endmember ΣCO_2 concentrations *vs.* endmember F concentration for all PACMANUS, NE Pual and Vienna Woods fluids 223

5.7. Endmember δD_{H2O} and $\delta^{18}O_{H2O}$ values from Vienna Woods and PACMANUS vent fields, with axes expanded to show compositions of mantle-derived water and subduction-related volcanic vapors 225

5.8. Measured $^{87}Sr/^{86}Sr$ ratios versus measured Mg/Sr ratios for select Vienna Woods and PACMANUS fluids 227

5.9. Endmember K, Li and Cs concentrations *vs.* endmember Rb concentration for Vienna Woods, PACMANUS and NE Pual fluids 229

5.10. Endmember SiO_2 concentrations and extrapolated vent temperatures for Vienna Woods and PACMANUS fluids 231

5.11. Endmember Li, Rb, K and Cs concentrations *vs.* corresponding endmember Cl concentration for Vienna Woods, PACMANUS and NE Pual vent fluids 233

5.12. $\delta^{34}S$ values for dissolved H_2S ($\delta^{34}S_{H2S}$) versus endmember ΣCO_2 Concentrations 235

5.13. Maximum measured vent temperatures (T_{max}) for co-located vent fluids at Roman Ruins and Fenway versus their lowest measured Mg concentrations (Mg_{min}) 237

5.14. Plots of endmember Ca/Cl ratios, endmember Sr/Cl ratios, lowest measured fluid pH(25°C) and endmember Fe/Mn ratios from Vienna Woods and Pual Ridge vent fluids *vs.* the lowest measured Mg concentration (Mg_{min}) for each fluid 239

5.15. Plot of measured molar Ca/Cl ratios ("*in situ*") and corresponding "*corrected*" values (adjusted for anhydrite precipitation) versus lowest measured Mg concentrations (Mg_{min}) for closely co-located PACMANUS vent fluids 241

CHAPTER 6.

6.1 Cartoon showing major processes influencing the evolution of fluid compositions in back-arc hydrothermal systems 277

CHAPTER 1

Introduction

Seafloor hydrothermal systems associated with the generation of oceanic crust represent a dramatic expression of heat and mass transfer from the interior of the Earth. In addition to profound effects on ocean chemistry, convective circulation of seawater through volcanically active oceanic crust leads to the formation of metal sulfide deposits. In addition, seafloor hot springs are often invoked as ideal settings from which early microbial life could have emerged. Since the initial discovery of low temperature venting at the Galápagos Spreading Center in 1977 (CORLISS *et al.*, 1979), our understanding of the composition and diversity of hydrothermal solutions has expanded greatly. During convection through oceanic crust of basaltic composition, O_2-replete seawater reacts with crustal rock, typically producing hot, reducing, acidic and metal-rich solutions that are depleted in Mg and SO_4 and variably enriched or depleted in Cl (BUTTERFIELD *et al.*, 2003). In hydrothermal systems where alteration of ultramafic rock (serpentinization) is occurring, such as Rainbow (CHARLOU *et al.*, 2002) and Lost City (KELLEY *et al.*, 2001; KELLEY *et al.*, 2005), more H_2-rich solutions are produced as a result of the oxidation of the ferrous iron component of olivine. Depending on the conditions of water-rock interaction either acidic or alkaline fluids can be produced in these systems (KLEIN *et al.*, 2009; MCCOLLOM and BACH, 2009). Our understanding of key geochemical parameters such as fluid redox and pH, and the mobility and behavior of metals in hydrothermal solutions has also advanced (*e.g.* SEYFRIED, 1987; SEEWALD and SEYFRIED, 1990; SEYFRIED and DING, 1995; TIVEY *et al.*, 1995; ALLEN and SEYFRIED, 2003; CRADDOCK, 2008; KLEIN *et al.*, 2009; MCCOLLOM and BACH, 2009). While these inorganic aspects of vent fluid geochemistry are reasonably well constrained,

what is less well understood is the formation and transformation of carbon species in hydrothermal solutions, especially in ultramafic geologic settings where highly reducing fluids contain high concentrations of CH_4 and other hydrocarbons of purported non-biological (abiotic) origin (HOLM and CHARLOU, 2001; CHARLOU *et al.*, 2002; MCCOLLOM and SEEWALD, 2007; PROSKUROWSKI *et al.*, 2008; KONN *et al.*, 2009). In addition, though water-rock interactions in backarc environments may broadly resemble those of basalt-hosted systems in some respects (BUTTERFIELD *et al.*, 2003), our understanding of the role of acidic magma-derived solutions in influencing hydrothermal fluid chemistry in these environments is currently limited by a lack of comprehensive geochemical investigations (GAMO *et al.*, 2006; YANG and SCOTT, 2006). This thesis presents a series of independent studies addressing these two emergent areas of inquiry in the geochemistry of hydrothermal solutions.

The origin of reduced carbon compounds in seafloor hydrothermal fluids is currently a subject of considerable interest (MCCOLLOM and SEEWALD, 2007; PROSKUROWSKI *et al.*, 2008; KONN *et al.*, 2009). Since the discovery of seafloor hot springs, hydrothermal systems have been discussed as a plausible setting for the emergence of early life on Earth (CORLISS *et al.*, 1981) and the potential for synthesis of prebiotic organic compounds in hydrothermal solutions figures prominently in arguments for a hyperthermophilic hydrothermal origin of life (HOLM, 1992). However, our understanding of the role hydrothermal systems may have played in providing the key prebiotic compounds for the emergence of life is still largely speculative. The expansion in recent decades of theoretical organic geochemistry has illustrated that thermodynamic drives may exist for the formation of a variety of organic species during hydrothermal circulation through the oceanic crust (SHOCK, 1990, 1992; SHOCK and SCHULTE, 1998) but several aspects of carbon transformations and organic syntheses in hydrothermal systems are poorly understood. Experimental investigations of organic synthesis under realistic hydrothermal conditions have

largely focused on hydrocarbon formation by mineral catalysis (FOUSTOUKOS and SEYFRIED, 2004; MCCOLLOM and SEEWALD, 2006; FU *et al.*, 2007). However, hydrocarbon formation in the absence of catalytic minerals has largely been ignored. Chapter 2 of this thesis specifically addresses the possibility of aqueous CH_4 formation *via* intermediate oxidation state carbon compounds, thereby challenging previously held assumptions that CO_2 reduction without mineral catalysis is kinetically inhibited.

While the synthesis of aliphatic hydrocarbon components is an important prerequisite for the formation of any primitive cellular structures, other organic functional groups are clearly required for early life to emerge in a hydrothermal setting. Theories postulating that primitive chemoautotrophism emerged as the earliest form of life all invoke an abiotic supply of methanethiol (CH_3SH) for the synthesis of thioester – the functional group involved in metabolism (DE DUVE, 1991; HUBER and WACHTERSHAUSER, 1997; MARTIN and RUSSELL, 2006; RUSSELL and HALL, 2006). Chapter 3 represents the first known survey of the distribution of CH_3SH in present day vent fluids and discusses possible origins.

The use of stable isotope measurements has become an important tool in elucidating processes of abiotic hydrocarbon production (SHERWOOD LOLLAR *et al.*, 2002; PROSKUROWSKI *et al.*, 2008). Chapter 4 represents an experimental investigation of the feasibility of hydrogen isotope exchange between low molecular weight hydrocarbons and water and the findings of this chapter have important implications for the utility of hydrogen isotopes in elucidating abiotic hydrocarbon production, in addition to contributing to our understanding of factors influencing the hydrogen isotope composition of hydrocarbons in petroleum systems.

While the Chapters 2 through 4 deal predominantly with carbon transformations in hydrothermal solutions, Chapter 5 deviates from this theme and presents a detailed survey of the chemistry of hydrothermal fluids from a felsic-hosted hydrothermal system in a backarc

environment. Backarc spreading centers (those formed behind volcanic arcs associated with subduction zones) are known to host a large fraction (~20%) of hydrothermal systems discovered to date (ISHIBASHI and URABE, 1995) yet the chemistry of fluids in these systems still remains poorly characterized. Backarc hydrothermal systems represent the closest modern analog to Kuroko-type volcanic-hosted massive sulfide ore deposits (FRANKLIN *et al.*, 1981; HERZIG and HANNINGTON, 1995) and the role of magma-derived fluids in influencing crustal alteration and massive sulfide formation is currently of great interest (GAMO *et al.*, 2006; YANG and SCOTT, 2006). The identification of magmatic signatures is therefore a major focus of Chapter 5 and this study provides useful insight into magmatic-hydrothermal processes in backarc settings.

REFERENCES

ALLEN, D. E. and SEYFRIED, W. E. (2003) Compositional controls on vent fluids from ultramatic-hosted hydrothermal systems at mid-ocean ridges: An experimental study at 400°C, 500 bars. *Geochimica et Cosmochimica Acta* **67**(8), 1531-1542.

BUTTERFIELD, D., SEYFRIED, W. E., and LILLEY, M. (2003) Composition and evolution of hydrothermal fluids. In: *Dahlem Workshop Report: Energy and Mass Transfer in Marine Hydrothermal Systems*, (*Ed:* P. E. Halbach, V. Tunnicliffe, and J. R. Hein), **89**, Dahlem University Press. pp. 123-161.

CHARLOU, J. L., DONVAL, J. P., FOUQUET, Y., JEAN-BAPTISTE, P., and HOLM, N. (2002) Geochemistry of high H_2 and CH_4 vent fluids issuing from ultramafic rocks at the Rainbow hydrothermal field (36°14'N, MAR). *Chemical Geology* **191**(4), 345-359.

CORLISS, J. B., DYMOND, J., GORDON, L. I., EDMOND, J. M., VON HERZEN, R. P., BALLARD, R. D., GREEN, K., WILLIAMS, D., BAINBRIDGE, A., CRANE, K. *et al.* (1979) Submarine thermal springs on the Galapagos Rift. *Science* **203**, 1073-1083.

CORLISS, J. B., BAROSS, J. A., and HOFFMAN, S. E. (1981) An hypothesis concerning the relationship between submarine hot springs and the origin of life on Earth. *Oceanologica Acta* **4**(Supplement), 59-69.

CRADDOCK, P. R. (2008) Geochemical Tracers of Processes Affecting the Formation of Seafloor Hydrothermal Fluids and Deposits in the Manus Back-arc Basin. Ph.D. Thesis. MIT-WHOI Joint Program in Oceanography, MIT.

DE DUVE, C. (1991) *Blueprint for a Cell: The Nature and Origin of Life.* N. Patterson.

FOUSTOUKOS, D. I. and SEYFRIED, W. E. (2004) Hydrocarbons in hydrothermal vent fluids: The role of chromium-bearing catalysts. *Science* **304**(5673), 1002-1005.

FRANKLIN, J., LYNDON, J. W., and SANGSTER, D. F. (1981) Volcanic-associated massive sulfide deposits. *Economic Geology* **75**, 485-627.

FU, Q., SHERWOOD LOLLAR, B., HORITA, J., LACRAMPE-COULOUME, G., and SEYFRIED, W. (2007) Abiotic formation of hydrocarbons under hydrothermal conditions: Constraints from chemical and isotopic data. *Geochimica et Cosmochimica Acta* **71**(8), 1982-1998.

GAMO, T., ISHIBASHI, J., TSUNOGAI, U., OKAMURA, K., and CHIBA, H. (2006) Unique geochemistry of submarine hydrothermal fluids from arc-back-arc settings of the Western Pacific. In: *Back-Arc Spreading Systems: Geological, Biological, Chemical, and Physical Interactions*, (*Ed:* D. M. Christie, C. R. Fisher, S.-M. Lee, and S. Givens), AGU Monograph, **166**, American Geophysical Union. pp. 147-161.

HERZIG, P. M. and HANNINGTON, M. D. (1995) Polymetallic massive sulfides at the modern seafloor - a review. *Ore Geology Reviews* **10**(2), 95-115.

HOLM, N. G. (1992) *Marine Hydrothermal Systems and the Origin of Life: Report of SCOR Working Group 91.* Reprinted from: Origins of Life and Evolution of the Biosphere, Vol. 22 (1-4), 1992. Springer.

HOLM, N. G. and CHARLOU, J. L. (2001) Initial indications of abiotic formation of hydrocarbons in the Rainbow ultramafic hydrothermal system, Mid-Atlantic Ridge. *Earth And Planetary Science Letters* **191**(1-2), 1-8.

HUBER, C. and WACHTERSHAUSER, G. (1997) Activated acetic acid by carbon fixation on (Fe,Ni)S under primordial conditions. *Science* **276**(5310), 245-247.

ISHIBASHI, J. and URABE, T. (1995) Hydrothermal activity related to arc-backarc magmatism in the Western Pacific. In: *Backarc Basins: Tectonics and Magmatism*, (*Ed:* B. Taylor), Plenum Press. pp. 451-495.

KELLEY, D. S., KARSON, J. A., BLACKMAN, D. K., FRUH-GREEN, G. L., BUTTERFIELD, D. A., LILLEY, M. D., OLSON, E. J., SCHRENK, M. O., ROE, K. K., LEBON, G. T. et al. (2001) An off-axis hydrothermal vent field near the Mid-Atlantic Ridge at 30°N. *Nature* **412**(6843), 145-149.

KELLEY, D. S., KARSON, J. A., FRÜH-GREEN, G. L., YOERGER, D. R., SHANK, T. M., BUTTERFIELD, D. A., HAYES, J. M., SCHRENK, M. O., OLSON, E. J., PROSKUROWSKI, G. et al. (2005) A serpentinite-hosted ecosystem; the Lost City hydrothermal field. *Science* **307**(5714), 1428-1434.

KLEIN, F., BACH, W., JONS, N., MCCOLLOM, T., MOSKOWITZ, B., and BERQUO, T. (2009) Iron partitioning and hydrogen generation during serpentinization of abyssal peridotites from 15 degrees N on the Mid-Atlantic Ridge. *Geochimica et Cosmochimica Acta* **73**(22), 6868-6893.

KONN, C., CHARLOU, J. L., DONVAL, J. P., HOLM, N. G., DEHAIRS, F., and BOUILLON, S. (2009) Hydrocarbons and oxidized organic compounds in hydrothermal fluids from Rainbow and Lost City ultramafic-hosted vents. *Chemical Geology* **258**(3-4), 299.

MARTIN, W. and RUSSELL, M. J. (2006) Review: On the origin of biochemistry at an alkaline hydrothermal vent. *Philosophical Transactions Of The Royal Society Of London Series B: Biological Sciences*, Page FirstCite, DOI 10.1098/rstb.2006.1881, URL: http://dx.doi.org/10.1098/rstb.2006.1881.

MCCOLLOM, T. M. and SEEWALD, J. S. (2006) Carbon isotope composition of organic compounds produced by abiotic synthesis under hydrothermal conditions. *Earth and Planetary Science Letters* **243**(1-2), 74-84.

MCCOLLOM, T. M. and SEEWALD, J. S. (2007) Abiotic synthesis of organic compounds in deep-sea hydrothermal environments. *Chemical Reviews* **107**, 382-401.

MCCOLLOM, T. M. and BACH, W. G. (2009) Thermodynamic constraints on hydrogen generation during serpentinization of ultramafic rocks. *Geochimica et Cosmochimica Acta* **73**(3), 856-875.

PROSKUROWSKI, G., LILLEY, M. D., SEEWALD, J. S., FRUH-GREEN, G. L., OLSON, E. J., LUPTON, J. E., SYLVA, S. P., and KELLEY, D. S. (2008) Abiogenic hydrocarbon production at Lost City hydrothermal field. *Science* **319**(5863), 604-607.

RUSSELL, M. J. and HALL, A. J. (2006) The onset and early evolution of life. In: *Evolution of Early Earth's Atmosphere, Hydrosphere, and Biosphere - Constraints from Ore Deposits: Geological Society of America Memoir 198*, (*Ed:* S. E. Kesler and H. Ohmoto), Geological Society of America. pp. 1-32.

SEEWALD, J. S. and SEYFRIED, W. E. (1990) The effect of temperature on metal mobility in subseafloor hydrothermal systems: constraints from basalt alteration experiments. *Earth and Planetary Science Letters* **101**(2-4), 388-403.

SEYFRIED, W. E. (1987) Experimental and theoretical constraints on hydrothermal alteration processes at mid-ocean ridges. *Annual Review of Earth and Planetary Sciences* **15**, 317-335.

SEYFRIED, W. E. and DING, K. (1995) Phase equilibria in subseafloor hydrothermal systems: a review of the role of redox, temperature, pH and dissolved Cl on the chemistry of hot spring fluids at mid-ocean ridges. In: *Seafloor Hydrothermal Systems: Physical, Chemical, Biological, and Geological Interactions*, (*Ed:* S. E. Humphris, R. A. Zierenberg, L. S. Mullineaux, and R. E. Thomson), AGU Monograph, **91**, American Geophysical Union. pp. 248-272.

SHERWOOD LOLLAR, B., WESTGATE, T. D., WARD, J. A., SLATER, G. F., and LACRAMPE-COULOUME, G. (2002) Abiogenic formation of alkanes in the Earth's crust as a minor source for global hydrocarbon reservoirs. *Nature* **416**(6880), 522-524.

SHOCK, E. L. (1990) Geochemical constraints on the origin of organic compounds in hydrothermal systems. *Origins Of Life And Evolution Of The Biosphere* **20**(3-4), 331-367.

SHOCK, E. L. (1992) Chemical Environments Of Submarine Hydrothermal Systems. *Origins Of Life And Evolution Of The Biosphere* **22**(1-4), 67-107.

SHOCK, E. L. and SCHULTE, M. D. (1998) Organic synthesis during fluid mixing in hydrothermal systems. *Journal Of Geophysical Research-Planets* **103**(E12), 28513-28527.

TIVEY, M. K., HUMPHRIS, S. E., THOMPSON, G., HANNINGTON, M. D., and RONA, P. A. (1995) Deducing patterns of fluid flow and mixing within the TAG active hydrothermal mound using mineralogical and geochemical data. *Journal Of Geophysical Research-Solid Earth* **100**(B7), 12527-12555.

YANG, K. and SCOTT, S. D. (2006) Magmatic fluids as a source of metals in seafloor hydrothermal systems. In: *Back-Arc Spreading Systems: Geological, Biological, Chemical, and Physical Interactions*, (*Ed:* D. M. Christie, C. R. Fisher, S.-M. Lee, and S. Givens), AGU Monograph, **166**, American Geophysical Union. pp. 163-184.

CHAPTER 2

Experimental investigation of CO_2 reduction to CH_4 under hydrothermal conditions

ABSTRACT

Abiotic synthesis of CH_4 in ridge-crest hydrothermal fluids is often presumed to occur on the surfaces of catalytically active minerals. However, aqueous reduction of carbon dioxide represents an alternative pathway to form reduced carbon compounds such as CH_4, carbon monoxide (CO), methanol (CH_3OH) and formic acid (HCOOH). To investigate whether CH_3OH is a metastable intermediary crucial to hydrothermal CH_4 production, aqueous fluids containing CO_2 and H_2 (added in the form of labeled $H^{13}COOH$) were heated at 325 and 300°C at 350 bar in a flexible-cell gold-Ti hydrothermal apparatus without added mineral catalysts, and the concentrations of CO_2, H_2, CH_4 and CH_3OH were monitored as a function of time over a multi-year period. CH_4 production increased with time at 325°C before reaching a constant rate. In contrast, the rate of CH_3OH production decreased with time as a metastable equilibrium with CO_2 and H_2 was attained relatively quickly at 325°C. To test the sensitivity of CH_4 production to CH_3OH concentration, the experiment was cooled from 325 to 300°C. Upon cooling, concentrations of CH_3OH increased due to the strong temperature dependence of CO_2-H_2-CH_3OH equilibrium. The rate of CH_4 production increased further despite the 25°C temperature decrease, strongly suggesting that formation of CH_4 from CO_2 is controlled by the concentration of the CH_3OH intermediate. Injection of H_2S to the experimental solution did produce ^{13}C-labelled

CH_3SH from $H^{13}COOH$ but direct reduction of CO_2 to CH_3SH was not observed, suggesting that CH_3SH does not fulfill the same role as CH_3OH in regulating the formation rate of CH_4. This study indicates that, even in the absence of heterogeneous catalysts, aqueous synthesis of CH_4 from CO_2 is rapid enough to be observable on a laboratory timescale, and may be a significant source of CH_4 to hydrothermal fluids at unsedimented mid-ocean ridge systems such as those hosted in ultramafic rock.

1. INTRODUCTION

Constraining abiogenic (non-biological) sources of methane (CH_4) is critical to elucidating its production on this planet and on other Solar System bodies such as Mars and Titan (*e.g.* GLEIN *et al.*, 2008; GLEIN *et al.*, 2009; MUMMA *et al.*, 2009). Methane production has long been associated with serpentinization of ultramafic rock (ABRAJANO *et al.*, 1988; SHERWOOD *et al.*, 1988; ABRAJANO *et al.*, 1990; CHARLOU and DONVAL, 1993; CHARLOU *et al.*, 1998; KELLEY *et al.*, 2001; PROSKUROWSKI *et al.*, 2008) and the origin of methane in black smoker fluids has been the subject of considerable discussion ever since seafloor hydrothermal activity was first discovered in 1977 (WELHAN, 1988; KELLEY and FRUH-GREEN, 1999; MCCOLLOM and SEEWALD, 2007). In the absence of a thermogenic (*i.e.* organic matter pyrolysis), microbial or magmatic origin, non-biological chemical reactions have been invoked as potential mechanisms to generate CH_4 in reducing hydrothermal fluids. The term "abiotic synthesis" in hydrothermal fluids refers to the non-biological reduction of oxidized single carbon compounds (CO_2 or CO) to CH_4 and other organic species. Thermodynamic assessments indicate that, at elevated temperatures and pressures, the generation and subsequent cooling of H_2-rich aqueous fluids during hydrothermal alteration of basaltic and ultramafic crust strongly favors this process (SHOCK, 1992; SHOCK and SCHULTE, 1998). The possibilities for catalysis by minerals such as magnetite (Fe_3O_4, FU et al., 2007), Fe-Ni alloy (HORITA and BERNDT, 1999) or chromite ($FeCr_2O_4$, FOUSTOUKOS and SEYFRIED, 2004) in oceanic hydrothermal systems enhances the potential for abiotic organic synthesis and these environments have been extensively discussed as a favorable setting from which early life could have emerged (CORLISS *et al.*, 1981; BAROSS and HOFFMAN, 1985; SCHULTE and SHOCK, 1995). The production of methane is also vital to the maintenance of microbial ecosystems in present day hydrothermal vent and plume environments,

where methanotrophs can represent a large fraction of the microbial population (BAROSS and DEMING, 1995; COWEN *et al.*, 2002; KELLEY *et al.*, 2002; KELLEY *et al.*, 2004).

A widely cited mechanism responsible for abiotic hydrocarbon synthesis in hydrothermal fluids is the Fischer-Tropsch reaction (CHARLOU *et al.*, 1998; CHARLOU *et al.*, 2002). In its original industrial context, the Fischer-Tropsch reaction refers to the reduction of gas-phase mixtures of CO and H_2 to CH_4 and longer chain *n*-alkanes by polymerization on the surface of a transition metal catalyst (ANDERSON, 1984). Whether abiotic CH_4 production in hydrothermal systems indeed occurs by the Fischer-Tropsch mechanism is as yet unknown. Formation of CH_4 alone may be possible by a Sabatier-type process, with Fe-Ni alloy catalysts (HORITA and BERNDT, 1999). For clarity, MCCOLLOM and SEEWALD (2007) recommended the use of the term 'Fischer-Tropsch-type' (FTT) synthesis when referring to purported hydrothermal reduction of CO_2 or CO by heterogeneous (mineral) catalysis, as this does not mistakenly imply any specific reaction mechanism or generation of C–C bonds. The potential relevance of mineral-catalyzed synthesis to seafloor hydrothermal systems has lead to numerous experimental studies attempting to simulate the process in the laboratory (BERNDT *et al.*, 1996; MCCOLLOM and SEEWALD, 2001; RUSHDI and SIMONEIT, 2001; FOUSTOUKOS and SEYFRIED, 2004; FU *et al.*, 2007).

Despite the widespread interest in mineral-catalyzed pathways for the production of hydrocarbons, CH_4 concentrations in many ultramafic-hosted vent fluids are inconsistent with a single polymerization-type formation mechanism. For example, CH_4 concentrations in vent fluids at the Lost City hydrothermal site are elevated relative to the predicted log-linear increase in *n*-alkane abundance with decreasing carbon number for polymerization of hydrocarbons (ANDERSON, 1984; PROSKUROWSKI *et al.*, 2008; CHARLOU *et al.*, 2002). In addition to possible biogenic sources (BRADLEY *et al.*, 2009), abiotic mechanisms may be responsible for these elevated abundances. It has largely been assumed that uncatalyzed aqueous reduction of CO_2 to

CH_4 by H_2 is kinetically prohibited (HORITA and BERNDT, 1999; LUTHER, 2004) and with the exception of recent work by SEEWALD *et al.* (2006), there have been few studies of hydrothermal CO_2 reduction in the absence of heterogeneous catalysts. SEEWALD *et al.* (2006) observed formation of minor quantities of CH_4 and other single carbon compounds from CO_2 in the absence of mineral catalysts or gas phase reactants during laboratory experiments and proposed a pathway for sequential reduction of CO_2 to CH_4 *via* a series of single carbon intermediates. Excluding the formation of C–C bonds, aqueous reactions among single carbon compounds in the C-H-O system are limited to the carbonate system (CO_2, HCO_3^-, CO_3^{2-}), carbon monoxide (CO), formic acid/formate ($HCOOH/HCOO^-$), formaldehyde (CH_2O), methanol (CH_3OH) and CH_4. The reduction of CO_2 to CO (known as the water-gas shift (WGS) reaction) is relatively rapid (on the order of hours to days) at 150–300°C and reversible in the absence of mineral catalysis (SEEWALD *et al.*, 2006). If complete equilibrium between aqueous CO_2, H_2 and the single carbon compounds in Figure 2.1 were attained under hydrothermal conditions, CH_4 would be the dominant reduced species. The reductive pathway proposed by SEEWALD *et al.* (2006) does not, however, consider the possible role of reduced sulfur (S) species in carbon dioxide reduction. Reduced S is ubiquitous in hydrothermal systems (either as dissolved hydrogen sulfide (H_2S, <1–20 mmol/kg, VON DAMM, 1995) or in the form of sulfide minerals). Given the large number of oxidation states of sulfur and its inherent reactivity in many natural redox reactions, the possibility exists that simple sulfur-bearing compounds may actually be involved in numerous aqueous organic reactions in hydrothermal fluids and play an as yet undetermined role in abiotic synthesis. Aqueous sulfur species have been shown to enhance reaction rates of simple hydrocarbons under hydrothermal conditions (SEEWALD, 2001) and reduced S species are known to act as free radical shuttles (LEIF and SIMONEIT, 2000). The addition of reduced S to the aqueous C-O-H system allows for several possible S-bearing intermediate oxidation state carbon

species (Figure 2.1), the stability and behavior of which under hydrothermal conditions is unknown. There have been few studies of organosulfur compounds under hydrothermal conditions (HEINEN and LAUWERS, 1996) but there is extensive interest in the role they may have played in the origin of primitive metabolism (HUBER and WACHTERSHAUSER, 1997; MARTIN and RUSSELL, 2006; MARTIN *et al.*, 2008).

This study builds on the experimental work of SEEWALD *et al.* (2006), which suggested that the rate of aqueous CH_4 production in the absence of mineral catalysis may be governed by redox-dependant metastable equilibrium between CO_2 and the intermediates HCOOH, CO, CH_2O and CH_3OH. Metastable equilibrium is defined as any equilibrium energy state of a system other than the lowest energy state (ANDERSON, 2005). If CH_3OH abundance is governed by metastable equilibrium with CO_2 and its subsequent reduction to CH_4 is kinetically inhibited, then methanol may represent the overall rate-limiting step in CO_2 reduction. Furthermore, the possibility that its S-bearing analog, methanethiol (CH_3SH), could be a rate-limiting precursor was not investigated. Thermodynamic data are currently limited to the *n*-alkyl thiols (SCHULTE and ROGERS, 2004), but Figure 2.2 shows that the stability of CH_3SH with respect to CO_2 and H_2 is greater than that of CH_3OH. This study therefore attempts to constrain the relative importance of methanol and methanethiol as a potential reaction intermediates in CO_2 reduction in the absence of mineral catalysis. The findings of this study have significant implications for the potential of subsurface hydrothermal fluids to generate CH_3OH and CH_3SH, and to produce CH_4 without the involvement of heterogeneous catalysis.

2. METHODS

2.1. Experimental Apparatus and Design

The experiment was performed by heating an aqueous solution of formic acid (HCOOH) in a flexible-cell hydrothermal apparatus in the presence and absence of H_2S. The apparatus used consists of a gold reaction cell (with titanium closure piece, Figure 2.3) contained within a steel pressure vessel which uses H_2O as a pressurizing fluid (SEYFRIED, 1987). There are several advantages in using this type of reaction cell instead of traditional fixed-volume reactors, and the apparatus has been successfully used to study a variety of aqueous organic reactions under hydrothermal conditions (SEEWALD, 2001; MCCOLLOM and SEEWALD, 2003a,b; SEEWALD *et al.*, 2006; FU *et al.*, 2007). External control of *in situ* pressure and temperature conditions in the reaction cell allows the elimination of a vapor phase headspace. This is particularly important in studying aqueous CH_4 production rates, as reactants may partition into the headspace and undergo rapid reduction. Fluid samples are removed from the reaction cell by means of a titanium capillary tube and valve leading from the closure piece, without disturbing the pressure and temperature conditions of the cell contents. Rapid cooling of fluid samples upon removal from the reaction cell also minimizes retrograde reactions that can occur during prolonged quenching (SEEWALD, 2001). Prior to the addition of fluid, the gold reaction cell was flame treated in air to several hundred degrees Celsius to anneal the gold and ensure combustion of any potential organic contaminants.

Because the objective of the experiment was to investigate factors controlling the production of CH_4 in the absence of heterogeneous catalysts, minerals were not added to the reaction cell. Although the possibility exists that some of the reactions studied may have been catalyzed by the reaction cell materials, previous experiments using the same reaction system suggest that neither gold nor TiO_2 are catalytically active with respect to a variety of organic

reactions at experimental conditions (BELL *et al.*, 1994; MCCOLLOM and SEEWALD, 2003a; SEEWALD *et al.*, 2006). The titanium closure piece/capillary tube was heated overnight at 400°C in air to form an inert TiO_2 layer on all surfaces in contact with the fluid. Prior to pressurization of the reaction cell, the reaction cell headspace was purged with argon before closure to remove air.

In order to circumvent the technical difficulties of dissolving large quantities of gaseous species into the reaction cell, aqueous formic acid (HCOOH) was used as a source of both CO_2 and H_2 during the experiment. Previous experiments have shown that HCOOH undergoes near quantitative decarboxylation to aqueous CO_2 and H_2 in less than 48h under hydrothermal conditions (MCCOLLOM and SEEWALD, 2003a, 2006; SEEWALD *et al.*, 2006). Isotopically-labeled formic acid (99% $H^{13}COOH$, Cambridge Isotopes Labs) was used to allow differentiation between *bona fide* reaction products (*i.e.* formed from HCOOH or CO_2) and compounds derived from background sources such as thermal decomposition of background dissolved organic carbon (DOC).

Stage (1) of the experiment consisted of heating 39.4g of a solution containing 123mmol/kg $H^{13}COOH$ and 9.83mmol/kg NaCl at 325°C and 35 MPa for 956 days. The NaCl was added as a conservative tracer to monitor potential leakage of the reaction cell contents into the surrounding NaCl-free pressurizing fluid. Chemical disequilibrium was induced after 956 days by reducing the temperature (at 35 MPa) to 300°C and the subsequent evolution of dissolved species concentrations was monitored as a function of time (Stage (2)). The purpose of cooling the reaction cell was to investigate the effects of temperature and carbon speciation on the rate of CH_4 formation from CO_2. As can be seen from Figure 2.2, the overall reactions for CH_3OH and CH_4 formation from CO_2 and H_2 are thermodynamically favored at lower temperatures. The pressure vessel temperature was stable at 300°C within 6 hours of cooling the furnace, thereby

ensuring near-instantaneous disequilibrium on the timescale of these reactions. After 1575 days, the effect of sulfur addition to the aqueous C-O-H system was examined by injection () of 20.5g of a solution containing 40mmol/kg sodium sulfide (Na_2S) adjusted to pH 4 to 5 with hydrochloric acid, thereby yielding a solution of NaCl and H_2S (Stage (3)). The injected solution also contained 132mmol/kg $H^{13}COOH$ to replenish the CO_2 and H_2 inventory of the reaction cell solution.

2.2. Analysis of Dissolved Species

Throughout the course of the experiment, separate ~0.5–1g fluid samples were taken in duplicate on a given sampling event with glass/Teflon gas-tight syringes for analysis of dissolved species. Total dissolved CO_2 ($\Sigma CO_2 = [CO_{2(aq)}] + [HCO_3^-] + [CO_3^{2-}]$), CH_4 and C_1–C_5 hydrocarbons were analyzed using a purge and trap system interfaced directly to a gas chromatograph (GC) with a Porapak Q packed column and serially connected thermal conductivity (TCD) and flame ionization detectors (FID). Quantitative extraction of all carbonate species as $CO_{2(g)}$ was accomplished by injection of fluid samples into a He purge cell containing a 25 wt% phosphoric acid solution. During Stage (3) of the experiment, methanethiol concentrations were also determined by purge-and-trap GC-FID and total dissolved sulfide ($\Sigma H_2S = H_2S + HS^- + S^{2-}$) was determined gravimetrically following precipitation as Ag_2S. Dissolved H_2 was analyzed on a GC using a 5Å molecular sieve packed column with TCD, following headspace extraction with N_2 gas. Cl was analyzed by ion exchange chromatography on a Dionex DX500 system with conductivity detection. Concentrations of total formic acid ($\Sigma HCOOH = HCOOH + HCOO^-$) were also determined by ion chromatography using an IonPac® ICE-AS1 ion exclusion column. Methanol concentrations were determined by split injection of aqueous samples onto a HP 6890 GC with an EC-WAX column and flame ionization detector.

To monitor incorporation of the ^{13}C label into CH_3OH, CH_3SH and CH_4, selected fluid samples were analyzed by gas chromatography-mass spectrometer (Hewlett-Packard 5973 mass selective detector). The analytical uncertainty of all dissolved species measurements is estimated at ±5% (2s).

3. RESULTS

3.1. CO_2 and H_2

Rapid production of CO_2 and H_2 in equimolar concentrations (~120mmol/kg) was observed within 78 days of initial heating (Table 2.1), consistent with decomposition of HCOOH which decreased to <0.3mmol/kg. This is consistent with previous use of HCOOH which revealed that CO_2-H_2-HCOOH equilibration is rapid and occurs in less than 48 hours at temperatures of ≥300°C (SEEWALD *et al.*, 2006). CO_2 concentrations, initially 120mmol/kg, remained relatively constant throughout the experiment but decreased slightly at the end of the 325°C phase (Figure 2.4). H_2 concentrations appeared to decrease monotonically from the initial value of 118mmol/kg to 61mmol/kg by the end of the 300°C phase of the experiment (Figure 2.4). Based on the concentrations of CH_4 and CH_3OH after 1560 days (Table 2.1) and the stoichiometry of the overall reduction reactions (Figure 2.2), production of these species can only account for the consumption of ~17mmol/kg of the initial H_2 concentration. Constant Cl^- concentrations (Table 2.1) indicate that the reaction cell maintained integrity during the experiment, precluding leakage as the cause for the observed decrease. It may be possible that the long duration of this experiment facilitated slow diffusion of H_2 through the reaction cell materials. Alternatively, reduction of the TiO_2 surface of the closure piece to Ti or formation of a titanium (II) carbonate phase may have occurred. Though there are no thermodynamic data for the latter, it may explain the loss of both H_2 and CO_2 towards the end of the 325°C phase. The subsequent increase in CO_2 upon cooling might therefore reflect the effect of temperature on the solubility of such phases.

3.2. CH_4 and CH_3OH formation

The long time scale of this experiment allowed substantial quantities of aqueous CH_4 and CH_3OH to be generated (Table 2.1). The average rate of CH_4 production increased with time during the 325°C phase from 0.5μmol kg^{-1} day^{-1} (prior to 78 days) to 1.0μmol kg^{-1} day^{-1} at 851 days, though CH_4 concentrations increased much more slowly than CH_3OH (Figure 2.4). Following the temperature reduction to 300°C, CH_4 concentrations in Stage (2) steadily increased at a similar average rate to the latter portion of Stage (1) but then increased to 1.6 μmol kg^{-1} day^{-1} in the final stages of the 300°C phase. By the end of the experiment, ~1% of the total carbon in the fluid had been converted to CH_4.

In contrast to CH_4, production of CH_3OH was initially rapid at both 325 and 300°C and slowed with time. Concentrations of CH_3OH increased during the early stages of the experiment before reaching a constant value (~1.2mmol/kg) by the end of Stage (1), (Figure 2.4). After the temperature was reduced to 300°C at 956 days, production of CH_3OH increased, with concentrations rapidly rising to 3.5mmol/kg by the end of Stage (2). Though less pronounced than Stage (1), the rate of CH_3OH formation gradually decreased with time in Stage (2) also (Figure 2.4).

Extensive incorporation of the ^{13}C label into both CH_3OH and CH_4 was evident, based on GC-MS analysis of samples taken at 1560 and 78 days, respectively (Figure 2.5). Incorporation of the ^{13}C label was not detected in any of the C_{2+} hydrocarbons analyzed. This confirms that CH_3OH and CH_4 are predominantly *bona fide* reaction products of CO_2 or HCOOH reduction, and not derived from thermal decomposition of the background DOC of the solution. The dissolved organic carbon content of the Milli-Q water used to make the initial solution is estimated to be ~40μmol/kg (B. Van Mooy, *pers. comm.*). Hence, it is likely that the observed

C_{2+} compounds were merely derived from thermal decomposition of the background DOC in the solution.

3.3. Other C species

Concentrations of C_2–C_5 hydrocarbons appeared to increase during the 325°C phase but subsequently remained constant throughout the remainder of the experiment and were low overall (<30μmol/kg) relative to CH_4 (Table 1). The postulated intermediate formaldehyde (Figure 2.1) was not observed during the course of the experiment, though it would not have been detected at levels below ~10^{-7}mol/kg. It is also possible that formaldehyde-methanediol equilibrium could be occurring, which could explain the observed lack of formaldehyde. At room temperatures, formaldehyde in solution predominantly exists as methanediol (ANSLYN and DOUGHERTY, 2005), a species which could not be analyzed. There are no thermodynamic data for diols under hydrothermal conditions to evaluate this possibility, however. Furthermore, given the large concentrations of CO_2 used in this experiment, accurate mass balance on the abundance of reduced species present at much lower abundances is not possible.

3.4. Sulfur-bearing species

The injection of the Na_2S and HCOOH solution produced a solution composition similar to Stages (1) and (2) with CO_2 concentrations of 108mmol/kg, H_2 concentrations of 85mmol/kg except with the addition of H_2S at concentrations at 20–24mmol/kg (Figure 2.4). CO_2 concentrations remained relatively constant while H_2 concentrations decreased steadily in a similar manner to the previous stages. Rapid production of CH_3SH occurred immediately after injection at the start of Stage (3), with a maximum concentration of 1.1mmol/kg. However, production abruptly ceased when HCOOH decomposition to CO_2 and H_2 was complete and

CH_3SH concentrations subsequently decreased with time to low values (<0.2mmol/kg) by the end of Stage (3). Incorporation of the ^{13}C label into CH_3SH was evident (Figure 2.5) indicating that it was not derived from background contamination. In contrast to the previous stages, CH_4 production was initially rapid but slowed with time (Figure 2.5) and although dilution occurred due to injection, CH_3OH concentrations did not subsequently vary outside of analytical error. The average rate of CH_4 production during Stage (3) was 1.9μmol/d.

4. DISCUSSION

4.1. Thermodynamic constraints on metastable equilibrium

Interpretation of the analytical results of this experiment in a thermodynamic context indicates that equilibrium between CO_2, H_2 and CH_3OH is rapid enough to be observable on laboratory timescales. The extent to which aqueous species may have attained a state of thermodynamic equilibrium (metastable or stable) during the experiment can be evaluated by calculating the chemical affinity (A) for a given reaction according to the following relationship:

$$A = -\Delta_r G = -RT \ln (Q_r / K_{eq}) \qquad (1)$$

Where R is the universal gas constant, T is temperature in Kelvin, Q_r is the reaction quotient and K_{eq} is the equilibrium constant for the reaction in question. Positive values of A indicate a thermodynamic drive for the reaction to proceed from left to right as written (*i.e.* $A = -\Delta_r G$ for a given reaction). At thermodynamic equilibrium, values of Q and K_{eq} are equal and A equals zero. Requisite thermodynamic data for these calculations were generated from the SUPCRT92 thermodynamic database JOHNSON *et al.* (1992), with additional data from SHOCK (1995). Given the presence of solely non-ionic or univalent species and the low solution ionic strength (of order $\sim 10^{-2}$), activity coefficients of unity were assumed for all aqueous species due to the low concentration of dissolved ions in solution and the concomitant lack of significant 'salting out' effects (GARRELS and CHRIST, 1965; ANDERSON, 2005). Due to uncertainties in the thermodynamic data used to perform these calculations, an affinity of exactly zero at equilibrium should not be expected. Calculated affinities of 0±4kJ/mol are typically assumed to represent equilibrium (SEEWALD, 2001), consistent with the errors estimated by SHOCK and HELGESON (1990) in derivation of $\Delta_r G^o$ values. Evaluation of chemical affinities for both CH_3OH ($A_{Methanol}$) and CH_4 ($A_{Methane}$) formation reactions shown in Figure 2.2 reveals that CO_2-H_2-CH_3OH equilibration was essentially complete by the end of each of the three stages as values approach

within 4kJ/mol of zero (Figure 2.6). Following the temperature reduction to 300°C (956 days), $A_{Methanol}$ increased markedly, consistent with the strong temperature dependence of the K_{eq} for CH_3OH production (Figure 2.2), but rapidly returned to equilibrium towards the end of the experiment as CH_3OH concentrations increased. The lack of variation in CH_3OH concentrations in Stage (3) reflects a decreased drive for CH_3OH production due to decreased H_2 activity. In contrast to $A_{Methanol}$, affinities for the formation of CH_3SH by the reduction of CO_2 (reaction shown in Figure 2.2) were high (27.0 – 34.3kJ/mol) throughout Stage (3) and, rather than approach equilibrium values, actually increased with time (Figure 2.6). $A_{Methane}$ also remained 1 to 2 orders of magnitude higher than $A_{Methanol}$ for all of the experiment (Figure 2.6), indicating a consistent strong thermodynamic drive for CH_4 production to proceed.

In the absence of analytical constraints on all species involved in the reductive pathway of SEEWALD *et al.* (2006), (Figure 2.1), speciation calculations may be used to further constrain the composition of the experimental solutions expected for equilibrium. By allowing an idealized initial fluid composition (120 mmol/kg CO_2 and H_2) to reach equilibrium according to the reactions shown in black in Figure 2.1, in addition to the reactions of the carbonate system, a theoretical equilibrium fluid composition may be calculated for each phase of the experiment by simultaneous solving the respective mass balance and mass action expressions. Two models of the experimental solution composition were tested using this approach and predicted concentrations compared to measurements. The first scenario assumed that CH_4 formation does not occur due to kinetic inhibition, thereby allowing the calculation of a theoretical *metastable* equilibrium composition in which CO_2 is allowed to reach equilibrium with the aqueous species HCO_3^-, CO_3^{2-}, HCOOH, $HCOO^-$, CO, CH_2O and CH_3OH only. In the second scenario, the kinetic inhibition was removed and CO_2 was allowed to equilibrate with CH_4 in addition to the above

species. This latter case differs from the former in that it represents the total equilibrium state of the fluid.

Examination of Figures 2.7 (A) and (D) reveals that the assumption of kinetic inhibition of methane is a more realistic approximation of the real system composition, which closely matches this model. The measured abundances of CH_3OH are greatly in excess of what total equilibrium would predict (Figures 2.7 (C) and (D)). Thus, metastable equilibrium between CO_2 and CH_3OH represents the best explanation for the observed variations in fluid chemistry. Although measured CH_3OH concentrations did not quite reach the value predicted for metastable equilibrium by the end of the 300°C phase, the values agree to within a factor of 3. Losses of H_2 (to which equilibrium CH_3OH abundance is highly sensitive) in the experiment relative to the speciation model conditions are likely to be responsible for this offset.

Measured concentrations of CH_3SH during Stage (3) did not approach values predicted for equilibrium with CO_2, H_2 and H_2S (Figure 2.7(E)) and were almost 2 orders of magnitude too low by the end of Stage (3). Figure 2.7 (E) shows that CH_3SH would be far more abundant than CH_3OH if it reached metastable equilibrium with CO_2, H_2 and H_2S, a situation that was never realized during the experiment. Combined with the affinity considerations above, this provides compelling evidence for kinetic inhibition of CH_3SH formation from CO_2, H_2 and H_2S. In contrast, CH_3OH remained in equilibrium with CO_2 and H_2 in the presence of H_2S (Figure 2.7(E)).

4.2. The relative roles of CH_3OH and CH_3SH in abiotic synthesis of CH_4

Significant quantities of CH_4 and CH_3OH were formed by reduction of CO_2 during the course of this experiment and rates of CH_4 production appear to have been regulated by CO_2-H_2-CH_3OH metastable equilibrium. By reducing the temperature of the system, the effect of temperature on CH_3OH stability was evident. According to Figure 2.2, the drop in temperature of

25°C corresponded to an almost ten-fold increase in CH_3OH abundance (*cf.* Figures 2.7(A) and (B)). Despite the enhanced thermodynamic drive, lower CH_4 production rates might have been expected at 300°C due to a strong positive correlation of reaction kinetics with temperature. However, if CH_3OH reduction is the rate-limiting step and its equilibrium abundance influences CH_4 production rates, then the loss of any kinetic advantages available to the reaction of CH_3OH to form CH_4 at 325°C could potentially be offset by increased CH_3OH concentrations at 300°C. Increased CH_3OH concentrations after cooling were accompanied by increases in CH_4, and the average CH_4 production rate during Stage (2) exceeded that of Stage (1), despite the lower temperature of the former. The increase in CH_4 production rates with time during both stages noted above strongly suggests a dependency on CH_3OH concentrations, which were initially low but increased until metastable equilibrium with CO_2 was obtained. By limiting the abundance of CH_3OH, metastable CO_2-H_2-CH_3OH equilibrium may therefore influence the production rate of CH_4.

The data from the H_2S free stage of the experiment may be used to derive estimates of the rate constant, k, for CH_4 formation from CH_3OH at both 325°C and 300°C. Assuming the rate of reaction is first order with respect to both the concentration of H_2 and CH_3OH, an equation of the following form can be used to estimate k:

$$d[CH_4] / dt = k\,[CH_3OH][H_2]$$

where t is time in days and [i] is the measured concentration of species 'i'. Using average rates of CH_4 formation and concentration data from 851 days and 1560 days, estimated values of k at 325°C and 300°C are calculated to be 0.9×10^{-8} and 1.2×10^{-8} $\mu mol\ kg^{-1} day^{-1}$, respectively.

In contrast to CH_3OH, CH_3SH does not appear to exert the same influence on CH_4 production rates as metastable CO_2-H_2-H_2S-CH_3SH equilibrium was never attained. It is likely that, rather than being a product of direct CO_2 reduction, CH_3SH formed during the earliest

portion of Stage (3) as a result of HCOOH decomposition in the presence of H_2S. This may have been facilitated by intermediates such as CO or other species which could have been present in large quantities before HCOOH decomposition was complete. This is consistent with the lack of CH_3SH production subsequent to the transformation of HCOOH to CO_2 and H_2. A possible explanation for kinetic inhibition is that direct reduction of CO_2 to S-bearing intermediates inherently requires reaction of both H_2S and H_2 with CO_2 (Figure 2.1), which due to molecular collision considerations, may be kinetically inhibited. The decrease in CH_4 production rate with time in Stage (3) suggests that formed CH_3SH subsequently reacted to produce CH_4, producing lesser amounts with time as the supply of CH_3SH was exhausted. However, given that concentrations of CH_3SH did not achieve metastable equilibrium with CO_2, the presence of H_2S does not appear to substantially affect the rate of formation of CH_4 in the absence of high concentrations of HCOOH.

4.3. Implications for hydrothermal systems

4.3.1 CH_3OH and CH_4 formation

In ultramafic-hosted hydrothermal systems, aqueous CO_2 and H_2 concentrations are typically an order of magnitude lower than those used in this study (see MCCOLLOM and SEEWALD, 2007 for review). The abundance of CH_3OH and other intermediates in seafloor hydrothermal systems will be regulated by the residence time of fluids in high-temperature reaction zones, as well as the physical and chemical characteristics of the subsurface environment. CH_3OH abundances will be a strong function of the temperature structure of the subseafloor environment and will be more abundant at lower temperatures. Measured vent temperatures in ultramafic hydrothermal systems investigated to date span a wide range (28–365°C, CHARLOU *et al.*, 2002; PROSKUROWSKI *et al.*, 2008), but theoretical considerations estimate subsurface

temperatures in the range of 200–400°C (ALLEN and SEYFRIED, 2004; FOUSTOUKOS *et al.*, 2008). Recent thermodynamic modeling of serpentinization processes indicates that associated H_2 production is likely to be maximal in the temperature range of 200–315°C (KLEIN et al., 2009; MCCOLLOM and BACH, 2009). Thus, the increased stability of CH_3OH within this lower temperature range in conjunction with elevated H_2 activities could result in substantial CH_4 production without mineral catalysis in systems where serpentinization is occurring at these conditions. The findings of this experiment therefore have significant implications for CH_4 production in such systems.

In contrast to temperature, subsurface residence times of hydrothermal fluids are much less constrained, but estimates from studies of short-lived radionuclides in vent fluids from various sites along the Juan de Fuca Ridge indicate that the residence times for fluids in the high temperature (>200°C) regions of the hydrothermal reservoir are on the order of years (KADKO and MOORE, 1988; KADKO and BUTTERFIELD, 1998), consistent with estimates based on geophysical constraints (FISHER, 2003). Thus, there is likely to be sufficient time for CO_2-H_2-CH_3OH equilibrium to be achieved in subseafloor hydrothermal fluids and if fluids within the lower temperature range have longer subsurface residence times than hotter (~400°C) fluids, increased CH_4 production might be possible despite slower kinetics.

An important implication of this study is the possibility that aqueous CH_4 production could proceed at reasonable rates in natural systems without the need to invoke heterogeneous catalysis. The general view that mineral-catalyzed mechanisms are the only plausible pathway for abiotic CH_4 synthesis has lead to many experimental studies using catalysts such as iron-nickel alloy and chromium (HORITA and BERNDT, 1999; FOUSTOUKOS and SEYFRIED, 2004). Although transition metals are present in basaltic and ultramafic crust, it has been largely ignored that catalytic surfaces may be effectively 'poisoned' by the abundant reduced sulfur species in

hydrothermal systems (HAYATSU and ANDERS, 1981; MILLER and BADA, 1988) and such experiments typically have not included any S forms. It is widely known that S is detrimental to the Fischer-Tropsch reaction in particular (LIU *et al.*, 1994; RHODES *et al.*, 2000). Thus, the applicability of this type of synthesis to S-rich natural hydrothermal systems is still a matter of debate. The possibility of homogeneous reduction also offers an explanation for the excess CH_4 relative to the Anderson-Schulz-Flory distribution of *n*-alkanes at the Lost City hydrothermal site (PROSKUROWSKI *et al.*, 2008). Reaction zone conditions in this system are estimated to be in the vicinity of 250°C (ALLEN and SEYFRIED, 2004; FOUSTOUKOS *et al.*, 2008), which would be favorable for the production of H_2 and CH_3OH. While it is possible that CH_4 synthesis from CH_3OH could also occur in basalt-hosted systems, there may be kinetic issues associated with the drastically lower H_2 concentrations typical of these systems.

This study also has significant implications for methanol synthesis in hydrothermal systems. Previous experimental studies of magnetite-catalyzed gas phase reactions indicate that abiotic synthesis of large quantities of CH_3OH could be achieved in seafloor hydrothermal systems during short-lived diking-eruptive events, which are known to release large quantities of CO_2 and H_2 (HOLLOWAY and O'DAY, 2000; VOGLESONGER *et al.*, 2001). Such events are also typically associated with intense 'megaplumes', and large increases in observed CH_4 concentrations (see KELLEY *et al.*, 2004 for review). The data presented here show that methanol formation occurs readily in an aqueous phase and the CO_2-H_2-CH_3OH equilibration timescale is comparable to estimates of residence times for fluids in ridge-crest hydrothermal systems. Hence, unless significant catalysis is occurring, it is unlikely that the short (weeks to months) timescales of diking-eruptive events could lead to significant CH_3OH production in the aqueous phase. However, as yet, there have been no reported measurements of CH_3OH concentrations in vent fluids to test hypotheses for the importance of methanol in hydrothermal systems. Table 2.2

shows predicted CH_3OH abundances for two highly reducing vent fluids from the Mid-Atlantic Ridge sites 'Rainbow' and 'Logatchev', and these concentrations may be measurable if analytical methods are developed.

4.3.2 CH_3SH formation

The results presented here provide compelling evidence for kinetic inhibition of aqueous CH_3SH formation from CO_2, H_2 and H_2S. There is extensive interest in the formation of CH_3SH by CO_2 reduction in ultramafic-hosted hydrothermal fluids as it is considered a possible precursor in the synthesis of thioester (HUBER and WACHTERSHAUSER, 1997; MARTIN and RUSSELL, 2006; RUSSELL and HALL, 2006; MARTIN *et al.*, 2008). The latter is the key functional group of the Acetyl-CoA enzyme, and prebiotic thioester formation is a crucial component of theories which postulate that primitive metabolism preceded the emergence of RNA-like material on the early Earth (DE DUVE, 1991; HUBER and WACHTERSHAUSER, 1997; RUSSELL and HALL, 2006). In CHAPTER 2, the distribution of CH_3SH in hydrothermal fluids from a variety of geologic settings of varying redox states is shown to be inconsistent with CO_2 reduction as a formation mechanism and likely reflects other, possibly non-abiotic, sources. Combined, these observations suggest the potential for CH_3SH synthesis in seafloor hydrothermal fluids by this mechanism is much more limited than previously thought.

5. CONCLUSIONS

A long term hydrothermal experiment has demonstrated significant aqueous CO_2 reduction to CH_4 in the absence of mineral catalysts on timescale analogous to fluid residence times in hydrothermal systems. Long term production rates of CH_4 are influenced by the equilibrium abundance of its metastable precursor, CH_3OH, the stability of which is highly dependant on temperature and redox. The experimental data indicate that reduction of CO_2 to CH_3OH is rapid under hydrothermal conditions while reduction of CH_3OH to CH_4 is comparatively slow, but does proceed at measurable rates. Aqueous reduction of CO_2 to CH_4 *via* CH_3OH thus represents a likely pathway to form significant quantities of CH_4 in unsedimented seafloor hydrothermal systems. Despite slower kinetics than mineral-catalyzed mechanisms, CH_4 production may be associated with maximal H_2 production during serpentinization at 200–315°C due to the enhanced stability of methanol at these temperatures relative to much hotter subsurface conditions. By addition of H_2S, the potential role of CH_3SH in CH_4 formation appears to be limited as direct reduction of CO_2 to the former did not readily occur. The aqueous reduction of CO_2 to CH_4 appears to be an unavoidable consequence of the strong chemical and thermal gradients present in seafloor hydrothermal systems.

ACKNOWLEDGEMENTS

I would like to thank Dr. P. Saccocia for the initial setup of the experiment in 2003. I would also like to thank S. Sylva for his analytical expertise and assistance with instrumentation and sampling. This work was supported by the National Science Foundation grant OCE-0136954.

Table 2.1
Concentrations of aqueous species measured during heating at 325-300°C and 35MPa

Time (days)	ΣHCOOH mmol/kg	H_2 mmol/kg	ΣCO_2 mmol/kg	ΣH_2S mmol/kg	CH_3OH mmol/kg	CH_4 mmol/kg	CH_3SH mmol/kg	Cl^- mmol/kg	ΣC_2-C_5 mmol/kg
			Stage (1) Temperature at 325°C						
0.0	123	na	na	na	na	na	na	9.5	0.0
25.2	na	na	na	na	na	na	na	10	0.0
78.1	0.3	118	120	na	0.5	0.04	na	10	0.01
851	0.2	88	116	na	1.3	0.82	na	9.5	0.03
953	0.3	85	104	na	1.2	0.86	na	9.5	0.03
956			***Stage (2) Temperature reduced to 300°C***						
981	0.4	90	101	na	1.3	0.86	na	9.5	0.03
1037	0.2	82	106	na	1.5	0.91	na	9.6	0.03
1161	0.8	76	115	na	2.3	0.94	na	9.3	0.03
1560	na	61	117	na	3.5	1.60	na	na	0.04
1575			***Stage (3) Injected solution of HCOOH, Na_2S and HCl at 300°C***						
1579	5.1	85	108	20	1.6	0.50	1.0	53	0.01
1586	0.6	88	114	22	1.9	0.54	1.1	52	0.01
1677	1.8	79	105	na	1.8	0.83	0.31	58	0.02
1875	na	67	105	24	1.8	1.09	0.12	56	0.02

na = not analyzed

ΣC_2-C_5 = Sum of straight chain alkane and alkene compounds with carbon numbers 2 to 5

The analytical uncertainty of all dissolved species measurements is estimated at ±5% (2σ)

Table 2.2.

Predicted concentrations of methanol in equilibrium with measured CO_2 and H_2 for two representative fluids from high temperature ultramafic-hosted hydrothermal systems

Vent Site	Temp. (°C)	Depth (m)	CO_2 (mM)	H_2 (mM)	*CH_3OH* (μM)*
Logatchev (14°45'N, MAR)	350	3000	10.1	12.0	*0.025*
Rainbow (36°14'N, MAR)	365	2300	16	16	*0.23*

Temperatures are measured exit temperatures

MAR = Mid-Atlantic Ridge, * = *predicted*

Data from Charlou *et al.* (2002)

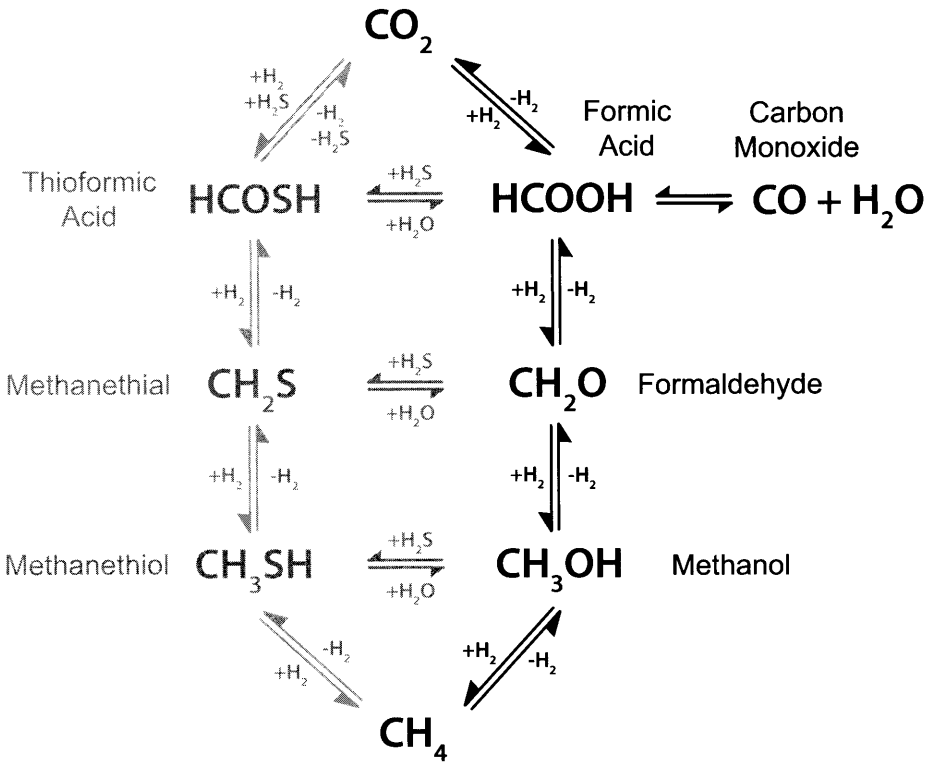

Figure 2.1. Model for the sequential aqueous reduction of CO_2 to CH_4 by H_2 *via* a series of intermediate oxidation state single carbon compounds. The pathway in black is that proposed by SEEWALD *et al.* (2006) for the system C-O-H (excluding carbon-carbon bonds), while that in grey represents an alternative possible reaction pathway with S-bearing intermediates in the analogous C-O-S-H system. Because of the addition of S, redox independent substitution reactions between S-bearing and oxygenated species with similar carbon oxidation states are also theoretically possible. Carbonyl sulfide (COS) and carbon disulfide (CS_2) are not included as they do not represent a change in carbon oxidation state from that of CO_2.

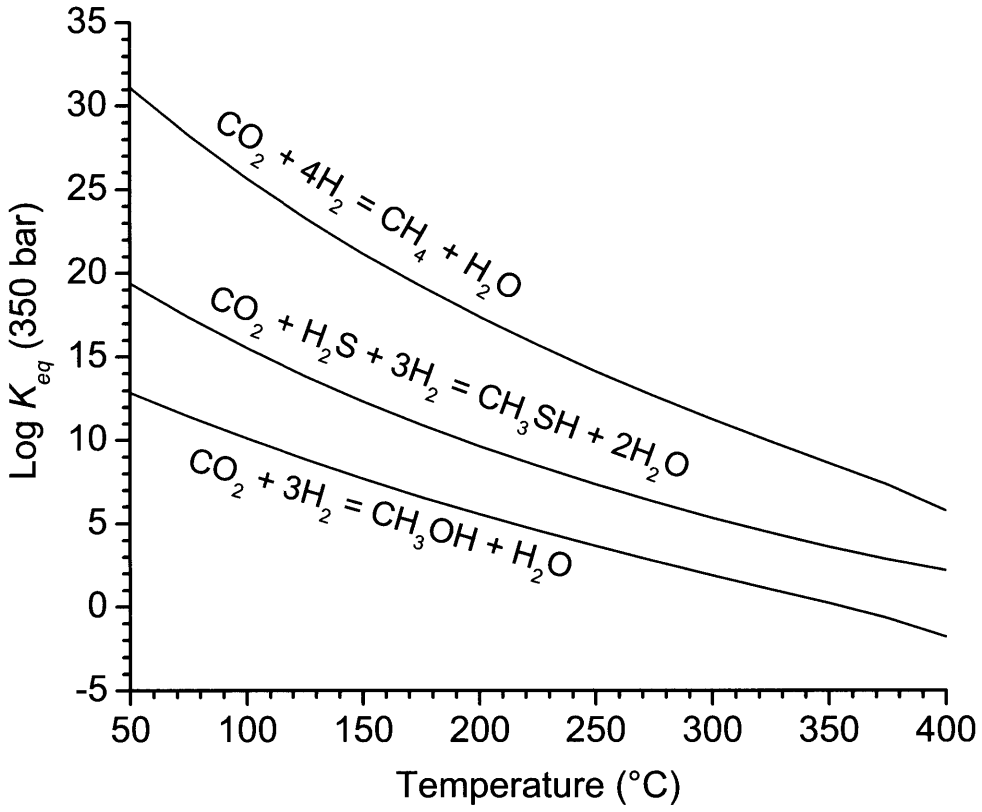

Figure 2.2. Temperature dependence of the equilibrium constants (K_{eq}) for CH_3OH, CH_3SH and CH_4 formation by overall CO_2 reduction. All reactions are favored to proceed from right to left as written at lower temperatures, with CH_4 formation exhibiting stronger temperature dependency than CH_3OH and CH_3SH formation. Requisite thermodynamic data for the construction of this figure were taken from the SUPCRT92 database (JOHNSON *et al.*, 1992) with additional data from AMEND and HELGESON (1997), SHOCK and HELGESON (1990) and SCHULTE and ROGERS (2004).

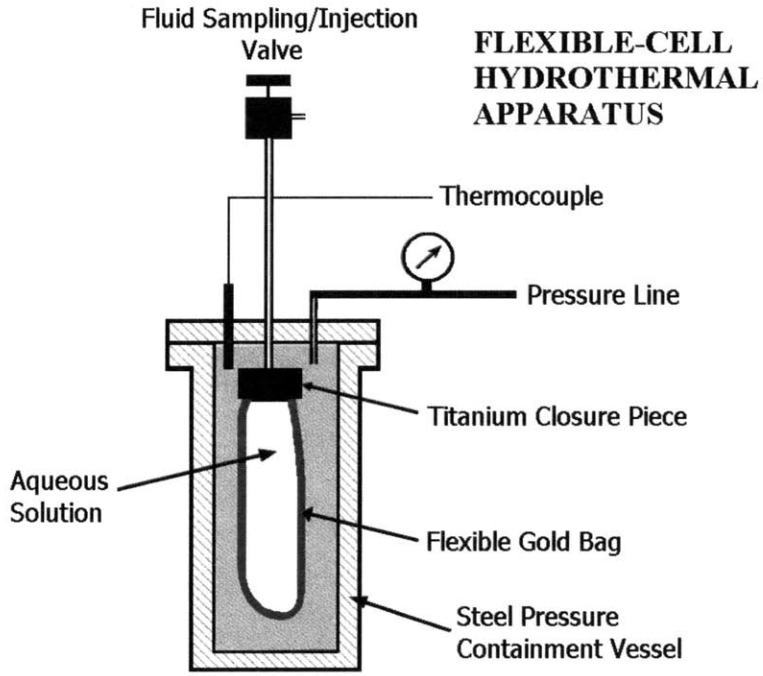

Figure 2.3. Schematic of the SEYFRIED (1987) design of flexible-cell hydrothermal reactor and pressure containment vessel. The entire apparatus is kept at desired conditions inside a temperature-controlled furnace. The *in situ* temperature is monitored using thermocouple temperature probes adjacent to the pressure vessel. Pressure is adjusted using a HPLC pump/bleed system attached to the pressure line. Adapted from MCCOLLOM and SEEWALD (2001).

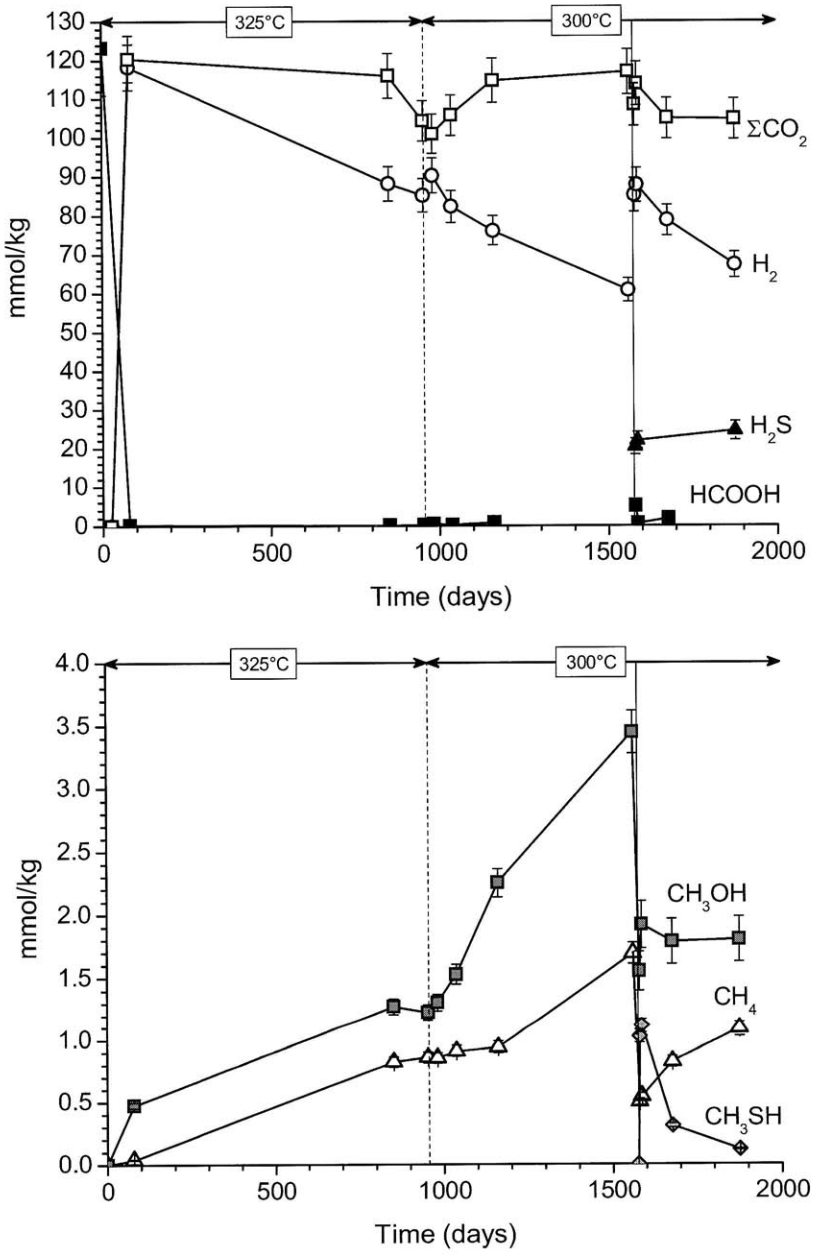

Figure 2.4. Measured concentrations of dissolved species as a function of time during the 325°C and 300°C phases of the experiment. The dashed vertical line at 956 days indicates the perturbation of equilibrium by rapid cooling of the pressure vessel. The solid vertical line at 1575 days represents injection of a solution of H_2S, $H^{13}COOH$ and NaCl. 2s analytical uncertainties are plotted for selected species. CH_4 accumulation in solution was initially slow but increased to a constant rate by the end of the 325°C phase.

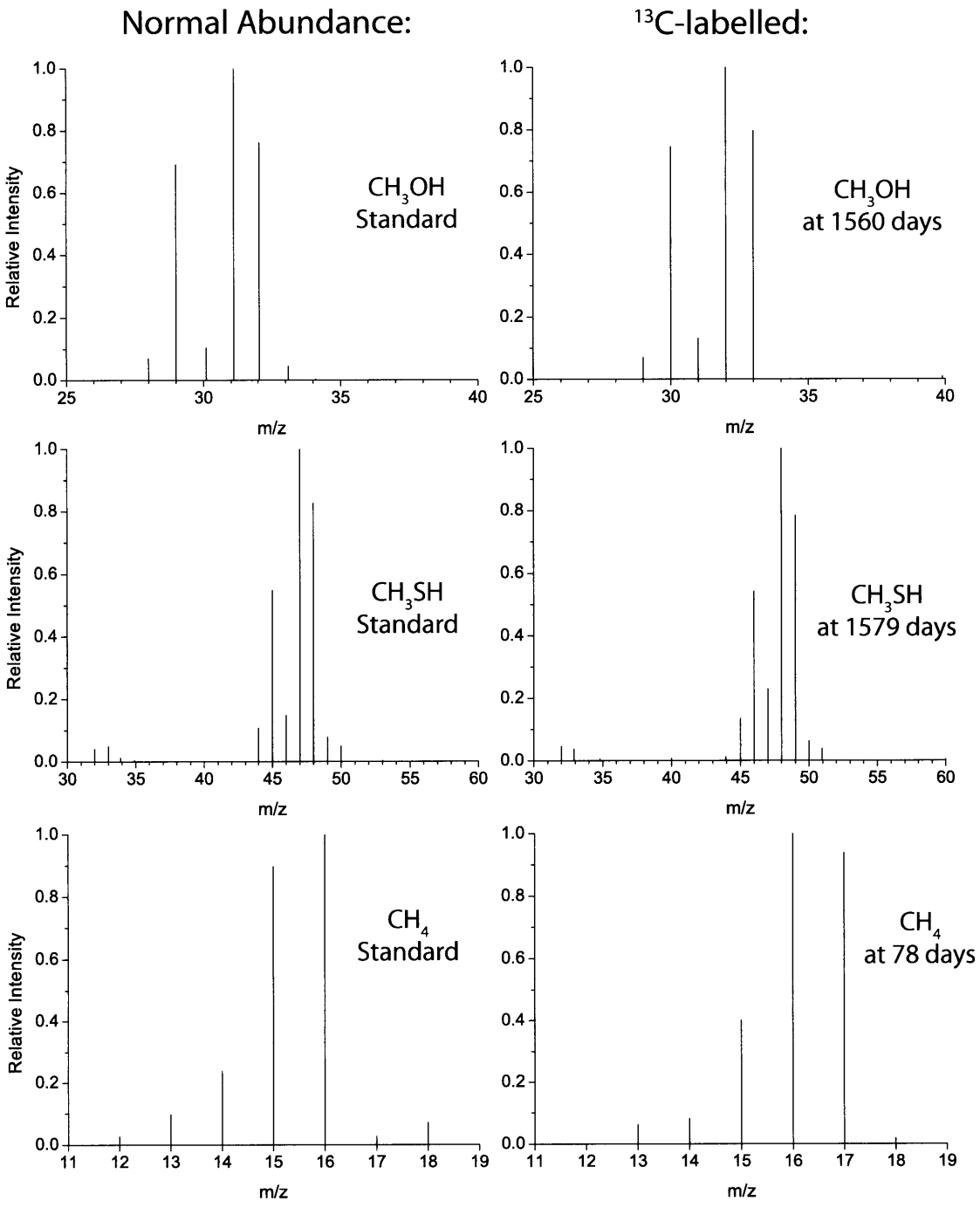

Figure 2.5. Mass spectrum of natural ^{13}C abundance CH_3OH, CH_3SH and CH_4 standards compared with ^{13}C-labeled forms in experimental samples. Extensive incorporation of the ^{13}C label into all three species, as evidenced by the m/z shift of 1, necessitates that production of both compounds must have occurred *via* the reduction of labeled HCOOH and/or CO_2.

Figure 2.6. Thermodynamic affinities for the production of CH_3OH ($A_{Methanol}$), CH_3SH (A_{CH3SH}) and CH_4 ($A_{Methane}$) by the overall reactions shown in Figure 2.2 during the experiment. The dashed vertical line at 956 days represents the drop in temperature from 325°C to 300°C and the solid vertical line at 1575 days represents injection of a solution containing $H^{13}COOH$, NaCl and H_2S. $A_{Methane}$ remained large throughout the experiment. In contrast, $A_{Methanol}$ appears to have achieved equilibrium ($A = 0 \pm 4$kJ/mol) on the timescales of all three stages. A_{CH3SH} (black triangles, right axis) increased gradually during the last stage of the experiment. Requisite thermodynamic data for the construction of this figure were taken from the SUPCRT92 database (JOHNSON *et al.*, 1992) with additional data from SHOCK and HELGESON (1990), AMEND and HELGESON (1997) and SHULTE and ROGERS (1990).

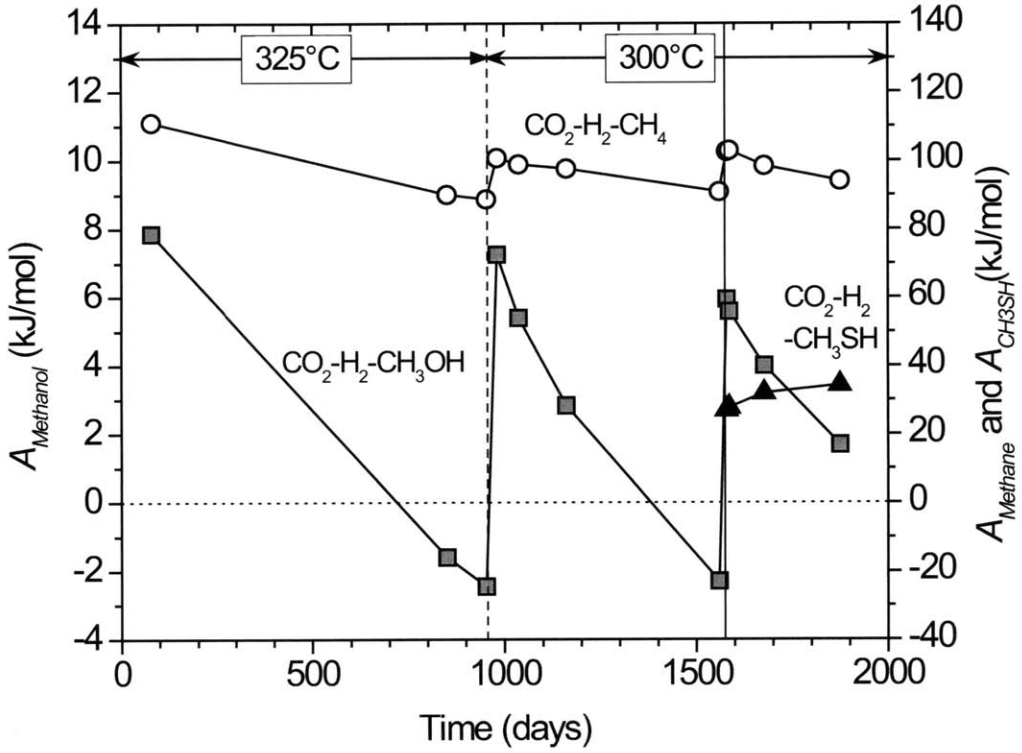
325°C
300°C
CO2-H2-CH4
CO2-H2-CH3OH
CO2-H2
-CH3SH
A Methanol (kJ/mol)
A Methane and A CH3SH (kJ/mol)
Time (days)
14
12
10
8
6
4
2
0
-2
-4
140
120
100
80
60
40
20
0
-20
-40
0
500
1000
1500
2000

Figure 2.6.

Figure 2.7. Equilibrium abundances of aqueous species as a function of pH at 35MPa for a model solution initially containing 120mmol/kg total CO_2 and H_2 at temperatures of **(A)**, 325°C, and **(B)**, 300°C, assuming metastable equilibrium between CO_2 (and the carbonate system), H_2, CO, HCOOH, $HCOO^-$, CH_2O and CH_3OH in the absence of CH_4 formation. Diagrams **(C)**, 325°C and **(D)**, 300°C, allows CO_2 to equilibrate with CH_4 in addition to the species above. The dashed vertical lines in **(A)** and **(B)** represent the calculated *in situ* fluid composition of the model solution at the specified temperature. For comparison, measured concentrations of CO_2 (*grey squares*), H_2 (*open circles*) and CH_3OH (*black circles*) at the end of Stage (1), **(A)**, and Stage (2), **(B)**, are shown. **(E)** represents the same reaction system and conditions as **(B)**, except for the addition of 20 mmol/kg total H_2S, and the introduction of CH_3SH formation by the overall reaction shown in Figure 2.2. The measured CH_3SH concentration at the end of Stage (3) is shown (*grey circle*). H_2S/HS^- dissociation is included, but dissociation of CH_3SH is not included due to a lack of thermodynamic data for CH_3S^-. Requisite thermodynamic data for the construction of this figure were taken from the SUPCRT92 database JOHNSON *et al.* (1992), with additional data from SHOCK (1995), SHOCK and HELGESON (1990) and SCHULTE and ROGERS (2004).

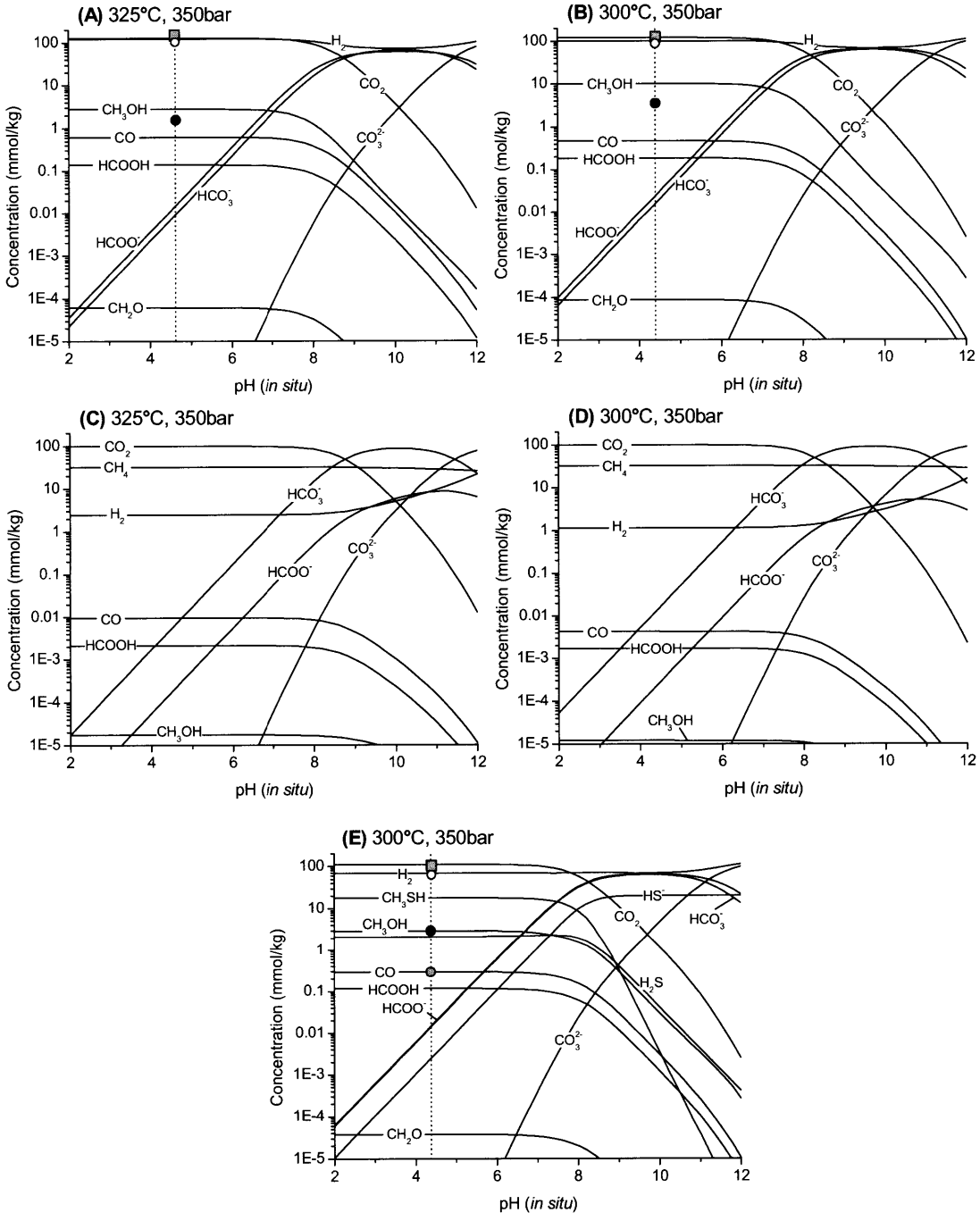
(A) 325°C, 350bar
(B) 300°C, 350bar
(C) 325°C, 350bar
(D) 300°C, 350bar
(E) 300°C, 350bar
Concentration (mmol/kg)
Concentration (mol/kg)
pH (in situ)
H2
CO2
CH3OH
CO
HCOOH
HCO3-
HCOO-
CO3 2-
CH2O
CH4
CH3SH
HS-
H2S

Figure 2.7

REFERENCES

ABRAJANO, T. A., STURCHIO, N. C., BOHLKE, J. K., LYON, G. L., POREDA, R. J., and STEVENS, C. M. (1988) Methane Hydrogen Gas Seeps, Zambales Ophiolite, Philippines - Deep Or Shallow Origin. *Chemical Geology* **71**(1-3), 211-222.

ABRAJANO, T. A., STURCHIO, N. C., KENNEDY, B. M., LYON, G. L., MUEHLENBACHS, K., and BOHLKE, J. K. (1990) Geochemistry Of Reduced Gas Related To Serpentinization Of The Zambales Ophiolite, Philippines. *Applied Geochemistry* **5**(5-6), 625-630.

ALLEN, D. E. and SEYFRIED, W. E. (2004) Serpentinization and heat generation: Constraints from Lost City and Rainbow hydrothermal systems. *Geochimica et Cosmochimica Acta* **68**(6), 1347-1354.

ANSLYN, E.V. and DOUGHERTY, D.A. (2005) *Modern Physical Organic Chemistry*. University Science.

AMEND, J. P. and HELGESON, H. C. (1997) Group additivity equations of state for calculating the standard molal thermodynamic properties of aqueous organic species at elevated temperatures and pressures. *Geochimica et Cosmochimica Acta* **61**(1), 11-46.

ANDERSON, G. (2005) *Thermodynamics of Natural Systems*. Cambridge University Press.

ANDERSON, R. B. (1984) *The Fischer-Tropsch Reaction*. Academic Press.

BAROSS, J. A. and HOFFMAN, S. E. (1985) Submarine Hydrothermal Vents And Associated Gradient Environments As Sites For The Origin And Evolution Of Life. *Origins Of Life And Evolution Of The Biosphere* **15**(4), 327-345.

BAROSS, J. A. and DEMING, J. W. (1995) Growth at high temperatures: Isolation and taxonomy, physiology and ecology. In: *The Microbiology of Deep-Sea Hydrothermal Vents*, (*Ed:* D. M. Karl), CRC Press. pp. 169-218.

BELL, J. L. S., PALMER, D. A., BARNES, H. L., and DRUMMOND, S. E. (1994) Thermal-Decomposition Of Acetate: III. Catalysis By Mineral Surfaces. *Geochimica et Cosmochimica Acta* **58**(19), 4155-4177.

BERNDT, M. E., ALLEN, D. E., and SEYFRIED, W. E. (1996) Reduction of CO_2 during serpentinization of olivine at 300 °C and 500 bar. *Geology* **24**(4), 351-354.

BRADLEY, A. S., HAYES, J. M., and SUMMONS, R. E. (2009) Extraordinary ^{13}C enrichment of diether lipids at the Lost City Hydrothermal Field indicates a carbon-limited ecosystem. *Geochimica et Cosmochimica Acta* **73**(1), 102-118.

CHARLOU, J. L. and DONVAL, J. P. (1993) Hydrothermal Methane Venting Between 12°N And 26°N Along The Mid-Atlantic Ridge. *Journal Of Geophysical Research-Solid Earth* **98**(B6), 9625-9642.

CHARLOU, J. L., DONVAL, J. P., FOUQUET, Y., JEAN-BAPTISTE, P., and HOLM, N. (2002) Geochemistry of high H_2 and CH_4 vent fluids issuing from ultramafic rocks at the Rainbow hydrothermal field (36°14'N, MAR). *Chemical Geology* **191**(4), 345-359.

CHARLOU, J. L., FOUQUET, Y., BOUGAULT, H., DONVAL, J. P., ETOUBLEAU, J., JEAN-BAPTISTE, P., DAPOIGNY, A., APPRIOU, P., and RONA, P. A. (1998) Intense CH_4 plumes generated by serpentinization of ultramafic rocks at the intersection of the 15°20'N fracture zone and the Mid-Atlantic Ridge. *Geochimica et Cosmochimica Acta* **62**(13), 2323-2333.

CORLISS, J. B., BAROSS, J. A., and HOFFMAN, S. E. (1981) An hypothesis concerning the relationship between submarine hot springs and the origin of life on Earth. *Oceanologica Acta* **4**(Supplement), 59-69.

COWEN, J. P., WEN, X. Y., and POPP, B. N. (2002) Methane in aging hydrothermal plumes. *Geochimica et Cosmochimica Acta* **66**(20), 3563-3571.

DE DUVE, C. (1991) *Blueprint for a Cell: The Nature and Origin of Life*. N. Patterson.

FISHER, A. T. (2003) Geophysical constraints on hydrothermal circulation: observations and models. In: *Dahlem Workshop Report: Energy and Mass Transfer in Marine Hydrothermal Systems*, (*Ed:* P. E. Halbach, V. Tunnicliffe, and J. R. Hein), **89**, Dahlem University Press. pp. 29-52.

FOUSTOUKOS, D. I. and SEYFRIED, W. E. (2004) Hydrocarbons in hydrothermal vent fluids: The role of chromium-bearing catalysts. *Science* **304**(5673), 1002-1005.

FOUSTOUKOS, D. I., SAVOV, I. P., and JANECKY, D. R. (2008) Chemical and isotopic constraints on water/rock interactions at the Lost City hydrothermal field, 30°N Mid-Atlantic Ridge. *Geochimica et Cosmochimica Acta* **72**(22), 5457-5474.

FU, Q., SHERWOOD LOLLAR, B., HORITA, J., LACRAMPE-COULOUME, G., and SEYFRIED, W. (2007) Abiotic formation of hydrocarbons under hydrothermal conditions: Constraints from chemical and isotopic data. *Geochimica et Cosmochimica Acta* **71**(8), 1982-1998.

GARRELS, R. M. and CHRIST, C. L. (1965) *Solutions, Minerals, and Equilibria*. Harper & Row.

GLEIN, C. R., ZOLOTOV, M. Y., and SHOCK, E. L. (2008) The oxidation state of hydrothermal systems on early Enceladus. *Icarus* **197**(1), 157-163.

GLEIN, C. R., DESCH, S. J., and SHOCK, E. L. (2009) The absence of endogenic methane on Titan and its implications for the origin of atmospheric nitrogen. *Icarus* **204**(2), 637-644.

HAYATSU, R. and ANDERS, E. (1981) Organic compounds in meteorites and their origins. *Topics in Current Chemistry* **99**, 1-37.

HEINEN, W. and LAUWERS, A. M. (1996) Organic sulfur compounds resulting from the interaction of iron sulfide, hydrogen sulfide and carbon dioxide in an anaerobic aqueous environment. *Origins Of Life And Evolution Of The Biosphere* **26**(2), 131-150.

HOLLOWAY, J. R. and O'DAY, P. A. (2000) Production of CO_2 and H_2 by diking-eruptive events at mid-ocean ridges: Implications for abiotic organic synthesis and global geochemical cycling. *International Geology Review* **42**(8), 673-683.

HORITA, J. and BERNDT, M. E. (1999) Abiogenic methane formation and isotopic fractionation under hydrothermal conditions. *Science* **285**(5430), 1055-1057.

HUBER, C. and WACHTERSHAUSER, G. (1997) Activated acetic acid by carbon fixation on (Fe,Ni)S under primordial conditions. *Science* **276**(5310), 245-247.

JOHNSON, J. W., OELKERS, E. H., and HELGESON, H. C. (1992) SUPCRT92 - A software package for calculating the standard molal thermodynamic properties of minerals, gases, aqueous species, and reactions from 1 to 5000 bar and 0 to 1000°C. *Computers & Geosciences* **18**(7), 899-947.

KADKO, D. and MOORE, W. (1988) Radiochemical Constraints On The Crustal Residence Time Of Submarine Hydrothermal Fluids - Endeavor Ridge. *Geochimica et Cosmochimica Acta* **52**(3), 659-668.

KADKO, D. and BUTTERFIELD, D. A. (1998) The relationship of hydrothermal fluid composition and crustal residence time to maturity of vent fields on the Juan de Fuca Ridge. *Geochimica et Cosmochimica Acta* **62**(9), 1521-1533.

KELLEY, D. S. and FRUH-GREEN, G. L. (1999) Abiogenic methane in deep-seated mid-ocean ridge environments: insights from stable isotope analyses. *Journal of Geophysical Research, [Solid Earth]* **104**(B5), 10439-10460.

KELLEY, D. S., BAROSS, J. A., and DELANEY, J. R. (2002) Volcanoes, fluids, and life at mid-ocean ridge spreading centers. *Annual Review Of Earth And Planetary Sciences* **30**, 385-491.

KELLEY, D. S., LILLEY, M. D., and FRÜH-GREEN, G. L. (2004) Volatiles in submarine environments: food for life. In: *The Subseafloor Biosphere at Mid-Ocean Ridges*, (*Ed:* W. S. D. Wilcock, E. F. DeLong, D. S. Kelley, J. A. Baross, and S. C. Cary), AGU Monograph, **144**, American Geophysical Union. pp. 167-189.

KELLEY, D. S., KARSON, J. A., BLACKMAN, D. K., FRUH-GREEN, G. L., BUTTERFIELD, D. A., LILLEY, M. D., OLSON, E. J., SCHRENK, M. O., ROE, K. K., LEBON, G. T. *et al.* (2001) An off-axis hydrothermal vent field near the Mid-Atlantic Ridge at 30°N. *Nature* **412**(6843), 145-149.

KLEIN, F., BACH, W., JONS, N., MCCOLLOM, T., MOSKOWITZ, B., and BERQUO, T. (2009) Iron partitioning and hydrogen generation during serpentinization of abyssal peridotites from 15 degrees N on the Mid-Atlantic Ridge. *Geochimica et Cosmochimica Acta* **73**(22), 6868-6893.

LEIF, R. N. and SIMONEIT, B. R. T. (2000) The role of alkenes produced during hydrous pyrolysis of a shale. *Organic Geochemistry* **31**(11), 1189-1208.

LIU, Z. T., ZHOU, J. L., and ZHANG, B. J. (1994) Poisoning Of Iron Catalyst By Cos In Syngas For Fischer-Tropsch Synthesis. *Journal Of Molecular Catalysis* **94**(2), 255-261.

LUTHER, G. W. (2004) Activation of Diatomic and Triatomic Molecules for the Synthesis of Organic Compounds: Metal Catalysis at the Subseafloor Biosphere. In: *The Subseafloor Biosphere at Mid-Ocean Ridges, AGU Monograph*, (*Ed:* W. S. D. Wilcock, E. F. DeLong, D. S. Kelley, J. A. Baross, and S. C. Cary), **144**, American Geophysical Union. pp. 191-198.

MARTIN, W. and RUSSELL, M. J. (2006) Review: On the origin of biochemistry at an alkaline hydrothermal vent. *Philosophical Transactions Of The Royal Society Of London Series*

B: Biological Sciences, Page FirstCite, DOI 10.1098/rstb.2006.1881, URL: http://dx.doi.org/10.1098/rstb.2006.1881.

MARTIN, W., BAROSS, J., KELLEY, D., and RUSSELL, M. J. (2008) Hydrothermal vents and the origin of life. *Nature Reviews Microbiology* **6**(11), 805-814.

MCCOLLOM, T. M. and SEEWALD, J. S. (2001) A reassessment of the potential for reduction of dissolved CO2 to hydrocarbons during serpentinization of olivine. *Geochimica et Cosmochimica Acta* **65**(21), 3769-3778.

MCCOLLOM, T. M. and SEEWALD, J. S. (2003a) Experimental constraints on the hydrothermal reactivity of organic acids and acid anions: I. Formic acid and formate. *Geochimica et Cosmochimica Acta* **67**(19), 3625-3644.

MCCOLLOM, T. M. and SEEWALD, J. S. (2003b) Experimental study of the hydrothermal reactivity of organic acids and acid anions: II. Acetic acid, acetate, and valeric acid. *Geochimica et Cosmochimica Acta* **67**(19), 3645-3664.

MCCOLLOM, T. M. and SEEWALD, J. S. (2006) Carbon isotope composition of organic compounds produced by abiotic synthesis under hydrothermal conditions. *Earth and Planetary Science Letters* **243**(1-2), 74-84.

MCCOLLOM, T. M. and SEEWALD, J. S. (2007) Abiotic synthesis of organic compounds in deep-sea hydrothermal environments. *Chemical Reviews* **107**, 382-401.

MCCOLLOM, T. M. and BACH, W. G. (2009) Thermodynamic constraints on hydrogen generation during serpentinization of ultramafic rocks. *Geochimica et Cosmochimica Acta* **73**(3), 856-875.

MILLER, S. L. and BADA, J. L. (1988) Submarine hot springs and the origin of life. *Nature* **334**, 609-611.

MUMMA, M. J., VILLANUEVA, G. L., NOVAK, R. E., HEWAGAMA, T., BONEV, B. P., DISANTI, M. A., MANDELL, A. M., and SMITH, M. D. (2009) Strong Release of Methane on Mars in Northern Summer 2003. *Science* **323**(5917), 1041-1045.

PROSKUROWSKI, G., LILLEY, M. D., SEEWALD, J. S., FRUH-GREEN, G. L., OLSON, E. J., LUPTON, J. E., SYLVA, S. P., and KELLEY, D. S. (2008) Abiogenic hydrocarbon production at Lost City hydrothermal field. *Science* **319**(5863), 604-607.

RHODES, C., RIDDEL, S. A., WEST, J., WILLIAMS, B. P., and HUTCHINGS, G. J. (2000) The low-temperature hydrolysis of carbonyl sulfide and carbon disulfide: a review. *Catalysis Today* **59**(3-4), 443-464.

RUSHDI, A. I. and SIMONEIT, B. R. (2001) Lipid formation by aqueous Fischer-Tropsch-type synthesis over a temperature range of 100 to 400°C. *Origins of life and evolution of the biosphere* **31**(1-2), 103-118.

RUSSELL, M. J. and HALL, A. J. (2006) The onset and early evolution of life. In: *Evolution of Early Earth's Atmosphere, Hydrosphere, and Biosphere - Constraints from Ore Deposits: Geological Society of America Memoir 198*, (*Ed:* S. E. Kesler and H. Ohmoto), Geological Society of America. pp. 1-32.

SCHULTE, M. and SHOCK, E. (1995) Thermodynamics Of Strecker Synthesis In Hydrothermal Systems. *Origins Of Life And Evolution Of The Biosphere* **25**(1-3), 161-173.

SCHULTE, M. D. and ROGERS, K. L. (2004) Thiols in hydrothermal solution: standard partial molal properties and their role in the organic geochemistry of hydrothermal environments. *Geochimica et Cosmochimica Acta* **68**(5), 1087-1097.

SEEWALD, J. S. (2001) Aqueous geochemistry of low molecular weight hydrocarbons at elevated temperatures and pressures: Constraints from mineral buffered laboratory experiments. *Geochimica et Cosmochimica Acta* **65**(10), 1641-1664.

SEEWALD, J. S., ZOLOTOV, M. Y., and MCCOLLOM, T. (2006) Experimental investigation of single carbon compounds under hydrothermal conditions. *Geochimica et Cosmochimica Acta* **70**(2), 446-460.

SEYFRIED, W., D.R. JANECKY AND M.E. BERNDT (1987) Rocking autoclaves for hydrothermal experiments II: The flexible reaction-cell system. In: *Hydrothermal Experimental Techniques*, (*Ed:* G. C. Ulmer and H. L. Barnes), Wiley. pp. 216-239.

SHERWOOD, B., FRITZ, P., FRAPE, S. K., MACKO, S. A., WEISE, S. M., and WELHAN, J. A. (1988) Methane Occurrences In The Canadian Shield. *Chemical Geology* **71**(1-3), 223-236.

SHOCK, E. L. (1992) Chemical Environments Of Submarine Hydrothermal Systems. *Origins Of Life And Evolution Of The Biosphere* **22**(1-4), 67-107.

SHOCK, E. L. (1995) Organic-Acids In Hydrothermal Solutions - Standard Molal Thermodynamic Properties Of Carboxylic-Acids And Estimates Of Dissociation-Constants At High-Temperatures And Pressures. *American Journal Of Science* **295**(5), 496-580.

SHOCK, E. L. and HELGESON, H. C. (1990) Calculation of the thermodynamic and transport properties of aqueous species at high pressures and temperatures: Standard partial molal properties of organic species. *Geochimica et Cosmochimica Acta* **54**(4), 915-945.

SHOCK, E. L. and SCHULTE, M. D. (1998) Organic synthesis during fluid mixing in hydrothermal systems. *Journal Of Geophysical Research-Planets* **103**(E12), 28513-28527.

VOGLESONGER, K. M., HOLLOWAY, J. R., DUNN, E. E., DALLA-BETTA, P. J., and O'DAY, P. A. (2001) Experimental abiotic synthesis of methanol in seafloor hydrothermal systems during diking events. *Chemical Geology* **180**(1-4), 129-139.

VON DAMM, K. L. (1995) Controls on the chemistry and temporal variability of seafloor hydrothermal systems. In: *Seafloor Hydrothermal Systems: Physical, Chemical, Biological, and Geological Interactions*, (*Ed:* S. E. Humphris, R. A. Zierenberg, L. S.

Mullineaux, and R. E. Thomson), AGU Monograph, **91**, American Geophysical Union. pp. 222-247.

WELHAN, J. A. (1988) Origins of methane in hydrothermal systems. *Chemical Geology* **71**(1-3), 183-198.

CHAPTER 3

Insights into the origin of methanethiol in seafloor hydrothermal fluids

ABSTRACT

Abiotic (non-biological) synthesis of methanethiol (CH_3SH) in hydrothermal solutions is considered an important first step in the emergence of primitive chemoautotrophism as the earliest form of life. However, little is known about the origin and distribution of CH_3SH in seafloor hydrothermal fluids. This chapter reports the first known measurements of CH_3SH concentrations in 'black smoker' fluids collected from ultramafic-, basalt- and sediment-hosted settings. Concentrations in relatively oxidizing (H_2-poor) basalt-hosted fluids (TAG, Lucky Strike, 9°50'N East Pacific Rise) are comparable to those in more reducing ultramafic systems (Lost City, Rainbow) despite differences in dissolved H_2 concentrations of several orders of magnitude. When considered in a thermodynamic context, this distribution is therefore inconsistent with formation of CH_3SH by abiotic CO_2 reduction. CH_3SH abundances in Guaymas Basin vent fluids indicate that thermogenic sources (pyrolysis of sedimentary organic matter) are possible, while enrichments in low temperature fluids at Rainbow and 9°50'N suggest that fluid-microbe interactions may be a source to sediment-starved systems. In the absence of microbial/thermogenic sources, the only abiotic pathway that could account for CH_3SH distributions in high temperature black smoker fluids is partial oxidation of CH_4 with H_2S. The latter would represent a fundamental paradigm shift in our understanding of abiotic synthesis in hydrothermal systems, which is typically viewed as a solely reductive process.

1. INTRODUCTION

Since their discovery, seafloor hydrothermal fluids have been proposed as a source of abiotic organic compounds necessary for early life to emerge on a prebiotic (Hadean-Archaean) Earth (CORLISS *et al.*, 1981; BAROSS and HOFFMAN, 1985; HOLM, 1992; MARTIN *et al.*, 2008). Hypotheses which postulate that the earliest form of life consisted of primitive chemoautotrophism in reducing hydrothermal settings (DE DUVE, 1991; HUBER and WACHTERSHAUSER, 1997; MARTIN and RUSSELL, 2006) all invoke the existence of a geological supply of simple thiol molecules in the prebiotic environment as a precursor for the synthesis of thioester (R-CO-S-R'). The latter is the key functional group of the Acetyl-CoA enzyme central to the autotrophic metabolisms of primitive methanogens and acetogens (FUCHS, 1989). Conversion of CO and CH_3SH to methyl thioacetate (CH_3-CO-S-CH_3 – the simplest thioester) has been demonstrated in the presence of Fe and Ni sulfide minerals and water (HUBER and WACHTERSHAUSER, 1997). The requisite supply of CH_3SH to the prebiotic environment has traditionally been assumed to be abiotic reduction of CO_2 (typically the dominant form of carbon in hydrothermal solutions) by H_2 in the presence of reduced sulfur (HUBER and WACHTERSHAUSER, 1997; MARTIN and RUSSELL, 2006) – as suggested by thermodynamic considerations (SCHULTE and ROGERS, 2004) and experimental evidence (HEINEN and LAUWERS, 1996; HUBER and WACHTERSHAUSER, 1997). However, the abundance of CH_3SH in modern vent fluids has hitherto not been characterized and its origin is therefore poorly constrained. Investigations of abiotic organic compounds in hydrothermal fluids have to date focused on the origin of linear hydrocarbons and oxygenated organic compounds, such as those found at Rainbow and Lost City (HOLM and CHARLOU, 2001; CHARLOU *et al.*, 2002; MCCOLLOM and SEEWALD, 2007; PROSKUROWSKI *et al.*, 2008; KONN *et al.*, 2009). The fundamental assumption regarding the origin of CH_3SH and therefore chemoautotrophic life therefore requires testing.

In 2008 a survey of CH_3SH abundance in vent fluids from several mid-ocean ridge environments was conducted along with accompanying temperature, dissolved CO_2, CO, CH_4, H_2, and H_2S measurements in order to elucidate geochemical processes that could produce CH_3SH under hydrothermal conditions. Fluids were collected from three bare-rock hydrothermal systems hosted in basalt, including Lucky Strike (LANGMUIR *et al.*, 1997; VON DAMM *et al.*, 1998) and TAG (THOMPSON *et al.*, 1985; TIVEY *et al.*, 1995) on the Mid-Atlantic Ridge (MAR) and 9°50'N (HAYMON *et al.*, 1993; PROSKUROWSKI *et al.*, 2008) on the East Pacific Rise. Two bare-rock systems hosted in peridotite were also sampled, including Rainbow (CHARLOU *et al.*, 2002) and Lost City (KELLEY *et al.*, 2001; PROSKUROWSKI *et al.*, 2008) on the Mid-Atlantic Ridge. To assess the influence of hydrothermal alteration of sedimentary organic matter on CH_3SH formation, additional fluid samples were taken at the sediment-covered Guaymas Basin hydrothermal system (WELHAN and LUPTON, 1987).

2. METHODS

Fluid samples were collected using isobaric gas-tight samplers (SEEWALD *et al.*, 2002) during a July-August 2008 cruise to the Mid-Atlantic Ridge with ROV *Jason II* and an October-November 2008 cruise with DSV *Alvin* to the Guaymas Basin and EPR. In most cases, high temperature fluids were sampled, but in the case of the 9°50'N site, sets of paired high temperature and associated nearby low temperature vents were targeted for comparison. Maximum vent temperatures were measured in real-time during sampling. Dissolved CH_3SH, H_2, H_2S and CO concentrations were determined at sea within hours of recovery. CH_3SH was analyzed by purge and trap gas chromatography (GC) with flame ionization detection (FID). CH_3SH was quantitatively sparged from acidified fluid aliquots with helium, cryo-focused at -78°C on *n*-octane-coated silica, then thermally desorbed at 145°C onto a Carbograph 1SC packed column. GC analysis was conducted isothermally at 40°C. Due to potentially surface-reactive nature of gaseous CH_3SH (SIMO, 1998; WARDENCKI, 1998), de-activated glass and PTFE-coated tubing were used wherever possible in the purge and trap method. Errors of reproducibility for measured CH_3SH were variable (mean 2s error ±16%, range ±0.4% to ±68%) with the greatest errors associated with lowest concentrations. CH_4, H_2 and CO were analyzed by GC as per SEEWALD *et al.* (2006). H_2S was determined either gravimetrically onshore after precipitation as Ag_2S at sea or potentiometrically at sea by Ag/AgCl electrode. pH(25°C) was also measured potentiometrically by Ag/AgCl electrode. Dissolved inorganic carbon (ΣCO_2), C_{2+} hydrocarbon and $\delta^{13}C_{CH4}$ fluid aliquots were stored in evacuated glass serum vials (with butyl rubber stoppers) and were analyzed after acidification by injecting volumes of headspace gas directly onto a Porapak Q packed column with TCD and FID. ΣCO_2 data were corrected for partitioning between headspace-fluid phases. Mg was determined by ion chromatography. Analytical uncertainties (2s) are ±10% for measured H_2S, CO, H_2, C_{2+} hydrocarbon concentrations and ±5%

for Mg, ΣCO_2, and CH_4. $\delta^{13}C_{CH4}$ values were determined on selected samples by isotope ratio monitoring-gas chromatography mass spectrometry using a Finnegan DeltaPlus XL mass spectrometer interfaced to an Agilent 6890 gas chromatograph through a GCIII interface (combustion furnace held at 950°C). The pooled standard deviation (2s) of all $\delta^{13}C_{CH4}$ values was 0.3‰.

Because hydrothermal fluids are conventionally assumed to be devoid of Mg due to water-rock reaction at elevated temperatures (BISCHOFF and DICKSON, 1975; MOTTL and HOLLAND, 1978; SEYFRIED and BISCHOFF, 1981), endmember compositions are calculated by extrapolating measured concentrations of individual species in multiple fluid samples from a given orifice to zero Mg concentration using a linear least squares regression weighted to pass through ambient bottom seawater concentrations (VON DAMM *et al.*, 1985). For fluids that have undergone extensive mixing, such as the low temperature fluids at 9°50'N, endmember compositions may not reflect a composition existing in the hydrothermal system if the species in question is added or removed from solution during the mixing process. However, zero Mg endmembers are calculated here to elucidate such non-conservative behavior during mixing of low Mg, high temperature fluids with seawater.

3. RESULTS

Measured concentrations of CH_3SH, H_2S, ΣCO_2, CO, CH_4 and associated Mg concentrations are shown in Table 3.1 for all collected samples and corresponding endmember compositions and lowest measured pH(25°C) values are shown in Table 3.2. This survey of three hydrothermal settings (basaltic, ultramafic and sediment-covered) reveals several key features in the distribution of CH_3SH (Table 3.2). The range of endmember concentrations was greatest in fluids from the Guaymas Basin hydrothermal site (8.1nmol/L to $17x10^3$nmol/L). Concentrations were lowest in fluids at Lost City (1.4–1.9nmol/L). A key observation is that for many moderate to high temperature (>150°C) vent fluids in hydrothermal systems devoid of sediment, endmember CH_3SH concentrations are reasonably uniform despite large changes in aqueous H_2 concentrations (Table 3.2). The range of endmember concentrations at Lucky Strike and TAG (5.6–23.4 nmol/L), as well as that of >150°C fluids at 9°50'N (4.0 – 11 nmol/L), overlaps that of the more H_2-rich fluids at Rainbow (7.4 to $2.9x10^2$ nmol/L). Within the Rainbow fluids, higher endmember concentrations of CH_3SH (55 – $2.9x10^2$ nmol/L) are associated with the lower temperature fluids Ecurie and Mussel Beach, while the high temperature (350 – 367°C) fluids have a much narrower range (7.4 – 12 nmol/L).

4. DISCUSSION

Carbon dioxide, which is predominantly derived from magmatic degassing, represents the dominant form of oxidized C in many hydrothermal fluids (VON DAMM, 1995; KELLEY *et al.*, 2002). Because there are strong thermodynamic drives for CO_2 reduction to organic compounds at subsurface conditions encountered by circulating hydrothermal fluids (SHOCK, 1990, 1992; SHOCK and SCHULTE, 1998), it is generally considered the main C substrate for abiotic organic synthesis and is the assumed substrate for CH_3SH formation in models for the origin of chemoautotrophism (HUBER and WACHTERSHAUSER, 1997; MARTIN and RUSSELL, 2006; RUSSELL and HALL, 2006; MARTIN *et al.*, 2008). Reduction of CO_2 to CH_3SH can be summarized by the following overall reaction:

$$CO_2 + H_2S + 3H_2 \leftrightarrow CH_3SH + 2H_2O \qquad (1)$$

The stoichiometry of reaction (1) indicates that at a given temperature and pressure, increases in dissolved H_2 should result in disproportionately large increases in CH_3SH at equilibrium. As shown in Figure 3.1, CH_3SH stability also increases dramatically with decreasing temperature. To compare observed concentrations with reaction (1) predictions, the equilibrium concentration of CH_3SH according to reaction (1) is calculated at the temperature and pressure of all vent fluids sampled using thermodynamic data at conditions (SCHULTE and ROGERS, 2004) and endmember ΣCO_2, H_2S and H_2 abundances as mass balance constraints. These calculations assume metastable equilibrium between ΣCO_2, H_2 and the reduced species CO, HCOOH (and $HCOO^-$), CH_2O, CH_3OH in accordance with the experimental observations of SEEWALD *et al.* (2006) and those presented in CHAPTER 2, in addition to equilibrium between ΣCO_2, H_2, H_2S and CH_3SH. ΣCO_2 speciation H_2S dissociation are also considered. Activity coefficients of unity were assumed for all aqueous species in the absence of constraints on non-ideal behavior (GARRELS and CHRIST, 1965; ANDERSON, 2005). pH (25°) values were used for all calculations. Most *in*

situ pH values for high temperature fluids are up to 1 pH unit higher (GERMAN and VON DAMM, 2003). However, this has no effect on predicted CH_3SH abundance for any of the fluids presented here. Equilibrium between ΣCO_2, H_2 and CH_4 is suppressed based on the sluggish equilibration timescale of this reaction (see CHAPTER 2).

The most striking observation is that the abundance of CH_3SH does not vary substantially between the systems sampled relative to the distribution predicted by reaction (1), (Figure 3.2(A)). When fluids with similarly high temperatures (350–370°C) are compared at TAG and Rainbow, reaction (1) predicts a range of concentrations of $\sim 10^7$ mol/L yet observed CH_3SH concentrations vary by less than an order of magnitude. Furthermore, measured concentrations at TAG and Lucky Strike, where H_2 concentrations are extremely low relative to Rainbow, are both far in excess of equilibrium values predicted for reaction (1) while the reverse is true in fluids with higher H_2 concentrations (Rainbow and 9°50N) and measured concentrations are below predicted values (Figure 3.2(A)). It is difficult to assess the significance of measured concentrations at Lost City given the uncertainties involved in predicting CH_3SH abundances for reaction (1) at the high pH of Lost City fluids (10.5–10.6 at 25°C and 1 atm). Concentrations of ΣCO_2 are exceedingly low and consequently associated with large uncertainties. Furthermore, thermodynamic data for deprotonated methanethiol (CH_3S^-) which has a pK_a of 10.5 (at 25°C, 1 atm) are lacking at conditions relevant to Lost City. Acidity constants for many organic acids gradually increase with increasing temperature (SHOCK, 1992), but below 100°C the pK_a of CH_3SH may not increase to an extent to warrant neglecting dissociation effects. However, though predictions may not be possible, concentrations were lowest in the Lost City fluids of all sampled. While our predicted values refer to vent *T-P* conditions at the seafloor, it is unlikely that the dichotomy in CH_3SH abundance between H_2-rich and H_2-poor fluids reflects equilibrium elsewhere within these hydrothermal systems (*i.e.* during recharge or reaction zone *T-P* conditions). By calculating

the reaction quotient for the mass action according to reaction (1), the temperature dependence of the equilibrium constant for reaction (1) can be used to calculate apparent temperatures of equilibration according to the reaction. Apparent temperatures of equilibration according to reaction (1) are 436–456°C at Rainbow, slightly greater than expected reaction zone temperatures (ALLEN and SEYFRIED, 2004), but a much lower temperature of equilibration (222°C) is apparent at TAG, where reaction zone conditions are in excess of 363°C. Apparent temperatures of equilibration are also low at Lucky Strike (222–242°C) relative to measured temperatures (270–308°C). At 9°50'N, measured temperatures for high temperature fluids (221–363°C) overlap the range of apparent temperatures of equilibration (236–361°C). These apparent temperatures are inconsistent with equilibrium according to reaction (1) occurring at reaction zone conditions in all these systems. Therefore, this strongly suggests that equilibrium according to reaction (1) is kinetically inhibited in the majority of hydrothermal fluids. This is consistent with the results of CHAPTER 2, which suggest that equilibrium between CO_2, H_2 and H_2S is kinetically inhibited in the absence of mineral catalysts. This may be a result of the complexities of multiple reduction steps and the inherent requirements of CO_2, H_2 and H_2S reaction. Alternatively, if equilibrium is indeed occurring at depth within the Rainbow system alone, it may be the result of mineral catalysis by Fe-Ni phases unique to ultramafic rock (KLEIN and BACH, 2009). It has been suggested that reduction of CO is much more favorable for CH_3SH synthesis relative to CO_2, but in all vent fluids from bare rock hydrothermal systems where CO abundance was determined, chemical affinities for CO equilibrium with CO_2 and H_2 are near zero (0.9–5.8kJ/mol). This is consistent with previous experimental observations of rapid CO_2-H_2-CO equilibrium under hydrothermal conditions (SEEWALD *et al.*, 2006).

Sluggish kinetics for reaction (1) alone cannot explain the excess CH_3SH relative to equilibrium at TAG and Lucky Strike, hence other sources of CH_3SH must be examined. CH_4 is

the other dominant form of carbon in hydrothermal fluids and in many low H_2 fluids there are net thermodynamic drives for CH_4 oxidation to CO_2 (MCCOLLOM and SEEWALD, 2007). A possible consequence of this may be that partial oxidation of CH_4 occurs by reaction with H_2S to form CH_3SH:

$$CH_4 + H_2S \leftrightarrow CH_3SH + H_2 \qquad (2)$$

Though reaction (2) has not been demonstrated experimentally, formation of alkyl thiols by hydrocarbon sulfidation is thought to occur in petroleum deposits (KREIN, 1993; ZHANG *et al.*, 2008). Predicted CH_3SH concentrations can be calculated according to reaction (2) using measured CH_4, H_2S and H_2 concentrations and assuming activity coefficients of 1 as for reaction (1) predictions. Based on these calculations, CH_3SH is in apparent equilibrium with CH_4 in the high temperature Rainbow fluids and in many low H_2 fluids (Lucky Strike and TAG) it is closer to equilibrium with CH_4 than CO_2 (Figure 3.2(B)). The temperature and redox dependency of reaction (2) is directly opposite to reaction (1) and would be favored under higher temperature, more oxidizing conditions (Figure 3.1).

CH_3SH was most abundant (1.5–1.7μmol/L) at Guaymas Basin (Table 3.1) where hydrothermal alteration of immature organic-rich sediments (composed primarily of hemipelagic diatomaceous ooze) contributes several classes of thermogenic organic compounds to vent fluids (WELHAN and LUPTON, 1987; SIMONEIT *et al.*, 1988). While it is possible that high CO concentrations in some Guaymas fluids (above that of equilibrium with CO_2) could drive CH_3SH production (SCHULTE and ROGERS, 2004), it is more likely that CH_3SH is derived either from incipient alteration of sedimentary organic matter or decomposition of the resulting products. Vents with μmol/L levels of CH_3SH (Theme Park, Cathedral Hill and Sulfide Spires) are characterized by lower temperatures and than vents with lower (nmol/L) CH_3SH (Rebecca's Roost and Toadstool). C_1/C_2+C_3 *n*-alkane ratios (SEEWALD, unpubl. data) for the latter (124–

132) are much higher than those of the former (55–60) and the association of high CH_3SH concentrations with C_{2+} hydrocarbons between these two groups of fluids suggests that similar processes are controlling both hydrocarbon and CH_3SH concentrations. Lower C_1/C_2+C_3 ratios are indicative of lower thermal maturities, as dissolved C_{2+} hydrocarbons ultimately decompose to CH_4 with increasing thermal stress (CRUSE and SEEWALD, 2006). Alkyl thiols in petroleum reservoirs are also typically associated with lower thermal maturities (KREIN, 1993) but may form by hydrocarbon reactions with H_2S during hydrous pyrolysis (ZHANG *et al.*, 2008).

The compositions of several moderate to low temperature fluids from bare-rock systems suggest that thermogenic or biogenic sources of CH_3SH to vent fluids are also possible. Two moderate temperature (180–191°C) fluids at Rainbow (Ecurie and Mussel Beach) are substantially enriched in CH_3SH relative to high temperature (>350°C) fluids there (Table 3.1). The temperatures and compositions of the latter at Rainbow are relatively uniform, reflecting a common source fluid (CHARLOU *et al.*, 2002). The moderate temperature fluids, however, have similar endmember ΣCO_2, H_2 and H_2S concentrations to the higher temperature fluids, which strongly suggest they formed by conductive cooling of the latter. Of the moderate temperature fluids, Ecurie vent has a lower $\delta^{13}C_{CH4}$ value (-19.9‰) relative to the uniform high temperature fluids (-17.1 to -17.9‰), indicating net addition of ^{13}C-depleted CH_4. This could reflect addition of small quantities of CH_4 of a thermogenic origin (MCCOLLOM and SEEWALD, 2007), and possible sources include thermal decomposition of vent biomass material or dissolved organic carbon (DOC). The former has yet to be conclusively demonstrated in hydrothermal settings, but DOC depletions relative to seawater in some high temperature vent fluids suggest pyrolysis of the latter may occur (LANG *et al.*, 2006). It is possible that thermogenic processes may be contributing CH_3SH to high temperature fluids in bare rock systems, and the apparent equilibration of reaction (2) in some instances merely reflects approach from the direction of

excess CH_3SH. Further work is needed to constrain the possible contributions from pyrolysis of biomass material.

At 9°50'N, two sets of paired high temperature fluids and nearby diffuse flow fluids (Table 3.2) show clear CH_3SH enrichments associated with CH_4 enrichments in the latter relative to their parent fluids. Crab Spa vent (23°C) was observed to be venting 5.7–6.1 nmol/L measured CH_3SH concentrations over the course of 3 days. While biomass decomposition is possible, active microbial methane production and consumption has been inferred (PROSKUROWSKI *et al.*, 2008) in diffuse fluids at 9°50'N and these enrichments could reflect microbial activity. CH_3SH has been implicated as an intermediate in anaerobic methane oxidation (MORAN *et al.*, 2008), evidence for which has been detected at Guaymas Basin (TESKE *et al.*, 2002).

The results of this survey challenge the validity of the assumed formation pathway for CH_3SH in seafloor hydrothermal solutions. Current models for the origin of chemoautotrophic life in ultramafic hydrothermal settings analogous to Lost City invoke formation of CH_3SH by CO_2 or CO reduction at temperatures in the vicinity of 100°C (MARTIN and RUSSELL, 2006). Given the apparent disequilibrium between CO_2, H_2, H_2S and CH_3SH evident in most high temperature fluids (>150°C) from bare-rock hydrothermal systems, and the possibility of CH_3SH formation from CH_4 (which is more energetically favorable under higher temperature, more oxidizing conditions), such a source is not supported by the data presented here. In addition, yields of thioester reported in the experiments of HUBER and WACHTERSHAUSER (1997) were extremely low – less than 10% of CH_3SH was converted to methyl thioacetate on the timescale of the experiments. Given the low (nmol/L) concentrations of CH_3SH present in vent fluids compared to these experiments (~100μmol/L), this suggests that thioester yields in natural hydrothermal fluids may be much lower than previously assumed.

4. CONCLUSIONS

A survey of CH_3SH abundance in seafloor hydrothermal fluids reveals that in bare rock hydrothermal settings the abundance of CH_3SH does not vary substantially with redox conditions, as would be expected for a species purported to be derived from abiotic CO_2 reduction. Enrichments in vent fluids from the sedimented Guaymas Basin site and low temperature fluids at 9°50'N East Pacific Rise suggest that thermogenic and biogenic sources to vent fluids are possible. Further speculation on the origin of CH_3SH in vent fluids and the exact nature of microbial or thermogenic processes contributing to dissolved abundances is limited by a paucity of observations of these processes. However, our results do provide compelling evidence that CO_2 reduction to CH_3SH is kinetically inhibited under hydrothermal conditions despite favorable thermodynamic conditions in ultramafic systems. If CH_3SH formation in present day vent fluids is governed either by thermogenic processes or by high temperature CH_4 oxidation, this implies that the feasibility of sustained abiotic thioester synthesis from CH_3SH in low temperature reducing hydrothermal settings may be more limited than previously assumed. The possibility that reworking or pyrolysis of preexisting organic matter, either biomass or seawater-derived DOC, could contribute organic compounds of prebiotic relevance to vent fluids requires much further investigation.

ACKNOWLEDGEMENTS

I would like to thank N.J. Pester, M. Rough and W.E. Seyfried for providing Mg, H_2S and pH data for the Mid-Atlantic Ridge sites. Thanks also to Peter Saccocia and Marcel van der Meer for assistance with H_2 and CO analysis during the Mid-Atlantic Ridge expedition. Field sampling was made possible by NSF grants MCB-0702677 (Seewald and Sievert), OCE-0549829 (Seewald).

Table 3.1. Measured concentrations of dissolved species

Site (depth), Vent	Sample	Mg (mmol/kg)	CH_3SH (nmol/L)	CH_3SH error 2s (n)	H_2S (mmol/L)	H_2 (mmol/L)	ΣCO_2 (mmol/kg)	CO (µmol/L)	CH_4 (mmol/L)
Rainbow (2300m)									
PP27/Exo2	J2-353-IGT3	6.9	6.7	nd	2.73	10.7	19.6	4.5	1.66
	J2-353-CGT-RED	7.0	6.5	nd	2.97	10.6	17.8	4.4	1.65
Stylo1	J2-354-IGT5	4.2	7.6	0.8 (4)	1.89	15.0	23.4	6.6	1.87
	J2-354-CGT-BLUE	3.9	6.1	0.9 (3)	2.33	14.8	22.3	6.5	1.84
CMSt.P&P	J2-354-IGT3	3.5	7.2	1.0 (3)	1.85	14.8	20.6	6.9	1.85
	J2-354-CGT-YELLOW	49.5	1.1	0.1 (3)	0.09	1.5	na	0.4	0.18
X11	J2-355-IGT4	4.0	15.0	2.4 (3)	1.75	15.4	19.7	6.3	1.92
	J2-355-CGT-RED	9.1	5.7	0.5 (3)	1.69	13.6	17.4	5.9	1.72
Ecurie	J2-354-IGT4	33.8	93	6.2 (4)	0.61	4.8	11.2	2.7	0.88
	J2-354-IGT8	13.2	223	9.8 (3)	1.40	9.4	18.7	5.9	1.68
Mussel Beach	J2-355-IGT8	7.2	48	4.0 (3)	1.54	14.4	21.8	7.3	1.75
Lost City (750m)									
Beehive	J2-361-CGT-BLUE	6.5	1.6	0.6 (3)	0.21	9.1	n/d	BD	0.93
	J2-361-CGT-WUXI	2.3	2.5	1.5 (4)	0.47	10.1	0.19	BD	1.04
	J2-361-IGT5	1.4	1.4	0.9 (4)	0.07	10.1	0.32	BD	1.03
Marker 6	J2-362-IGT4	1.2	1.3	0.4 (3)	0.22	10.26	0.15	BD	1.13
Lucky Strike (1700m)									
Isabel	J2-357-IGT5	2.8	6.1	1.7 (3)	3.06	0.03	106	BD	0.83
US 4	J2-357-IGT3	2.3	5.3	1.3 (4)	3.22	0.05	127	BD	0.66
Crystal	J2-358-IGT8	2.9	23.0	3.0 (3)	3.07	0.04	110	BD	0.76
	J2-358-CGT-RED	31.2	7.5	0.9 (4)	1.51	0.02	48.9	BD	0.32
Medea	J2-359-IGT2	4.2	5.4	0.7 (3)	2.17	0.06	90.3	BD	0.82
	J2-359-CGT-YELLOW	3.8	5.6	0.7 (3)	2.51	0.06	91.2	BD	0.83
TAG (3600m)									
Black Smoker Complex	J2-363-IGT5	3.9	11.6	2.5 (3)	4.70	0.10	4.94	BD	0.13
	J2-363-CGT-RED	5.9	10.2	0.5 (2)	4.54	0.09	4.47	BD	0.12
9°50' N (2500m)									
Tica	4464-IGT1	4.1	3.6	0.6 (3)	8.22	0.37	92.5	0.81	0.091
Crab Spab	4464-IGT4	50.3	6.1	0.1 (3)	0.17	0.003	7.26	BD	0.010
	4464-IGT5	50.5	5.7	0.3 (3)	0.19	0.003	7.26	BD	0.012
	4466-IGT3	50.0	5.9	nd	0.29	0.006	7.47	BD	0.009
L Vent (hi-T)	4467-IGT1	4.3	7.8	0.03 (2)	5.18	0.72	8.81	0.20	0.071
	4467-IGT5	8.9	9.8	0.6 (3)	4.60	0.70	8.18	0.18	0.070
L Vent (lo-T)	4467-IGT6	41.1	17.8	1.3 (3)	1.00	0.028	3.93	BD	0.037
L Vent, Marker 8	4468-IGT4	9.1	7.5	0.6 (3)	4.73	0.63	8.19	BD	0.066
Bio9 (HOBO)	4469-IGT4	3.3	4.3	0.8 (3)	10.2	0.92	86.9	1.64	0.076
	4469-IGT5	3.0	3.2	0.3 (3)	11.0	0.87	86.7	nd	0.075
Trick or Treat	4469-IGT1	5.7	11.1	3.0 (3)	17.1	1.0	60.4	nd	0.058
	4469-IGT3	2.5	10.0	0.8 (3)	18.3	1.2	66.1	1.88	0.066
Guaymas Basin (2000m)									
Theme Park	4458-IGT1	3.5	1.4E+04	3.6E3 (3)	6.38	0.50	43.9	nd	41.5
	4458-IGT8	31.9	6.5E+03	0.8E3 (3)	2.82	0.23	21.1	nd	18.8
Cathedral Hill	4459-IGT5	41.0	3.5E+03	0.2E3 (3)	1.85	0.12	9.8	6.27	10.3
Sulfide Spires	4461-IGT5	12.9	1.3E+04	1.9E3 (3)	5.33	0.42	31.8	75.6	32.8
	4461-IGT8	32.3	6.1E+03	0.8E3 (3)	2.88	0.24	21.0	25.7	19.3
Toadstool	4462-IGT5	11.3	8.5	nd	6.10	2.10	41.8	BD	49.7
	4462-IGT6	2.42	6.1	nd	7.89	2.63	47.6	BD	61.0
Rebecca's Roost	4462-IGT1	3.12	14.1	1 (2)	7.49	3.06	45.8	BD	54.5
	4462-IGT4	5.64	5.1	2 (2)	7.27	2.96	43.6	BD	53.6

Mg and H_2S data from MAR sites provided by N.Pester. CH_3SH error represents the 2s analytical error associated with *n* measurements. 2s analytical uncertainties associated with H_2S, ΣCO_2 and CH_4 are ±5%, and those for CO are ±10%.

Table 3.2 Endmember concentrations (extrapolated to zero Mg) and lowest measured pH values

Site (depth), Vent	T_{max} (°C)	pH (25°)	H_2 (mmol/L)	H_2S (mmol/L)	ΣCO_2 (mmol/kg)	CO (mmol/L)	CH_4 (mmol/L)
Rainbow (2300m)							
PP27/Exo2	350	3.4	12.3	3.3	21.3	5.1	1.9
Stylo1	367	3.3	16.1	2.3	24.6	7.1	2.0
CMSt.P&P	365	3.3	16.0	2.1	22.3	6.9	2.0
X11	364	3.1	16.5	2.0	20.9	7.0	2.1
Ecurie	191	3.0	12.6	1.9	24.8	7.8	2.3
Mussel Beach	180	3.0	16.7	1.8	25.0	8.5	2.0
Lost City (750m)							
Beehive	96	10.6	10.4	0.3	0.18	BD	1.1
Marker 6	96	10.5	10.4	0.2	0.11	BD	1.1
Lucky Strike (1700m)							
Isabel	292	3.8	0.028	3.2	111.7	BD	0.9
US 4	299	3.9	0.053	3.4	132.7	BD	0.7
Crystal	308	3.6	0.041	3.3	116.7	BD	0.8
Medea	270	3.7	0.063	2.5	98.0	BD	0.9
TAG (3600m)							
Black Smoker Complex	363	3.3	0.1	5.1	5.0	BD	0.2
9°50' N (2500m)							
Tica	275	3.8	0.40	8.9	99.8	0.88	0.099
Crab Spa[a]	23	5.7	0.059	3.3	78.4	BD	0.15
L Vent (hi-T)	246	3.8	0.81	5.6	9.4	0.22	0.080
L Vent (lo-T)[b]	78	5.8	0.12	4.2	9.5	BD	0.15
L Vent, Marker 8	221	4.2	0.75	5.7	9.4	n/d	0.080
Bio9 (HOBO)	363	3.5	0.95	11.3	92.0	1.8	0.081
Trick or Treat	280	3.8	1.2	19.1	68.3	2.0	0.067
Guaymas Basin (2000m)							
Theme Park	249	5.7	0.54	6.8	47.2	n/d	44.8
Cathedral Hill	172	5.7	0.51	7.7	33.8	26	43.2
Sulfide Spires	218	4.5	0.56	7.0	42.7	92	44.2
Toadstool	299	6.1	2.7	8.0	50.8	n/d	63.5
Rebecca's Roost	278	6.1	3.3	8.0	48.4	n/d	58.8
Seawater	3	**8**	0	0	2.2	0	0

[a,b] Low temperature 'Crab Spa' and 'L Vent (lo-T)' fluids are considered to have been derived from nearby 'Tica' and 'L Vent (hi-T)/Marker 8' high temperature fluids, respectively. The end-member compositions of all vents were calculated by extrapolating measured compositions to zero Mg using linear least squares regression. 'Crab Spa' and 'L Vent (lo-T)' endmembers required large extrapolations and do not reflect represent an existing composition, but are useful in demonstrating the deviation from conservative dilution of their parent fluids. pH(25°C) values represent the lowest measured values of all samples for a given vent fluid.

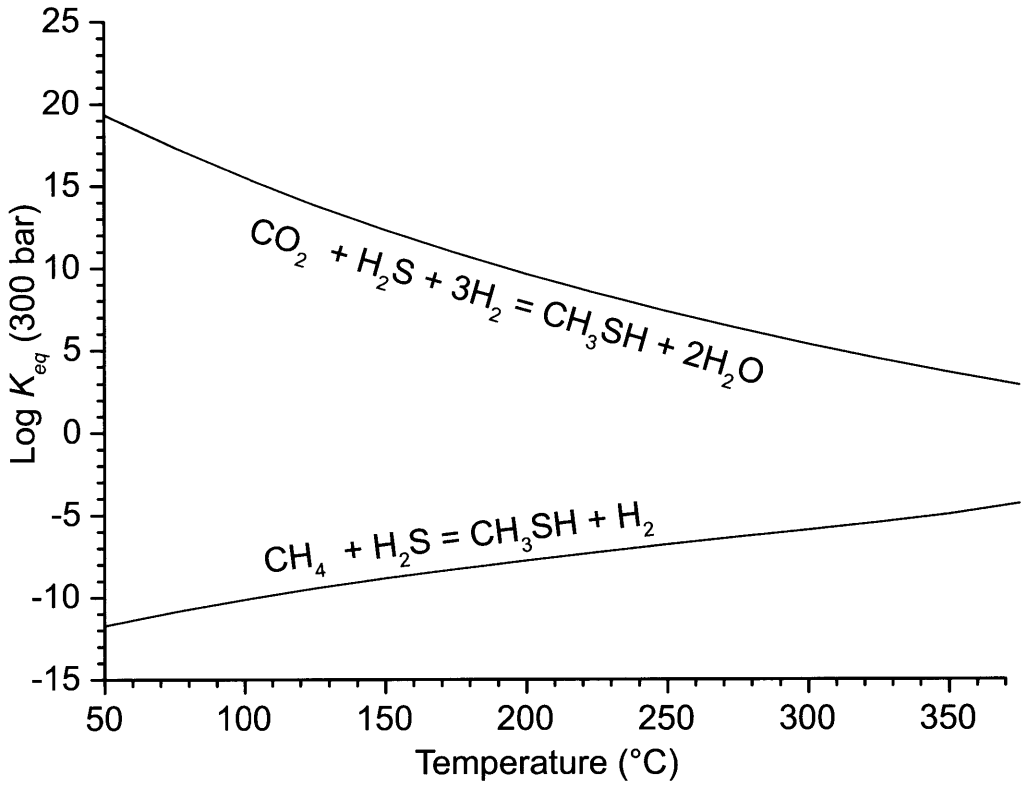

Figure 3.1.

Equilibrium constants (Log K_{eq}) for the formation of CH_3SH from either CO_2 (reduction) or CH_4 (oxidation) as a function of temperature at 300 bar. Formation of CH_3SH by CO_2 reduction is favored under lower temperature, more reducing conditions, whereas formation from CH_4 is favored under higher temperature, more oxidizing conditions. Thermodynamic data for the construction of this figure were obtained from the SUPCRT92 database (JOHNSON *et al.*, 1992) with additional data from SHOCK and HELGESON (1990) and SCHULTE and ROGERS (2004).

Figure 3.2.

Predicted concentration (open symbols) of CH_3SH according to reaction (1), **(A)**, and reaction (2), **(B)** as a function of measured H_2 concentrations. Measured concentrations are shown as filled symbols. Activity coefficients of unity are assumed for all neutral species. Only moderate to high temperature vents (>150°C) from bare rock hydrothermal systems are plotted for clarity.

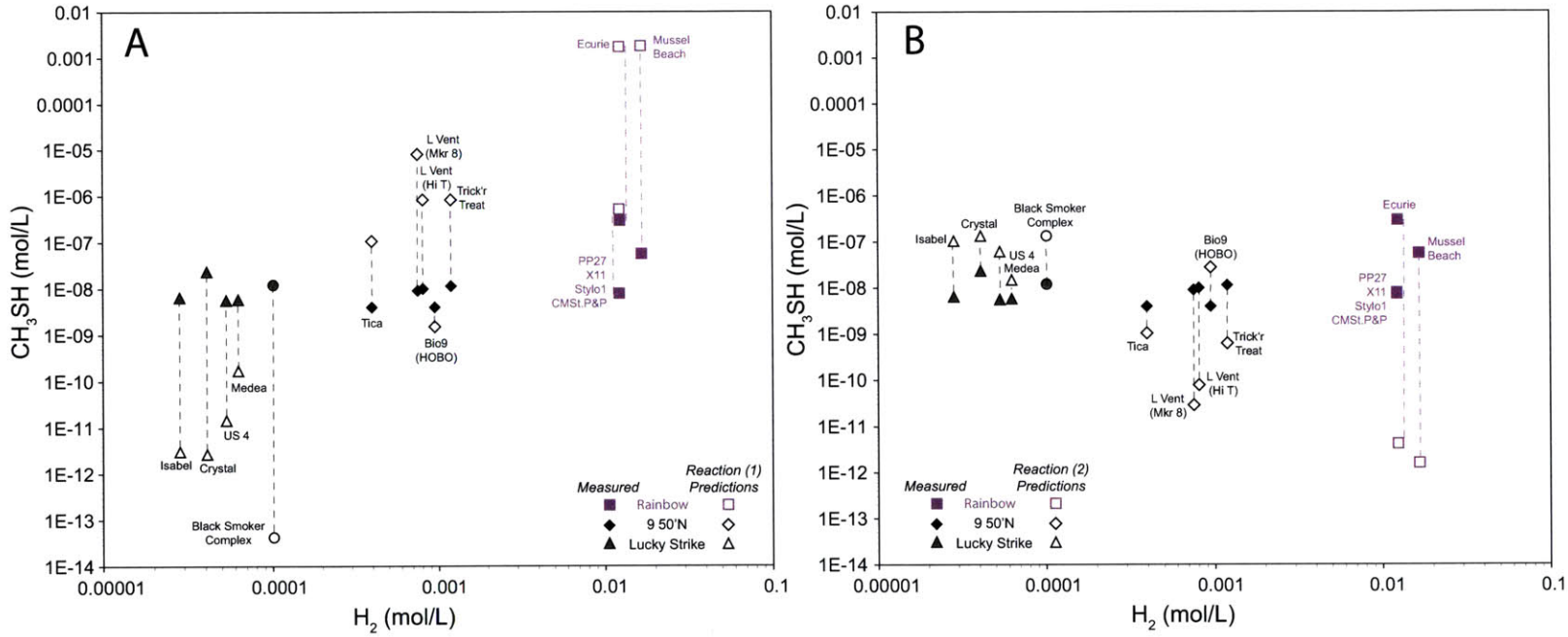
A
B
CH_3SH (mol/L)
H_2 (mol/L)
0.01
0.001
0.0001
1E-05
1E-06
1E-07
1E-08
1E-09
1E-10
1E-11
1E-12
1E-13
1E-14
0.00001
0.0001
0.001
0.01
0.1
Ecurie
Mussel Beach
L Vent (Mkr 8)
L Vent (Hi T)
Trick'r Treat
PP27
X11
Stylo1
CMSt.P&P
Tica
Bio9 (HOBO)
Medea
US 4
Isabel
Crystal
Black Smoker Complex
Reaction (1) Predictions
Measured
Rainbow
9 50'N
Lucky Strike
Reaction (2) Predictions

Figure 3.2

REFERENCES

ALLEN, D. E. and SEYFRIED, W. E. (2004) Serpentinization and heat generation: Constraints from Lost City and Rainbow hydrothermal systems. *Geochimica Et Cosmochimica Acta* **68**(6), 1347-1354.

ANDERSON, G. (2005) *Thermodynamics of Natural Systems*. Cambridge University Press.

BAROSS, J. A. and HOFFMAN, S. E. (1985) Submarine Hydrothermal Vents And Associated Gradient Environments As Sites For The Origin And Evolution Of Life. *Origins Of Life And Evolution Of The Biosphere* **15**(4), 327-345.

BISCHOFF, J. L. and DICKSON, F. W. (1975) Seawater-basalt interaction at 200°C and 500 bars: Implications for origin of sea-floor heavy-metal deposits and regulation of seawater chemistry. *Earth and Planetary Science Letters* **25**, 385-397.

CHARLOU, J. L., DONVAL, J. P., FOUQUET, Y., JEAN-BAPTISTE, P., and HOLM, N. (2002) Geochemistry of high H_2 and CH_4 vent fluids issuing from ultramafic rocks at the Rainbow hydrothermal field (36°14'N, MAR). *Chemical Geology* **191**(4), 345-359.

CORLISS, J. B., BAROSS, J. A., and HOFFMAN, S. E. (1981) An hypothesis concerning the relationship between submarine hot springs and the origin of life on Earth. *Oceanologica Acta* **4**(Supplement), 59-69.

CRUSE, A. M. and SEEWALD, J. S. (2006) Geochemistry of low-molecular weight hydrocarbons in hydrothermal fluids from Middle Valley, northern Juan de Fuca Ridge. *Geochimica Et Cosmochimica Acta* **70**(8), 2073-2092.

DE DUVE, C. (1991) *Blueprint for a Cell: The Nature and Origin of Life*. N. Patterson.

FUCHS, G. (1989) Alternative pathways of autotrophic CO_2 fixation. In: *Autotrophic bacteria*, (*Ed:* H. G. Schlegel and B. Bowien), Science Tech Publishers. pp. 365-382.

GARRELS, R. M. and CHRIST, C. L. (1965) *Solutions, Minerals, and Equilibria*. Harper & Row.

GERMAN, C. and VON DAMM, K. L. (2003) Hydrothermal Processes. In: *The Treatise on Geochemistry*, (*Ed:* K. K. Turekian and H. D. Holland), **6.07**, Elsevier. pp. 181-222.

HAYMON, R. M., FORNARI, D. J., VONDAMM, K. L., LILLEY, M. D., PERFIT, M. R., EDMOND, J. M., SHANKS, W. C., LUTZ, R. A., GREBMEIER, J. M., CARBOTTE, S. et al. (1993) Volcanic-Eruption Of The Mid-ocean Ridge Along The East Pacific Rise Crest At 9°45-52'N - Direct Submersible Observations Of Sea-Floor Phenomena Associated With An Eruption Event In April, 1991. *Earth And Planetary Science Letters* **119**(1-2), 85-101.

HEINEN, W. and LAUWERS, A. M. (1996) Organic sulfur compounds resulting from the interaction of iron sulfide, hydrogen sulfide and carbon dioxide in an anaerobic aqueous environment. *Origins Of Life And Evolution Of The Biosphere* **26**(2), 131-150.

HOLM, N. G. (1992) *Marine Hydrothermal Systems and the Origin of Life: Report of SCOR Working Group 91.* Reprinted from: Origins of Life and Evolution of the Biosphere, Vol. 22 (1-4), 1992. Springer.

HOLM, N. G. and CHARLOU, J. L. (2001) Initial indications of abiotic formation of hydrocarbons in the Rainbow ultramafic hydrothermal system, Mid-Atlantic Ridge. *Earth And Planetary Science Letters* **191**(1-2), 1-8.

HUBER, C. and WACHTERSHAUSER, G. (1997) Activated acetic acid by carbon fixation on (Fe,Ni)S under primordial conditions. *Science* **276**(5310), 245-247.

JOHNSON, J. W., OELKERS, E. H., and HELGESON, H. C. (1992) SUPCRT92 - A software package for calculating the standard molal thermodynamic properties of minerals, gases, aqueous species, and reactions from 1 to 5000 bar and 0 to 1000°C. *Computers & Geosciences* **18**(7), 899-947.

KELLEY, D. S., BAROSS, J. A., and DELANEY, J. R. (2002) Volcanoes, fluids, and life at mid-ocean ridge spreading centers. *Annual Review Of Earth And Planetary Sciences* **30**, 385-491.

KELLEY, D. S., KARSON, J. A., BLACKMAN, D. K., FRUH-GREEN, G. L., BUTTERFIELD, D. A., LILLEY, M. D., OLSON, E. J., SCHRENK, M. O., ROE, K. K., LEBON, G. T. et al. (2001) An off-axis hydrothermal vent field near the Mid-Atlantic Ridge at 30°N. *Nature* **412**(6843), 145-149.

KLEIN, F. and BACH, W. G. (2009) Fe-Ni-Co-O-S Phase Relations in Peridotite-Seawater Interactions. *Journal Of Petrology* **50**(1), 37-59.

KONN, C., CHARLOU, J. L., DONVAL, J. P., HOLM, N. G., DEHAIRS, F., and BOUILLON, S. (2009) Hydrocarbons and oxidized organic compounds in hydrothermal fluids from Rainbow and Lost City ultramafic-hosted vents. *Chemical Geology* **258**(3-4), 299.

KREIN, E. B. (1993) Organic sulfur in the geosphere: analysis, structures and chemical processes. In: *Supplement S: The chemistry of Sulphur-containing functional groups*, (*Ed:* S. Patai and Z. Rappoport), Wiley. pp. 975-1032.

LANG, S. Q., BUTTERFIELD, D. A., LILLEY, M. D., JOHNSON, H. P., and HEDGES, J. I. (2006) Dissolved organic carbon in ridge-axis and ridge-flank hydrothermal systems. *Geochimica Et Cosmochimica Acta* **70**(15), 3830-3842.

LANGMUIR, C., HUMPHRIS, S., FORNARI, D., VANDOVER, C., VONDAMM, K., TIVEY, M. K., COLODNER, D., CHARLOU, J. L., DESONIE, D., WILSON, C. et al. (1997) Hydrothermal vents near a mantle hot spot: The Lucky Strike vent field at 37 degrees N on the Mid-Atlantic Ridge. *Earth And Planetary Science Letters* **148**(1-2), 69-91.

MARTIN, W. and RUSSELL, M. J. (2006) Review: On the origin of biochemistry at an alkaline hydrothermal vent. *Philosophical Transactions Of The Royal Society Of London Series*

B: Biological Sciences, Page FirstCite, DOI 10.1098/rstb.2006.1881, URL: http://dx.doi.org/10.1098/rstb.2006.1881.

MARTIN, W., BAROSS, J., KELLEY, D., and RUSSELL, M. J. (2008) Hydrothermal vents and the origin of life. *Nature Reviews Microbiology* **6**(11), 805-814.

MCCOLLOM, T. M. and SEEWALD, J. S. (2007) Abiotic synthesis of organic compounds in deep-sea hydrothermal environments. *Chemical Reviews* **107**, 382-401.

MORAN, J. J., BEAL, E. J., VRENTAS, J. M., ORPHAN, V. J., FREEMAN, K. H., and HOUSE, C. H. (2008) Methyl sulfides as intermediates in the anaerobic oxidation of methane. *Environmental Microbiology* **10**(1), 162-173.

MOTTL, M. J. and HOLLAND, H. D. (1978) Chemical exchange during hydrothermal alteration of basalt by seawater-I. Experimental results for major and minor components of seawater. *Geochimica et Cosmochimica Acta* **42**(8), 1103-1115.

PROSKUROWSKI, G., LILLEY, M. D., and OLSON, E. J. (2008) Stable isotopic evidence in support of active microbial methane cycling in low-temperature diffuse flow vents at 9°50'N East Pacific Rise. *Geochimica et Cosmochimica Acta* **72**(8), 2005-2023.

PROSKUROWSKI, G., LILLEY, M. D., SEEWALD, J. S., FRUH-GREEN, G. L., OLSON, E. J., LUPTON, J. E., SYLVA, S. P., and KELLEY, D. S. (2008) Abiogenic hydrocarbon production at Lost City hydrothermal field. *Science* **319**(5863), 604-607.

RUSSELL, M. J. and HALL, A. J. (2006) The onset and early evolution of life. In: *Evolution of Early Earth's Atmosphere, Hydrosphere, and Biosphere - Constraints from Ore Deposits: Geological Society of America Memoir 198*, (*Ed:* S. E. Kesler and H. Ohmoto), Geological Society of America. pp. 1-32.

SCHULTE, M. D. and ROGERS, K. L. (2004) Thiols in hydrothermal solution: standard partial molal properties and their role in the organic geochemistry of hydrothermal environments. *Geochimica Et Cosmochimica Acta* **68**(5), 1087-1097.

SEEWALD, J. S., ZOLOTOV, M. Y., and MCCOLLOM, T. (2006) Experimental investigation of single carbon compounds under hydrothermal conditions. *Geochimica Et Cosmochimica Acta* **70**(2), 446-460.

SEEWALD, J. S., DOHERTY, K. W., HAMMAR, T. R., and LIBERATORE, S. P. (2002) A new gas-tight isobaric sampler for hydrothermal fluids. *Deep-Sea Research Part I-Oceanographic Research Papers* **49**(1), 189-196.

SEYFRIED, W. E. and BISCHOFF, J. L. (1981) Experimental seawater-basalt interaction at 300°C, 500 bars, chemical exchange, secondary mineral formation and implications for the transport of heavy-metals. *Geochimica et Cosmochimica Acta* **45**(2), 135-147.

SHOCK, E. L. (1990) Geochemical constraints on the origin of organic compounds in hydrothermal systems. *Origins Of Life And Evolution Of The Biosphere* **20**(3-4), 331-367.

SHOCK, E. L. (1992) Chemical Environments Of Submarine Hydrothermal Systems. *Origins Of Life And Evolution Of The Biosphere* **22**(1-4), 67-107.

SHOCK, E. L. and HELGESON, H. C. (1990) Calculation of the thermodynamic and transport properties of aqueous species at high pressures and temperatures: Standard partial molal properties of organic species. *Geochimica et Cosmochimica Acta* **54**(4), 915-945.

SHOCK, E. L. and SCHULTE, M. D. (1998) Organic synthesis during fluid mixing in hydrothermal systems. *Journal Of Geophysical Research-Planets* **103**(E12), 28513-28527.

SIMO, R. (1998) Trace chromatographic analysis of dimethyl sulfoxide and related methylated sulfur compounds in natural waters. *Journal Of Chromatography A* **807**(2), 151-164.

SIMONEIT, B. R. T., KAWKA, O. E., and BRAULT, M. (1988) Origin Of Gases And Condensates In The Guaymas Basin Hydrothermal System (Gulf Of California). *Chemical Geology* **71**(1-3), 169-182.

TESKE, A., HINRICHS, K. U., EDGCOMB, V., GOMEZ, A. D., KYSELA, D., SYLVA, S. P., SOGIN, M. L., and JANNASCH, H. W. (2002) Microbial diversity of hydrothermal sediments in the Guaymas Basin: Evidence for anaerobic methanotrophic communities. *Applied And Environmental Microbiology* **68**(4), 1994-2007.

THOMPSON, G., MOTTL, M. J., and RONA, P. A. (1985) Morphology, Mineralogy And Chemistry Of Hydrothermal Deposits From The TAG Area, 26°N Mid-Atlantic Ridge. *Chemical Geology* **49**(1-3), 243-257.

TIVEY, M. K., HUMPHRIS, S. E., THOMPSON, G., HANNINGTON, M. D., and RONA, P. A. (1995) Deducing patterns of fluid flow and mixing within the TAG active hydrothermal mound using mineralogical and geochemical data. *Journal Of Geophysical Research-Solid Earth* **100**(B7), 12527-12555.

VON DAMM, K. L. (1995) Controls on the chemistry and temporal variability of seafloor hydrothermal systems. In: *Seafloor Hydrothermal Systems: Physical, Chemical, Biological, and Geological Interactions*, (*Ed:* S. E. Humphris, R. A. Zierenberg, L. S. Mullineaux, and R. E. Thomson), AGU Monograph, **91**, American Geophysical Union. pp. 222-247.

VON DAMM, K. L., EDMOND, J. M., GRANT, B., and MEASURES, C. I. (1985) Chemistry of submarine hydrothermal solutions at 21°N, East Pacific Rise. *Geochimica et Cosmochimica Acta* **49**(11), 2197-2220.

VON DAMM, K. L., BRAY, A. M., BUTTERMORE, L. G., and OOSTING, S. E. (1998) The geochemical controls on vent fluids from the Lucky Strike vent field, Mid-Atlantic Ridge. *Earth and Planetary Science Letters* **160**(3-4), 521-536.

WARDENCKI, W. (1998) Problems with the determination of environmental sulphur compounds by gas chromatography. *Journal Of Chromatography A* **793**(1), 1-19.

WELHAN, J. A. and LUPTON, J. (1987) Light Hydrocarbon Gases In Guaymas Basin Hydrothermal Fluids: Thermogenic Versus Abiogenic Origin. *AAPG Bulletin* **71**(2), 215-223.

ZHANG, T. W., AMRANI, A., ELLIS, G. S., MA, Q. S., and TANG, Y. C. (2008) Experimental investigation on thermochemical sulfate reduction by H2S initiation. *Geochimica Et Cosmochimica Acta* **72**(14), 3518-3530.

CHAPTER 4

Rapid hydrogen isotope ($^2H/^1H$) exchange between aqueous *n*-alkanes and water under hydrothermal conditions: implications for the isotopic composition of abiogenic and thermogenic hydrocarbons

ABSTRACT

Experiments were conducted to investigate $^2H/^1H$ exchange between aqueous hydrocarbons and water under hydrothermal conditions. C_1–C_5 *n*-alkanes were heated in aqueous solutions of varying initial $^2H/^1H$ ratio in the presence of a pyrite-pyrrhotite-magnetite mineral redox buffer at 323°C and 350 bar using a Au-Ti flexible cell hydrothermal apparatus. Extensive and completely reversible incorporation of water-derived H into C_3–C_5 *n*-alkanes was observed on timescales of months. In contrast, comparatively minor exchange was observed for CH_4 and ethane. Isotopic exchange is facilitated by rapid reversible equilibration of *n*-alkanes and their corresponding alkenes and water-derived H_2. Rates of δ^2H variation in C_{3+} *n*-alkanes decreased with time, consistent with an apparent approach to steady-state isotopic compositions regulated by alkane-water isotopic equilibrium. Substantially slower exchange rates were observed for ethane relative to C_3–C_5 *n*-alkanes, suggesting that alkane/alkene abundances and isomerization reactions may dramatically enhance rates of H incorporation in longer chain hydrocarbons. Thus, in reducing aqueous environments, reaction mechanisms exist that allow rapid $^2H/^1H$ exchange of alkyl-H with water at elevated temperatures and pressures on relatively short geological timescales. The proximity of some abiogenic and thermogenic alkane δ^2H values to values predicted for

equilibrium fractionation with ambient water suggests that this process may occur in natural systems.

1. INTRODUCTION

Compound-specific stable hydrogen isotope (^1H and ^2H) measurements of carbon-bound hydrogen (TOBIAS and BRENNA, 1997; BURGOYNE and HAYES, 1998; HILKERT *et al.*, 1999; SESSIONS, 2006) have recently become widespread in organic geochemistry. The hydrogen isotope composition of *n*-alkanes have been utilized to elucidate such diverse processes as abiogenic hydrocarbon formation (SHERWOOD LOLLAR *et al.*, 2002; FU *et al.*, 2007; PROSKUROWSKI *et al.*, 2008), formation and biodegradation of petroleum constituents (SCHOELL, 1983; WHITICAR et al., 1985; TANG *et al.*, 2005; SCHIMMELMANN *et al.*, 2006; BOREHAM *et al.*, 2008) and paleoenvironmental changes (SCHEFUSS *et al.*, 2005; SACHSE *et al.*, 2006; EGLINTON and EGLINTON, 2008). However, use of δ^2H measurements to infer primary isotopic influences (*i.e.* kinetic or equilibrium isotope effects associated with hydrocarbon formation) implicitly assumes the resistance of organic hydrogen to secondary exchange processes over pertinent geologic timeframes. There is growing evidence to suggest that exchange or incorporation of water-derived H into organic molecules can obscure primary isotopic signatures but there are still significant gaps in our understanding of this process (SESSIONS *et al.*, 2004; SCHIMMELMANN *et al.*, 2006).

Recently, studies of $^2H/^1H$ ratios have been expanded to the low molecular weight (LMW) *n*-alkanes (C_1 to C_5), which represent an important class of compounds in a variety of high temperature fluids. The formation of abiogenic LMW *n*-alkanes associated with serpentinization of ultramafic igneous crust is currently the subject of extensive interest (BERNDT *et al.*, 1996; MCCOLLOM and SEEWALD, 2001, 2007; FU *et al.*, 2007; PROSKUROWSKI *et al.*, 2008) and δ^2H measurements been used to infer mechanistic information regarding abiogenesis (SHERWOOD LOLLAR *et al.*, 2002). Moreover, C_1 to C_5 *n*-alkanes are abundantly present in oil and natural gas formed by thermal maturation of sedimentary organic matter (TISSOT and WELTE,

1984; HUNT, 1996) and there is interest in developing their $^{2}H/^{1}H$ signatures as maturation and correlation parameters for petroleum characterization (TANG *et al.*, 2007). Understanding the provenance of these hydrocarbons is crucial both for the management of natural gas resources and elucidating the potential for abiogenic organic synthesis in hydrothermal settings. The usefulness of $\delta^{2}H$ values in this respect is problematic, however, given the uncertainty in our understanding of controls on hydrocarbon $^{2}H/^{1}H$ ratios in water-rich environments.

A significant source of uncertainty stems from the fact that the susceptibility of hydrocarbons to isotopic exchange with ambient water at elevated temperatures is unclear. In addition to its obvious ubiquity in hydrothermal systems, water may be a reactive source of H not just during the generation of petroleum hydrocarbons but also during subsequent migration and accumulation processes (LEWAN, 1997; SEEWALD, 2003; SCHIMMELMANN *et al.*, 2006). While aliphatic H is typically considered to be the most isotopically conservative moiety under low temperature conditions (SCHIMMELMANN *et al.*, 2006), aqueous reaction paths at elevated temperatures could facilitate reversible exchange with water-derived H. Experiments conducted under hydrothermal conditions have shown that *n*-alkanes (below C_7 in length) and their corresponding *n*-alkenes rapidly attain reversible states of redox-dependant metastable equilibrium under redox-buffered conditions according to the following reaction (SEEWALD, 1994, 2001, 2003):

$$C_nH_{2n+2(aq)} = C_nH_{2n(aq)} + H_{2(aq)} \qquad (1)$$

Under progressively oxidizing conditions, further stepwise oxidation can occur *via* metastable ketone and alcohol intermediaries, leading to chain shortening and overall conversion of *n*-alkanes to CO_2 and CH_4. However, under reducing conditions the initial alkane-alkene reaction allows *n*-alkanes to persist in metastable reversible equilibrium with aqueous H_2, depending on redox conditions. Because the latter is ultimately derived from water and these reactions are

reversible, in theory reversible $^{2}H/^{1}H$ exchange may occur. This has not been verified and the timescales on which exchange could occur in natural systems are poorly constrained.

This chapter presents an experimental study of the potential for reversible $^{2}H/^{1}H$ exchange between dissolved C_1 to C_5 *n*-alkanes and water at hydrothermal conditions, and the timescales on which such exchange might occur. As such it increases our understanding of possible controls on isotopic variability in LMW hydrocarbons, which is essential for proper interpretation of stable hydrogen isotope compositions of alkane H in geologic fluids.

2. MATERIALS AND METHODS

2.1 Experimental Approach and Setup

All experiments in this study were conducted by heating dissolved mixtures of C_1 to C_5 *n*-alkanes in aqueous solutions of varying $^2H/^1H$ ratios within a flexible-cell hydrothermal apparatus of the type described by SEYFRIED (1987). The apparatus consists of a gold reaction cell equipped with titanium fittings and a capillary exit tube with sampling valve. The reaction cell is contained within a stainless steel pressure vessel (using de-ionized water as pressurizing fluid) and furnace. This apparatus has been used in numerous investigations of aqueous LMW organic compounds under hydrothermal conditions (MCCOLLOM and SEEWALD, 2001, 2003a,b; SEEWALD, 2001; SEEWALD *et al.*, 2006; FU *et al.*, 2007). A key feature is that it allows experiment to be conducted at constant pressure, thereby confining reactions to the aqueous phase. In addition, the capillary exit tube allows both removal of fluid aliquots for analysis of solution composition as a function of time and modification of reaction cell contents by injection of solutions without perturbing the temperature or pressure of the experiment. Rapid cooling of removed aliquots to room temperature also minimizes retrograde reactions that can occur during prolonged quenching. Both Au and TiO_2 are also the least catalytic surfaces for carbon-carbon bond cleavage that can fulfill the requirements of the apparatus (PALMER and DRUMMOND, 1986; BELL *et al.*, 1994; MCCOLLOM and SEEWALD, 2003a,b). Prior to use, the titanium fittings in contact with the reaction cell contents were previously heated in air for 24h at 400°C to form an inert TiO_2 surface layer.

Laboratory experiments have demonstrated that the stability of aqueous LMW *n*-alkanes is highly sensitive to the redox state of the fluid (SEEWALD, 1994, 2001). Hence, to demonstrate that variations in *n*-alkane $^2H/^1H$ ratios can be attributed to reversible $^2H/^1H$ exchange with water, rather than kinetic isotope effects associated with degradation/side reactions, it is crucial that the

latter be simultaneously limited. SEEWALD (2001) demonstrated that overall rates of *n*-heptane degradation by stepwise aqueous oxidation varied dramatically depending on the mineral redox buffer employed. Of the three buffers used (pyrite-pyrrhotite-magnetite (PPM), hematite-magnetite-pyrite (HMP) and hematite-magnetite (HM)), *n*-alkane degradation was slowest with the more reducing PPM mineral assemblage (SEEWALD, 2001), hence, this buffer was chosen for all experiments (Figure 4.1). The PPM assemblage buffers both $H_{2(aq)}$ and $H_2S_{(aq)}$ activities ($a_{H2(aq)}$ and $a_{H2S(aq)}$, respectively) *via* the following chemical reactions:

$$1.5FeS_{(s)} + H_2O_{(l)} = 0.75FeS_{2(s)} + 0.25Fe_3O_{4(s)} + H_{2(aq)} \quad (2)$$

$$FeS_{2(s)} + 2FeS_{(s)} + 4H_2O_{(l)} = Fe_3O_{4(s)} + 4H_2S_{(aq)} \quad (3)$$

The influence of this mineral assemblage on the oxidation state of the fluid is reflected in the abundance of dissolved H_2, which is directly related to O_2 fugacity by the disproportionation of water, which rapidly attains thermodynamic equilibrium at high temperatures:

$$H_2O_{(l)} = H_{2(aq)} + 0.5O_{2(aq)} \quad (4)$$

The effectiveness of the PPM mineral assemblage in buffering dissolved H_2 and H_2S concentrations on short (weekly) timescales has been demonstrated in numerous previous experiments (SEEWALD, 1994, 1997, 2001; MCCOLLOM and SEEWALD, 2003b). Accordingly, aqueous H_2S was not routinely measured to preserve the limited quantities of fluid in the reaction cell. In addition to the above practical considerations, the choice of the PPM assemblage also reflects a reasonable redox state encountered in seafloor hydrothermal systems (which range from lower to much higher f_{O2} values than the PPM triple point, SHOCK, 1992; SEYFRIED and DING, 1995; SEYFRIED *et al.*, 2004) and provides a source of S for the formation of catalytic S species that may facilitate organic reactions (SEEWALD, 2001).

Each experiment was set up by loading a mixture containing ~5g each of commercially synthesized (>99.9% pure) pyrite, pyrrhotite and magnetite powders into the reaction cell with

~30g of an Ar purged solution of a given δ^2H_{H2O} value. ^{2}H-enriched and ^{2}H-depleted solutions were made with dilutions of 99wt.% ^2H_2O and ^{2}H-depleted water (Cambridge Isotope Labs) with Milli-Q water, respectively. Both starting solutions contained a low but known concentration of NaCl to allow for detection of reaction cell leakage. Prior to pressurization of the reaction cell, the reaction cell gas headspace (~10mL) was purged repeatedly with Ar, evacuated, then loaded with a gaseous mixture of C_1 to C_5 *n*-alkanes of known δ^2H (with approximately equimolar carbon amounts per *n*-alkane) that subsequently dissolved during pressurization. The purpose of including CH_4 in the dissolved mixture was to examine if the lack of a corresponding alkene influenced exchangeability of H relative to the other *n*-alkanes. A small amount (<1.5g) of starting solution was then injected to completely flush the gas mixture into the reaction cell for subsequent dissolution during pressurization and heating. It has been demonstrated that commercial minerals of the purity used here do contain trace carbon contaminants arising from synthesis processes (SEEWALD, 1994, 2001; MCCOLLOM and SEEWALD, 2003a,b). As a result, C_1 to C_5 *n*-alkane concentrations employed in each experiment were intentionally >2 orders of magnitude larger than any contaminant hydrocarbon concentrations observed in previous studies to ensure *n*-alkane δ^2H values (δ^2H_{alkane}) during each experiment were unaffected by background levels.

In order to determine if δ^2H_{alkane} variations were a function of the initial $^2H/^1H$ ratio of the solution (δ^2H_{H2O}), two experiments were conducted with near-identical temperatures, pressures and dissolved *n*-alkane concentrations but initial δ^2H_{H2O} values higher and lower than the starting δ^2H_{alkane} values, respectively. Experiment 1 (113 days) was conducted at 323°C and 36MPa with an initial δ^2H_{H2O} of +507‰, whereas Experiment 2 (323°C and 35MPa for 226 days) had an initial δ^2H_{H2O} value of -802‰ during Stage (1). The reversibility of $^2H/^1H$ transfer between water and dissolved *n*-alkanes was confirmed by injecting 15.0g of a ^{2}H-spiked fluid (containing

10mmol/kg NaCl) into the reaction cell of Experiment 2 after 226 days, thereby raising the δ^2H_{H2O} value of the fluid to +352‰ (Stage (2)). This had the effect of diluting the abundances of dissolved hydrocarbons by ~50%. The injected fluid was not purged of O_2 with Ar gas prior to injection in order to limit evaporative effects on δ^2H_{H2O} values.

2.2 Analytical Methods

Concentrations of dissolved species were monitored as a function of time during each experiment by removing discrete fluid aliquots (in duplicate, typically <1g each) into glass/PTFE gas-tight syringes for immediate analyses (within 2h). Prior to each sampling event, an initial aliquot (<1g) was withdrawn to flush the capillary exit tube and discarded.

Concentrations of total dissolved inorganic carbon (ΣCO_2) and hydrocarbons (C_1 to C_5 *n*-alkanes, methylpropane (*iso*-butane) and C_2 to C_5 *n*-alkenes) were determined using purge and trap gas chromatography. Fluid aliquots were injected into a sparge cell containing ~1mL of 25wt.% phosphoric acid to completely purge ΣCO_2. The evolved gases were cryofocussed on *n*-octane-coated silica beads then transferred directly to a HP 5890 Series II gas chromatograph (GC) equipped with Porapak^{TM} Q column and serially connected thermal conductivity (TCD) and flame ionization (FID) detectors. Commercially available hydrocarbon and CO_2 gas standards were similarly cryofocussed and transferred to the GC column for calibration. Chromatographic separation of individual C_4 and C_5 *n*-alkene isomers in experimental samples was not possible by this method and reported concentrations therefore reflect the summation of all alkene isomers (denoted as ΣC_X alkenes, where X is the carbon number) eluting at the retention time of the corresponding terminal *n*-alkene standard. Furthermore, due to the co-elution of large methylpropane and *n*-butane peaks before and after comparatively small ΣC_4 alkene peaks, large errors are associated with concentrations of the latter. Accordingly, while their presence was

observed, they were not quantified. Analytical uncertainties (2s) are ±5% for C_1 to C_5 *n*-alkanes and ΣCO_2, and ±10% for alkenes and methylpropane.

Aqueous H_2 analyses were performed on a HP 5890 Series II GC by injection of extracted headspace gases from fluid aliquots onto a 5Å molecular sieve column with TCD detection (analytical error (2s) ±10%). Total dissolved sulfide (ΣH_2S) was determined gravimetrically for a single fluid sample at 218.8 days in Experiment 2, following acidification of the aliqout with a 25wt.% phosphoric acid solution and precipitation of evolved H_2S gas as Ag_2S in a 5wt.% $AgNO_3$ solution. pH (at 25°C and 1 atm) was also not monitored routinely but was measured potentiometrically on a single (1.4g) fluid sample at 287.9 days in Experiment 2 using a Ag/AgCl combination reference electrode. Concentrations of Cl and any dissolved C_1 to C_5 *n*-alkanoic acids formed were determined by ion chromatography on a Dionex DX500 system with electrochemical detection using an IonPac® AS15 ion exchange and IonPac® ICE-AS1 ion exclusion column, respectively. Analytical uncertainties (2s) are ±5% for Cl and ±10% for *n*-alkanoic acids.

Fluid aliquots for isotope analyses of dissolved hydrocarbons were also collected in glass gas-tight syringes and immediately transferred into evacuated glass serum vials with butyl rubber stoppers (BellCo Glass) until analyzed. To avoid contamination of samples by background levels of low molecular weight hydrocarbons present in butyl rubber, the stoppers were treated to avoid contamination by volatile organic compounds by boiling in 2N NaOH for 2–4hrs followed by rinsing and overnight immersion in Milli-Q water (OREMLAND *et al.*, 1987). δ^2H_{alkane} values for methane, ethane, propane, *n*-butane and *n*-pentane were determined by continuous flow Gas Chromatography/Pyrolysis/Isotope-Ratio Mass Spectrometry (GC/P/IRMS) on a Finnigan Delta^{Plus}XL mass spectrometer at WHOI interfaced to an Agilent 6890 GC through a GCCIII interface. The pyrolysis furnace was held at 1440°C for quantitative conversion of carbon-bound

H to H_2. Peaks of an organic working standard gas (propane, δ^2H_{alkane} = -150‰, externally calibrated against V-SMOW and SLAP) were periodically introduced downstream of the analytical (Alltech AT-Q) column for pyrolytic conversion as per analyte peaks prior to entry into the IRMS ion source. Mass-2 and -3 signals were processed using the ISODAT software package (ThermoElectron) and corrected for the H_3^+ factor (<5 ppm/mV) daily (SESSIONS, 2006). While the pooled standard deviation (2s precision) of all hydrocarbon δ^2H analyses is less than ±6‰, it is difficult to estimate the overall accuracy of our analyses given that the range of δ^2H values reported here (-489‰ to +114‰) is beyond that of any available LMW hydrocarbon δ^2H standards. Although we have corrected for H_3^+ production (an important source of bias), other effects of 'scale compression' (COPLEN, 1988) are possible for the extreme compositions encountered during our experiments. One potential source of inaccuracy that has been demonstrated in GC/P/IRMS analyses are 'memory effects', whereby a peak in a given chromatogram may be influenced by a preceding adjacent peak which differs in δ^2H by several hundred ‰ (WANG and SESSIONS, 2008). WANG and SESSIONS (2008) attribute such effects to uncharacterized GC (*i.e.* column) and surface adsorption processes during pyrolytic conversion, and while they have been constrained for lipid δ^2H analyses the potential effects for analyses of LMW *n*-alkanes with extreme δ^2H values are unknown. However, introduction of reference propane peaks of constant composition between analyte peaks of extreme δ^2H values within chromatograms from both experiments suggests variability due to pyrolytic conversion is less than ±10‰ for samples with the most extreme differences between *n*-alkane isotopic compositions.

The hydrogen isotope composition of water in experimental solutions (δ^2H_{H2O}) was determined using high-resolution laser absorption spectroscopy (DLT-100 Liquid Water Isotope Analyzer, Los Gatos Research Inc.) according to the method of WANG *et al.* (2009a). Precisions

were less than ±4‰ (2s) for all analyses. Independent analysis of the ^{2}H-enriched starting solution for Experiment 1 by conventional dual-inlet isotope-ratio mass spectrometry (Isotech Laboratories, Inc.) indicated a $\delta^{2}H_{H2O}$ value of +501±5‰, which is close to the value obtained by laser absorption spectroscopy (507±4‰).

All $\delta^{2}H$ values are expressed relative to the Vienna Standard Mean Ocean Water (V-SMOW) scale by the relation:

$$\delta^{2}H = [(^{2}H / ^{1}H)_{MEAS} / (^{2}H / ^{1}H)_{VSMOW}] - 1 \qquad (5)$$

where MEAS refers the measured isotope ratio for a given bulk molecule and $(^{2}H / ^{1}H)_{VSMOW}$ is 155.76×10^{-6} (HAGEMANN *et al.*, 1970). The permil (‰) symbol used with $\delta^{2}H$ values implies a factor of 10^{3} which is omitted from Eq. (5).

3. RESULTS

3.1 $^2H/^1H$ ratios

Based on H mass balance considerations, it is impossible for the composition of the water to change within analytical error due to isotope exchange with the dissolved hydrocarbons. This is confirmed by measurements of the initial (-802‰ and +352‰) and final (-798‰ and +354%) δ^2H_{H2O} values of both stages of Experiment 2 (Table 4.2). A mean value for each stage was therefore assumed. Though only one sample was taken, the above observation suggests that δ^2H_{H2O} values in Experiment 1 (+507‰) are unlikely to have varied outside of error and the value determined by laser absorption spectroscopy was used for consistency.

Several patterns of variability were observed during the experiments in the rates and directions of C_1 to C_5 *n*-alkane δ^2H changes (Figure 4.2). Firstly, the direction of change clearly varied depending upon the value of δ^2H_{H2O}. δ^2H values of all *n*-alkanes increased to varying degrees with time during Experiment 1 from initial values that were lower than that of the solution. In Stage (1) of Experiment 2, where initial *n*-alkane δ^2H values were initially much higher than that of the solution, the reverse occurred. These trends were reversed for all *n*-alkanes except CH_4 following injection of ^2H_2O-spiked water to raise the δ^2H value of the reaction cell water above that of the *n*-alkanes (Figure 4.2). Secondly, rates of δ^2H variation were consistently faster for the C_3 to C_5 *n*-alkanes relative to ethane (Figure 4.2). Methane δ^2H values varied least in both experiments with only a small increases and decreases (<30‰) evident, although in all cases the direction conformed to the higher homologues (Figure 4.2). δ^2H values for both compounds behaved in a similar fashion in both stages of Experiment 2, with negligible changes in δ^2H for methane and a slight increases or decreases for ethane.

Regardless of the δ^2H_{H2O} value, the rate of change of δ^2H_{alkane} values consistently decreased with time for the C_3 to C_5 *n*-alkanes. Such decreases in the rate of change of δ^2H_{alkane}

were not discernable for methane and ethane on the timescales of the experiments. In addition, rates of change for the C_3 to C_5 *n*-alkanes varied depending on the difference between the δ^2H_{H2O} and initial δ^2H_{alkane} values ($\Delta^2H_{H2O\text{-}alkane}$). Changes were most rapid in Stage (2) of Experiment 2 ($\Delta^2H_{H2O\text{-}alkane}$ of 780–840‰) and were slowest in Experiment 1 ($\Delta^2H_{H2O\text{-}alkane}$ of 600–640‰), with Stage (1) of Experiment 2 having intermediate rates and $\Delta^2H_{H2O\text{-}alkane}$.

3.2 Dissolved species concentrations

3.2.1 H_2 and H_2S concentrations

Concentrations of all dissolved species analyzed are shown in Table 4.1. Aqueous H_2 concentrations ranged from 0.26 to 0.65mmol/kg during both experiments. Assuming activity coefficients of 1 for neutral species, the narrow range of dissolved H_2 activities ($a_{H2(aq)}$,) in both Experiments 1 and 2 overlaps the $a_{H2(aq)}$ predicted by the triple point of the PPM mineral assemblage (Figure 4.1). The effectiveness of the assemblage in buffering the redox state of the fluid is evident in the rapid restoration of $a_{H2(aq)}$ to predicted values after fluid injection in Experiment 2. Based on the single H_2S measurement in Experiment 2, the PPM assemblage also appears to have buffered the activity of $H_2S_{(aq)}$ to near equilibrium values (Figure 4.1), consistent with previous experimental observations (SEEWALD, 1994, 2001; MCCOLLOM and SEEWALD, 2003b).

3.2.2 Dissolved hydrocarbon concentrations

With the exception of this first sampling event in Experiment 1, and taking into account the dilution effects of H_2O injection in Experiment 2, the abundances of methane, ethane and propane were relatively constant (within error) throughout both experiments (Figure 4.3). Gradual decreases in the concentrations of *n*-pentane and *n*-butane were observed with time in

Experiment 1 and during both stages of Experiment 2 (Table 4.1). Maximum overall losses in any given stage were <55% for *n*-pentane and <20% for *n*-butane. C_1 to C_5 *n*-alkane concentrations at 8.0 days in Experiment 1 were all ~25% lower than subsequent sampling events (Table 4.1). No such trend was observed in the Cl concentration over the same period and the same behavior was not observed in Experiment 2. This suggests that the solution may have been inhomogeneous with respect to the dissolved *n*-alkane mixture during the initial phase of Experiment 1, rather than addition of buffer-derived contaminant hydrocarbons. The pressure vessels are not equipped to ensure stirring/mixing of reaction cell contents and poor mixing of the starting solution and dissolved gases during loading the *n*-alkane mixture could have been responsible. Alternatively, operator error may have been responsible.

Concentrations of ethene and propene varied by less than a factor of 2 during both experiments (Figure 4.4). ΣC_5 alkenes initially increased with time during the first stage of Experiment 2 but did not vary substantially during the second stage or during Experiment 1. Gradual production of small amounts of methylpropane was observed in both experiments (Table 4.1).

3.2.3 ΣCO_2 and organic acid concentrations

The high concentrations of ΣCO_2 initially observed in both experiments (0.85–1.4mmol/kg, Table 4.1) most likely reflect thermocatalytic production of CO_2 from contaminant carbon in the mineral assemblage. Production during the early stages of experiments was observed in previous investigations which used the PPM assemblage (SEEWALD, 1994, 2001; MCCOLLOM and SEEWALD, 2003b). Thereafter however, ΣCO_2 increased gradually in both experiments, including Stage (2) of Experiment 2 (Figure 4.3). Excluding the first sampling events, mass balance on total dissolved carbon species (C_T, Table 4.1) indicates that C_T is

relatively invariant after the initial stages of both experiments. Therefore the mineral buffer cannot account for the gradual increases ΣCO_2 with time in both experiments. Sluggish oxidation of C_4 and C_5 hydrocarbons (as evidenced by their gradual decreases) is the most likely candidate to explain the formation of ΣCO_2 and is consistent with observations from previous experiments (SEEWALD, 2001). Increased ΣCO_2 likely contributed to the acidic pH (4.2 at 25°C and 1 atm) observed in Experiment 2.

Gradual accumulation of ethanoic and propanoic acid were observed throughout both experiments at concentrations <0.5mmol/kg (Table 4.1). Propanoic acid, though identified, was not present in quantifiable concentrations (above 0.1mmol/kg) except in the later part of Stage (1) of Experiment 2. As is the case for ΣCO_2, organic acids are also typical alteration products of *n*-alkane oxidation and formation of exclusively C_2 and C_3 *n*-alkanoic acids is consistent with the decomposition of C_4 and C_5 *n*-alkanes (SEEWALD, 2001). After injection of H_2O into the reaction cell contents in Experiment 2 (Table 4.1), the concentration of ethanoic acid decreased by <20% which is smaller than expected for the estimated dilution factor (2.1). In addition, decreases in *n*-pentane and *n*-butane (both ~70%) after dilution were smaller than expected. While the excess carbon present as ethanoic acid relative to that predicted by dilution (~0.4 mmol C/kg) fails to account for all C apparently lost from the C_4 and C_5 alkanes after dilution (~1.2 mmol C/kg), it does suggest that some oxidation of the latter occurred upon injection of H_2O, which was not sparged of O_2. Minor increases in propanoic acid and ΣCO_2 below analytical resolution may account for much of the remainder. Despite these losses, however, no significant changes in δ^2H values for *n*-butane and *n*-pentane were apparent, indicating that any decomposition had a minimal isotopic effect relative to the large observed variations in δ^2H values for these compounds.

4. DISCUSSION

4.1 Alkane-alkene equilibria

The extent to which ethane-ethene and propane-propene attained a state of thermodynamic equilibrium in both experiments can be demonstrated by calculating chemical affinities (A) according to the following relationship:

$$A \text{ (kJ/mol)} = -RT \ln (Q_r / K_{eq}) \qquad (6)$$

Where R is the universal gas constant, T is temperature in Kelvin, Q_r and K_{eq} are the reaction quotient and equilibrium constant for the form of reaction (1) in question at T and experimental pressure. Positive values of A indicate a thermodynamic drive for the reaction to proceed from left to right as written. At thermodynamic equilibrium, values of Q and K_{eq} are equal and the affinity reduces to zero. Uncertainties associated with affinity calculations are difficult to quantify, but based on errors in the derivation of $\Delta_r G^o$ values (SHOCK and HELGESON, 1990) calculated affinities of 0±4kJ/mol can in many cases be assumed to reflect attainment of equilibrium. As shown in Figure 4.5, thermodynamic affinities for ethane-ethene and propane-propene equilibria rapidly approached values within 4kJ/mol of zero in both experiments. These affinities were consistently maintained for both reactions with time and were rapidly restored following injection of H_2O in Experiment 2. Thus, as demonstrated by SEEWALD (2001), metastable thermodynamic equilibrium was attained between C_2 and C_3 *n*-alkanes and their corresponding terminal *n*-alkenes according to reaction (1) in both experiments.

Rapid equilibration of C_4 and C_5 *n*-alkanes and their corresponding *n*-alkenes is also likely to have occurred in both experiments, but it is difficult to demonstrate equilibrium for these reactions due to the potential for isomerization of alkenes. Numerous studies have shown that terminal alkene double bonds can migrate internally in aliphatic hydrocarbons (HOERING, 1984; WERES *et al.*, 1988; SISKIN *et al.*, 1990; LEIF and SIMONEIT, 1995, 2000; SEEWALD, 2001, 2001).

However, thermodynamic data for internal *n*-alkenes are lacking and analytical limitations precluded quantification of individual C_4 and C_5 *n*-alkene isomers in this study. For example, affinities for equilibrium between pentane and 1-pentene were in excess of -20kJ/mol for both experiments (Figure 4.4), which suggests an apparent excess of the latter relative to equilibrium predictions. This discrepancy is best explained by the presence of isomers other than 1-pentene (*i.e. cis*-2-pentene and *trans*-2-pentene) which contribute to the ΣC_5 *n*-alkene measurement. While contributions from branched C_5 alkene isomers (2-methylbut-1-ene, 3-methylbut-1-ene and 2-methylbut-2-ene) cannot be excluded, precursors for such compounds (likely branched C_5 alkanes) were not observed in substantial quantities in this study or previous experimental investigations (SEEWALD, 2001).

4.2 Reversible $^2H/^1H$ exchange and isotopic equilibrium

4.2.1 Alkane-alkene equilibrium and $^2H/^1H$ exchange

Experiments 1 and 2 demonstrate that the coupling of alkane-alkene equilibrium and water disproportionation (reactions (1) and (4)) represents an indirect but reversible mechanism for $^2H/^1H$ exchange between water and C_{2+} *n*-alkanes under hydrothermal conditions. H transfer to and from *n*-alkanes is facilitated by the sluggish nature of the stepwise oxidation pathway at the redox state employed, as demonstrated by the persistence of *n*-alkanes in solution. Relatively minor amounts of *n*-alkene are present at equilibrium relative to their corresponding *n*-alkanes (Table 4.1), and while kinetic isotope effects associated with the hydration of *n*-alkenes to alcohols are possible, they cannot explain the large reversible isotopic shifts demonstrated in the experiments. The losses (in excess of dilution) of *n*-butane and *n*-pentane observed upon injection of H_2O in Experiment 2 (Section 3.2.3) produced no noticeable change in δ^2H values

(Figure 4.2), suggesting that any inherent kinetic isotope effects are insignificant relative to the large shifts produced by alkane-alkene equilibrium.

According to SESSIONS *et al.* (2004), mechanisms by which $^{2}H/^{1}H$ ratios in organic molecules are altered by incorporation of exogenous H can be classified into five general categories. These consist of 'pure exchange' (where reactants and products are isotopically different but structurally and chemically identical), 'stereochemical exchange' (isotopic substitutions related to chiral inversions), 'constitutional exchange' (where reactants and products are constitutional isomers), and net transfer mechanisms such as 'addition' and 'loss' in which a reaction leads to a net transfer of H to or from the molecule. When viewed in isolation, the conversion of *n*-alkanes to *n*-alkenes technically implies an H 'loss' reaction (and the reverse 'addition') in the above classification. However, the requisite $H_{2(aq)}$ for alkene hydrogenation is ultimately provided by the disproportionation of water (reaction (4)) and both reactions (1) and (4) are rapid and reversible at elevated temperatures (SEEWALD, 1994, 2001). Hence, though the actual $^{2}H/^{1}H$ exchange takes place by a sequence of 'loss' and subsequent 'addition' transfer mechanisms, when coupled together reversible H transfer between water and *n*-alkanes is analogous to a 'pure exchange' mechanism in the absence of competing side reactions.

Overall exchange may be further enhanced by 'constitutional exchange' within the *n*-alkenes (C_3 and above) prior to hydrogenation back to their corresponding *n*-alkanes. It is widely acknowledged that terminal double bonds in aliphatic alkenes can rapidly migrate (*i.e.* isomerize) to internal positions under acidic conditions at elevated temperatures. SEEWALD (2001) observed rapid isomerization of 1-butene to all possible *n*-butene isomers on timescales of hours at 300°C following injection of the former into a PPM-buffered solution. Extensive double bond migration has also been demonstrated in several studies during hydrous pyrolysis of C_{10}, C_{14} and C_{16} terminal alkenes, leading to substantial ^{2}H incorporation where pure $^{2}H_2O$ was used (HOERING,

1984; WERES *et al.*, 1988; SISKIN *et al.*, 1990; LEIF and SIMONEIT, 1995, 2000). Double bond migration is known to be catalyzed by high H^+ activities (and possibly S species) and ionic strengths, suggesting it is the result of an ionic reaction mechanism (SISKIN *et al.*, 1990; LEIF and SIMONEIT, 2000). Variations in ΣC_5 *n*-alkene concentrations with time during both experiments (Figure 4.4) were minor, which suggests pentane may have achieved a state of metastable equilibrium with multiple individual *n*-alkene isomers though thermodynamic data do not exist to confirm this possibility. Hydrogenation of internal double bonds would therefore contribute to exchange on internal carbon positions in *n*-alkanes. As shown in Figure 4.6, both alkene isomerization and internal double bond hydrogenation imply that H at all carbon positions in an individual *n*-alkane is potentially exchangeable when considered within the framework of the overall alkane-alkene reaction.

A key observation from the experiments is the drastic difference in isotopic shifts for the C_{3+} hydrocarbons relative to ethane (Figure 4.2). While isomerization processes are undoubtedly a contributing factor, additional influences may also contribute to the rapid exchange in higher *n*-alkanes relative to ethane. One possible factor is that the equilibrium abundance of *n*-alkenes according to reaction (1) is substantially greater for C_{3+} *n*-alkanes than ethane. While in all cases metastable chemical equilibrium is attained, the rate at which isotopic exchange occurs will depend in part on the abundance of species involved in the exchange reaction. An examination of the equilibrium constants for reaction (1) shows that equilibrium constant for a given temperature are over an order of magnitude higher for the reactions of C_{3+} *n*-alkanes than ethane (Figure 4.7), implying equivalently lower alkane/alkene activity ratios at a given $a_{H2(aq)}$. Thus, higher alkane/alkene ratios may slow overall rates of exchange between water and *n*-alkanes.

4.2.2 Isotopic equilibrium and alkane δ^2H trends

Regardless of the δ^2H value of the solution, changes in the H isotope composition of the C_3 to C_5 *n*-alkanes slowed with time in both experiments (Figure 4.5). The absence of steady state δ^2H values, notwithstanding, this behavior provides compelling evidence that isotope equilibrium was being approached between some, if not all, of the *n*-alkanes and water. This is entirely consistent with the reversible nature of the alkane-alkene and water disproportionation reactions. When a reservoir of H (alkane H) is approaching isotopic equilibrium with another reservoir that is vastly in excess (*i.e.* water), the rate of change of $^2H/^1H$ ratios tends to follow pseudo first-order kinetics. SESSIONS *et al.* (2004, after ROBERTS and UREY, 1939) described this process by the general equation:

$$\frac{F_t - F_{eq}}{F_i - F_{eq}} = e^{-kt} \qquad (7)$$

Where F is the fractional abundance of ^2H ($= {}^2H/({}^2H + {}^1H)$) in the organic molecule *i*nitially, at time t, and at *eq*uilibrium and k refers to the rate constant of exchange. The equilibrium isotope fractionation factor can be derived from F_{eq} and the δ^2H_{H2O} value. The left hand side of this equation essentially represents the fraction of H atoms that remain unexchanged at time t, and at time i the left hand side equals 1 and approaches zero as $t \rightarrow \infty$. For *n*-alkanes, both the F_{eq} and k terms in the strictest sense will depend on the nature of carbon-bound H in question (*i.e.* methyl or methylene-bound H) and while equation (7) is exact for methane and ethane, more complex forms considering individual H positions are required to accurately model exchange in larger hydrocarbons (SESSIONS *et al.*, 2004). However, while the above equation refers to a 'pure exchange' scenario, the bulk H in C_{2+} *n*-alkanes will follow the form of equation (7) resulting in decreasing δ^2H changes in the bulk molecule per unit time as overall isotopic composition of alkane H nears an equilibrium state. Factors such as equilibrium alkane, alkene and H_2 activities,

alkene isomerization and other possible catalytic species, however, will undoubtedly influence the magnitude of the observed rate constant k for exchange (k_{obs}) in the bulk n-alkane molecule. Because of the exponential nature of the process, observed exchange rates will also vary depending on how far the bulk δ^2H value is from the equilibrium state at a given k_{obs}. Pseudo first-order behavior was not evident for ethane in the timescales of either experiment. However, it is possible that the sluggish rate of exchange compared to the C_{3+} n-alkanes is simply the manifestation of low ethene abundance and resulting effects on k_{obs} rather than proximity to equilibrium.

Significant advances have been made in theoretical predictions of equilibrium isotope fractionation factors ($\alpha_{o/w}$) between *o*rganic and *w*ater H (defined as the ratio of their respective isotopic ratios (R_o/R_w)) but these have been limited to low temperatures (KNYAZEV, 1992; SESSIONS *et al.*, 2004; SCHIMMELMANN *et al.*, 2006; WANG *et al.*, 2009a,b). Presently, little is known about the magnitude of $\alpha_{o/w}$ for C_1 to C_5 n-alkanes at conditions typical of hydrothermal systems and natural gas deposits. WANG *et al.* (2009a,b) recently derived estimates of $\alpha_{o/w}$ between 0 and 100°C for specific H moieties in a variety of organic compound classes, including linear alkanes and alkenes, using *ab initio* quantum mechanical calculations combined with experimental calibration to reduce uncertainties associated with the former. According to their estimates, C_1 to C_5 n-alkanes should be between 105 and 122‰ depleted in ^{2}H relative to V-SMOW at 100°C. Fractionation factors for the C_{3+} n-alkanes show little temperature dependence (<10‰) over the 100°C calibrated range (WANG *et al.*, 2009b). While isotopic equilibrium was not attained in either of the experiments presented here, minimum values of $\alpha_{o/w}$ can be estimated for propane, n-butane and n-pentane based on their final δ^2H values according to the expression:

$$\alpha_{o/w} = \frac{R_o}{R_w} = \frac{\delta^2 H_{alkane} + 1000}{\delta^2 H_{H2O} + 1000} \qquad (8)$$

Calculated minimum $\alpha_{o/w}$ values are 0.673, 0.708 and 0.739, respectively, for propane, *n*-butane and *n*-pentane in Experiment 1. In all likelihood the actual $\alpha_{o/w}$ values could be much higher but corresponding δ^2H_{alkane} values from Stage (1) of Experiment 2 (where equilibrium was approached from the opposite direction) only limit $\alpha_{o/w}$ values to less than ~4. Given the comparatively sluggish changes in ethane and methane δ^2H values, these calculations do not provide useful lower limits on $\alpha_{o/w}$ values for these compounds.

4.2.3 Variations in δ^2H_{meth}

Despite the lack of a comparable exchange mechanism, minor shifts (<30‰) were observed in methane δ^2H values that followed the direction of the higher hydrocarbons. While it is possible that these trends reflect sluggish exchange of methane H by some mechanism involving H abstraction and replacement, we cannot exclude additions of CH_4 from degradation of isotopically exchanged C_4–C_5 *n*-alkanes or other sources. Minor amounts of methane can be produced as an end product of the stepwise *n*-alkane oxidation pathway if decomposition of any acetic acid produced occurs by decarboxylation to CO_2 and CH_4 (KHARAKA *et al.*, 1983; PALMER and DRUMMOND, 1986; BELL *et al.*, 1994; SEEWALD, 2001). SEEWALD (2001) noted that ratios of CO_2 to CH_4 produced during *n*-heptane degradation were substantially higher under PPM-buffered conditions relative to more oxidizing conditions, indicating enhanced decarboxylation of acetic acid under more reducing conditions. Methane concentrations remained constant during both experiments except for the initial sample in Experiment 1 (Figure 4.3), and so contributions of methane within analytical error are required to have produced the observed isotopic shifts if exchange is not responsible. Based on the 2s analytical uncertainties of CH_4 concentrations, a maximum of ~0.3mmol CH_4/kg could have been produced in Experiment 1. Isotope mass balance indicates that to produce the observed +28‰ shift in δ^2H_{meth} values requires added CH_4 to

have a δ^2H value of ~380‰. Similar calculations for Stage (1) of Experiment 2 indicate that production of ~0.2mmol CH_4/kg (within 2s uncertainty) would require δ^2H_{meth} values of approximately -600‰ in the added CH_4. In both cases the required CH_4 compositions are between the δ^2H values of the water and the C_3–C_5 hydrocarbons. Production of methyl groups with such extreme $^2H/^1H$ ratios implies extensive intramolecular isotopic ordering in the heavily exchanged longer *n*-alkanes. Alternative possibilities include thermocatalytic production of labeled methane from carbon contaminants in the mineral buffer (SEEWALD, 1994). It is therefore equivocal whether the small shifts in CH_4 observed in this study truly represent reversible exchange.

4.3 Implications for natural systems

4.3.1 ^2H / ^1H ratios and abiogenesis in igneous environments

The abiogenic formation of aliphatic hydrocarbons during hydrothermal alteration of ultramafic crust has been extensively discussed (ABRAJANO *et al.*, 1988; SHERWOOD *et al.*, 1988; ABRAJANO *et al.*, 1990; CHARLOU *et al.*, 2002; PROSKUROWSKI *et al.*, 2006; MCCOLLOM and SEEWALD, 2007; KONN *et al.*, 2009). Though the exact mechanism for production of *n*-alkanes in highly-reducing crustal fluids is uncertain, it is assumed to be analogous to the industrial Fischer-Tropsch reaction and involves both reduction of inorganic carbon (CO_2 or CO) to methyl/methylene moieties and subsequent polymerization on a catalytic mineral surface (see review in MCCOLLOM and SEEWALD, 2007). In the last decade, $^2H/^1H$ ratios have been used to elucidate this phenomenon in addition to stable carbon isotope ratios (SHERWOOD LOLLAR *et al.*, 2002; FU *et al.*, 2007; PROSKUROWSKI *et al.*, 2008). Because of the larger relative mass difference between ^2H and ^1H, substantial kinetic H isotope fractionation could occur between homologues during abiogenic polymerization. As a result of investigations of putative abiogenic

C_1–C_4 *n*-alkanes recovered from saline fracture waters in crystalline basement rocks of the Canadian Shield, SHERWOOD LOLLAR *et al.* (2002) proposed a characteristic H isotope trend with carbon number whereby δ^2H_{meth} values (often below -400‰) are extremely low relative to the C_2–C_4 alkanes (δ^2H ~ -220 to -320‰), which show a trend of increasing δ^2H with increasing carbon number (Figure 4.8). This trend has subsequently been observed in several other Precambrian shield gases (SHERWOOD LOLLAR *et al.*, 2006, 2008) and is postulated to reflect preferential cleavage of ^{12}C–^{1}H bonds relative to ^{12}C–^{2}H bonds during the abiogenic polymerization process, putative kinetic effects associated with $^{13}C/^{12}C$ fractionation during polymerization.

The trends presented by SHERWOOD LOLLAR *et al.* (2002, 2006, 2008) have not been observed in purported abiogenic hydrocarbons from higher temperature settings (Figure 4.8), such as those present in vent fluids of the Lost City hydrothermal site (PROSKUROWSKI *et al.*, 2008) or those formed in abiotic synthesis experiments (FU *et al.*, 2007), leading to speculation that this reflects mechanistic differences. Based on the experimental observations of reversible exchange presented here, this discrepancy may actually reflect partial or complete alkane-water H isotope exchange in the latter cases. The recent advent of theoretical equilibrium fractionation factors for C_{2+} alkane H below 100°C mentioned above (WANG *et al.*, 2009a,b), combined with $\alpha_{o/w}$ values for CH_4-H_2O equilibrium (HORIBE and CRAIG, 1995) permits an evaluation of possible alkane-water equilibrium in the Canadian Shield gases and Lost City hydrothermal fluids. Using published δ^2H_{H2O} values, apparent values of $\alpha_{o/w}$ can be calculated from equation (8) for the Canadian shield (Kidd Creek Mine, SHERWOOD LOLLAR *et al.*, 2002) and Lost City vent fluid *n*-alkanes (PROSKUROWSKI *et al.*, 2008) at the reported temperatures in these studies.

As shown in Figure 4.9, the Kidd Creek Mine *n*-alkanes are far too depleted in ^{2}H relative to theoretical predictions for isotopic equilibrium with water. $\alpha_{o/w}$ for other low temperature (<100°C) microbial/abiogenic LMW *n*-alkanes from crystalline rock aquifers in the

Witwatersrand Basin, S. Africa (WARD *et al.*, 2004; LIN *et al.*, 2006; ONSTOTT *et al.*, 2006; SHERWOOD LOLLAR *et al.*, 2008) and Fennoscandian Shield (NURMI *et al.*, 1988; SHERWOOD LOLLAR *et al.*, 1993a,b) are also much lower than equilibrium predictions at the temperatures likely experienced by these systems. As previously suggested by SHERWOOD *et al.* (1988) and SHERWOOD LOLLAR *et al.* (1993b), the most likely explanation for the extremely negative δ^2H values of these hydrocarbons is that they formed by abiogenic or microbial reductive processes (likely at low temperatures) involving extremely ^2H-depleted $H_{2(aq)}$ (δ^2H_{H2} values as low as -695‰) that is present in these systems (SHERWOOD *et al.*, 1988; SHERWOOD LOLLAR *et al.*, 1993b; LIN *et al.*, 2006). Though some isotopic exchange cannot be discounted, the apparent lack of isotopic equilibrium between water and alkane H in these gases is reasonable given that the alkane-alkene mechanism may not be able to effectively promote H exchange in C_{2+} hydrocarbons at the low temperatures of the these systems (~35–60°C, SHERWOOD LOLLAR *et al.*, 2008). The drastic decrease in alkene stability according to reaction (1) with decreasing temperature (Figure 4.7), coupled with potential kinetic barriers for chemical equilibrium inherent at the low temperatures of these systems may simply preclude attainment of isotopic equilibrium despite the exceedingly long timescales of fluid isolation in these systems (on the order of tens of Ma, LIPPMANN *et al.*, 2003).

In stark contrast to the Precambrian shield gases, abiogenic C_1 to C_3 *n*-alkanes in vent fluids at Lost City are much more ^2H-enriched (δ^2H of -119 to -171‰, PROSKUROWSKI *et al.*, 2008) and at odds with the extremely negative δH values of $H_{2(aq)}$ there (-600 to -700‰, PROSKUROWSKI *et al.*, 2006) by the above reasoning. While these differences could reflect higher temperatures of abiogenesis or mechanistic effects, a likely explanation is that partial or near-complete alkane-water exchange has erased any highly ^2H-depleted signatures. $\alpha_{o/w}$ values for many of the Lost City fluids are slightly low relative to predictions (Figure 4.9) but are much

closer to apparent alkane-water equilibrium than the Kidd Creek gases and $\alpha_{ethane/w}$ values are in agreement with equilibrium values in some of the lower temperature fluids. The likelihood of ethane-water isotopic equilibrium mediated by reaction (1) is further supported by measurements of ethene concentrations in these fluids (1–40nmol/kg, PROSKUROWSKI *et al.*, 2008). Using the range of endmember ethane, ethene and H_2 concentrations reported by PROSKUROWSKI *et al.* (2008) apparent temperatures of ethane-ethene equilibrium according to reaction (1) are all >300°C, indicating substantial ethane-ethene disequilibrium at the observed vent temperatures (<91°C). However, there is extensive theoretical evidence to suggest that Lost City fluids have cooled conductively during upflow and are considerably hotter (in the vicinity of 250°C) at depth (ALLEN and SEYFRIED, 2004; FOUSTOUKOS *et al.*, 2008). It is therefore possible that the ethane-ethene reaction records higher temperatures deeper in the hydrothermal system due to a lack of re-equilibration upon cooling, as has been observed in the Middle Valley hydrothermal system (CRUSE and SEEWALD, 2006). The discrepancy of apparent isotopic equilibrium between ethane and water at the lower temperatures of venting but lack of chemical ethane-ethene equilibrium could be explained if alkane $\alpha_{o/w}$ values are similarly insensitive to changing temperature above 100°C. While the alkane-alkene mechanism cannot promote CH_4-H_2O exchange, the ^{2}H-enriched nature of CH_4 is also suggestive of isotopic equilibrium at temperatures significantly greater than measured values. Many of the $\alpha_{o/w}$ values for CH_4 at Lost City (0.849–0.877, Figure 4.9) are higher than the predicted values of HORIBE and CRAIG (1995) below 100°C, but are suggestive of CH_4-H_2O isotopic equilibrium within a temperature range of 140–280°C. While the derivation of HORIBE and CRAIG (1995) lacks experimental verification, this range is consistent with the above estimates of reaction zone conditions (ALLEN and SEYFRIED, 2004; FOUSTOUKOS *et al.*, 2008). Furthermore, higher temperature isotopic equilibrium between the pairs CH_4-H_2 and H_2O-H_2, as proposed by PROSKUROWSKI *et al.* (2006), inherently implies CH_4-H_2O equilibrium.

Results of the experiments suggest that, with increasing temperatures, alkane-alkene equilibria may promote H isotopic exchange and possibly equilibrium between abiogenic *n*-alkanes and water. In other ultramafic-hosted hydrothermal systems where abiogenic hydrocarbon formation has been proposed, such as Rainbow and Logatchev (HOLM and CHARLOU, 2001; CHARLOU *et al.*, 2002; SCHMIDT *et al.*, 2007), reaction zone temperatures are considerably higher than Lost City. Maximum measured vent fluid temperatures at both of these locations are in excess of 350°C and reaction zone conditions are thought to be nearer 400°C (ALLEN and SEYFRIED, 2003; SEYFRIED *et al.*, 2004). The experiments presented here suggest substantial H isotope exchange between the C_{2+} alkanes and water can occur on timescales of months to years at 323°C, and even greater rates of isotope exchange are likely at the higher temperatures of these systems due to the enhanced stability of alkenes (Figure 4.7) according to reaction (1). Although greater alkene abundances could enhance overall stepwise oxidation of *n*-alkanes according to the mechanism of SEEWALD (2001), the highly reducing conditions evident in these systems (SEYFRIED *et al.*, 2004) may sufficiently retard oxidation such that, as was observed in the experiments presented here, isotopic exchange proceeds much faster than competing chemical degradation reactions. Given that estimates of crustal residence times for hydrothermal solutions based on radioisotope methods (KADKO, 1996; KADKO and BUTTERFIELD, 1998) and geophysical considerations (FISHER, 2003) are on the order of years, sufficient time for isotopic equilibrium may be provided. Though H isotope data are lacking for C_{2+} alkanes at sites other than Lost City, the demonstration of ethane-ethene and propane-propene equilibria at reaction zone conditions in the sedimented Middle Valley hydrothermal system (CRUSE and SEEWALD, 2006) suggests that alkane-water exchange may be commonplace in hydrothermal fluids with measurable C_{2+} *n*-alkanes. Hence, the alkane ^{2}H-depletions noted by SHERWOOD LOLLAR *et al.* (2002) are unlikely to be evident among abiogenic hydrocarbons in seafloor

hydrothermal fluids and may be a unique feature of Precambrian Shield gases. This is consistent with the only experimental study to date on H isotope variations during Fischer-Tropsch-type synthesis, which did not observe any ^{2}H depletion in methane relative to ethane at 400°C (Figure 4.8). Should such depletions be noted in hydrocarbons from higher temperature hydrothermal systems, ambiguities could arise if partial exchange has occurred only in the higher (C_{2+}) hydrocarbons but exchange in methane has been sluggish.

4.3.2 $^{2}H/^{1}H$ signatures in thermogenic hydrocarbons

In environments where hydrocarbon formation is occurring by thermogenic processes, the potential for alkene-mediated H exchange between LMW *n*-alkanes and water will clearly depend on the availability of aqueous fluids, in addition to redox and temperature. Water is a ubiquitous feature in sedimentary basins and there is substantial evidence to suggest it plays an important role in both the thermal maturation of sedimentary organic matter and the migration of generated light ($<C_5$) hydrocarbons (LEWAN *et al.*, 1979; TISSOT and WELTE, 1984; LEWAN, 1997). In addition, oil and gas deposits are invariably associated with basinal brine fluids of connate or infiltrated paleometeoric origin (KHARAKA and CAROTHERS, 1986). LMW *n*-alkanes are among the more soluble constituents of petroleum and, in some cases, can be extensively removed from discrete hydrocarbon phases by processes such as water washing (TISSOT and WELTE, 1984; HUNT, 1996). The efficacy of exchange will also depend on the redox state of aqueous fluids in which hydrocarbons are dissolved due to the nature of the alkane-alkene reaction. Though buffered redox conditions are a necessary experimental tool, they are not a prerequisite for oxidation of alkanes to alkenes (SEEWALD, 2001). All that is required is the availability of sufficient oxidizing agents to consume H_2 (which would accumulate given the dominating effect of organic matter of fluid redox) and create a thermodynamic drive that maintains alkene stability.

SEEWALD (2001) reviewed several possible oxidants that are known to be present in sedimentary basins, including SO_4, which is present in evaporite minerals and as a major ion in basinal brines (KHARAKA and CAROTHERS, 1986), Fe(III)-bearing minerals such as aluminosilicates, hematite and magnetite (SURDAM and CROSSEY, 1985; SURDAM *et al.*, 1993) and pyrite (which can react with H_2 and CO_2 to form $FeCO_3$ and H_2S), all of which can consume H_2 by being reduced. If conditions are sufficiently reducing such that stepwise oxidation occurs much slower than alkane-alkene equilibration, then H exchange between undegraded alkanes and water could conceivably proceed. The temperature dependence of alkane/alkene ratios will also influence the likelihood of exchange. However, while light ($<C_{10}$) hydrocarbons typically form below ~200°C where alkene stability may be orders of magnitude lower (Figure 4.7) according to reaction (1), the slow timescales of thermal maturation and migration in petroleum-producing systems (on the order of Ma) may be sufficient to facilitate isotopic exchange.

Despite the advent of compound-specific $^2H/^1H$ analyses, there have been relatively few published studies of δ^2H values of thermogenic C_2–C_5 alkanes. However, common features of thermogenic natural gases reported to date are gradually increasing δ^2H values with increasing carbon number (see Figure 4.8) and overall ^2H-enrichment in the homologous series with increasing thermal maturity (SCHOELL, 1983; BARKER and POLLOCK, 1984; WHITICAR *et al.*, 1985; SHERWOOD LOLLAR *et al.*, 2002; EDWARDS *et al.*, 2007; BOREHAM *et al.*, 2008). As is the case for the higher *n*-alkanes, this is traditionally viewed as the kinetic isotope effect of C–C bond cleavage which favors reaction of ^2H-depleted larger molecules in cracking reactions (SCHIMMELMANN *et al.*, 2004). $C(^2H^1H)$–$C(^1H_2)$ bonds are stronger, and therefore considered slower to react, than $C(^1H_2)$–$C(^1H_2)$ bonds and quenching of generated alkyl radicals is likely to favor incorporation of ^1H relative to ^2H (SACKETT, 1978; SCHIMMELMANN *et al.*, 2004).

Both the typical ^2H depletions reported for thermogenic gases and the trend of gradually increasing δ^2H with carbon number are, however, equally consistent with isotopic equilibration with water H. Taking the example of thermogenic wet (C_{2+} rich) gases from southwestern Ontario reported by SHERWOOD LOLLAR *et al.* (1994, 2002), C_{2+} alkanes there are depleted in ^2H relative to average saline groundwaters of this region by between 70–140‰ (apparent $\alpha_{o/w}$ values of approximately 0.85 to 0.92). This depletion overlaps the range of equilibrium fractionation factors (Figure 4.9) derived by WANG *et al.* (2009b) at 100°C ($\alpha_{o/w}$ values of 0.87–0.89). If the equilibrium $\alpha_{o/w}$ values for alkane H are similarly insensitive to temperature up to 200°C, the likely temperatures of maturation (SHERWOOD LOLLAR *et al.*, 1994), the compositions of these gases would be consistent with equilibrium exchange with water. In addition to these depletions, the gradual increase of ~0–30‰ with each increase in carbon number that is typical of all reported thermogenic gases (SHERWOOD LOLLAR *et al.*, 2002; EDWARDS *et al.*, 2007; BOREHAM *et al.*, 2008) could be explained by the predicted chain length dependency of alkane-water equilibrium H isotope effects. According to the data of WANG *et al.* (2009b), calculated $\alpha_{o/w}$ values for ethane/water (0.878), propane/water (0.886), *n*-butane/water (0.890) and *n*-pentane/water (0.895) equilibrium at 100°C also increase with carbon number. While the magnitude of these offsets increases at lower temperatures (*cf.* Figure 4.9) the trend does not change. This chain length dependency is related to the inductive electron-donating (+I) effect of terminal methyl ($-CH_3$) groups on adjacent internal methylene ($-CH_2-$) positions which increases stiffness in C–H bonds of the latter, thereby favoring slightly greater degrees of ^2H substitution (HARTSHORN and SHINER, 1972; WANG *et al.*, 2009b). With increasing chain lengths beyond *n*-pentane, this effect gradually decreases due to increasing quantities of internal methylene groups (with uniform $\alpha_{o/w}$ values) but it has the capability to produce strikingly similar trends to those observed in thermogenic LMW hydrocarbons.

While hydrocarbons beyond C_5 were not examined in this investigation, experimental evidence suggests that alkane-alkene reactions could also mediate extensive H exchange in much longer chain alkanes. In a series of hydrous pyrolysis experiments using pure ^2H_2O at 330–350°C, LEIF and SIMONEIT (2000) demonstrated extensive double bond migration and concomitant ^2H incorporation during reaction of the terminal alkenes 1,13-tetradecadiene ($C_{14}H_{26}$) and 1-hexadecene ($C_{16}H_{32}$) with immature organic-rich shale. These short experiments (<72h) were conducted in traditional fixed volume reactors without intentional redox buffering but minor amounts of ^2H-labeled alkanes were observed to form by reduction of these probe molecules. This strongly suggests that reversible alkane-alkene reactions enabled H isotope exchange in C_{10}–C_{16} hydrocarbons in the presence of the highly reducing shale and its kerogen complement, suggesting that this mechanism is not limited to the shorter chain homologues. This is especially significant given the clear chain length dependency of exchange rates observed in the experiments here. It has become increasingly recognized in recent years that δ^2H values of bulk sedimentary organic matter and its individual hydrocarbon constituents initially increase during thermal maturation but approach relatively a constant offset of ~80–110‰ below that of associated waters, even with further increases in thermal maturity (SCHIMMELMANN *et al.*, 1999, 2001, 2006). The estimation of compound specific fractionation factors between alkane H and water lead WANG *et al.* (2009b) to conclude that this offset can best be explained by isotopic exchange toward equilibrium between these two H reservoirs. While SCHIMMELMANN *et al.* (1999, 2001) argued that this exchange likely takes place as a result of reactions largely limited to the maturation process (*e.g.* cracking, isomerization, rearrangement etc.), the alkane-alkene mediated exchange demonstrated here could easily occur subsequent to the main stage of oil formation and would also allow for comprehensive exchange of all aliphatic H in hydrocarbons.

Further constraints are required to confirm that the composition of thermogenic LMW hydrocarbons reflects isotopic equilibrium with associated waters. These include detailed evaluations of the isotopic composition of individual thermogenic gas constituents and associated waters in the context of their thermal history, in addition to better estimates of alkane-water fractionations at higher temperatures to confirm if temperature independence. However, the observations of near equilibrium isotopic compositions in at least some thermogenic gases and the increased recognition of exchange in higher molecular weight petroleum constituents provides compelling evidence that the H isotopic composition of thermogenic hydrocarbons may be governed by equilibrium rather than kinetic isotope effects both during maturation processes. This has important implications for the use of hydrogen isotopes as maturity indicators and correlation parameters for thermogenic hydrocarbons (TANG *et al.*, 2005, 2007). Whereas the extent of isotopic fractionation during kinetically controlled processes will vary as a function of time and temperature, equilibrium fractionation will only vary as a function of temperature and to a lesser extent pressure.

5. CONCLUSIONS

This chapter presents experimental evidence of $^{2}H/^{1}H$ exchange between low molecular weight ($<C_5$) aqueous *n*-alkanes and water under hydrothermal conditions. Transfer of H isotopes is mediated by rapid reversible metastable equilibria between *n*-alkanes and their corresponding *n*-alkenes, coupled with the disproportionation of water which ultimately provides requisite H for hydrogenation. In the absence of competing subsequent oxidation of *n*-alkenes, rates of exchange are sufficiently rapid that drastic changes in alkane $\delta^{2}H$ values timescales of years at 323°C. Much faster rates of exchange are observed for longer chains alkanes due to factors such as higher equilibrium alkene abundances and internal isomerization of terminal *n*-alkenes prior to hydrogenation. The evidence for exchange in methane is equivocal, but if it occurs, rates are substantially slower than the higher homologues.

Based on recent theoretical estimates of equilibrium fractionation between hydrocarbon H and water H, previously reported gases from the Canadian Shield of putative abiogenic origin are too depleted in ^{2}H relative to equilibrium fractionation effects and are thus unlikely to have experienced extensive exchange with water. This is consistent with thermodynamic predictions of exceedingly high equilibrium alkane/alkene ratios which would hinder exchange at the low temperatures (<60°C) experienced by these aqueous hydrocarbons. Abiogenic hydrocarbons from the higher temperature Lost City hydrothermal field are, in contrast, more likely to have undergone exchange following synthesis at reaction zone conditions. The proximity of many of these hydrocarbon $^{2}H/^{1}H$ ratios to values predicted for isotopic equilibrium with water suggests that the observed disparity between these and the Canadian Shield hydrocarbons reflects exchange effects subsequent to abiogenesis. Though further confirmation is needed, the H isotopic composition of many thermogenic gases is also suggestive isotopic equilibrium with water, rather than kinetic isotope effects related to thermal maturation. This is consistent with the

emerging realization of extensive exchange in higher petroleum hydrocarbons that have experienced elevated temperatures.

ACKNOWLEDGEMENTS

The author wished to thank Prof. Alex Sessions for kindly undertaking the hydrogen isotopic analyses of water samples from this study. Sean Sylva carried out hydrogen isotope analyses of hydrocarbon samples. This work was funded by DOE Grant DE-FG02-97ER14746 and NSF grant OCE-0549829.

Table 4.1 Concentrations of aqueous species during heating of C_1 to C_5 *n*-alkane mixtures at 323°C and 35MPa with a pyrite-pyrrhotite-magnetite (PPM) mineral assemblage

Time[a]	Cl	H_2	ΣH_2S	pH	ΣCO_2	CH_4	Ethane	Ethene	Propane	Propene	*n*-Butane	methyl propane	*n*-Pentane	ΣC_5 alkenes[b]	Ethanoic acid	Propanoic acid	C_T[c]
days	mm	mm	mm	(25°C)	mm	mm	mm	mm	mm	mm	mm	mm	mm	mm	mm	mm	mm
Experiment 1:								Initial fluid enriched in ^2H									
8.0	213	0.26	na	na	0.85	3.85	2.16	na	1.05	2.6E-04	0.974	0.01	0.346	0.031	na	na	-
47.1	210	0.49	na	na	1.3	5.25	2.90	5.9E-05	1.39	4.9E-04	1.27	0.04	0.425	0.016	0.25	<0.1	24
112.1	210	0.64	na	na	1.7	5.37	2.88	9.3E-05	1.30	7.1E-04	1.15	0.13	0.370	0.040	0.18	<0.1	24
Experiment 2:								**Stage (1)** Initial fluid (31.6g) depleted in ^2H									
4.0	9.9	0.33	na	na	1.4	3.97	2.11	8.3E-05	1.09	4.1E-04	0.784	0.013	1.22	0.054	0.18	<0.1	-
18.8	10.1	0.27	na	na	1.9	4.01	2.05	5.1E-05	1.13	7.1E-04	0.845	0.018	1.39	0.073	0.23	<0.1	25
114.9	10.5	0.29	na	na	3.3	3.99	2.16	8.4E-05	1.08	1.0E-03	0.755	0.027	1.09	0.22	0.45	0.12	25
218.8	11.5	0.29	10.6	na	5.6	4.14	2.09	7.1E-05	0.991	7.2E-04	0.638	0.028	0.906	0.30	0.49	0.10	27
226.0								**Stage (2)** Injected 15.0g of ^2H_2O-spiked water into reaction cell containing 13.6g H_2O									
227.8	9.7	0.27	na	na	2.5	1.87	0.937	2.5E-05	0.413	3.4E-04	0.218	0.010	0.257	0.10	0.41	<0.1	11
243.9	9.9	0.27	na	na	2.9	1.98	0.990	1.6E-05	0.433	3.2E-04	0.234	0.011	0.271	0.11	0.36	<0.1	12
287.9	9.9	0.65	na	4.2	3.2	1.97	0.962	1.7E-05	0.422	3.4E-04	0.211	0.010	0.220	0.10	0.36	<0.1	12
340.8	na	na	na	na	na	na	na	na	na	na	na	na	na	na	na	na	-

mm = mmol/kg fluid. [a]Time after the initial heatup of experiment. [b]ΣC_5 alkenes = sum of all coeluted C_5 alkene isomers eluting at the retention time of *n*-pent-1-ene. [c]C_T = sum of all dissolved carbon species. na = not analyzed.

Table 4.2 Hydrogen isotope compositions of dissolved C_1 to C_5 *n*-alkanes and corresponding solutions during heating with a pyrite-pyrrhotite-magnetite (PPM) mineral assemblage

Time[a] **days**	Temp. °C	Solution δ^2H_{H2O} (‰)	Methane δ^2H (‰)	Ethane δ^2H (‰)	Propane δ^2H (‰)	*n*-Butane δ^2H (‰)	*n*-Pentane δ^2H (‰)
Experiment 1: Initial fluid enriched in ^2H							
0.0	-	507	-194	-142	-113	-136	-93.9
8.0	324	na	-194	-144	-100	-100	-54.0
47.1	324	na	-190	-115	-14.6	-4.87	28.7
112.1	323	na	-162	-91.7	14.4	66.7	114
Experiment 2: Initial fluid depleted in ^2H							
0.0	-	-802	-165	-142	-113	-136	-93.9
4.0	323	na	-165	-144	-156	-157	-116
18.8	323	na	-166	-152	-190	-198	-174
114.9	323	na	-188	-186	-346	-408	-398
218.8	323	-798	-187	-233	-430	-490	-473
226.0		---------- Injected ^2H_2O-spiked solution ----------					
227.8	323	352	-215	-248	-429	-489	-478
243.9	323	na	-212	-248	-363	-401	-393
287.9	323	na	-213	-238	-249	-246	-243
340.8	323	na[b]	-208	-219	-158	-118	-83.7

[a]Time after the initial heatup of experiment. Initial (time zero) δ^2H values are those prior to loading of materials into reaction cell. [b]The δ^2H_{H2O} value determined after termination of Expt. 2 was +354‰.

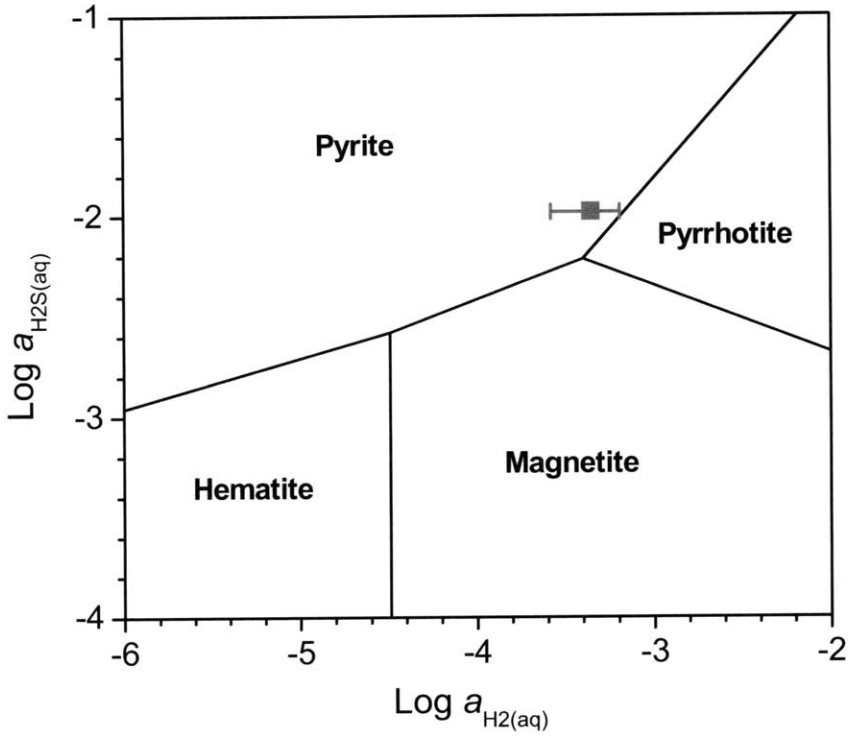

Figure 4.1. Activity diagram showing the phase relations in the system Fe-S-O-H at 325°C and 35MPa. Requisite data for the construction of this figure were obtained from the SUPCRT92 database (JOHNSON *et al.*, 1992). Because pyrrhotite is non-stoichiometric, equilibrium constants for reactions (2) and (3) in Section 2.1 reduce to $a_{H2(aq)}/a_{FeS(s)}^{1.5}$ and $a_{H2S(aq)}^{4}/a_{FeS(s)}^{2}$. To calculate equilibrium values of $a_{H2(aq)}$ and $a_{H2S(aq)}$ requisite activities for pyrrhotite at conditions were calculated from the data of TOULMIN and BARTON (1964). The *horizontal gray line* denotes the range of aqueous H_2 activities observed during both Experiments 1 and 2. The *gray square* denotes the concentration of H_2S measured in a single sample at 218.8 days in Experiment 2.

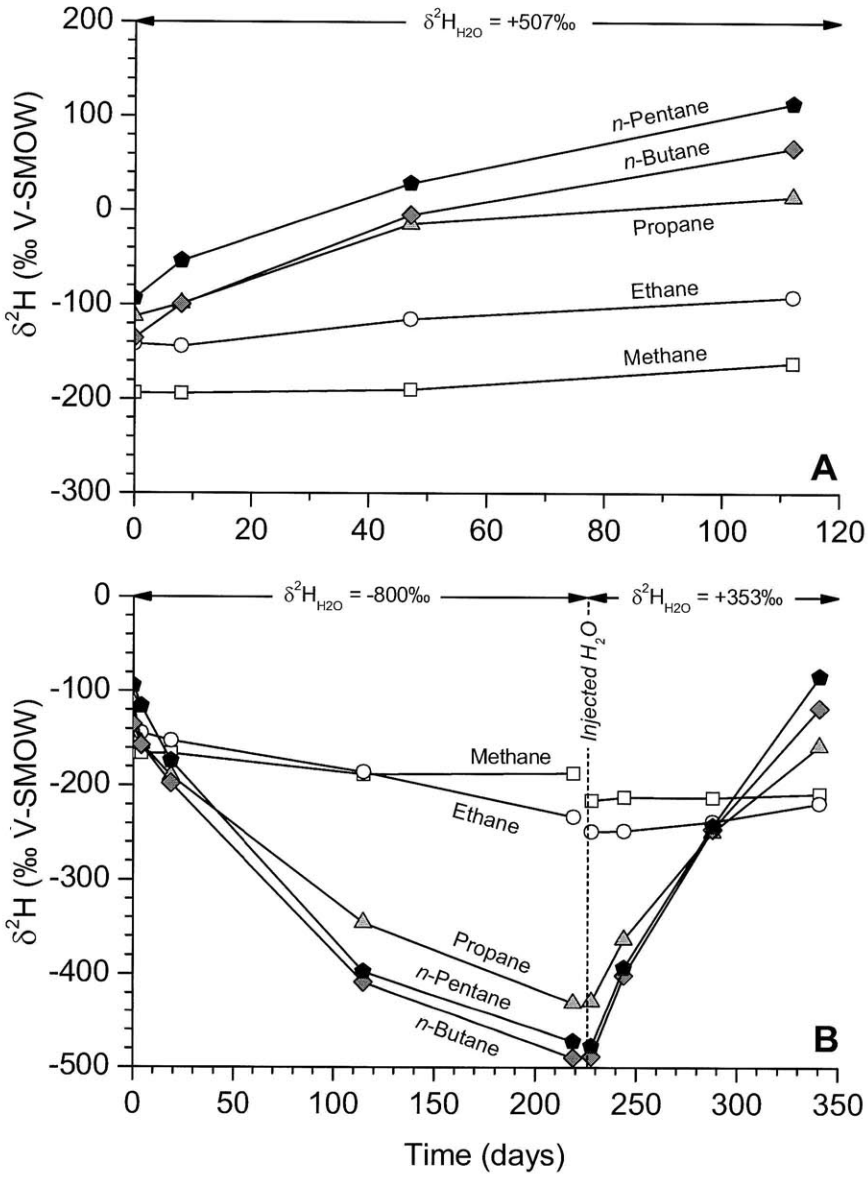

Figure 4.2. C_1 to C_5 *n*-alkane δ^2H values from Experiment 1 **(A)** and Experiment 2 **(B)** as a function of time at 323°C and 35MPa. The vertical dashed line at 226 days in Experiment 2 represents injection of ^2H-spiked water to raise the δ^2H_{H2O} value of the solution in the reaction cell. The pooled standard deviation of all *n*-alkane δ^2H analyses (±6‰, 2s) is smaller than the data symbols. Mean values of δ^2H_{H2O} are plotted for each experimental stage.

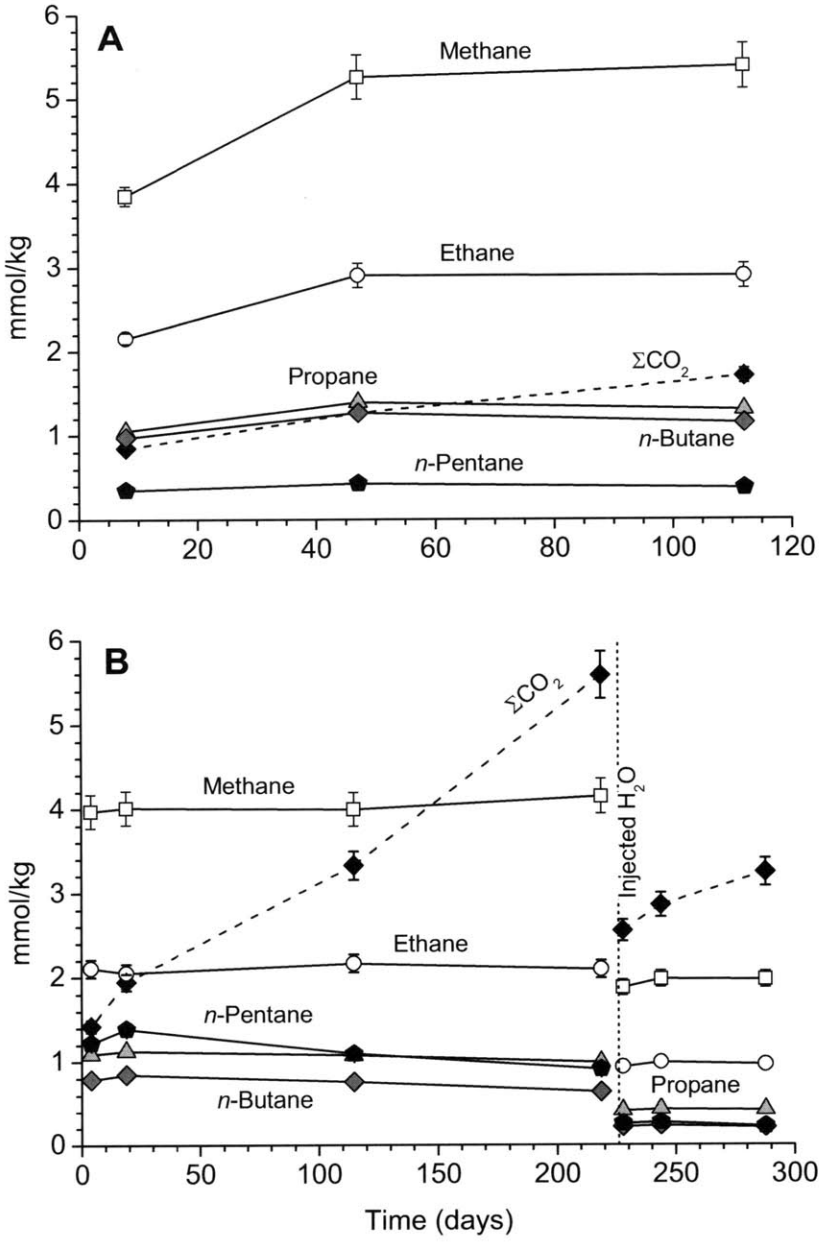

Figure 4.3. Concentrations of C_1 to C_5 *n*-alkanes and ΣCO_2 from Experiment 1 **(A)** and Experiment 2 **(B)** as a function of time at 323°C and 35MPa. The vertical dashed line at 226 days in Experiment 2 represents injection of ^2H-spiked water. Error bars represent 2s analytical uncertainties, which are smaller than the data symbols for propane, *n*-butane and *n*-pentane. Concentrations of dissolved species were not monitored after 300 days in Experiment 2.

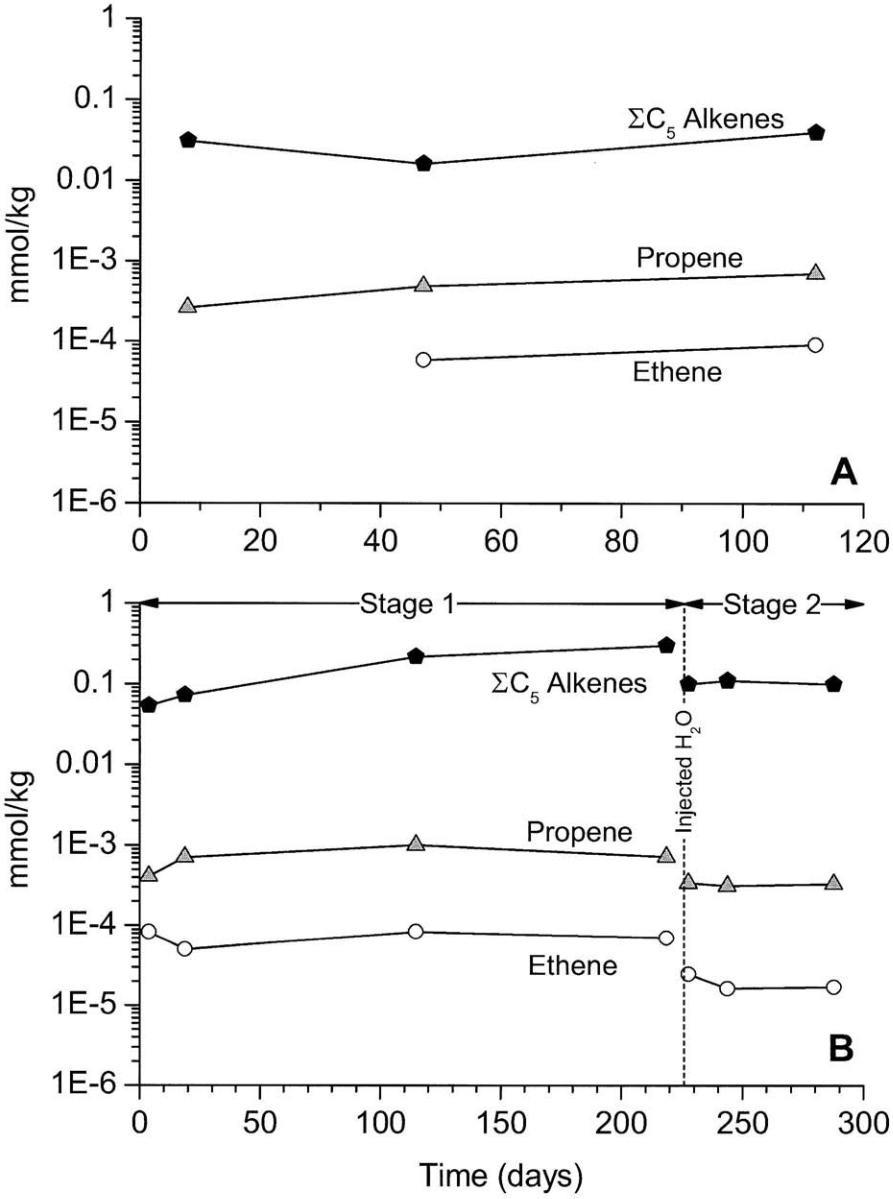

Figure 4.4. Concentrations of C_2, C_3 and C_5 *n*-alkenes in Experiment 1 **(A)** and Experiment 2 **(B)** as a function of time at 323°C and 35MPa. The vertical dashed line at 226 days in Experiment 2 represents injection of ^{2}H-spiked water. Concentrations of dissolved species were not monitored after 300 days in Experiment 2.

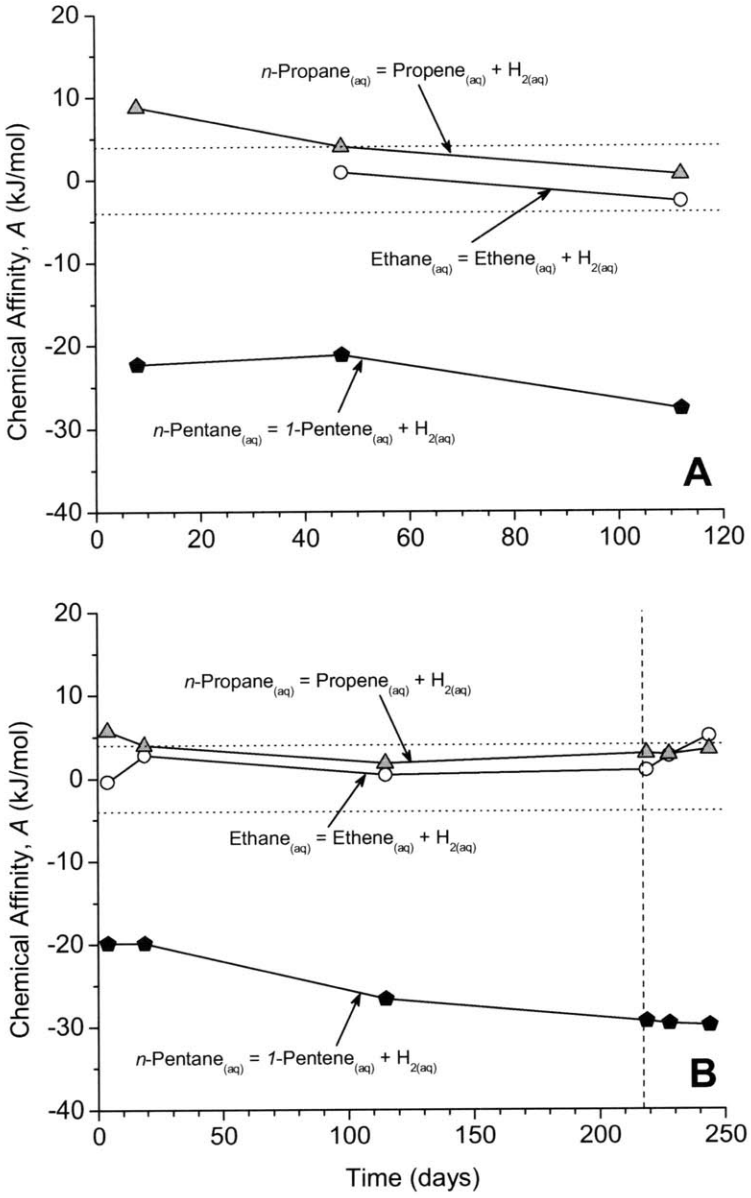

Figure 4.5. Chemical affinities (calculated using equation (6)) for oxidation of C_2, C_3 and C_5 *n*-alkanes to their corresponding terminal *n*-alkenes according to reaction (1) as a function of time at 323°C and 35MPa in Experiment 1 **(A)** and Experiment 2 **(B)**. The vertical dashed line at 226 days in Experiment 2 represents injection of ^{2}H-spiked water. Horizontal dotted lines represent the uncertainty associated with attainment of equilibrium (0±4kJ/mol, SHOCK and HELGESON, 1990).

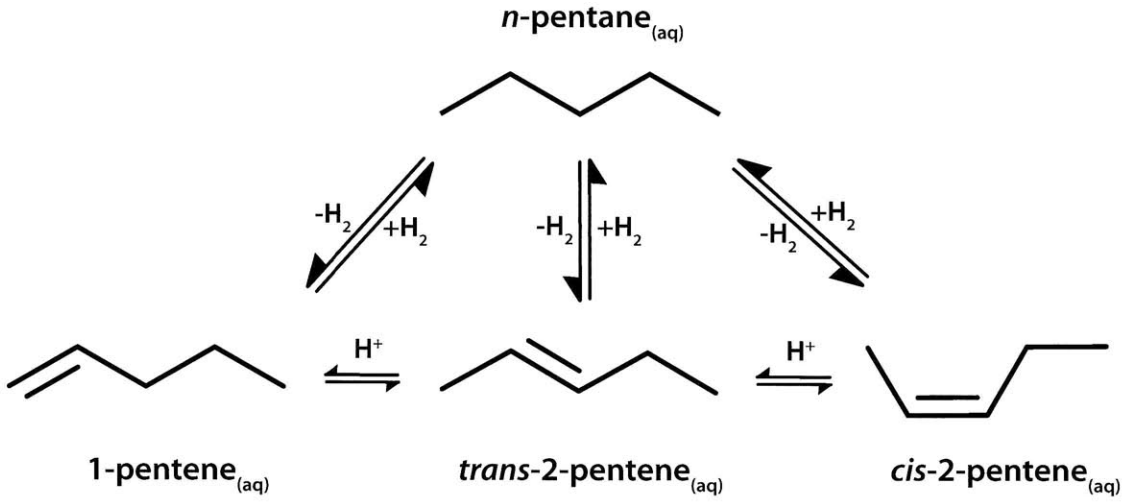

Figure 4.6. Proposed mechanism for the reversible equilibration of *n*-pentane with individual pentene isomers allowing exchange of all H atoms at each carbon position throughout the molecule. Similar mechanisms could be drawn for other *n*-alkanes with multiple potential alkene isomers.

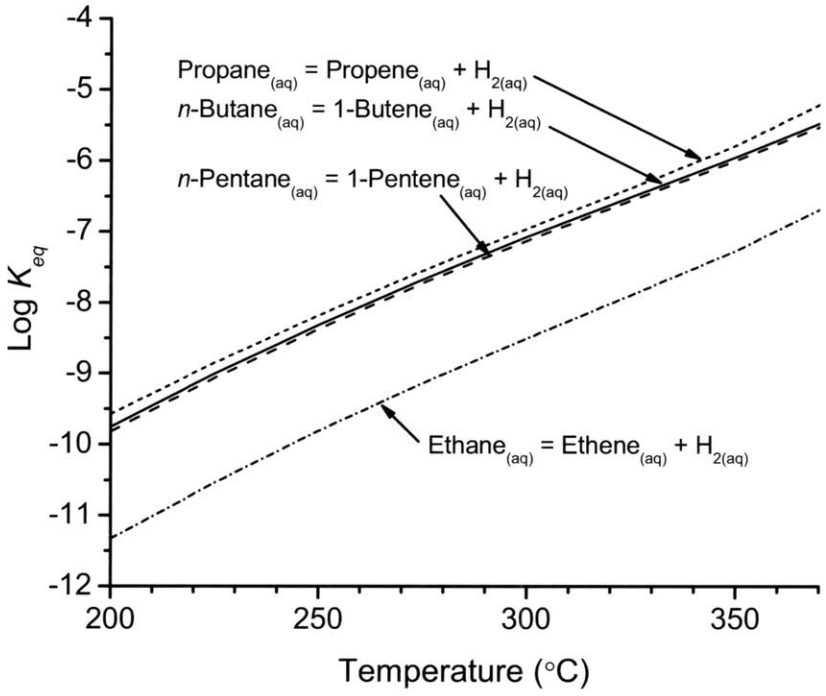

Figure 4.7. Equilibrium constants (K_{eq}) for reactions between C_2 to C_5 *n*-alkenes and their corresponding terminal *n*-alkenes as a function of temperature. Requisite data for the construction of this figure are taken from the SUPCRT92 database (JOHNSON *et al.*, 1992) with additional data from SHOCK and HELGESON (1990).

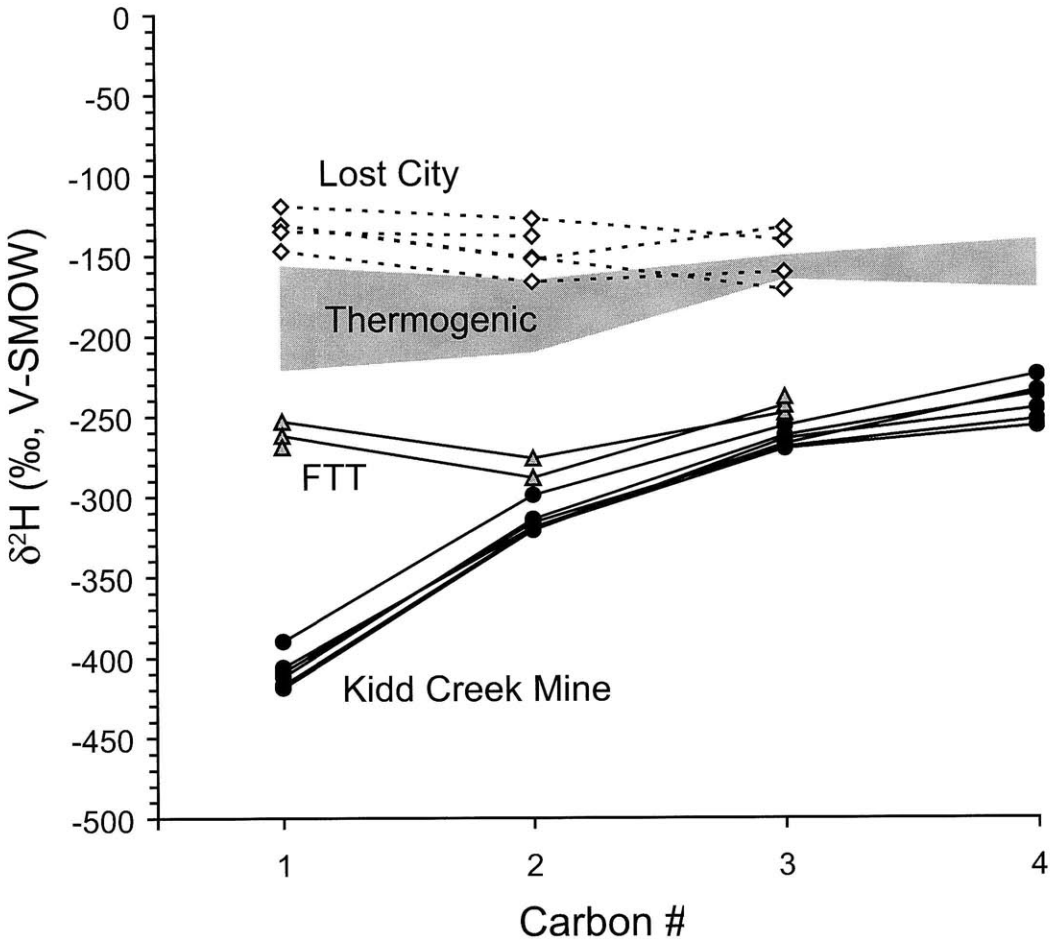

Figure 4.8. Isotopograms showing the δ^2H values of *n*-alkanes as a function of chain length for the Kidd Creek Mine abiogenic gases (*black dots*, SHERWOOD LOLLAR *et al.*, 2002), thermogenic gases from Southwest Ontario gas fields (*gray area*, SHERWOOD LOLLAR *et al.*, 1994, 2002), Lost City vent fluids (*open diamonds*, PROSKUROWSKI *et al.*, 2008) and alkanes produced by experiment aqueous Fischer-Tropsch-type (FTT) synthesis at 400°C (FU *et al.*, 2007). δ^2H values for *n*-butane were not reported for the latter two studies.

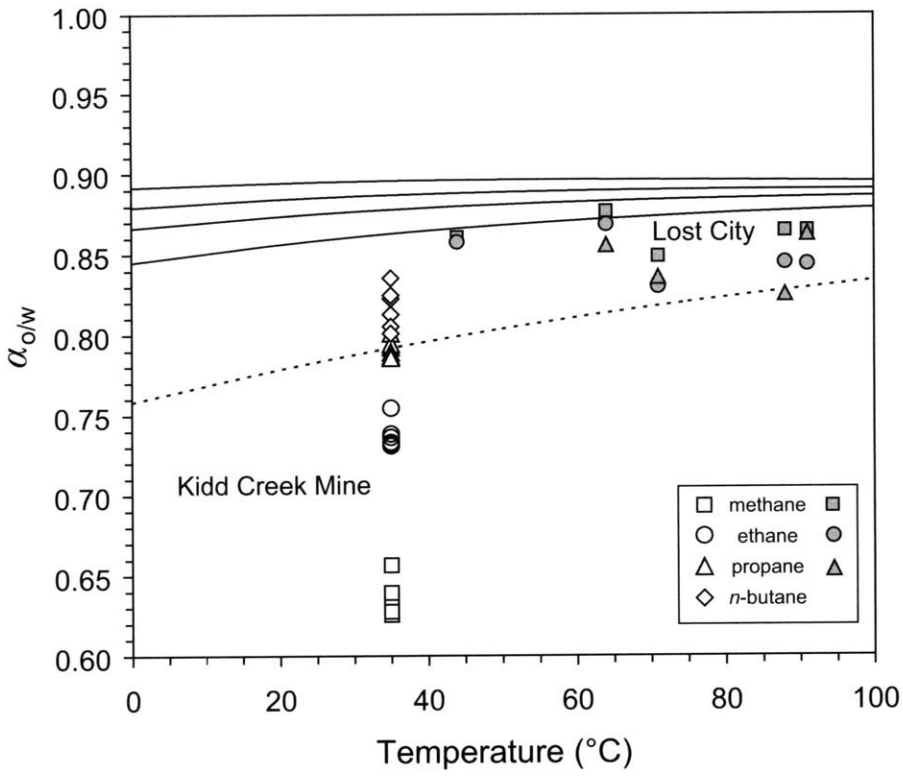

Figure 4.9. Plot of theoretical alkane-water equilibrium fractionation factors for ethane ($\alpha_{ethane/w}$), propane ($\alpha_{propane/w}$), *n*-butane ($\alpha_{butane/w}$) and *n*-pentane ($\alpha_{pentane/w}$) H calculated as a function of temperature from the data of WANG *et al.* (2009b). $\alpha_{methane/w}$ values (dashed line) are calculated as a function of temperature from the data of HORIBE and CRAIG (1995). Also plotted are the apparent $\alpha_{o/w}$ values for Kidd Creek Mine (open symbols, SHERWOOD LOLLAR *et al.*, 2002) and Lost City vent fluid (gray symbols, PROSKUROWSKI *et al.*, 2008) *n*-alkanes. For the Kidd Creek Mine gases, fracture waters are of relatively uniform temperature (~35°C, SHERWOOD LOLLAR *et al.*, 2008) and an average δ^2H_{H2O} value of -71‰ is chosen based on the range (-68 to -74‰) reported by SHERWOOD *et al.* (1988). For Lost City, accompanying vent fluid temperatures (PROSKUROWSKI *et al.*, 2008) are plotted and an average δ^2H_{H2O} value of +5‰ is chosen based on the range (+2 to +7‰) reported by PROSKUROWSKI *et al.* (2006).

REFERENCES

ABRAJANO, T. A., STURCHIO, N. C., BOHLKE, J. K., LYON, G. L., POREDA, R. J., and STEVENS, C. M. (1988) Methane Hydrogen Gas Seeps, Zambales Ophiolite, Philippines - Deep Or Shallow Origin. *Chemical Geology* **71**(1-3), 211-222.

ABRAJANO, T. A., STURCHIO, N. C., KENNEDY, B. M., LYON, G. L., MUEHLENBACHS, K., and BOHLKE, J. K. (1990) Geochemistry Of Reduced Gas Related To Serpentinization Of The Zambales Ophiolite, Philippines. *Applied Geochemistry* **5**(5-6), 625-630.

ALLEN, D. E. and SEYFRIED, W. E. (2003) Compositional controls on vent fluids from ultramatic-hosted hydrothermal systems at mid-ocean ridges: An experimental study at 400°C, 500 bars. *Geochimica et Cosmochimica Acta* **67**(8), 1531-1542.

ALLEN, D. E. and SEYFRIED, W. E. (2004) Serpentinization and heat generation: Constraints from Lost City and rainbow hydrothermal systems. *Geochimica et Cosmochimica Acta* **68**(6), 1347-1354.

BARKER, J. F. and POLLOCK, S. J. (1984) The geochemistry and origin of natural gases in southern Ontario. *Bulletin of Canadian Petroleum Geology* **32**(3), 313-326.

BELL, J. L. S., PALMER, D. A., BARNES, H. L., and DRUMMOND, S. E. (1994) Thermal-Decomposition Of Acetate: III. Catalysis By Mineral Surfaces. *Geochimica et Cosmochimica Acta* **58**(19), 4155-4177.

BERNDT, M. E., ALLEN, D. E., and SEYFRIED, W. E. (1996) Reduction of CO_2 during serpentinization of olivine at 300 °C and 500 bar. *Geology* **24**(4), 351-354.

BOREHAM, C. J., EDWARDS, D. S., HOPE, J. M., CHEN, J. H., and HONG, Z. H. (2008) Carbon and hydrogen isotopes of neo-pentane for biodegraded natural gas correlation. *Organic Geochemistry* **39**(10), 1483-1486.

BURGOYNE, T. W. and HAYES, J. M. (1998) Quantitative production of H_2 by pyrolysis of gas chromatographic effluents. *Analytical Chemistry* **70**(24), 5136-5141.

CHARLOU, J. L., DONVAL, J. P., FOUQUET, Y., JEAN-BAPTISTE, P., and HOLM, N. (2002) Geochemistry of high H_2 and CH_4 vent fluids issuing from ultramafic rocks at the Rainbow hydrothermal field (36°14'N, MAR). *Chemical Geology* **191**(4), 345-359.

COPLEN, T. B. (1988) Normalization of Oxygen and Hydrogen Isotope Data. *Chemical Geology* **72**(4), 293-297.

CRUSE, A. M. and SEEWALD, J. S. (2006) Geochemistry of low-molecular weight hydrocarbons in hydrothermal fluids from Middle Valley, northern Juan de Fuca Ridge. *Geochimica et Cosmochimica Acta* **70**(8), 2073-2092.

EDWARDS, D. S., BOREHAM, C. J., HOPE, J. M., PRESTON, J. C., LEPOIDEVIN, S., BUCKLER, T., and HONG, Z. (2007) Molecular and stable isotope (D/H AND $^{13}C/^{12}C$) compositions of natural gas from the Exmouth Plateau and Rankin Platform, Carnarvon Basin, Australia. In: *The 23rd International Meeting on Organic Geochemistry, Torquay, England, 9th-14th September 2007. Book of Abstracts,* pp. 335-336.

EGLINTON, T. I. and EGLINTON, G. (2008) Molecular proxies for paleoclimatology. *Earth And Planetary Science Letters* **275**(1-2), 1-16.

FISHER, A. T. (2003) Geophysical constraints on hydrothermal circulation: observations and models. In: *Dahlem Workshop Report: Energy and Mass Transfer in Marine Hydrothermal Systems*, (Ed: P. E. Halbach, V. Tunnicliffe, and J. R. Hein), **89**, Dahlem University Press. pp. 29-52.

FOUSTOUKOS, D. I., SAVOV, I. P., and JANECKY, D. R. (2008) Chemical and isotopic constraints on water/rock interactions at the Lost City hydrothermal field, 30°N Mid-Atlantic Ridge. *Geochimica et Cosmochimica Acta* **72**(22), 5457-5474.

FU, Q., SHERWOOD LOLLAR, B., HORITA, J., LACRAMPE-COULOUME, G., and SEYFRIED, W. (2007) Abiotic formation of hydrocarbons under hydrothermal conditions: Constraints from chemical and isotopic data. *Geochimica et Cosmochimica Acta* **71**(8), 1982-1998.

HAGEMANN, R., NIEF, G., and ROTH, E. (1970) Absolute isotopic scale for deuterium analysis of natural waters: absolute D/H ratio for SMOW. *Tellus* **22**(6), 712-715.

HARTSHORN, S. R. and SHINER, V. J. (1972) Calculation of H/D, $^{12}C/^{13}C$, and $^{12}C/^{14}C$ fractionation factors from valence force fields derived for a series of simple organic molecules. *Journal of the American Chemical Society* **94**(26), 9002-9012.

HILKERT, A. W., DOUTHITT, C. B., SCHLUTER, H. J., and BRAND, W. A. (1999) Isotope ratio monitoring gas chromatography mass spectrometry of D/H by high temperature conversion isotope ratio mass spectrometry. *Rapid Communications In Mass Spectrometry* **13**(13), 1226-1230.

HOERING, T. C. (1984) Thermal reactions of kerogen with added water, heavy water and pure organic substances. *Organic Geochemistry* **5**(4), 267-278.

HOLM, N. G. and CHARLOU, J. L. (2001) Initial indications of abiotic formation of hydrocarbons in the Rainbow ultramafic hydrothermal system, Mid-Atlantic Ridge. *Earth And Planetary Science Letters* **191**(1-2), 1-8.

HORIBE, Y. and CRAIG, H. (1995) D/H fractionation in the system methane-hydrogen-water. *Geochimica et Cosmochimica Acta* **59**(24), 5209-5217.

HUNT, J. M. (1996) *Petroleum Geochemistry and Geology*. 2nd Ed. W.H. Freeman and Company.

JOHNSON, J. W., OELKERS, E. H., and HELGESON, H. C. (1992) SUPCRT92 - A software package for calculating the standard molal thermodynamic properties of minerals, gases, aqueous species, and reactions from 1 to 5000 bar and 0 to 1000°C. *Computers & Geosciences* ***18(7), 899-947.***

KADKO, D. (1996) Radioisotopic studies of submarine hydrothermal vents. *Reviews Of Geophysics* **34**(3), 349-366.

KADKO, D. and BUTTERFIELD, D. A. (1998) The relationship of hydrothermal fluid composition and crustal residence time to maturity of vent fields on the Juan de Fuca Ridge. *Geochimica et Cosmochimica Acta* **62**(9), 1521-1533.

KHARAKA, Y. K. and CAROTHERS, W. W. (1986) Oxygen and Hydrogen Isotope Geochemistry of Deep Basin Brines. In: *Handbook of Environmental Isotope Geochemistry: Volume 2 - The Terrestrial Environment, B,* (Ed: P. Fritz and J. C. Contes), Elsevier. pp. 305-360.

KHARAKA, Y. K., CAROTHERS, W. W., and ROSENBAUER, R. J. (1983) Thermal Decarboxylation of Acetic Acid - Implications for Origin of Natural Gas. *Geochimica et Cosmochimica Acta* **47**(3), 397-402.

KNYAZEV, D. A., MYASOEDOV, N.F., BOCHAREV, A.V. (1992) The theory of the equilibrium isotope effects of hydrogen. *Russian Chemical Reviews* **61**, 204-220.

KONN, C., CHARLOU, J. L., DONVAL, J. P., HOLM, N. G., DEHAIRS, F., and BOUILLON, S. (2009) Hydrocarbons and oxidized organic compounds in hydrothermal fluids from Rainbow and Lost City ultramafic-hosted vents. *Chemical Geology* **258**(3-4), 299.

LEIF, R. N. and SIMONEIT, B. R. T. (1995) Ketones in hydrothermal petroleums and sediment extracts from Guaymas Basin, Gulf of California. *Organic Geochemistry* **23**(10), 889-904.

LEIF, R. N. and SIMONEIT, B. R. T. (2000) The role of alkenes produced during hydrous pyrolysis of a shale. *Organic Geochemistry* **31**(11), 1189-1208.

LEWAN, M. D. (1997) Experiments on the role of water in petroleum formation. *Geochimica et Cosmochimica Acta* **61**(17), 3691-3723.

LEWAN, M. D., WINTERS, J. C., and MCDONALD, J. H. (1979) Generation of oil-like pyrolyzates from organic-rich shales. *Science* **203**(4383), 897-899.

LIN, L. H., WANG, P. L., RUMBLE, D., LIPPMANN-PIPKE, J., BOICE, E., PRATT, L. M., LOLLAR, B. S., BRODIE, E. L., HAZEN, T. C., ANDERSEN, G. L. *et al.* (2006) Long-term sustainability of a high-energy, low-diversity crustal biome. *Science* **314**(5798), 479-482.

LIPPMANN, J., STUTE, M., TORGERSEN, T., MOSER, D. P., HALL, J. A., LIN, L., BORCSIK, M., BELLAMY, R. E. S., and ONSTOTT, T. C. (2003) Dating ultra-deep mine waters with noble gases and Cl-36, Witwatersrand Basin, South Africa. *Geochimica et Cosmochimica Acta* **67**(23), 4597-4619.

MCCOLLOM, T. M. and SEEWALD, J. S. (2001) A reassessment of the potential for reduction of dissolved CO2 to hydrocarbons during serpentinization of olivine. *Geochimica et Cosmochimica Acta* **65**(21), 3769-3778.

MCCOLLOM, T. M. and SEEWALD, J. S. (2003a) Experimental constraints on the hydrothermal reactivity of organic acids and acid anions: I. Formic acid and formate. *Geochimica et Cosmochimica Acta* **67**(19), 3625-3644.

MCCOLLOM, T. M. and SEEWALD, J. S. (2003b) Experimental study of the hydrothermal reactivity of organic acids and acid anions: II. Acetic acid, acetate, and valeric acid. *Geochimica et Cosmochimica Acta* **67**(19), 3645-3664.

MCCOLLOM, T. M. and SEEWALD, J. S. (2007) Abiotic synthesis of organic compounds in deep-sea hydrothermal environments. *Chemical Reviews* **107**, 382-401.

NURMI, P. A., KUKKONEN, I. T., and LAHERMO, P. W. (1988) Geochemistry and origin of saline groundwaters in the Fennoscandian Shield. *Applied Geochemistry* **3**, 185-230.

ONSTOTT, T. C., LIN, L. H., DAVIDSON, M., MISLOWACK, B., BORCSIK, M., HALL, J., SLATER, G., WARD, J., LOLLAR, B. S., LIPPMANN-PIPKE, J. *et al.* (2006) The origin and age of biogeochemical trends in deep fracture water of the Witwatersrand Basin, South Africa. *Geomicrobiology Journal* **23**(6), 369-414.

OREMLAND, R. S., MILLER, L. G., and WHITICAR, M. J. (1987) Sources And Flux Of Natural Gases From Mono Lake, California. *Geochimica et Cosmochimica Acta* **51**(11), 2915-2929.

PALMER, D. A. and DRUMMOND, S. E. (1986) Thermal decarboxylation of acetate. Part I. The kinetics and mechanism of reaction in aqueous solution. *Geochimica et Cosmochimica Acta* **50**(5), 813-823.

PROSKUROWSKI, G., LILLEY, M. D., KELLEY, D. S., and OLSON, E. J. (2006) Low temperature volatile production at the Lost City Hydrothermal Field, evidence from a hydrogen stable isotope geothermometer. *Chemical Geology* **229**(4), 331-343.

PROSKUROWSKI, G., LILLEY, M. D., SEEWALD, J. S., FRUH-GREEN, G. L., OLSON, E. J., LUPTON, J. E., SYLVA, S. P., and KELLEY, D. S. (2008) Abiogenic hydrocarbon production at Lost City hydrothermal field. *Science* **319**(5863), 604-607.

ROBERTS, I. and UREY, H. C. (1939) Kinetics of exchange of Oxygen between Benzoic Acid and Water. *Journal of the American Chemical Society* **61**, 2580-2584.

SACHSE, D., RADKE, J., and GLEIXNER, G. (2006) δD values of individual n-alkanes from terrestrial plants along a climatic gradient - Implications for the sedimentary biomarker record. *Organic Geochemistry* **37**(4), 469-483.

SACKETT, W. M. (1978) Carbon and hydrogen isotope effects during thermo-catalytic production of hydrocarbons in laboratory simulation experiments. *Geochimica et Cosmochimica Acta* **42**(6), 571-580.

SCHEFUSS, E., SCHOUTEN, S., and SCHNEIDER, R. R. (2005) Climatic controls on central African hydrology during the past 20,000 years. *Nature* **437**(7061), 1003-1006.

SCHIMMELMANN, A., LEWAN, M. D., and WINTSCH, R. P. (1999) D/H isotope ratios of kerogen, bitumen, oil, and water in hydrous pyrolysis of source rocks containing kerogen types I, II, IIS, and III. *Geochimica et Cosmochimica Acta* **63**(22), 3751-3766.

SCHIMMELMANN, A., SESSIONS, A. L., and MASTALERZ, M. (2006) Hydrogen isotopic (D/H) composition of organic matter during diagenesis and thermal maturation. *Annual Review Of Earth And Planetary Sciences* **34**, 501-533.

SCHIMMELMANN, A., BOUDOU, J. P., LEWAN, M. D., and WINTSCH, R. P. (2001) Experimental controls on D/H and $^{13}C/^{12}C$ ratios of kerogen, bitumen and oil during hydrous pyrolysis. *Organic Geochemistry* **32**(8), 1009-1018.

SCHIMMELMANN, A., SESSIONS, A. L., BOREHAM, C. J., EDWARDS, D. S., LOGAN, G. A., and SUMMONS, R. E. (2004) D/H ratios in terrestrially sourced petroleum systems. *Organic Geochemistry* **35**(10), 1169-1195.

SCHMIDT, K., KOSCHINSKY, A., GARBE-SCHONBERG, D., DE CARVALHO, L. M., and SEIFERT, R. (2007) Geochemistry of hydrothermal fluids from the ultramafic-hosted Logatchev hydrothermal field, 15°N on the Mid-Atlantic Ridge: Temporal and spatial investigation. *Chemical Geology* **242**(1-2), 1-21.

SCHOELL, M. (1983) Genetic Characterization of Natural Gases. *AAPG Bulletin* **67**(3), 546-546.

SEEWALD, J. (1997) Mineral redox buffers and the stability of organic compounds under hydrothermal conditions. *Mat. Res. Soc. Symp. Proc.* **412**, 317-331.

SEEWALD, J. S. (1994) Evidence For Metastable Equilibrium Between Hydrocarbons Under Hydrothermal Conditions. *Nature* **370**(6487), 285-287.

SEEWALD, J. S. (2001) Model for the origin of carboxylic acids in basinal brines. *Geochimica et Cosmochimica Acta* **65**(21), 3779-3789.

SEEWALD, J. S. (2001) Aqueous geochemistry of low molecular weight hydrocarbons at elevated temperatures and pressures: Constraints from mineral buffered laboratory experiments. *Geochimica et Cosmochimica Acta* **65**(10), 1641-1664.

SEEWALD, J. S. (2003) Organic-inorganic interactions in petroleum-producing sedimentary basins. *Nature* **426**(6964), 327-333.

SEEWALD, J. S., ZOLOTOV, M. Y., and MCCOLLOM, T. (2006) Experimental investigation of single carbon compounds under hydrothermal conditions. *Geochimica et Cosmochimica Acta* **70**(2), 446-460.

SESSIONS, A. L. (2006) Isotope-ratio detection for gas chromatography. *Journal Of Separation Science* **29**(12), 1946-1961.

SESSIONS, A. L., SYLVA, S. P., SUMMONS, R. E., and HAYES, J. M. (2004) Isotopic exchange of carbon-bound hydrogen over geologic timescales. *Geochimica et Cosmochimica Acta* **68**(7), 1545-1559.

SEYFRIED, W., FOUSTOUKOS, D. I., and ALLEN, D. E. (2004) Ultramafic-hosted hydrothermal systems at Mid-Ocean Ridges: Chemical and physical constraints on pH, redox, and carbon reduction reactions. In: *Mid-Ocean Ridges: Hydrothermal Interactions between the Lithosphere and Oceans,* (Ed: C. German, J. Lin, and L. Parson), AGU Monograph, **148**, American Geophysical Union. pp. 267-285.

SEYFRIED, W., D.R. JANECKY AND M.E. BERNDT (1987) Rocking autoclaves for hydrothermal experiments II: The flexible reaction-cell system. In: *Hydrothermal Experimental Techniques,* (Ed: G. C. Ulmer and H. L. Barnes), Wiley. pp. 216-239.

SEYFRIED, W. E. and DING, K. (1995) Phase equilibria in subseafloor hydrothermal systems: a review of the role of redox, temperature, pH and dissolved Cl on the chemistry of hot spring fluids at mid-ocean ridges. In: *Seafloor Hydrothermal Systems: Physical,*

Chemical, Biological, and Geological Interactions, (Ed: S. E. Humphris, R. A. Zierenberg, L. S. Mullineaux, and R. E. Thomson), AGU Monograph, **91**, American Geophysical Union. pp. 248-272.

SHERWOOD, B., FRITZ, P., FRAPE, S. K., MACKO, S. A., WEISE, S. M., and WELHAN, J. A. (1988) Methane Occurrences In The Canadian Shield. *Chemical Geology* **71**(1-3), 223-236.

SHERWOOD LOLLAR, B., FRAPE, S. K., WEISE, S. M., FRITZ, P., MACKO, S. A., and WELHAN, J. A. (1993a) Abiogenic Methanogenesis In Crystalline Rocks. *Geochimica et Cosmochimica Acta* **57**(23-24), 5087-5097.

SHERWOOD LOLLAR, B., FRAPE, S. K., FRITZ, P., MACKO, S. A., WELHAN, J. A., BLOMQVIST, R., and LAHERMO, P. W. (1993b) Evidence For Bacterially Generated Hydrocarbon-Gas In Canadian Shield And Fennoscandian Shield Rocks. *Geochimica et Cosmochimica Acta* **57**(23-24), 5073-5085.

SHERWOOD LOLLAR, B., WEISE, S. M., FRAPE, S. K., and BARKER, J. F. (1994) Isotopic constraints on the migration of hydrocarbon and helium gases of southwestern Ontario. *Bulletin of Canadian Petroleum Geology* **42**(3), 283-295.

SHERWOOD LOLLAR, B., WESTGATE, T. D., WARD, J. A., SLATER, G. F., and LACRAMPE-COULOUME, G. (2002) Abiogenic formation of alkanes in the Earth's crust as a minor source for global hydrocarbon reservoirs. *Nature* **416**(6880), 522-524.

SHERWOOD LOLLAR, B., LACRAMPE-COULOUME, G., SLATER, G. F., WARD, J., MOSER, D. P., GIHRING, T. M., LIN, L. H., and ONSTOTT, T. C. (2006) Unravelling abiogenic and biogenic sources of methane in the Earth's deep subsurface. *Chemical Geology* **226**(3-4), 328-339.

SHERWOOD LOLLAR, B., LACRAMPE-COULOUME, G., VOGLESONGER, K., ONSTOTT, T. C., PRATT, L. M., and SLATER, G. F. (2008) Isotopic signatures of CH_4 and higher

hydrocarbon gases from Precambrian Shield sites: A model for abiogenic polymerization of hydrocarbons. *Geochimica et Cosmochimica Acta* **72**(19), 4778-4795.

SHOCK, E. L. (1992) Chemical Environments Of Submarine Hydrothermal Systems. *Origins Of Life And Evolution Of The Biosphere* **22**(1-4), 67-107.

SHOCK, E. L. and HELGESON, H. C. (1990) Calculation of the thermodynamic and transport properties of aqueous species at high pressures and temperatures: Standard partial molal properties of organic species. *Geochimica et Cosmochimica Acta* **54**(4), 915-945.

SISKIN, M., BRONS, G., KATRITZKY, A. R., and BALASUBRAMANIAN, M. (1990) Aqueous Organic Chemistry.1. Aquathermolysis - Comparison with Thermolysis in the Reactivity of Aliphatic Compounds. *Energy & Fuels* **4**(5), 475-482.

SURDAM, R. C. and CROSSEY, L. J. (1985) Organic Inorganic Reactions During Progressive Burial - Key To Porosity And Permeability Enhancement And Preservation. *Philosophical Transactions Of The Royal Society Of London Series A-Mathematical Physical And Engineering Sciences* **315**(1531), 135-156.

SURDAM, R. C., JIAO, Z. S., and MACGOWAN, D. B. (1993) Redox Reactions Involving Hydrocarbons And Mineral Oxidants - A Mechanism For Significant Porosity Enhancement In Sandstones. *AAPG Bulletin* **77**(9), 1509-1518.

TANG, Y. C., ELLIS, G. S., and MA, Q. S. (2007) Use of carbon and hydrogen stable isotopic composition to quantitatively assess natural gas generation. *Geochimica et Cosmochimica Acta* **71**(15), A1001-A1001.

TANG, Y. C., HUANG, Y. S., ELLIS, G. S., WANG, Y., KRALERT, P. G., GILLAIZEAU, B., MA, Q. S., and HWANG, R. (2005) A kinetic model for thermally induced hydrogen and carbon isotope fractionation of individual n-alkanes in crude oil. *Geochimica et Cosmochimica Acta* **69**(18), 4505-4520.

TISSOT, B. P. and WELTE, D. H. (1984) *Petroleum Formation and Occurrence*. 2nd Ed. Springer-Verlag.

TOBIAS, H. J. and BRENNA, J. T. (1997) On-line pyrolysis as a limitless reduction source for high-precision isotopic analysis of organic-derived hydrogen. *Analytical Chemistry* **69**(16), 3148-3152.

TOULMIN, P., III and BARTON, P. B., JR. (1964) A thermodynamic study of pyrite and pyrrhotite. *Geochimica et Cosmochimica Acta* **28**, 641-671.

WANG, Y. and SESSIONS, A. L. (2008) Memory Effects in Compound-Specific D/H Analysis by Gas Chromatography/Pyrolysis/Isotope-Ratio Mass Spectrometry. *Analytical Chemistry* **80**(23), 9162-9170.

WANG, Y., SESSIONS, A., NIELSEN, R. J., and GODDARD, W. A., III (2009a) Equilibrium $^{2}H/^{1}H$ fractionations in organic molecules: I. Experimental calibration of ab initio calculations. *Geochimica et Cosmochimica Acta* **73**(23), 7060-7075.

WANG, Y., SESSIONS, A., NIELSEN, R. J., and GODDARD, W. A., III (2009b) Equilibrium $^{2}H/^{1}H$ fractionations in organic molecules. II: Linear alkanes, alkenes, ketones, carboxylic acids, esters, alcohols and ethers. *Geochimica et Cosmochimica Acta* **73**(23), 7076-7086.

WARD, J. A., SLATER, G. F., MOSER, D. P., LIN, L. H., LACRAMPE-COULOUME, G., BONIN, A. S., DAVIDSON, M., HALL, J. A., MISLOWACK, B., BELLAMY, R. E. S. *et al.* (2004) Microbial hydrocarbon gases in the Witwatersrand Basin, South Africa: Implications for the deep biosphere. *Geochimica et Cosmochimica Acta* **68**(15), 3239-3250.

WERES, O., NEWTON, A. S., and TSAO, L. (1988) Hydrous Pyrolysis of Alkanes, Alkenes, Alcohols and Ethers. *Organic Geochemistry* **12**(5), 433-444.

WHITICAR, M. J., FABER, E., and SCHOELL, M. (1985) Hydrogen and Carbon Isotopes of C_1 To C_5 Alkanes in Natural Gases. *AAPG Bulletin* **69**(2), 316 (abstr.).

CHAPTER 5

Geochemistry of hydrothermal fluids from the PACMANUS, Northeast Pual and Vienna Woods vent fields, Manus Basin, Papua New Guinea

(A modified version of this Chapter has been submitted to *Geochimica et Cosmochimica Acta*, December 11th, 2009, and is currently under review as a coauthored paper with Jeffrey S. Seewald, Peter Saccocia, Emily Walsh, Wolfgang Bach, Paul Craddock, Wayne C. Shanks, Sean Sylva, Thomas Pichler, Martin Rosner)

ABSTRACT

Processes controlling the composition of seafloor hydrothermal fluids in silicic backarc/near-arc crustal settings remain poorly constrained despite growing evidence for extensive magmatic-hydrothermal activity in such environments. In order to assess the effects of water-rock interaction with varying substrate compositions and magmatic fluid degassing on hydrothermal fluid chemistry, we conducted a survey of vent fluid compositions from two contrasting regions of the Manus backarc basin, Papua New Guinea - the felsic-hosted PACMANUS and nearby Northeast (NE) Pual hydrothermal vent fields (located on Pual Ridge near the active New Britain Arc) and the more arc-distal basalt-hosted Vienna Woods field. In 2006, fluid samples were collected from 18 discrete vents at PACMANUS/NE Pual and 3 at Vienna Woods using both gas-tight and syringe-style samplers. High temperature fluids at

Vienna Woods were characterized by uniform endmember temperatures (273–285°C) and major element compositions, low dissolved CO_2 concentrations (4.4mmol/kg) and high measured pH (4.2–4.9 at 25°C). Temperatures and compositions were highly variable at PACMANUS and a large, newly discovered vent area (Fenway) was observed to be vigorously venting boiling (358°C) fluid. All PACMANUS/NE Pual fluids are characterized by negative δD_{H2O} values, in contrast to positive values at Vienna Woods, suggesting substantial magmatic water input to circulating fluids at the former. Low measured pH (25°C) values (~2.6 to 2.7), high endmember CO_2 (up to 272 mmol/kg) and negative $\delta^{34}S_{H2S}$ values (down to -2.7‰) in some vent fluids are also consistent with degassing of acid-volatile species from evolved magma. Dissolved CO_2 at PACMANUS is enriched in ^{13}C (-4.1‰ to -2.3‰) relative to Vienna Woods (-5.2‰ to -5.7‰) suggesting a contribution of slab-derived carbon to the former. The mobile elements (e.g. Li, K, Rb, Cs and B) are also greatly enriched in PACMANUS and NE Pual fluids reflecting increased abundances in the crust there relative to the Vienna Woods field. Variations in alkali and dissolved gas abundances with Cl at PACMANUS and NE Pual suggest that phase separation has affected fluid chemistry despite the low temperatures of many vents. These fluids further differ from those at Vienna Woods in that substantial modification has taken place as a result of seawater entrainment. Almost all PACMANUS and NE Pual samples have consistently high measured Mg concentrations, indicating subsurface seawater entrainment is pervasive there. Trends of increasingly non-conservative SO_4 behavior, decreasing endmember Ca/Cl and Sr/Cl ratios with increased Mg indicate extensive subsurface anhydrite deposition is occurring. Decreased pH and endmember Fe/Mn ratios in higher Mg fluids indicate that sulfide deposition is also occurring as a result of mixing/cooling and leading to secondary acidity production. Several low temperature (≤80°C) fluids at PACMANUS and NE Pual also show evidence for anhydrite dissolution and water-rock interaction (B fixation) subsequent to seawater entrainment. This

study demonstrates that arc proximity has the potential to profoundly influence vent fluid compositions in back-arc settings and provides useful insights into hydrothermal processes occurring there.

1. INTRODUCTION

Hydrothermal activity in back-arc basins shares many common physical and chemical processes with mid-ocean ridge (MOR) settings, including water-rock reaction, magmatic volatile degassing, phase separation and subsurface fluid mixing. In back-arc hydrothermal systems, however, the proximity to a subduction zone and eruption of magmas with higher water contents relative to mid-ocean ridge basalt (MORB) results in a broader range of degassed volatiles capable of influencing vent fluid chemistry (de Ronde, 1995; Ishibashi and Urabe, 1995; Yang and Scott, 2006). In contrast to MOR settings, where CO_2 is the dominant volatile degassed, the exsolution of large quantities of H_2O and CO_2 from water-rich silicic magmas can be accompanied by acid-volatile species such as SO_2, HCl and HF. Subsequent entrainment of water-rich magmatic fluids into existing hydrothermal circulation cells could substantially lower pH, thereby influencing the transport of dissolved metals and styles of crustal alteration (Gamo et al., 1997; Gena et al., 2001; Gamo et al., 2006; Yang and Scott, 2006). Moreover, magmatic fluids have long been proposed as an additional source of economically important metals (i.e. Cu, Zn, Ag and Au) in excess of that feasible by rock leaching alone (Yang and Scott, 1996; Sun et al., 2004; Simmons and Brown, 2006; Yang and Scott, 2006). Many large volcanic-hosted massive sulfide deposits (Kuroko-type) are thought to have formed in arc and back-arc magmatic-hydrothermal settings (Franklin et al., 1981; Herzig and Hannington, 1995). Thus, models for the formation of metal sulfide deposits in back-arc environments require an understanding of the role of magmatic fluids in metal transport and deposition.

Discharge of magmatic fluids directly into the water column has been observed above submarine arc volcanoes (Embley et al., 2006; Nakagawa et al., 2006; Lupton et al., 2008) and seamounts (Cheminée et al., 1991; Gamo et al., 1993; de Ronde et al., 2005; Resing et al., 2007), and contributions of magmatic acid-volatile species and water to hydrothermal fluids have been

reported in a few locations (Sedwick et al., 1992; McMurtry et al., 1993; Gamo et al., 1997; Zengqian et al., 2005; Nakagawa et al., 2006). In general, however, active magmatic-hydrothermal systems hosted in felsic crust have been historically under-sampled despite the prevalence of hydrothermal activity associated with back-arc volcanism in the western Pacific (Ishibashi and Urabe, 1995).

In 1999 the Ocean Drilling Program (ODP) drilled into an active felsic-hosted hydrothermal system at the PACMANUS site in the Eastern Manus Volcanic Zone, Papua New Guinea (Fig. 5.1 and Fig. 5.2). Subsequent investigations of alteration assemblages recovered in drill-cores indicated a complex system affected by both temporally and spatially variable magmatic acid-volatile inputs and subsurface mixing of hydrothermal fluids with seawater (Bach et al., 2003; Roberts et al., 2003; Lackschewitz et al., 2004; Paulick et al., 2004; Paulick and Bach, 2006; Binns et al., 2007). In addition to magmatic inputs, pervasive entrainment and mixing of seawater, as indicated by ODP Leg 193, may be an important process that influences vent fluid chemistry in back-arc hydrothermal systems.

In 2006 we conducted a detailed chemical and isotopic survey of vent fluids at the near-arc hydrothermal fields on Pual Ridge (PACMANUS and Northeast (NE) Pual), and the more distal basalt-hosted Vienna Woods field, to examine the effects of substrate composition, magmatic fluid inputs, and subsurface mixing on vent fluid geochemistry. Here, we demonstrate that present hydrothermal activity at Pual Ridge is influenced by variable inputs of acidic magmatic solutions to seawater-derived vent fluids at depth, in addition to processes of water/rock reaction and phase separation. We further show that widespread seawater entrainment prior to venting modifies the composition of resulting mixtures and partially obscures the effects of magmatic fluid inputs. In contrast, the geochemistry of vent fluids at Vienna Woods is similar

in many respects to other temporally stable hydrothermal systems commonly sampled in MOR settings.

2. GEOLOGICAL SETTING

The Manus Basin is a young (ca. 3.5Ma old), rapidly opening (137mm/yr) back-arc basin in the northeastern portion of the Bismarck Sea (Fig. 5.1a), tectonically bordered to the north by the presently inactive Manus Trench and to the south by the Willaumez Rise and the active New Britain Trench (Taylor, 1979a; Taylor et al., 1994; Tregoning, 2002; Lee and Ruellan, 2006). Volcanism associated with basin extension occurs along a series of spreading centers and rifts between three major transform faults (Taylor, 1979a; Taylor et al., 1994; Martinez and Taylor, 1996). Approximately 250km from the active New Britain Arc in the center of the basin, spreading occurs along the 120km-long Manus Spreading Center (MSC), bounded by the Willaumez and Djual transform faults (Fig. 5.1a). Predominantly MORB-like basaltic lavas erupt along the MSC (Sinton et al., 2003) and numerous areas of hydrothermal activity have been reported, the largest of which is the unsedimented Vienna Woods field (Both et al., 1986; Tufar, 1990; Lisitsyn et al., 1993). In contrast, the eastern Manus Basin, between the Djual and Weitin transform faults, is an extensional transform zone within remnant Eocene-Oligocene island-arc crust that is thought to have formed during previous southwestward subduction along the Manus Trench (Binns and Scott, 1993; Binns et al., 2007). As such, it is probably the precursor of a back-arc spreading center like the MSC. Volcanism associated with the incipient rifting of existing intermediate/felsic crust has produced a complex series of *en echelon* neovolcanic ridges (such as Pual Ridge, Fig. 5.1b) and volcanic domes, known as the Eastern Manus Volcanic Zone (EMVZ, Fig. 5.1a), of basaltic to rhyodacitic composition (Binns and Scott, 1993; Kamenetsky et al., 2001; Sinton et al., 2003). These edifices possess isotopic, major and trace element characteristics similar to subaerial volcanoes of the New Britain Arc indicating strong arc affinities (Sinton et al., 2003; Pearce and Stern, 2006). Due to the proximity of the EMVZ to the New Britain Arc (<100km), the relative influences of the mantle wedge, subducting slab and

remnant arc crust on melt production and volcanism are highly complex (Sinton et al., 2003; Pearce and Stern, 2006). Several large areas of hydrothermal activity have been discovered in the EMVZ (Fig. 5.1a) in the last two decades, including the DESMOS caldera (Gamo et al., 1993; Gamo et al., 1997), SuSu Knolls (Binns et al., 1997; Moss and Scott, 2001; Tivey et al., 2006; Hrischeva et al., 2007) and PACMANUS vent fields (Binns and Scott, 1993).

2.1 Hydrothermal Vent Fields

2.1.1 Vienna Woods

Current hydrothermal activity at the Vienna Woods field (Fig. 5.2a) is confined to an area of approximately 100m by 150m at a water depth of 2780m within the rift zone of the MSC (~0.5km south of the neo-volcanic zone). Though the site is hosted in basalt that is compositionally similar to MORB, substrate composition along the MSC is variable and more intermediate compositions occur to the south and north of Vienna Woods (Shaw et al., 2004). The rift zone itself is comprised of basaltic pillow lavas/sheet flows with minimal sediment cover and occasional 1-2m wide along-axis fissures. Hydrothermal activity in 2006 consisted of three main clusters of tall (5–12m high) active sulfide structures separated by 100–150m and generally aligned along these fissures, in addition to numerous smaller inactive chimneys. All fluids sampled were relatively clear in color with little visible precipitate upon mixing with seawater.

2.1.2 PACMANUS and Northeast Pual

The PACMANUS (*P*apua New Guinea-*A*ustralia-*C*anada-*MANUS*) vent field, originally discovered during the 1991 expedition of the same name, consists of several discrete vent areas distributed over a 1.5km section of Pual Ridge (Fig. 5.1b, (Binns and Scott, 1993). Pual Ridge is a 20km long, Y-shaped neovolcanic edifice located 80km from Rabaul Volcano on the New

Britain Arc (Fig. 5.1b). With a ridge crest at 1600–1700m depth, it is 1–1.5km in width and stands ~500m above the sedimented basaltic to andesitic seafloor of the EMVZ (Binns et al., 2007). Erupted lavas consist of highly vesicular and blocky dacite/rhyodacite with some rhyolite and the ridge itself is constructed of stacked, subhorizontal flows up to 30m thick with negligible to minor sediment cover (Binns and Scott, 1993; Paulick et al., 2004; Yang and Scott, 2005). Based on the composition of erupted lavas, Yang and Scott (2002) proposed that the entire ridge represents a single calc-alkaline trend that may have been generated by fractional crystallization of a single volatile-rich mafic magma source. While conclusive evidence for magma bodies beneath Pual Ridge is currently lacking, a faint and discontinuous seismic reflector was observed at ~2km depth in 2002 (Lee, 2003; Binns et al., 2007). Based on the Cl and H_2O contents of volcanic glasses from Pual Ridge and solubility constraints, Sun et al. (2007) also suggested that a magma chamber might be located near this depth. In contrast to Vienna Woods, meter-scale fissures are noticeably absent on the surface of Pual Ridge.

The five main areas of hydrothermal activity previously visited at PACMANUS include Roman Ruins, Roger's Ruins, Satanic Mills, Snowcap and Tsukushi. These are distributed between two broad highs along the crest of Pual Ridge at depths ranging from 1640m to 1710m (Fig. 5.1b, Fig. 5.2b and 5.2c). To the north, hydrothermal activity at the Roman Ruins and smaller Roger's Ruins areas in 2006 (Fig. 5.2b) consisted of focused black or gray smoker fluids venting from multi-spired, sulfide chimney complexes up to 10m tall. Areas of hydrothermal activity to the south encircle the Snowcap Dome (Fig. 5.2c). Similar styles of venting through smaller sulfide structures were evident at Satanic Mills and diffuse fluid also appeared to be flowing from a nearby depression tentatively identified as the drill hole of ODP Leg 193 Site 1191A (Fig. 5.2c). A 5.3°C temperature anomaly (above ambient) was measured ~15cm beneath the surface of the drilling mud/bore-hole cuttings, which were covered by a white microbial mat

(Tivey et al., 2006). At Tsukushi, sulfide structures were found to be largely inactive in 2006 and only a single low temperature fluid (62°C) exiting from an oxide mound fissure was sampled. The Snowcap vent area is a broad knoll of mostly diffuse venting with a small area of moderate temperature focused venting (<180°C) confined to the western flank (Fig. 5.2c). In contrast to Roman/Roger's Ruins, Satanic Mills and Tsukushi areas where sulfide structures are located atop rugged surficial lava flows, the Snowcap area is heavily sedimented with hydrothermal precipitate/volcaniclastic debris, and lava outcrops are rare. Several outcrops of heavily bleached rocks cemented with native sulfur were observed near active vents, presumably reflecting advanced argillic alteration by acid-sulfate type fluids (Brimhall and Ghiorso, 1983; Gena et al., 2001; Binns et al., 2007). However, no 'white smoker activity' similar to the DESMOS caldera site (Gamo et al., 1997; Gamo et al., 2006) has been observed anywhere on Pual Ridge. A new site, Fenway, was discovered ~200m south of Satanic Mills at 1710m depth during this expedition (Fig. 5.2c). The core area of the Fenway site is a 40m diameter two-tiered mound composed of chimney debris, massive anhydrite-sulfide breccia and coarse anhydrite sand. At its summit (1710m depth), a large black smoker chimney complex was found to be vigorously venting the highest temperature fluids (358°C) observed in the PACMANUS field to date. Several areas of diffuse venting, including some emanating from anhydrite sand/talus, and occasional gray/black smoker fluids were observed on the flanks of the mound.

Another discrete area of hydrothermal activity was discovered during this expedition ~8km from PACMANUS on the northeast limb of Pual Ridge and named Northeast (NE) Pual (Fig. 5.1b). Fluids venting at NE Pual were predominantly low temperature/diffuse in nature in 2006 with maximum measured temperatures of 35°C. The presence of extensive biological activity (snails, shrimp, mussel beds and microbial mats) and inactive sulfide chimneys suggests hydrothermal activity in this area is waning.

3. METHODS

3.1 Sample collection

All hydrothermal fluid samples were collected during the July–August 2006 MGLN06MV expedition to the Manus Basin aboard the R/V *Melville*. Fluids were collected using 150mL titanium isobaric gas-tight (IGT) fluid samplers (Seewald et al., 2002) and 755mL titanium syringe 'major' samplers (Von Damm et al., 1985) deployed from the ROV *Jason II*. The temperatures of fluids collected with IGT samplers were monitored in real-time during collection using thermocouple temperature probes mounted adjacent to sampler snorkel tips. Only maximum temperatures for a given vent fluid are reported (uncertainty ±2°C) and temperatures were not measured in real time during deployment of the 'major' samplers. Two to three fluid samples were taken per discrete vent at all sites visited (typically two IGT samplers and one 'major' sampler) resulting in a total of 57 samples from 21 discrete vents at Vienna Woods and Pual Ridge (Table 5.1). In most cases, fluids were sampled after removing sulfide chimney structures.

After recovery of the ROV, fluid samples were processed on board the ship as soon as possible (typically within 12h). Fluids from IGT samplers were used for the analysis of both volatile (H_2, CH_4, CO, CO_2, H_2S) and dissolved inorganic constituents, whereas only the latter were analyzed from the 'major' samplers as they are not gas-tight. Fluid aliquots for major element (Na, Cl, Ca, K, SiO_2, SO_4, Br, F) and trace metal (Fe, Mn, Li, B, Sr, Rb, Cs, Al) determination were transferred to acid-cleaned high-density polyethylene (HDPE) Nalgene™ bottles and analyzed onshore. Aliquots for trace metal analysis were acidified with analytical-grade Optima® HCl prior to storage. Subsamples of acidified aliquots were diluted 100-fold onboard ship and stored for shore-based measurement of aqueous silica (SiO_2). Prior to storage, separate fluid aliquots were sparged with N_2 to remove all dissolved H_2S for analysis of SO_4

concentration and S isotopic composition ($\delta^{34}S_{SO4}$). Fluid aliquots for the onshore determination of aqueous ΣCO_2 concentration and the stable carbon isotope composition of ΣCO_2 ($\delta^{13}C_{CO2}$) and CH_4 ($\delta^{13}C_{CH4}$) were stored in evacuated 25mL serum vials sealed with butyl rubber stoppers. Fluid aliquots were also flame sealed in glass ampoules for H_2O stable hydrogen (δD_{H2O}) and oxygen ($\delta^{18}O_{H2O}$) isotope analysis.

3.2 Analytical methods

Aqueous H_2, CH_4 and CO concentrations were determined onboard ship by molecular sieve gas chromatograph (GC) with thermal conductivity detection (for H_2 and CH_4) and helium ionization detection (for CO) following a syringe headspace extraction. pH (at 25°C, 1 atm) was measured potentiometrically onboard ship using a Ag/AgCl combination reference electrode. Concentrations of total dissolved sulfide (ΣH_2S, hereafter abbreviated as H_2S) were determined gravimetrically at WHOI following shipboard precipitation as Ag_2S in a 5wt.% $AgNO_3$ solution. Ag_2S precipitates were stored in $AgNO_3$ solution for $\delta^{34}S$ analysis of H_2S ($\delta^{34}S_{H2S}$). Dissolved inorganic carbon (ΣCO_2, hereafter abbreviated as CO_2) concentrations were determined onshore after acidification of fluids with 25wt.% phosphoric acid by injecting aliquots of headspace gas directly onto a GC with a Porapak™ Q packed column and a thermal conductivity detector. These data were corrected to account for CO_2 partitioning between the headspace and fluid phases within each individual serum vial. Dissolved gas concentrations are expressed in concentration units of either mmol/L fluid (H_2S, H_2, CO and CH_4) for gases analyzed at sea or mmol/kg fluid (CO_2) for species analyzed in shore-based laboratories. The analytical uncertainty (2s) was ±10% for H_2, CH_4, CO and H_2S concentrations, ±5% for CO_2 concentrations and ±0.02 for pH(25°C) measurements.

The concentrations of the major elements (Mg, Na, Cl, Ca, K, SO_4, Br and F) were determined by ion chromatography. Concentrations of Fe, Mn, Li, Sr, Rb, Cs and Al were determined by inductively coupled plasma-mass spectrometry (ICP-MS) at WHOI (see Craddock (2008) for details). Dissolved SiO_2 and B concentrations were determined by inductively coupled plasma-optical emission spectrometry (ICP-OES) at the University of South Florida. To correct for the effects of sulfide precipitate formation within the fluid samplers, reported Fe data represent the 'total' concentrations obtained by summation of the dissolved and precipitated Fe fractions from a given sampler (Trefry et al., 1994; Craddock, 2008). The analytical uncertainty (2s) was ±5% for Mg, Na, Cl, Ca, K, SO_4, Br, and F concentrations, ±10% for Sr, Li, Rb, Cs, Fe, Mn and Al concentrations and ±2% for SiO_2 and B concentrations.

$\delta^{13}C_{CO2}$ and $\delta^{13}C_{CH4}$ values were determined at WHOI on a subset of samples by isotope ratio monitoring-gas chromatography mass spectrometry (irm-GC/MS) using a Finnigan Delta^{Plus}XL mass spectrometer interfaced to an Agilent 6890 gas chromatograph through a GCCIII interface (combustion furnace was held at 950°C for carbon isotope analysis). The pooled standard deviation (1s) is 0.3‰ for both $\delta^{13}C_{CO2}$ and $\delta^{13}C_{CH4}$ datasets. $\delta^{34}S_{H2S}$ measurements were conducted on Ag_2S precipitates with an automated elemental analyzer interfaced with an isotope ratio mass spectrometer at the USGS, Denver. SO_4 in selected fluid samples was precipitated as $BaSO_4$ prior to $\delta^{34}S_{SO4}$ determination by the same method. Analytical uncertainty on all $\delta^{34}S$ data is ±0.3‰ (2s). Oxygen isotope compositions of vent fluid H_2O ($\delta^{18}O_{H2O}$) were analyzed using an automated CO_2 equilibration device on a VG Optima mass spectrometer at the USGS, Denver. Hydrogen isotope compositions (δD_{H2O}) of vent fluid H_2O were analyzed as H_2 on a Finnigan MAT 252 mass spectrometer at the USGS, Denver. H_2 was prepared by the Zn reduction technique (Kendall and Coplen, 1985) following salt removal by

vacuum distillation. Analytical uncertainty (1s) for $\delta^{18}O_{H2O}$ and δD_{H2O} values are estimated to be 0.1 and 1.5‰, respectively.

Strontium isotope analyses ($^{87}Sr/^{86}Sr$) of fluids were conducted on a Finnigan MAT 261 thermal ionization mass spectrometer at the Freie Universität Berlin by static multi-collection (for further details see Eickmann et al. (2009)). External reproducibility of $^{87}Sr/^{86}Sr$ data is estimated to be on the order of 0.00007 (2s) based on three individually processed aliquots of IAPSO reference seawater ($^{87}Sr/^{86}Sr$ 0.709134 (±0.000066, 2s, n=3). Both this and the value for ambient bottom seawater in the Manus Basin (Table 5.1) are within error of the published value for seawater (0.70916, Banner (2004)). With the exception of $^{87}Sr/^{86}Sr$, all stable isotope data are reported using standard delta notation. For the isotope of interest, *A*, δA is defined by the following expression:

$$\delta A\ (‰) = \left[\frac{R_S - R_{STD}}{R_{STD}} \right] x\ 1000$$

Where R_S and R_{STD} are the isotope ratios of the sample and standard, respectively. $\delta^{13}C_{CO2}$ values are expressed relative to the V-PDB scale, while all $\delta^{34}S$ data are and CDT scales. $\delta^{18}O_{H2O}$ and δD_{H2O} values are both expressed relative to V-SMOW, with $\delta^{18}O_{H2O}$ values representing isotope activity ratios and δD_{H2O} values representing concentration ratios as per convention (Shanks et al. 1995; Shanks, 2001).

3.3 Calculation of endmember compositions

The fluid samplers used in this study have finite snorkel and valve dead volumes that were filled with bottom seawater prior to deployment. Vent fluids can mix with seawater prior to venting at the seafloor (due entrainment within vent structures or in the subseafloor plumbing system) and/or during the sampling process (contamination), hence the composition of collected

fluids invariably reflects two-component mixing of seawater and a hydrothermal fluid 'endmember'. The latter is conventionally assumed to be devoid of Mg, reflecting the composition of fluids prior to any mixing with seawater. This assumption is based on experimental evidence for near-quantitative removal of Mg from seawater during hydrothermal interactions with basalt, andesite, and rhyolite at reaction zone conditions typical of seafloor hydrothermal systems (Bischoff and Dickson, 1975; Mottl and Holland, 1978; Seyfried and Bischoff, 1981; Hajash and Chandler, 1982; Shiraki et al., 1987; Ogawa et al., 2005). It has been suggested that the highly acidic nature of many backarc basin fluids may reverse Mg uptake reactions thereby invalidating the assumption that a near-zero Mg composition exists prior to seawater admixing (Gamo et al., 1997; Douville et al., 1999; Butterfield et al., 2003). For the purposes of our interpretations, however, calculated 'endmember' compositions are assumed to contain no Mg as per convention. This assumes all Mg in our samples is seawater-derived and while we proceed with the conventional approach, we acknowledge some unknown proportion may not be. Our interpretations would not change significantly if compositions were extrapolated to an arbitrary Mg value (e.g. the lowest observed Mg in a given vent field (Douville et al., 1999)). Extrapolation of compositions to the lowest measured Mg concentration at each vent (in an attempt to remove effects of sampling-related seawater contamination only) would preclude meaningful comparisons between fluids for species unaffected by seawater admixing prior to venting, due to variable dilution/concentration effects between vents with differing seawater entrainment. However, while anomalous endmember values can implicate seawater entrainment in modifying pre-existing endmember fluid compositions, they do not represent realistic compositions in cases where non-conservative species behavior has occurred during mixing. In such instances we occasionally discuss compositions at lowest measured Mg concentrations ('minimum Mg') in addition to endmember values.

Endmember compositions were calculated by extrapolating measured concentrations of individual species in multiple fluid samples from a given orifice to zero Mg concentration using a linear least squares regression weighted to pass through ambient bottom seawater concentrations (Tables 5.1 and 5.2; Von Damm et al., 1985). Endmember $\delta^{18}O_{H2O}$ and δD_{H2O} values were calculated by extrapolation to zero Mg as per species concentrations. Measured $\delta^{13}C_{CO2}$ values were corrected to endmember values assuming 2.3 mmol/kg CO_2 in entrained seawater (see Cruse and Seewald, 2006). In cases where multiple samples from a given vent orifice were analyzed, endmember $\delta^{13}C_{CO2}$, $\delta^{13}C_{H2S}$ and $\delta^{34}S_{H2S}$ values were averaged. Endmember $^{86}Sr/^{86}Sr$ ratios were calculated by extrapolating measured molar Mg/Sr ratios to zero according to the method of (Albarède et al., 1981).

4. RESULTS

4.1 Temperature

Focused high-temperature fluids with near zero measured Mg concentrations were sampled from each of the three main structures at Vienna Woods (Fig. 5.2a, Table 5.1). Despite being located 100–150m apart, the three fluids exhibited a narrow range of temperatures (273–285°C) and compositions (Tables 5.1 and 5.2) suggesting that the Vienna Woods field is fed by a common source fluid. Measured temperatures, pH (25°C) and endmember fluid composition have remained relatively constant since previous expeditions in 1990 and 1995 (Lisitsyn et al., 1993; Auzende et al., 1996; Gamo et al., 1997; Douville et al., 1999; Fourre et al., 2006). In general, almost all aspects of the chemistry of fluids venting at Vienna Woods are similar to observations from basalt-hosted hydrothermal systems in MOR settings (Von Damm, 1995; German and Von Damm, 2003).

At Pual Ridge, focused fluids were sampled from 18 discrete orifices (Fig. 5.2b and 5.2c, Tables 5.1 and 5.2). Vent fluids sampled at Pual Ridge in 2006 show a wide range of temperatures in comparison to Vienna Woods. The hottest fluids were observed at the summit of the Fenway mound, where samples taken at F2 and F3 vents had maximum temperatures of 343°C and 358°C, respectively (Table 5.1). Fluids at F3 vent exhibited a 'flashing' phenomenon whereby exiting fluid was highly reflective under ROV lighting, but changed to smoke-like precipitate a few cm above the orifice. The phenomenon can be attributed to vigorous two-phase fluid venting (Massoth et al., 1989; Hannington et al., 2001; Stoffers et al., 2006). At a depth of 1710m (~171bar pressure) the fluid at F3 lies on the 2-phase boundary for a 3.2wt.% NaCl solution (Bischoff and Rosenbauer, 1985) consistent with subcritical boiling (Fig. 5.3). Measured temperatures at other vent areas on Pual Ridge were considerably lower than this.

4.2 Mg and SO_4

For most IGT samples taken at Vienna Woods, measured Mg is less than 1.6mmol/kg - the estimated maximum contribution of 'dead volume' seawater Mg for the sampler type (<4mL, Seewald et al., 2002). Measured Mg concentrations from all IGT samples (3.63 – 50.6mmol/kg) at Pual Ridge, however, are greater than the expected 'dead volume' contribution (Table 5.1, Fig. 5.4). The lowest Mg samples at the former (less than 10% of seawater Mg) were all from vents with temperatures greater than 300°C (Table 5.1). Many fluids sampled with both IGT and 'major' samplers have three near-identical measured Mg concentrations for different sampler types (RMR1, SM3, SC2, TK1, F2 and NP1 in Table 5.1). Sample sets from other vent fluids have two similar Mg values with a third (often suspected of accidental seawater entrainment) having much higher Mg (RMR2, RGR2, SC1, F1 and F5). It is unlikely that such consistently high Mg in repeat samples of a given vent fluid (with different sampler types) could be the result of accidental entrainment of near-identical amounts of seawater during each sampling event. These observations indicate that fluids exiting at the seafloor at Pual Ridge in 2006 all contain high concentrations of Mg relative to Vienna Woods fluids where Mg is near zero.

For all Vienna Woods samples, both measured Mg and SO_4 concentrations decrease linearly to near zero (Fig. 5.4). In contrast, SO_4 abundances in Pual Ridge vent fluids deviate from this behavior and both positive and negative endmember SO_4 concentrations are apparent. $\delta^{34}S_{SO4}$ values for all Pual Ridge fluids (Table 5.1) lie within a narrow range (+20.1 to +21.8‰) indicative of seawater-derived SO_4 (+20.99‰; Rees et al., 1978). Consequently, we do not explicitly calculate zero Mg endmember SO_4 concentrations are not as these would not reflect real compositions. Combined with high measured Mg concentrations, the predominance of seawater SO_4 suggests that many (if not all) fluids venting at the seafloor at Pual Ridge mixed with seawater prior to venting. Low temperature fluids at Fenway (F5, 80°C) and NE Pual (NP1,

35°C) are unique in that measured SO_4 concentrations are similar to or slightly greater than ambient seawater, but Mg concentrations are lower (Table 5.1). Samples from both fluids therefore trend toward positive apparent endmember SO_4 concentrations (Fig. 5.4).

4.3 pH

Endmember pH values were not calculated because of the numerous reactions that influence pH during seawater entrainment, both during sampling and in the subsurface. The pH's (measured at 25°C) in low Mg (<5mmol/kg) samples from Vienna Woods are mildly acidic, ranging from 4.22 to 4.92. In contrast, the pH of all PACMANUS fluids ranges from 2.32 to 5.90 (Table 5.1) and all high temperature (>250°C) fluid samples at PACMANUS (excluding those suspected of seawater contamination during sampling) fall within a narrow range of 2.32 to 2.96. The low temperature NE Pual fluid had relatively high pH (6.88–6.94). These values are significantly lower than Vienna Woods, but comparable to values previously reported for other arc/back-arc hydrothermal systems (Fouquet et al., 1991a; Fouquet et al., 1993; Gamo et al., 1997; Nakagawa et al., 2006; Takai et al., 2008).

4.4 H_2, H_2S, CH_4, CO and CO_2

In general, endmember concentrations of H_2, H_2S, CH_4 and CO_2 in Vienna Woods fluids are uniform and relatively low compared to the known range of MOR fluid compositions (Von Damm, 1995; German and Von Damm, 2003). At Pual Ridge, however, significant variability is evident in endmember H_2, H_2S, CH_4 and CO_2 both between vent areas and within each area (Table 5.2). With the exception of the high value of fluid F3 (306μM), all endmember H_2 concentrations are below 104μM. H_2 is generally low in fluids with lower measured exit temperatures, such as the Satanic Mills, Snowcap, and F5 fluids (Table 5.2, Fig. 5.5a).

Endmember H_2S ranges from 2.8mM at Roger's Ruins to 20.8mM in high-temperature Fenway fluids and is highest in fluids with lower endmember Cl (Fig. 5.5c). $\delta^{34}S_{H2S}$ values for PACMANUS are highly variable, with positive values (0.0 to +4.4‰) at Roman and Roger's Ruins but lower values (-2.7 to +2.6‰) at Satanic Mills, Snowcap and Fenway. The latter values are lower than the published range for unsedimented hydrothermal systems (+1.4 to +8.6‰; Shanks, 2001).

Endmember CO_2 values range from 4.38 to 4.48 mmol/kg at Vienna Woods and are comparable to the previously reported value for the site (6mM; Ishibashi et al., 1996). $\delta^{13}C_{CO2}$ values range from -5.2‰ to -5.7‰ and are within the range of basaltic CO_2 reported near Vienna Woods (-4.3‰ to -11.3‰; Shaw et al., 2004). With the exception of NE Pual, all fluids at Pual Ridge have substantially higher endmember CO_2 concentrations, ranging from 7.04mmol/kg (at Roger's Ruins) to 274mmol/kg at Satanic Mills (Table 5.2). Ishibashi et al. (1996) previously reported values of 20–40mM for the PACMANUS area but these data are minimum estimates because the samples were not acquired with gas-tight samplers. The highest CO_2 concentrations, found in the lower Cl fluids at Snowcap and Satanic Mills (Fig. 5.5b, Table 5.2), are among the highest reported to date for vent fluids (Karl et al., 1988; Butterfield et al., 1990; Sakai et al., 1990a,b; Von Damm, 1995; German and Von Damm, 2003; Lupton et al., 2006) and are comparable to those observed in black smoker fluids at the back-arc JADE site, Okinawa Trough (Sakai et al., 1990b). In addition to the higher concentrations relative to Vienna Woods, CO_2 is more ^{13}C-enriched at PACMANUS, with endmember $\delta^{13}C_{CO2}$ values varying from -4.1‰ to -2.3‰ (Table 5.2).

At all PACMANUS areas, endmember CH_4 concentrations are at the lower end of known compositions from MOR systems (German and Von Damm, 2003) but highly variable, ranging from 13.5μM at Fenway (F2) to a maximum of 78.1μM at Snowcap (SC2). Highest endmember

CH_4 concentrations are also evident in fluids with lower Cl contents (Fig. 5.5d). $\delta^{13}C_{CH4}$ values (Table 5.2) at PACMANUS (-7.4‰ to -15.2‰) are higher than Vienna Woods (-20.7‰ to -20.8‰), but values from both areas overlap the range observed for other unsedimented MOR hydrothermal fluids (-8.0‰ to -20.8‰, (McCollom and Seewald, 2007). CO concentrations are also variable at PACMANUS (highest endmember CO concentration (0.17μM) at F3 vent) but CO was not detected in Vienna Woods fluids (Table 5.2).

4.5 Cl, Br and F

Whilst endmember Cl concentrations are uniformly 25–30% higher than ambient seawater at Vienna Woods, much greater variability is evident at Pual Ridge (Table 5.2). Fluids at Roger's and Roman Ruins are all enriched in Cl relative to seawater, with endmember concentrations of 551 – 731mmol/kg, whereas the other vent areas are both enriched and depleted relative to seawater, reaching a minimum value of 388mmol/kg (Table 5.2). Fluids at Tsukushi, NE Pual and Fenway are enriched and depleted in Cl relative to seawater and fall within the above range. Endmember Br and Cl values at both Vienna Woods and Pual Ridge correlate well with each other and the majority of fluids have Br/Cl ratios close to that of ambient seawater (1.5, Table 5.3). In contrast to Vienna Woods fluids, which are uniformly depleted in F, all Pual Ridge fluids are variably enriched in fluoride relative to seawater (Fig. 5.6). Endmember F values at PACMANUS are the highest reported to date for seafloor hydrothermal systems (Von Damm, 1995; German and Von Damm, 2003). F also exhibits similar variability to CO_2 between vent fluids at Pual Ridge, with the highest concentrations of both at Snowcap, Satanic Mills and Fenway (Fig. 5.6).

4.6 $\delta^{18}O_{H2O}$ and δD_{H2O}

All vent waters at Vienna Woods have positive endmember δD_{H2O} and $\delta^{18}O_{H2O}$ values (Fig. 5.7), resembling observations from MOR hydrothermal systems (Shanks et al., 1995; Shanks, 2001). In contrast, though all PACMANUS fluids have endmember $\delta^{18}O_{H2O}$ values greater than those of Vienna Woods, the majority of δD_{H2O} values are substantially lower than seawater (Fig. 5.7). Thus, all PACMANUS fluid lie on a broad array of positive $\delta^{18}O_{H2O}$ and negative δD_{H2O} values, the latter being among the most negative found to date in seafloor hydrothermal fluids (de Ronde, 1995; Shanks et al., 1995; Gamo et al., 1997; Shanks, 2001). Though there is no discernable trend between the individual vent areas (Fig. 5.7), the lowest δD_{H2O} value is at Snowcap (SC2).

4.7 Alkalis, alkaline earths and B

Because Na and other ionic species tend to co-vary with Cl due to charge balance constraints, concentrations are typically normalized to Cl to eliminate this variability (Von Damm, 1995). All fluids from both Pual Ridge and Vienna Woods have lower endmember Na/Cl ratios than seawater (0.85), ranging from 0.76–0.84 at PACMANUS/NE Pual and 0.74–0.76 at Vienna Woods (Table 5.3).

Both absolute and Cl-normalized endmember K, Rb and Cs concentrations are much higher in Pual Ridge fluids relative to Vienna Woods fluids (Tables 5.2 and 5.3), consistent with the higher abundances of these elements in EMVZ crustal rock relative to the MSC (Sinton et al., 2003). The maximum K endmember concentration at PACMANUS (96.8mmol/kg, versus 21.2mmol/kg at Vienna Woods) is one the highest reported to date and consistent with previously reported endmember values at PACMANUS (80–90mmol/kg; Gamo et al., 1996a). Pual Ridge

fluids have a broader range of endmember Li concentrations (0.475–1.33mmol/kg) than Vienna Woods (1.07–1.16mmol/kg) but endmember Li/Cl ratios overlap in both areas (Table 5.3).

With the exception of NE Pual which has an endmember Ca concentration of 84.8mmol/kg, Pual Ridge fluids have much lower Ca contents (0.508 – 27.1mmol/kg) compared to Vienna Woods (70.7 – 80.9mmol/kg). These trends are also apparent on a Cl-normalized basis (Table 5.3). There is substantial inter- and intra-field variability at PACMANUS with some fluids even having lower endmember Ca/Cl ratios than seawater (Table 5.3). The highest endmember Ca/Cl ratios are in the low temperature F5 and NP1 fluids (Table 5.2).

Endmember Sr concentrations are also much lower at PACMANUS compared to Vienna Woods (Tables 5.2 and 5.3), with NE Pual having anomalously high Sr. Sr exhibits similar variability to Ca in Pual Ridge fluids and the elements tend to co-vary on a Cl-normalized basis. At Snowcap, measured Sr values extrapolate to an apparent negative endmember of -14.9μmol/kg, indicating significant non-conservative Sr behavior. The highest endmember Sr concentration (352μmol/kg) and Sr/Cl ratio are at F5 and NP1 vents (Table 5.2). Endmember $^{87}Sr/^{86}Sr$ ratios for PACMANUS fluids (Table 5.2) range from 0.69768 to 0.70429 and are lower than the Vienna Woods endmember (0.70435).

As shown in Tables 5.2 and 5.3, B is uniformly depleted (<0.246mmol/kg) relative to seawater (0.426mmol/kg) in Vienna Woods fluids but highly enriched in high temperature fluids at PACMANUS (up to 2.17mmol/kg). These upper values are high relative to MOR hydrothermal fluids (German and Von Damm, 2003), but within the range observed in other back-arc vent fluids (Ishibashi and Urabe, 1995). All low temperature fluids at Pual Ridge (F5, TK1 and NP1) are depleted in B below the level expected for conservative mixing of a fluid devoid of B with B-replete seawater. These compositions therefore yield apparent negative

endmember B concentrations, indicating substantial non-conservative mixing behavior (Table 5.2).

4.8 Fe, Mn, Al and SiO_2

Vienna Woods fluids were either clear or gray in color in 2006, which is consistent with the uniformly low endmember Fe (0.124–0.165mmol/kg; Table 5.2). Endmember Fe contents of Pual Ridge vent fluids are generally much higher and range from 0.076mmol/kg at Snowcap (SC1) to 14.6mmol/kg at Fenway (F2). The latter value is high compared to most MOR vent fluids to date (Butterfield and Massoth, 1994; Von Damm, 1995; Charlou et al., 2002; Gallant and Von Damm, 2006). Fluids with the highest endmember Fe contents (F2 and F3 at Fenway) also have the highest measured temperatures but Cl values <30% higher than seawater (Tables 5.1 and 5.2). There is also substantial variability between vent areas and within them at PACMANUS, with higher Mg fluids typically yielding lower endmember Fe values on a Cl-normalized basis (Table 5.2).

All Pual Ridge fluids are greatly enriched in Mn relative to Vienna Woods (Table 5.2), with endmembers ranging from 2.31 to 4.79mmol/kg. Similar to Fe, such Mn values are also among the highest reported for vent fluids to date (Ishibashi and Urabe, 1995; Von Damm, 1995; German and Von Damm, 2003). In contrast to Fe, however, there was less variability in Mn between vent areas or within them. Endmember Al contents at Vienna Woods are relatively uniform (6.6–7.5μmol/kg) and while they much more variable in high temperature fluids at Pual Ridge (6.1–14.6μmol/kg), concentrations are comparable between the two sites. Endmember SiO_2 concentrations are also variable at Pual Ridge compared to Vienna Woods (14.6–15.3mmol/kg), ranging from 11.3 to 23.9mmol/kg (Table 5.2).

5. DISCUSSION

Convective hydrothermal systems driven by magmatic heat sources are expected to share several basic features regardless of host rock (substrate) composition and tectonic setting. Seawater is typically assumed to enter the crust via a diffuse and poorly constrained 'recharge' zone and is subsequently heated to progressively higher temperatures. The hottest part of the hydrothermal reservoir – the 'reaction' or 'root' zone – is most likely adjacent to or above the magmatic intrusion, and is characterized by relatively low water/rock ratios. When buoyancy forces are sufficient to expel high temperature fluids from the hydrothermal reservoir, fluids rise toward the seafloor through a 'discharge' or 'upflow' zone under much higher water/rock ratios (Alt, 1995; Alt and Bach, 2003). Processes that can modify the composition of black smoker fluids during transit through such systems include: (i) water-rock (and/or sediment) interaction, (ii) phase separation, (iii) input of magmatic volatile species and (iv) and subsurface mixing with crustal seawater (Von Damm, 1995; German and Von Damm, 2003). Given the similarity of hydrothermal interactions (i) between seawater and basalt, andesite and rhyolite under experimental conditions (Bischoff and Dickson, 1975; Mottl and Holland, 1978; Seyfried and Bischoff, 1981; Hajash and Chandler, 1982; Shiraki et al., 1987; Ogawa et al., 2005), processes of Mg-fixation and anhydrite precipitation are expected to control Mg, Ca and SO_4 abundance during recharge of seawater into the crust at both Pual Ridge and Vienna Woods vent fields. Similarly, the abundances of other major elements (Na, Ca) are likely to be buffered by fluid-mineral equilibria under reaction zone conditions, albeit at different compositions (Seyfried, 1987; Butterfield et al., 2003). In addition, phase separation (ii) should influence the abundances of elements if *P-T* conditions within the hydrothermal reservoir reach the 2-phase boundary. Entrainment of magmatic volatiles (iii) most likely occurs near the 'reaction' zone, due to close proximity to the magma. Because of the relatively inert nature of MORB-derived volatiles, this

process is unlikely to significantly alter the acidity of high temperature fluids in typical mid-ocean ridge (MOR) systems (Butterfield et al., 2003). However, felsic-hosted magmatic hydrothermal systems are likely to differ substantially in this respect due to compositional differences in degassed volatiles (Yang and Scott, 2006). Significant modification of high temperature fluids by subsurface mixing (iv) has been recognized in MOR sites, such as the TAG hydrothermal mound on the Mid-Atlantic Ridge (Edmond et al., 1995; Tivey et al., 1995; Gamo et al., 1996b), North Cleft on the Juan de Fuca Ridge (Butterfield and Massoth, 1994) and Kairei Field, Central Indian Ridge (Gallant and Von Damm, 2006) and depends on the hydrologic regime in the 'upflow' zone. In the following discussion we examine the evidence for these four processes in the chemistry of Pual Ridge and Vienna Woods vent fields.

5.1 Influence of water/rock reaction and substrate composition on fluid compositions

5.1.1 Fluid-mineral equilibria

Elements whose abundances are controlled by temperature and pressure dependant fluid-mineral equilibrium reactions, such as Ca and Na (Berndt et al., 1989; Berndt and Seyfried, 1993), exhibit similar trends in Manus Basin fluids to MOR hydrothermal systems and do not differ substantially as a function of substrate composition between Vienna Woods and Pual Ridge. While few experimental studies have examined felsic rock-seawater interactions under hydrothermal conditions, early experimental work has demonstrated that seawater interactions with more silicic rock compositions (rhyolite and andesite) broadly resemble those with basalt for many of these 'solubility-controlled' species (Hajash and Chandler, 1982; Shiraki et al., 1987). Endmember Na/Cl ratios from Pual Ridge fluids overlap those at Vienna Woods and all are lower than the seawater ratio, suggesting removal of Na by albitization (Table 5.3). Though absolute Ca abundances in fluids from Pual Ridge have been variably modified by subsurface anhydrite

deposition or dissolution (see below), endmember Ca/Cl ratios from fluids with lowest Mg (<5mmol/kg) are greater than seawater (Table 5.2), suggesting Ca addition presumably by the same process. Both Ca/Cl and Na/Cl ratios in the lowest Mg fluids at PACMANUS are within the ranges observed in unsedimented hydrothermal systems in MOR settings, suggesting that the compositional differences in substrate at Pual Ridge do not influence these elements substantially.

In addition to Ca and Na, Sr abundance in hydrothermal fluids is also considered to be solubility-controlled (Berndt et al., 1988; Von Damm, 1988) and fluids from the Manus Basin also reflect this. Despite higher crustal abundances of Sr in crustal rocks of the EMVZ (Sinton et al., 2003), Sr/Cl ratios in the lowest Mg fluids at Pual Ridge are lower than corresponding ratios at Vienna Woods. Like Ca/Cl and Na/Cl, Sr/Cl ratios in both settings are within the range observed in MOR hydrothermal systems (Gallant and Von Damm, 2006), suggesting similar solubility control. Even though endmember $^{87}Sr/^{86}Sr$ ratios at PACMANUS are variable (Fig. 5.8) due to non-conservative Sr behavior during seawater admixing (Section 5.4), endmember ratios calculated for lowest Mg fluids at Vienna Woods (0.70435) and PACMANUS (0.70394–0.70428) are consistent with a predominantly rock-derived source of Sr. Crustal $^{87}Sr/^{86}Sr$ ratios from Pual Ridge and surrounding areas fall in a narrow range of 0.703446–0.703690, while MSC basalts have a ratio of 0.703275 (Kamenetsky et al., 2001; Marty et al., 2001; Sinton et al., 2003). A possible explanation for the slightly higher $^{87}Sr/^{86}Sr$ ratios in fluids least affected by subsurface mixing is that the Sr represents a mixture of seawater- and rock-derived Sr. Berndt et al. (1988) proposed a fluid reaction path model to explain the relationship between Sr abundance and $^{87}Sr/^{86}Sr$ ratios in MOR vent fluids whereby incomplete seawater Sr removal occurs during recharge (by anhydrite deposition), followed by subsequent addition of rock-derived Sr by dissolution of Ca- and Sr-bearing primary plagioclase minerals in high temperature reaction zones. Early stage precipitation would remove Sr without changing its isotopic composition

while subsequent addition of rock Sr from plagioclase dissolution would give rise to decreased $^{87}Sr/^{86}Sr$ ratios and increased Sr concentrations.

Despite the high temperature of some fluids at PACMANUS (e.g. 358°C at F3), none of the sampled fluids are devoid of Mg as is typical at Vienna Woods and other MOR hydrothermal fluids. While we argue below (Section 5.4) that the majority of Mg in Pual Ridge fluids must be seawater-derived, an additional source of Mg cannot be excluded for the hottest fluid (F3). Two of the three samples from F3 have consistent measured Mg (4.52 and 4.74 mmol/kg, Table 5.1) and temperatures (358 and 356°C, respectively). It is unlikely that these concentrations reflect entrainment of identical amounts of seawater during sampling, and they are greater than can be attributed to the dead volume of the IGT samplers (which accounts for <1.6mmol/kg Mg in any given IGT sample). This implies a Mg content of ~3 mmol/kg as the F3 fluid exited the seafloor at a temperature that places it on the boiling curve at seafloor pressure. It is unreasonable to conclude that this Mg could be derived from seawater mixing prior to venting as the required ~5% mix of seawater would cool the fluid by ~20°C below the two-phase boundary. The possibility exists that admixing of small amounts of a hotter seawater-like fluid occurred deep in the system and boiling occurred in response to decompression during upflow, but it is hard to envision a scenario whereby Mg-bearing seawater penetrates deep-seated reaction zones in such a hot and active system. An alternative explanation to account for this small, but significant concentration of Mg, is that it reflects the enhanced solubility of Mg-aluminosilicates at the exceedingly low pH of this fluid (2.74). Indeed, the solubility of Mg in hydrothermal systems in general, can be represented by the reaction:

$$Mg^{2+} + 4/3SiO_{2(aq)} + 4/3H_2O = 1/3Mg_3Si_4O_{10}(OH)_2 + 2H^+ \quad (3)$$

where talc ($Mg_3Si_4O_{10}(OH)_2$) is used to represent more compositionally complex phases (Seyfried, 1987). The stoichiometry of this reaction indicates that at equilibrium the activity of Mg^{2+} will

vary inversely with the square of H^+ activity. Accordingly, because vent fluids at PACMANUS are characterized by pH values within a range of 2 to 3 while pH typically varies from 3 to 4 in MOR systems (Von Damm, 1995; German and Von Damm, 2003), Mg activities at PACMANUS according to equation (3) or similar reactions may be 2 to 4 orders of magnitude higher at a given temperature, pressure and silica activity (Seyfried, 1987), possibly approaching the same order of magnitude as Mg contributions from sampler dead volume. Given the complex nature of Mg phases that may control Mg solubility (Seyfried, 1987) and limited thermodymanic data for these phases, however, further speculation is difficult. Regardless, the lowest measured Mg concentrations at PACMANUS are sufficiently close to zero that endmember compositions would not change substantially if these Mg values reflect true compositions prior to seawater admixing.

5.1.2 Alkalis and B

The influence of compositional differences in host rocks between the MSC and EMVZ is most apparent in the abundances of elements that are considered highly 'mobile' during fluid-rock interactions. Field and laboratory data indicate that alkali elements are almost quantitatively partitioned into the fluid phase during high temperature fluid-rock interaction with basalt and more silicic rock compositions (Seyfried et al., 1984; Von Damm et al., 1985; Von Damm, 1990; Ogawa et al., 2005). Endmember abundances of the alkalis K, Rb and Cs are highly elevated in PACMANUS fluids relative to Vienna Woods (Tables 5.2 and 5.3) and basalt-hosted MOR systems (German and Von Damm, 2003). This is entirely consistent with the greater abundances of these incompatible elements in arc-like EMVZ crust relative to the more mafic crust of the MSC (Kamenetsky et al., 2001; Sinton et al., 2003; Paulick et al., 2004; Monecke et al., 2007). In contrast to the other mobile alkalis, large differences in endmember Li concentrations are not evident between Vienna Woods and PACMANUS (Table 5.2). This observation is, however,

also consistent with limited data suggesting the Li content of EMVZ crust (~5–7ppm) does not differ from that of the MSC basalt (~5–8ppm) to the same extent as K, Rb and Cs (Sinton et al., 2003). In addition to differences in absolute abundances, endmember molar ratios of alkalis in Pual Ridge and Vienna Woods fluids are in reasonable agreement with the alkali ratios of the dominant rock compositions at each location (Fig. 5.9). B is also greatly enriched in most Pual Ridge fluids relative to Vienna Woods, consistent with greater B enrichment in more silicic rock compositions and the increased influence of recycled slab material as the arc is approached (Spivack and Edmond, 1987; Ryan and Langmuir, 1993). Because of the strong affinity of B for fluids, however, we cannot exclude magmatic degassing as an additional source of B to hydrothermal fluids at Pual Ridge (Ryan and Langmuir, 1993; Arnorsson and Andresdottir, 1995; Audetat et al., 1998).

If it is assumed that the mobile alkali elements Rb and Cs are quantitatively leached during hydrothermal alteration and do not undergo significant secondary mineral formation, effective water/rock (w/r) ratios can be calculated if fluid and rock concentrations are known (Von Damm et al., 1985). Rb and Cs contents vary widely in the EMB and along the MSC, however, as a result of highly varying substrate composition (Sinton et al., 2003). Using Rb (0.9ppm) and Cs (0.018ppm) contents from dredged basalt to the south of Vienna Woods (Sinton et al., 2003), calculated w/r ratios for fluids there vary from 0.5 to 0.6. Using values of Rb (27ppm) and Cs (0.8ppm) reported for Satanic Mills lava flows (Monecke et al., 2007), higher w/r ratios are calculated for high temperature (>200°C) fluids at Pual Ridge, varying from 5 to 6 for Rb and 2 to 3 for Cs. Differences between these locations notwithstanding, the relatively low values combined with the alkali ratio patterns discussed above indicate hydrothermal fluids at both Pual Ridge and Vienna Woods have reacted with fresh crustal rocks under rock-dominated conditions (Seyfried and Mottl, 1982).

5.1.3 Quartz-fluid equilibrium and dissolved SiO_2

SiO_2 contents in PACMANUS and NE Pual fluids, though highly variable, suggest considerable depths of hydrothermal circulation beneath Pual Ridge. The solubility of quartz in hydrothermal solutions is a strong function of temperature, pressure and to a lesser extent, salinity. Based on the assumption of quartz-fluid equilibrium at depth, dissolved SiO_2 is commonly used as an indicator of maximum *P-T* conditions encountered by hydrothermal fluids (Fournier, 1983; Von Damm et al., 1991; Foustoukos and Seyfried, 2007a). Using extrapolated (to zero Mg) vent temperatures and the quartz solubility data of (Von Damm et al., 1991), and SiO_2 contents, RMR2 and RGR1 compositions suggest quartz-fluid equilibrium at pressure of 400–700 bar (Fig. 5.10). While the upper limit may be excessive, the lower limit suggest circulation depths in the vicinity of a possible magma body ~2km beneath the seafloor at Pual Ridge (Lee, 2003; Binns et al., 2007; Sun et al., 2007). There is a high degree of variability between co-located vents (e.g. RMR1 and RMR2), however, and shallower equilibration pressures (<300 bars) are predicted for most other vents (Fig. 5.10). It has been suggested that the accuracy of the SiO_2 geobarometer in felsic-hosted systems may be affected by re-equilibration of SiO_2 with quartz-rich wall-rock occurs during fluid upflow (Ishibashi and Urabe, 1995). Abundant subsurface quartz-bearing vesicles and veins observed in ODP drillcores from postulated upflow zones suggest that some SiO_2 deposition has occurred during ascent of fluids to the seafloor at PACMANUS (Binns et al., 2007). While this process may be responsible for lower apparent equilibrium pressures, it cannot, however, explain the extremely high silica observed at RMR2 and RGR1.

In contrast, predicted equilibrium pressures (>1000bar) for all three vents at Vienna Woods imply an unreasonable depth of circulation there. A more plausible explanation is that extensive cooling of the Vienna Wood source fluid has occurred during upflow, as evidenced by

the low Fe contents (Table 5.2) and the high dissolved SiO_2 contents are merely a relic of much higher temperatures than those venting at the seafloor.

5.1.4 pH and metal mobility

The above observations suggest fluid-mineral buffering of major element abundances at depth. However, the pH of the lowest Mg samples at PACMANUS (2.62–2.74) is considerably more acidic than those observed during laboratory experiments that reacted seawater and rhyolite/dacite (3.5–4.5) at temperatures of 300–500°C (Hajash and Chandler, 1982; Shiraki et al., 1987). These experiments were conducted at 1 kbar pressure, however, which may be greater than reaction zone pressures encountered by fluids at PACMANUS where the seafloor pressure is ~170bar. Owing to effects on fluid density and species dissociation equilibria, lower pressures tend to yield slightly lower measured pH values buffered by heterogeneous equilibrium reactions (Seyfried, 1987). However, such uniformly low pH values, such as those at PACMANUS, are not common in basalt-hosted hydrothermal systems at similar depths (Butterfield et al., 2003). Such high acidity in black smoker fluids have only been observed in other arc and back-arc settings such as the Vai Lili (Fouquet et al., 1991a,b; Fouquet et al., 1993) and Mariner fields (Seewald et al., 2005; Takai et al., 2008) in the Lau Basin. Low pH values (2.39 to 2.66) at Mariner are suggested to be the result of magmatic acid volatile (SO_2) degassing from underlying magmas (Seewald et al., 2005; Takai et al., 2008). As discussed below, we propose that acidity-generating volatiles degassed at depth have contributed to the low pH values at PACMANUS also. In contrast, the much higher pH of Vienna Woods fluids (4.41–4.71) is more consistent with buffering by fluid-rock interactions alone.

The influence of acidity is apparent in the high Fe and Mn contents of PACMANUS fluids. Experiments have demonstrated that Fe and Mn solubility during hydrothermal alteration

of basalt and more felsic rock compositions is a complex and sensitive function of *in situ* pH, in addition to temperature, pressure and fluid composition (Mottl et al., 1979; Hajash and Chandler, 1982; Rosenbauer and Bischoff, 1983; Seyfried and Janecky, 1985; Seyfried, 1987; Seewald and Seyfried, 1990). At PACMANUS, endmember Fe concentrations from low Mg (<5mmol/kg) fluids range from 6.86 to 14.6mmol/kg, with corresponding endmember Mn concentrations of 3.01 to 4.72mmol/kg. These are among the highest Fe and Mn contents reported to date for either arc or back-arc basin hydrothermal fluids (Ishibashi and Urabe, 1995). Higher values have been observed at the basalt-hosted North Cleft system (Butterfield and Massoth, 1994) and the ultramafic-hosted Rainbow site (Charlou et al., 2002). In the case of North Cleft, high endmember Fe concentrations are associated with extremely high Cl contents (in excess of 1000mmol/kg) that greatly enhance Fe solubility at high temperature. The comparatively low endmember Cl (698mmol/kg) in the vent fluid (F2) with highest endmember Fe content (Table 5.2) indicates that factors other than Cl, such as pH, temperature and pressure are responsible. Fe and Mn solubility are expected to be greatest at relatively low pressures, high temperatures and low pH values (Seyfried, 1987). Given that temperatures at PACMANUS do not appear to be anomalously high or pressures anomalously low relative to other hydrothermal systems, the exceptionally high dissolved Fe and Mn contents most likely reflects the highly acidic nature of these fluids.

The Fe and Mn contents of Vienna Woods fluids are in good agreement with experimental observations of their mobility from crystalline basalt as a function of temperature (Seewald and Seyfried, 1990). The extremely low Fe contents of fluids there (Table 5.2) are consistent with the low temperatures of venting as Fe mobility in endmember fluids is rapidly diminished below 300°C in the absence of any seawater admixing. Mn in hydrothermal fluids, which has sluggish kinetics of re-precipitation upon cooling, tends to reflect much hotter

temperatures of mobilization. Based upon the experimental study of (Seewald and Seyfried, 1990), Mn concentrations in Vienna Woods fluids (Table 5.2) are more consistent with temperatures up to ~350°C. Such high temperatures in the reaction zone would reconcile the observations of high SiO_2 for the temperatures of venting that yield unreasonable apparent depths of quartz-fluid equilibrium (Fig. 5.10).

5.2 Phase separation and Cl variability

Vienna Woods and Pual Ridge fluids exhibit variable enrichments or depletions in endmember Cl relative to seawater (Table 5.2). While we can demonstrate much of this variability is due to phase separation, prior magmatic- or rock-derived Cl inputs cannot be ruled out in the case of Pual Ridge fluids. Cl variations in MOR hydrothermal fluids beyond that permissible by rock hydration effects are typically attributed to phase separation (Von Damm, 1990; Von Damm, 1995; German and Von Damm, 2003; Foustoukos and Seyfried, 2007b) and rock-derived Cl is typically not considered a significant source to mid-ocean ridge vent fluids due to the low Cl content of MORB (Michael and Schilling, 1989; Michael and Cornell, 1998). Silicic crustal rocks in back-arc environments, however, have higher Cl contents (Wallace, 2005; Aiuppa et al., 2009) and dredged dacites from the vicinity of Pual Ridge contain up to 0.84wt.% Cl (Sun et al., 2007). However, quantitative leaching of such dacite at the water/rock ratios calculated previously (2 to 6) could only increase vent fluid chlorinity by <120mmol/kg. Basalts from the MSC have lower Cl contents (<0.15wt.%, Sinton et al. 2003), and complete leaching at calculated water/rock ratios (~0.5) could only enrich Cl in Vienna Woods fluids by <50mmol/kg. Furthermore, while Cl enrichments might be possible, a solely rock-derived source of Cl cannot account for Cl depletions in Pual Ridge vent fluids. Input of Cl to Pual Ridge fluids from magmatic fluid degassing cannot be excluded, however, given the Cl-rich nature of Pual Ridge

magmas (Sun et al., 2007), and the chlorinity of magmatic fluids may be substantially higher or lower than seawater. While we demonstrate below that phase separation influences species abundances at Pual Ridge, we do acknowledge that hydrothermal fluids undergoing phase separation there may have initial chlorinities different from seawater.

Conclusive evidence for subcritical phase separation at seafloor pressures was found at the Fenway site where the maximum measured temperature of 358°C at F3 vent places this fluid on the two-phase boundary for a fluid of seawater salinity (Fig. 5.3) at a seafloor pressure of 171 bar (Bischoff and Rosenbauer, 1985). The observed flashing and variability in dissolved major element and gas concentrations between multiple fluid samples collected at F3 (Table 5.1) are consistent with active boiling and partial segregation of a 2-phase emulsion of immiscible vapor/brine during venting at the seafloor (Bischoff and Pitzer, 1985; Hannington et al., 2001; Stoffers et al., 2006). Measured exit temperatures (Fig. 5.3) for all other vent fluids at PACMANUS and Vienna Woods lie well below the seawater two-phase boundary at seafloor pressures. If phase separation at depth has contributed to Cl variability, these fluids must have undergone substantial cooling prior to venting at the seafloor. As discussed in Section 5.4, there is substantial evidence to indicate mixing-related and possibly conductive cooling at Pual Ridge. At Vienna Woods, the low measured Mg concentrations preclude seawater mixing as a heat loss mechanism and extensive conductive cooling (>100°C) is required to explain the low observed temperatures relative to the two-phase boundary (Fig. 5.3). As stated previously, Mn abundances in Vienna Woods fluids only suggest temperatures near 350°C and so it is possible that the high Cl endmembers do not reflect active phase separation at depth in 2006, but rather entrainment/depletion of residual brines formed during previous phase separation events (Shanks and Seyfried, 1987; Von Damm and Bischoff, 1987; Von Damm, 1988; Butterfield and Massoth, 1994; Butterfield et al., 1997; Schoofs and Hansen, 2000; Von Damm et al., 2005). Brine

entrainment would be consistent with the chronic venting of Cl-rich fluids at Vienna Woods since 1990 (Lisitsyn et al., 1993; Auzende et al., 1996; Gamo et al., 1997; Douville et al., 1999; Fourre et al., 2006) and the apparent absence of any Cl-depleted conjugate fluids.

Measured temperatures below the two-phase boundary, notwithstanding, systematic compositional variability between fluids within several PACMANUS vent areas strongly suggest that fluid other than F3 are also influenced by phase separation. Endmember concentrations of soluble alkali elements K, Li, Rb, and Cs show strong linear correlations with endmember Cl in areas with co-located vent fluids that extrapolate toward the origin (Fig. 5.11). Because these elements are readily mobilized from the crust during high temperature fluid-rock interaction (Seyfried et al., 1984; Von Damm et al., 1985; Von Damm, 1995) and they do not preferentially partition into the vapor phase (except under extreme conditions near halite saturation), alkali/Cl ratios are unaffected by phase separation (Berndt and Seyfried, 1990; Foustoukos and Seyfried, 2007b,c). This behavior implies phase separation and partial segregation of high and low salinity phases (Butterfield et al., 1994). Systematic variations in the endmember abundances of aqueous gases with Cl are also consistent with ongoing phase separation at PACMANUS. Endmember CO_2 and CH_4 concentrations at Fenway and Roman Ruins increase systematically with decreasing Cl (Figs. 5.5b and 5.5d), consistent with enhanced partitioning of volatile species into the lower salinity phases during phase separation. H_2 and H_2S are much more variable (Figs. 5.5a and 5.5c) but these species may behave non-conservatively during seawater admixing in the subsurface (see below). Processes in addition to phase separation, however, must be invoked to explain the extreme enrichments in dissolved CO_2 at Satanic Mills and Snowcap (Fig. 5.5b) and the lack of comparable enrichments in CH_4 (Fig. 5.5d). In general, it is difficult to attribute enrichments of this magnitude in seafloor hydrothermal fluids with partitioning of CO_2 into vapor phases

(Butterfield et al., 1990; Butterfield et al., 1994; Butterfield et al., 2003; Seewald et al., 2003), and additional sources of CO_2 such as magmatic degassing (discussed below) must be responsible.

5.3 Magmatic fluid input at Pual Ridge

The extensive vesicularity of felsic crust at Pual Ridge (Binns and Scott, 1993; Marty et al., 2001; Paulick et al., 2004) and the presence of vapor bubbles containing H_2O, CO_2 and sulfur precipitates in accompanying melt inclusions (Yang and Scott, 1996; Kamenetsky et al., 2001; Kamenetsky et al., 2002; Yang and Scott, 2002) indicate that the magmas that formed these lavas were super-saturated with a volatile phase during eruption and emplacement. Yang and Scott (2005) suggested that fractional crystallization of magmas beneath Paul Ridge could sustain pre-eruptive degassing on timescales of several decades, comparable to the lifetimes of hydrothermal systems. Given that a magma body 2km beneath the surface of Pual Ridge has been suggested (Lee, 2003; Binns et al., 2007; Sun et al., 2007) and the similar apparent depths of quartz-fluid equilibrium for some PACMANUS fluids discussed above, it is reasonable to assume circulating hydrothermal fluids there may reach sufficient depths to entrain fluids exsolved from degassing silicic magma.

5.3.1 Isotopic evidence for magmatic H_2O

Addition of magmatic water to Pual Ridge vent fluids is evident in the stark contrast in H_2O isotopic composition there compared to fluids at Vienna Woods (Fig. 5.7) and it is clear that other processes cannot account for this observation. The stable isotopic composition of vent fluid H_2O can record the integrated effects of three fundamental processes – water/rock (and/or sediment) interaction, phase separation and any contributions from extraneous magmatic waters. Hydration reactions between circulating hydrothermal fluids and igneous crust at high

temperatures invariably yield a trend of increasing $\delta^{18}O_{H2O}$ and δD_{H2O} values (relative to unmodified seawater) with decreasing water/rock ratios (Bowers and Taylor, 1985; Bowers, 1989; Shanks et al., 1995; Shanks, 2001). Incremental reaction path models of the isotopic evolution of these fluids indicate that the trajectory of such trends is a function of the mineral assemblage and the temperature of water/rock interaction, with increasing temperatures of reaction yielding greater δD_{H2O} increases relative to $\delta^{18}O_{H2O}$. Compared to the reaction path models of Shanks et al. (1995), values at Vienna Woods suggest interactions between basaltic mineral assemblages and hydrothermal fluid at ~300°C under water/rock ratios ≤ 1, in line with observed temperatures and water/rock ratios calculated above (~0.5). While the more positive endmember $\delta^{18}O_{H2O}$ values of the PACMANUS fluids are consistent with water/rock reaction at higher temperatures and/or lower water/rock ratios than Vienna Woods, alternate mechanisms must be invoked to explain the ubiquitous negative endmember δD_{H2O} values (Fig. 5.7).

Although phase separation is occurring at Pual Ridge (as discussed previously) and experimental studies have shown that both subcritical and supercritical phase separation processes occurring in seafloor hydrothermal systems can affect the hydrogen and oxygen isotopic composition of vent waters (Horita et al., 1995; Berndt et al., 1996; Shmulovich et al., 1999; Foustoukos and Seyfried, 2007b) this process cannot account for the observed hydrogen isotope composition of vent fluids there. Under most open- or closed-system scenarios for phase separation, vapor phases are slightly enriched in D relative to the heavily D-depleted brine phases while the reverse is true for oxygen isotope partitioning (Berndt et al., 1996; Foustoukos and Seyfried, 2007b). Examination of the PACMANUS fluids reveals no systematic variations in δD_{H2O} or $\delta^{18}O_{H2O}$ with endmember Cl (Table 5.2). Furthermore, low chlorinity fluids have consistently negative δD_{H2O} and positive $\delta^{18}O_{H2O}$, opposite to the trend expected for phase separation. While Berndt et al. (1996) propose that generation of a vapor phase with highly

negative δD_{H2O} and positive $\delta^{18}O_{H2O}$ values is conceivable under a scenario of combined water/rock reaction and open-system phase separation during isobaric heating (*i.e.* by subsurface dike emplacement), it requires segregation of a heavily distilled vapor (Foustoukos and Seyfried, 2007b). No such dilute vapors were observed at PACMANUS. Admixture of residual D-depleted brine (Shanks and Seyfried, 1987; Von Damm and Bischoff, 1987) could contribute to the negative δD_{H2O} values in high chlorinity Roman/Roger's Ruins (Table 5.2), the lack of any consistent δD_{H2O} trend with endmember Cl renders this unlikely.

Negative δD_{H2O} values and positive $\delta^{18}O_{H2O}$ values can be produced by extensive reaction of hydrothermal fluids with sedimentary overburden (Shanks et al., 1995; Von Damm et al., 2005). However, given the negligible sediment cover on the crest of Pual Ridge (Binns et al., 2007) and the lack of a thermogenic $\delta^{13}C_{CH4}$ signature (Table 5.2; Welhan, 1988; Cruse and Seewald, 2006), there is no evidence to suggest that PACMANUS fluids have interacted with sediments.

Given the failure of the above processes to account for the array of negative δD_{H2O} and positive $\delta^{18}O_{H2O}$ values at Pual Ridge, we propose that direct input of isotopically-distinct magmatic water to seawater-derived hydrothermal fluids is the most plausible explanation. The isotopic signature of 'juvenile' or mantle-derived magmatic water is estimated to have a narrow range of δD_{H2O} (–65±20‰) and $\delta^{18}O_{H2O}$ (+6±1‰), (Taylor, 1979b; Ohmoto, 1986). In contrast, waters degassed from silicic arc magmas (subduction-related volcanic vapors, SRVV) may have much higher δD_{H2O} (-10 to -30‰) and $\delta^{18}O_{H2O}$ (+6 to +10‰) values (Giggenbach, 1992; Hedenquist and Lowenstern, 1994). Degassing-related fractionation and slab-derived seawater inputs can both increase the δD_{H2O} value of magmatic waters at convergent margins (Taylor, 1986; Giggenbach, 1992; Taylor, 1997; Pineau et al., 1998; Shaw et al., 2008). While it is impossible to accurately constrain the isotopic composition of magmatic water added, the array of

PACMANUS isotopic compositions trends toward a D-depleted and highly ^{18}O-enriched component similar to the SRVV compositions and does not lie within the trends expected for simple mixing of hydrothermal fluids with δD_{H2O} values of -40 to -80‰ (Fig. 5.7) suggested for fluids from the nearby DESMOS hydrothermal system (Gamo et al., 1997). Although the observed isotopic compositions at PACMANUS could reflect the addition of SRVV to unmodified seawater isotopic compositions, it is hard to envision a scenario where seawater could reach high temperature environments in the vicinity of a degassing magma chamber without extensive isotopic modification. The most likely scenario is that SRVV-like compositions are mixing with evolved (seawater-derived) hydrothermal fluids that have experienced extensive fluid-rock interaction (analogous to Vienna Woods) and have increased δD_{H2O} and $\delta^{18}O_{H2O}$ values (Fig. 5.7).

A crude estimate of the minimum quantity of magmatic H_2O added to circulating fluids can be constrained by simple hydrogen isotope mass balance. For this calculation we assume that the effects of phase separation on δD_{H2O} are negligible, magmatic H_2O at all PACMANUS areas have a uniform δD_{H2O} of -30‰ (the lower limit of SRVV compositions (Giggenbach, 1992; Hedenquist and Lowenstern, 1994)) and the circulating fluids into which magmatic waters are entrained have δD_{H2O} values similar to Vienna Woods fluids (+2.4‰) due to prior water/rock reaction. With these assumptions in mind, a 1wt% magmatic H_2O fraction is required to produce the composition observed in Roman Ruins fluid RMR1 (the highest δD_{H2O} value in Fig. 5.7). Fluid at the Snowcap SC2 vent would require a 20wt% magmatic H_2O fraction, with the majority of fluids within these two extremes. While these estimates are speculative and highly variable, they do suggest substantial quantities of magmatic water are entrained by circulating hydrothermal fluids.

5.3.2 Magmatic CO_2, F, and Cl

Elevated abundances of aqueous CO_2 in PACMANUS vent fluids are consistent with a direct contribution of magmatic volatiles because CO_2 is invariably released from silicic magmas during cooling and crystallization (Carroll and Webster, 1994; Yang and Scott, 2006). Although some of the CO_2 observed in PACMANUS fluids may be derived from rock leaching, unaltered subseafloor dacites recovered by ODP drilling at Snowcap, Roman Ruins and Satanic Mills contain less than 500 ppm residual CO_2 (Paulick et al., 2004). Assuming quantitative mobilization, this limits the total amount of CO_2 that can be derived by substrate leaching to <6mmol/kg for the range of water/rock ratios calculated using alkali abundances (2 – 6). Concentrations of aqueous CO_2 in basalt-hosted mid-ocean ridge vent fluids that approach values observed at PACMANUS have also been attributed to active magmatic degassing (Butterfield et al., 2003; Lilley et al., 2003; Seewald et al., 2003). While primary CO_2 contents of parental magmas at PACMANUS are poorly constrained (Marty et al., 2001), weight percent additions of magmatic H_2O (estimated above) indicate that CO_2 is far less abundant than H_2O in the magmatic fluids being added. The exsolution of a water-dominated magmatic fluid suggests relatively shallow (crustal) magma chamber (Yang and Scott, 2006), consistent with the speculation of a fractionating silicic magma body beneath Pual Ridge (Lee, 2003; Yang and Scott, 2005; Binns et al., 2007; Sun et al., 2007).

Examination of the carbon isotopic composition of vent fluid CO_2 at PACMANUS (-4.1 to -2.3‰) reveals a more ^{13}C enriched CO_2 source relative to Vienna Woods fluids (-5.2 to -5.7‰), which likely reflects the closer proximity of the latter to the New Britain Arc (80km *vs.* 220km) and a larger contribution of more ^{13}C-enriched slab-derived carbon. $\delta^{13}C_{CO2}$ values in fluids from unsedimented hydrothermal systems measured to date range from -3.15‰ to -13.0‰ (Charlou et al., 1996; Charlou et al., 2002; McCollom and Seewald, 2007) but the majority of

typical basalt-hosted fluids range from -4‰ to -9‰ (Kelley et al., 2004), reflecting the composition of primitive mantle CO_2 (-5‰ to -8‰; Pineau et al., 1976; Taylor, 1986; Cartigny et al., 2001; Coltice et al., 2004). Based on the few studies conducted to date, dissolved CO_2 in back-arc hydrothermal fluids are typically more ^{13}C-enriched, with $\delta^{13}C_{CO2}$ values ranging from +0.4‰ at Mariner (Lau Basin) to -6.2‰ at White Lady (N.Fiji Basin), (Ishibashi et al., 1994; Takai et al., 2008). Vent fluid $\delta^{13}C_{CO2}$ values higher than putative mantle carbon values can arise from two potential processes – ^{13}C enrichment in the source magma due to slab-derived carbonate inputs and/or degassing-related fractionation effects. In the case of the latter, the CO_2 initially degassed from basaltic magmas can be enriched in ^{13}C by several per mil (i.e. 2.2 to 4.3‰ at >1100°C) relative to the undegassed bulk CO_2 reservoir (Javoy et al., 1978; Mattey, 1991). Such enrichments, however, are only associated with the earliest stages of CO_2 exsolution (Tsunogai et al., 1994) and cannot account for CO_2 observed in PACMANUS fluids since the extremely low CO_2 contents (Marty et al., 2001) and low $\delta^{13}C_{CO2}$ values observed in EMVZ lavas (down to -33.2‰; Shaw et al., 2004) suggest extensive degassing of crustal magmas. The ^{13}C-enriched nature of aqueous CO_2 at PACMANUS therefore may reflect the greater influence of slab-derived carbon on the magma source in this region of the basin. Subducted oceanic crust can contain sedimentary organic carbon/carbonate and carbonates formed during low temperature alteration of basaltic rocks (Alt and Teagle, 1999; Coltice et al., 2004), giving a bulk slab $\delta^{13}C$ value of approximately -1‰ (see Coltice et al., 2004). Numerous geochemical proxies (*e.g.* higher Ba/Nb and Cl/Nb ratios in dredged lavas) indicate greater subduction-related inputs to magmas in the EMVZ (and Pual Ridge) relative to the MSC (Kamenetsky et al., 2001; Sinton et al., 2003; Sun et al., 2004; Pearce and Stern, 2006; Park et al., in press) and inputs of slab-derived carbon have been suggested (Shaw et al., 2004). Trends of increasing $\delta^{13}C_{CO2}$ with arc proximity have been

observed in other back-arc vent fluids, such as the Lau Basin (Proskurowski et al., 2006) and the Okinawa Trough/Mariana Arc (cf. Sakai et al. (1990b) and Lupton et al. (2006)).

High concentrations of magmatic CO_2 in PACMANUS vent fluids are also accompanied by elevated fluoride (F) abundances (Fig. 5.6), which may reflect inputs of F to convecting hydrothermal fluids from magmatic degassing. Fluoride species are enriched in felsic magmas (Carroll and Webster, 1994) and are common constituents of exsolved magmatic gases in arc-type environments (Yang and Scott, 2006; Aiuppa et al., 2009). In contrast to Pual Ridge, vent fluids at Vienna Woods (Fig. 5.6) and MOR hydrothermal systems are depleted in F relative to seawater (Edmond et al., 1979a; Maris et al., 1984; Von Damm et al., 1985; Seyfried and Ding, 1995a; German and Von Damm, 2003). Despite this circumstantial evidence, however, we cannot discount additional rock-derived sources of F. The behavior of F in seafloor hydrothermal systems is not completely understood (Seyfried and Ding, 1995a) and limited experimental evidence suggests both mineralogical sources and sinks of F are possible during hydrothermal alteration of silicic rock compositions (Galluccio et al., 2009). Rock leaching has also been proposed as a source of F to some felsic-hosted terrestrial geothermal systems (Arnorsson et al., 1978). The F contents of unaltered Pual Ridge dacites (360 to 530ppm,; Paulick et al., 2004) are not substantially different from MSC basalts (~200ppm; Sinton et al., 2003) and typical MORB (~500ppm; Michael and Schilling, 1989). Even inefficient leaching at calculated w/r ratios (~0.5 for Vienna Woods, 2–6 for Pual Ridge) could yield aqueous F concentrations several times that of seawater in either setting. If mobilization of rock-derived F is occurring, some solubility control as a function of substrate must be invoked as F enrichments in Pual Ridge fluids and depletions at Vienna Woods do not reflect crustal compositions. Therefore, while the correlation of F with magmatic CO_2 is suggestive of a relationship, further constraints are needed on the mobility of F

in hydrothermal systems before the excess abundances relative to typical MOR hydrothermal fluids can be attributed to magmatic degassing with confidence.

In addition to CO_2 and F, magmatic fluids at Pual Ridge could also contain varying amounts of Cl but we cannot constrain such inputs, however, owing to the high quantities of seawater Cl and variability arising from phase separation. Exsolved magmatic fluids may also be characterized by chlorinities comparable to or much lower than seawater. At supercritical magmatic temperatures and shallow crustal pressures, Cl-bearing magmatic fluids can separate into low-Cl vapor phases containing the bulk of H_2O mass and small quantities of a Cl-rich brine condensate (Cline and Bodnar, 1991; Shinohara, 1994; Kelley and Früh-Green, 2000; Lowenstern, 2000; Webster, 2004). Additional lines of evidence, such as Br/Cl ratios, would not be useful in identifying the addition of magmatic fluids because molar Br/Cl ratios in high temperature (>700°C) fumaroles from western Pacific arc volcanoes (0.6 to 1.4; Goff and McMurtry, 2000; Snyder et al., 2002) approach those of the seawater value of 1.5. Most Pual Ridge fluids do not deviate from the latter ratio (Table 5.3).

5.3.3 Magmatic SO_2 input and disproportionation

There is some indirect evidence to suggest that magmatic fluids entrained by Pual Ridge vent fluids are accompanied by S species that could generate substantial acidity. We conclude, however, that much of the primary signature of magmatic S has likely been considerably overprinted by secondary processes subsequent to magmatic degassing and prior to seafloor venting. Exsolved CO_2 and H_2O-rich vapor bubbles in melt inclusions from Pual Ridge contain a host of sulfate- and sulfide-bearing minerals, indicating that sulfurous species have partitioned from magmas into exsolved aqueous fluids there (Kamenetsky et al., 2001; Kamenetsky et al., 2002; Yang and Scott, 2006). In contrast to basaltic magmas, where it exists mostly as sulfide,

total S in more oxidizing (higher f_{O2}) calc-alkaline magmas is predominantly in the forms SO_2 and SO_4 (Burnham, 1979; Carroll and Rutherford, 1988; Nilsson and Peach, 1993; Carroll and Webster, 1994). SO_2 strongly partitions into exsolved aqueous fluids during magmatic degassing (Burnham, 1979; Scaillet and Pichavant, 2003) and upon cooling below ~400°C, SO_2 can undergo either of the following disproportionation reactions (Iwasaki and Takejiro, 1960; Holland, 1965; Drummond, 1981; Kusakabe et al., 2000):

$$4SO_2 + 4H_2O \rightarrow H_2S + 3H_2SO_4 \qquad (1)$$

$$3SO_2 + 3H_2O \rightarrow S^0 + 2H_2SO_4 \qquad (2)$$

Where S^0 is zero-valent sulfur. According to Kusakabe et al.(2000), reaction (1) is more favored under higher temperatures and lower SO_2 contents than reaction (2). Both reactions are rapid, produce sulfuric acid (H_2SO_4, which generates acidity upon dissociation to HSO_4^- and H^+) and are associated with significant sulfur isotope fractionations between reactant SO_2 and the oxidized and reduced S products. H_2SO_4 is typically enriched in ^{34}S, while H_2S and S^0 are depleted in ^{34}S relative to precursor SO_2 (Ohmoto and Rye, 1979; Ohmoto and Goldhaber, 1997; Kusakabe et al., 2000). The SO_4 produced invariably has a $\delta^{34}S_{SO4}$ that is lower than seawater (+20.99‰; Rees et al., 1978), while negative $\delta^{34}S_{H2S}$ values would be expected for H_2S assuming an initial magma $\delta^{34}S$ near 0‰ (Ohmoto and Goldhaber, 1997).

Negative $\delta^{34}S_{H2S}$ values are observed in fluids from some areas of PACMANUS (Satanic Mills and Snowcap) and are associated with extremely high levels of magmatic CO_2 (Fig. 5.12). $\delta^{34}S_{H2S}$ values from unsedimented MOR hydrothermal systems range from +1.4‰ to +8.6‰, reflecting a mixture of both reduced seawater SO_4 and basaltic S (Shanks, 2001 and refs. therein). More negative values are possible in sedimented hydrothermal systems due to the presence of ^{34}S-depleted sedimentary sulfide minerals. The most negative $\delta^{34}S_{H2S}$ values (as low as -5.7‰) observed to date were in fluids from the DESMOS Caldera site to the east of Pual Ridge in 1995

and were attributed to magmatic SO_2 disproportionation (Gamo et al., 1997). As stated previously, there is no evidence to suggest fluids at Pual Ridge have interacted with sediments and the most plausible explanation for the above trend is that some of the H_2S in Satanic Mills and Snowcap fluids is derived either directly from magmatic SO_2 disproportionation, or possibly by reduction of magmatic SO_4 with low $\delta^{34}S_{SO4}$ values.

In contrast to $\delta^{34}S_{H2S}$, $\delta^{34}S_{SO4}$ values for all Pual Ridge fluids do not deviate significantly from that of seawater-derived SO_4 (Table 5.1) and are inconsistent with a magmatic origin for SO_4 in the fluids. The general absence of anomalous $\delta^{34}S_{SO4}$ compositions that might be expected from addition and disproportionation of magmatic SO_2, however, is not surprising considering the strong retrograde solubility of anhydrite as a function of temperature (Bischoff and Dickson, 1975; Bischoff and Seyfried, 1978; Mottl and Holland, 1978). If it is assumed that magmatic fluids are entrained (and therefore diluted) by circulating high-temperature fluids at considerable depth in the hydrothermal reservoir (possibly near the high temperature reaction zone) any SO_4 added could be quantitatively removed as anhydrite if a continuous supply of Ca is available from fluid-mineral equilibrium reactions. The widespread occurrence of anhydrite in the subsurface (Binns et al., 2007) and the extensive removal of seawater sulfate evident in present-day Snowcap fluids (Fig. 5.4) is an indication of the ability the former mechanism to overwhelm a magmatic source of SO_4.

Our observations are consistent with evidence to suggest variable magmatic SO_2 input and disproportionation has occurred in PACMANUS fluids in the past. Two independent investigations arising from ODP Leg 193 demonstrated $\delta^{34}S_{SO4}$ values as low as +16.6‰ (Craddock, 2008) and +18.1‰ (Roberts et al., 2003) in anhydrite deposited beneath Snowcap, with trends of decreasing $\delta^{34}S_{SO4}$ with increasing depth below the seafloor. These trends were interpreted to be the result of precipitation from fluids with variable mixtures of both seawater-

and magmatic SO_2-derived SO_4, with the proportion of the latter increasing with depth beneath the Snowcap dome. Several inactive outcrops of bleached volcaniclastic material cemented with native sulfur (S^0) were also found in the vicinity of Snowcap (Tivey et al., 2006), suggesting that acid-sulfate fluids may have reached the seafloor in the past.

The extremely high Fe contents of many PACMANUS fluids suggests that magmatic-derived acidity has lead to extensive dissolution of Fe from silicate minerals in the subsurface, which could have consumed H^+ and raised *in situ* pH. Measured pH values are still lower than experimental observations of equilibrium buffering by the andesite/dacite mineral assemblage (Hajash and Chandler, 1982; Shiraki et al., 1987), suggesting that titration of magmatic acidity may be incomplete. One possible explanation is that rocks in the upflow zones at Pual Ridge may be completely altered and characterized by mineral assemblages that are stable at low pH, as suggested by ODP Leg 193 observations beneath Snowcap (Binns et al., 2007). The latter would likely be incapable of buffering pH values to the same extent as fresh andesite/dacite mineral assemblages. While alkali abundances and ratios (Fig. 5.9) clearly indicate fluid interactions with fresh rock, this may simply reflect water-rock interaction prior to magmatic fluid addition.

5.3.4 Spatial variability of magmatic fluid inputs

Our data are remarkably consistent with ODP Leg 193 observations which demonstrated apparent spatial variability of magmatic inputs within the PACMANUS vent field. Observations of anomalous subsurface anhydrite $\delta^{34}S_{SO4}$ values, rare-earth element patterns and 'acid-sulfate' (quartz–illite–pyrophyllite–anhydrite) alteration assemblages were limited to the Site 1188 (beneath the Snowcap Dome) and were lacking at Site 1189 (Roman Ruins), (Bach et al., 2003; Roberts et al., 2003; Binns et al., 2007; Craddock, 2008). The data collected in 2006 demonstrates that vent fluids from Snowcap and the nearby Satanic Mills area clearly contain the

strongest signatures of H_2O, CO_2, H_2S, and possibly F of magmatic origin. What is perplexing, however, is that while there is a notable absence of extremely high concentrations of CO_2 and anomalous $\delta^{34}S_{H2S}$ values in Roman and Roger's Ruins vent fluids, δD_{H2O} and pH values there resemble those of low Mg fluids from Satanic Mills and are consistent with magmatic inputs. Given the poor constraints on compositional variability of magmatic fluids in backarc systems, the high degrees of dilution by circulating hydrothermal fluids, it may be that magmatic fluid compositions at Roman and Roger's Ruins contain lower amounts of CO_2 and SO_2, with small SO_2-derived $\delta^{34}S_{H2S}$ anomalies suffering extensive overprinting. While we acknowledge it is also possible that Roman and Roger's Ruins fluids may not be entraining magmatic fluids at depth, this would require some unknown alteration assemblage capable of buffering both pH and δD_{H2O} values to the same extent as the as Snowcap, Satanic Mills and Fenway fluids, and there is no evidence as yet to suggest this is plausible.

5.4 Subsurface seawater entrainment

The large number of sample sets taken from Pual Ridge vent fluids with consistently high measured Mg concentrations (Table 5.1) strongly suggests that fluids there have mixed with seawater prior to exiting at the seafloor. Mixing of seawater and hydrothermal fluids prior to venting has been recognized ever since hydrothermal activity was first discovered in 1977 at the Galapagos Spreading Center (Corliss et al., 1979; Edmond et al., 1979a,b; Butterfield and Massoth, 1994; Edmond et al., 1995; Tivey et al., 1995; Gamo et al., 1996b; Von Damm et al., 1998; Gallant and Von Damm, 2006). The hypothesis that extensive subsurface mixing is responsible for much of the Mg in Pual Ridge fluids can be tested by examining the relationship between Mg abundance and temperature for co-located vents. Lines depicting conservation of specific enthalpy and Mg during mixing of 3°C seawater and the hottest endmember fluids at

Roman Ruins and Fenway are shown in Figure 5.13. If other co-located fluids represent conservative mixtures of the hottest fluid and cold seawater they should fall on these mixing lines. Only fluids where at least 2 samples with consistent measured temperatures and Mg concentrations were collected are plotted to prevent ambiguity introduced by seawater contamination during sampling. Examination of Figure 5.13 reveals that the vents RMR4, RMR1 and RMR2 (Fig. 5.2b) display a clear conservative trend. At Fenway, the diffuse F5 vent appears to be a conservative mixture of seawater and the nearby F3 black smoker vent fluid. Vents RMR3, F2 and F4 fall below predicted temperatures, suggesting that in some cases conductive cooling may be occurring in addition to mixing. Temperature loss due to the former could explain the anomalously low apparent pressure of quartz-fluid equilibrium for F4 vent, and possibly other fluids also (Fig. 5.10). The agreement of measured temperatures and Mg concentrations with values predicted by the mixing model indicate a seawater source for the Mg in fluids and strongly suggests that entrained Mg behaves conservatively during mixing even at relatively high temperatures (>250°C).

SO_4 concentrations for the majority of PACMANUS fluids are lower than predicted for conservative mixing of seawater and an endmember hydrothermal fluid devoid of Mg and SO_4 (Fig. 5.4), yielding apparent negative endmember SO_4 concentrations at zero Mg. This further confirms fluids are venting with non-zero Mg concentrations and near zero SO_4, consistent with non-conservative behavior of SO_4 relative to Mg during the mixing process. This behavior increases with the extent of mixing in most cases (Fig. 5.4) and fluids with higher Mg concentrations yield lower endmember Ca/Cl and Sr/Cl ratios upon extrapolation to zero Mg (Fig. 5.14a and 5.14b). Collectively, these data indicate anhydrite precipitation is occurring during mixing in response to its low solubility at elevated temperatures, thereby removing Ca (and co-precipitating Sr) and seawater-derived SO_4 (Mottl and Holland, 1978; Shikazono and Holland,

1983; Berndt et al., 1988; Mills and Tivey, 1999). While unmixed hydrothermal fluid compositions can supply Sr in addition to that available in entrained seawater, in some cases losses are so great that Sr is also removed from the latter. Extrapolation of the SC1 fluid composition to zero Mg yields an apparent negative endmember Sr concentration and a near zero Ca concentration (Table 5.2). Such extreme Sr loss relative to Mg upon mixing provides and explanation for the implausible endmember $^{87}Sr/^{86}Sr$ ratio calculated at Snowcap (0.69768) which is beyond the range possible for crustal materials (Fig. 5.8; Banner, 2004).

In some cases, variable anhydrite precipitation is evident in multiple fluids sampled in close proximity to one another (*e.g.* RGR1 and RGR2 at Roger's Ruins, Figs. 5.2b and 5.4), suggesting that deposition may be occurring very near the seafloor or within sulfide structures themselves. Although mixing through 'leaky' walls of sulfide chimneys cannot be excluded at all vents (Haymon and Kastner, 1981; Goldfarb, 1983), consistently high Mg samples were collected from SM3 vent after the near complete removal of the sulfide chimney (<1m tall) and measured fluid temperatures before (279°C) and after removal (280–288°C) were similar. This suggests that mixing occurred beneath the seafloor and not within the removed structure at SM3. Shallow subsurface precipitation of anhydrite is entirely consistent with observations from ODP drillcores which indicate that the abundant anhydrite deposits beneath the seafloor at PACMANUS contain seawater-derived SO_4 (Roberts et al., 2003; Craddock, 2008). In cases where several vent fluids are in close proximity to one another and may be genetically related, the apparent variability in measured Ca/Cl ratios due to anhydrite deposition is greatly reduced when such Ca loss is corrected. Using the deviations in measured SO_4 concentrations from conservative behavior to estimate SO_4 losses and assuming equimolar Ca loss for measured compositions, adjusted Ca/Cl ratios in each case delineate trends between seawater and a much narrower range of endmember Ca/Cl (Fig. 5.15). This suggest co-located vents at Roman Ruins, Roman Ruins and Fenway each

reflect common source fluids that have undergone phase separation and partial segregation into fluids of differing Cl contents, followed by variable degrees of seawater entrainment into these fluids and concomitant anhydrite precipitation.

In addition to influence of mixing, some low temperature fluids at Pual Ridge, namely F5 vent and the NE Pual fluid (NP1), show evidence for extensive anhydrite dissolution and fixation of B. F5 vent (80°C) was a poorly focused flow vent emanating from anhydrite sand/talus on the north flank of the Fenway mound (Fig. 5.2c). In addition to the temperature and proximity considerations above, endmember alkali/Cl ratios (Table 5.3, Fig. 5.11) at F5 are similar to those venting at the summit black smoker complex (F2, F3 and F4 vents), further suggesting the fluid is a mixture of the latter and seawater. The striking feature of F5 and NP1 compositions are measured SO_4 concentrations (with near-seawater $\delta^{34}S_{SO4}$ values) that are elevated relative to concentrations predicted for conservative mixing of endmember fluids (devoid of Mg and SO_4) and seawater (Fig. 5.4). In addition to high apparent endmember Ca/Cl and Sr/Cl ratios (Table 5.3, Fig. 5.14a and 5.14b), these differences indicate that previously precipitated anhydrite is being re-dissolved by F5 and NP1 fluids, a likely consequence of the relatively low temperatures (<80°C) resulting from high degrees of mixing. Dissolution of anhydrite by active low temperature fluids has previously only been observed at 9°50'N on the East Pacific Rise (McDermott and Von Damm, 2008) and highlights the transient nature of Ca, Sr and SO_4 sinks in anhydrite. F5 and NP1 also differ from higher temperature Pual Ridge fluids in the behavior of B, as negative endmember concentrations are apparent upon extrapolation of measured B concentrations to zero Mg (Table 5.2). This implies removal of seawater-derived B in F5 and NP1 fluids in addition to the B complement of their parent hydrothermal fluids. The most plausible explanation for these depletions is that low temperature fixation reactions have decreased the abundances of B prior to venting. Laboratory and field studies have shown that

fixation of B from seawater solutions occurs during low temperature (<150°C) alteration of basaltic oceanic crust and likely sinks for B include alteration assemblages composed of ferric micas and smectites (Seyfried et al., 1984; Alt, 1995).

The pervasive nature of subsurface seawater entrainment apparent at Pual Ridge vent areas indicates a more open hydrologic regime beneath Pual Ridge compared to Vienna Woods and traditional MOR systems. Subsurface mixing at the TAG hydrothermal system was attributed to a 'leaky mound' model whereby seawater ingress is facilitated by the permeable anhydrite-sulfide breccia deposits of the TAG mound (Edmond et al., 1995; Humphris et al., 1995; Tivey et al., 1995; Humphris and Tivey, 2000). Aside from the Snowcap area, however, many of the mixed fluids at Pual Ridge are emanating from comparatively small sulfide structures atop rugged volcaniclastic flows. Meter-scale fissures were absent on the surface (Tivey et al., 2006), and it is possible fluid flow may instead be focused through contact zones between lava flows or subsurface networks of fractures/conduits (Binns et al., 2007). The possibility that the blocky, highly vesicular and brecciated volcaniclastic nature of lavas at Pual Ridge contributes to the mixing regime must also be considered. Monecke et al. (2007) demonstrated that hydrothermal alteration in glassy dacites from the surface of Pual Ridge is influenced by primary volcanic textures and that some fluid flow occurs through vesicles interconnected by perlitic cracks/quench fractures. Enhanced permeability and fluid flow due to volcanic textures has been suggested for other back-arc hydrothermal systems (Ishibashi and Urabe, 1995), and may be an inherent consequence of the volatile-rich nature of precursor magmas in these environments.

5.4.1 Secondary Acidity

An important consequence of the seawater entrainment and mixing beneath the seafloor at Pual Ridge is the deposition of iron sulfide minerals and production of secondary acidity in

addition to that derived from magmatic fluid input at depth. Cooling induced by seawater mixing reduces the stability of iron chloride complexes and the solubility of iron sulfides, resulting in the removal of Fe from solution. Iron sulfide deposition can be described by the reactions:

$$Fe^{2+} + H_2S_{(aq)} = FeS_{(s)} + 2H^+ \quad (3)$$

$$Fe^{2+} + 2H_2S_{(aq)} = FeS_{2(s)} + 2H^+ + H_{2(aq)} \quad (4)$$

$$Cu^+ + Fe^{2+} + 2H_2S_{(aq)} = CuFeS_{2(s)} + 0.5H_{2(aq)} + 3H^+ \quad (5)$$

All of these reactions result in the generation of acidity. Because of the higher Fe content (several mmol/kg) of Pual Ridge fluids relative to Cu (<1mmol/kg; Craddock, 2008), deposition of pyrrhotite (FeS) or pyrite (FeS_2) will likely have a greater impact of fluid pH than chalcopyrite ($CuFeS_2$). The extent of Fe precipitation at PACMANUS can be qualitatively assessed by examining Fe/Mn ratios, since Fe precipitation from high temperature vent fluids during cooling is a relatively rapid process while Mn precipitation is kinetically inhibited (Seewald and Seyfried, 1990). Accordingly, initial Fe/Mn ratios of endmember hydrothermal fluids should decrease with increased cooling (due to mixing), potentially resulting in substantial secondary acidity generation according to reactions 3 to 5. This is trend is observed for several PACMANUS vent areas, where both pH and endmember Fe/Mn ratios are lower in fluids with higher measured Mg (Fig. 5.14c and 5.14d). These data suggest that differences in pH between co-located higher- and lower-temperature vent fluids reflect local modification by mixing-induced sulfide precipitation reactions that decrease pH below the already low values. The impact of these reactions is considerable given the extremely high Fe contents of Pual Ridge fluids.

The apparent lack of abundant disseminated pyrrhotite in either the ODP drillcores (Binns et al., 2007), or in chimney structures (Craddock, 2008), suggests that pyrite precipitation (reaction (4)) is responsible for Fe removal, which is consistent with the relatively oxidizing redox conditions (as indicated by the aqueous H_2 concentrations) that fall at the low end of the

spectrum for ridge-crest hydrothermal fluids (Seyfried and Ding, 1995b; Von Damm, 1995). However, reaction (4) must produce equivalent moles of H_2 for each mole of Fe deposited and H_2 in Pual Ridge fluids does not approach the mmol/L levels expect for the quantities of Fe removal evident. Hence, an additional sink is required to consume H_2. The only species present in sufficient quantities that is capable of oxidizing H_2 in near-seafloor mixing zones is SO_4, which is abundantly present in entrained seawater and as anhydrite. Reduction of SO_4 by H_2 can be represented by the reaction:

$$HSO_4^- + H^+ + 4H_{2(aq)} = H_2S_{(aq)} + 4H_2O_{(l)} \qquad (6)$$

That each mole of SO_4 requires 4 moles of H_2 for complete reduction indicates that reaction (6) might be an efficient sink for H_2 generated by pyrite precipitation. Moreover, the kinetics of this reaction are greatly enhanced by the highly acidic nature of these fluids requiring timescales of a few hours to reach near-equilibrium states at pH and temperature conditions in subsurface environments (Ohmoto and Lasaga, 1982). In most cases, the decreases in pH observed for small amounts of seawater mixing are not as large as predicted from the apparent loss of Fe suggesting other reactions may be titrating secondary acidity generated by Fe-sulfide precipitation. This may reflect remobilization of other metals (*e.g.* Zn, Au, Ag and Pb) and 'zone refinement'. Tivey et al. (1995) demonstrated that remobilization of metals was occurring as a direct result of modification of high temperature fluids by seawater entrainment within the TAG hydrothermal mound.

6. SUMMARY

The concentrations of 23 dissolved species, in addition to select isotopic analyses, have been determined for 57 vent fluid samples collected from hydrothermal vent fields on the Manus Spreading Center (Vienna Woods) and Pual Ridge (PACMANUS and NE Pual) in the Manus back-arc basin. The sites differ substantially in both substrate type (mafic at Vienna Woods versus felsic at Pual Ridge) and proximity to the New Britain subduction zone (Pual Ridge is closest). Six areas of venting were sampled at PACMANUS, including a large area (Fenway) discovered during this expedition where vigorous 2-phase venting of 358°C fluid was observed, and one low temperature fluid was sampled at NE Pual. Distinct differences between the chemistries of fluids at Vienna Woods and Pual Ridge fluids indicate that while processes of water-rock interaction and phase separation are common to both, inputs of acidic magmatic fluids and entrainment of seawater into the subsurface exert substantial influence on high-temperature fluid chemistry at Pual Ridge.

All fluids at Vienna Woods are characterized by a high degree of uniformity and are compositionally similar to mid-ocean ridge basalt-hosted hydrothermal systems. Since the site was first sampled in 1990, the temperature and major element composition of fluids there have remained relatively constant. High absolute abundances and differing molar ratios of 'soluble' alkali elements and B in Pual Ridge fluids relative to those at Vienna Woods reflect hydrothermal interaction with the more arc-like crust of the Eastern Manus Volcanic Zone. Fluids from Pual Ridge demonstrate Cl variability which, combined with trends of 'soluble' elements and dissolved gas abundances with Cl, indicates that fluids have undergone phase separation even though measured exit temperatures for most vents are much lower than the 2-phase boundary for seawater. Vienna Woods are substantially cooler than the 2-phase boundary, hence either

extensive conductive cooling must be occurring or the chronic venting of high Cl fluids there reflects residual brine entrainment.

Measured pH (25°C) values in low Mg fluids at Pual Ridge differ from those of Vienna Woods in that values are far lower than that expected for equilibrium buffering by host rock mineral assemblages, suggesting the involvement magmatic fluids with acid-volatile constituents (*i.e.* SO_2). The extremely high dissolved metal contents and ubiquitous negative δD_{H2O} values found at PACMANUS are also consistent with the input of highly acidic magmatic fluids at depth to seawater-derived hydrothermal fluids. However, extremely high CO_2 concentrations (up to 274mmol/kg) and negative $\delta^{34}S_{H2S}$ values (down to -2.7‰) - both of which are strongly indicative of magmatic inputs - are limited to Snowcap, Satanic Mills and Fenway vent areas. $\delta^{13}C$ values of CO_2 at PACMANUS are higher than those of Vienna Woods indicating a greater influence of slab-derived carbon at the former, which is located much closer to the active New Britain Arc.

The ubiquity of non-zero measured Mg concentrations in Pual Ridge fluids relative to Vienna Woods indicates that subsurface entrainment seawater into hydrothermal fluids during upflow is pervasive at the former and the various vent areas delineate a spectrum of subsurface mixing regimes. Trends of increasing non-conservative SO_4 behavior, decreasing endmember Ca/Cl and Sr/Cl ratios with increased seawater admixing within vent areas demonstrate that subsurface precipitation of anhydrite is commonplace and is substantially modifying the Ca and Sr fluxes of high temperature fluids. Furthermore, these observations are accompanied in several cases by trends of decreasing endmember Fe/Mn ratios and decreasing measured pH(25°C) with increasing Mg, implying that iron sulfide deposition is also occurring in the subsurface and is leading to secondary acidity production.

ACKNOWLEDGEMENTS

This chapter represents a collaborative effort involving multiple researchers, including my primary advisor, Jeffrey Seewald. Peter Saccocia and Emily Walsh (Bridgewater State College) provided much needed assistance at sea in performing pH and H_2S analysis. W. Bach (University of Bremen) and M. Rosner (Freie Universität Berlin) performed Sr isotope analysis on collected fluids. P. Craddock performed Fe, Mn, Li, B, Sr, Rb and Cs concentration analyses. W. C. Shanks (USGS) performed all H_2O, H_2S, SO_4 stable isotope analyses. Stable carbon isotope analyses were performed by S. Sylva (WHOI). SiO_2 data were provided by T. Pichler (University of Bremen). I am grateful to the crew of the *R/V Melville* and *ROV Jason II* technical group for their expertise and assistance in successful completion of the dive program. I would also like to thank Maurice Tivey and the *ABE* technical group for providing SM2000 bathymetric maps for the manuscript prior to submission. The manuscript benefited from numerous helpful discussions with Margaret K. Tivey before submission. This study received financial support from NSF grant OCE-0327448.

Table 5.1.

Measured compositions of vent fluid samples from the Vienna Woods, PACMANUS and NE Pual vent fields, Manus Basin

Vent Field	Sample[b]	Mg	pH	Na	Cl	Ca	K	SiO_2	SO_4^{2-}	Br	F	Fe	Mn	Li
Area: **VENT**[a] (T_{max})		mm	(25°C)	mm	mm	mm	mm	mm	mm	mm	mm	mm	mm	mm
Vienna Woods														
VW1 (282°C)	J2-207-IGT7	3.36	4.77	520	694	76.6	20.6	14.3	1.88	1.03	0.023	0.148	0.328	1.02
	J2-207-IGT3	1.55	4.41	510	683	78.1	21.0	14.9	0.81	1.07	0.017	0.155	0.340	1.05
	J2-207-M2	1.44	4.92	506	677	77.3	20.7	-	-	1.05	0.022	0.141	0.341	1.03
VW2 (273°C)	J2-207-IGT4	1.02	4.22	509	687	79.5	21.0	14.7	0.72	1.05	0.021	0.162	0.358	1.14
VW3 (285°C)	J2-207-IGT8	1.11	4.71	504	663	69.5	20.0	14.4	0.87	1.01	0.019	0.127	0.207	1.06
	J2-207-IGT6+	14.9	5.37	494	644	53.5	17.2	10.4	7.83	0.971	0.034	0.082	0.151	0.759
PACMANUS														
Roman Ruins:														
RMR1 (314°C)	J2-208-IGT8	7.26	2.32	470	617	18.4	71.8	13.7	0.47	0.924	0.120	5.56	3.40	0.986
	J2-208-IGT5	7.59	2.35	485	619	18.6	71.3	13.4	0.64	0.923	0.120	5.62	3.28	0.957
	J2-208-M4	8.19	2.38	472	621	18.3	70.4	-	-	0.932	0.134	5.53	3.49	0.968
RMR2 (272°C)	J2-208-IGT2	15.9	2.34	434	549	10.6	50.6	16.6	2.61	0.808	0.097	-	2.26	0.620
	J2-208-IGT1	16.0	2.39	435	543	10.3	50.5	16.7	2.54	0.812	0.096	0.991	2.27	0.639
	J2-208-M2	27.0	2.65	443	551	10.5	38.5	-	-	0.784	0.091	0.681	1.70	0.453
RMR3 (278°C)	J2-213-IGT7+	22.7	3.16	508	648	18.8	58.8	11.6	10.6	0.993	0.117	4.32	2.58	0.778
	J2-213-M4	6.39	2.45	534	708	23.8	86.4	-	-	1.09	0.157	6.85	4.28	1.16
RMR4 (341°C)	J2-222-IGT1	3.63	2.68	495	650	22.3	77.2	17.8	0.42	1.00	0.116	6.47	2.83	1.06
	J2-222-M4	4.71	2.62	495	647	21.8	75.5	17.3	-	1.04	0.125	6.17	2.73	0.948
Roger's Ruins:														
RGR1 (320°C)	J2-213-IGT3	5.09	2.71	484	635	25.7	74.5	16.98	1.11	0.975	0.143	4.09	2.41	0.788
	J2-213-IGT4	7.61	2.73	487	634	24.2	70.1	16.15	2.59	0.968	0.146	3.89	2.30	0.765
	J2-213-M2	4.24	2.69	489	641	25.9	75.6	-	-	0.991	0.155	4.43	2.68	0.832
RGR2 (274°C)	J2-222-IGT4+	22.3	2.96	479	606	18.3	49.9	11.0	9.58	0.919	0.113	2.130	1.45	0.498
	J2-222-IGT3	8.96	2.56	481	631	22.4	68.6	15.8	1.50	0.969	0.128	3.173	2.15	0.753
	J2-222-M2	8.61	2.56	484	631	22.4	68.8	15.8	-	0.975	0.140	3.355	2.17	0.775
Satanic Mills:														
SM1 (295°C)	J2-209-IGT6	9.84	2.67	411	523	12.5	58.2	11.8	2.69	0.805	0.160	2.74	2.05	0.641
	J2-209-IGT7	8.95	2.71	409	521	12.5	59.3	12.0	2.18	0.799	0.162	2.79	2.14	0.638
	J2-209-M4	8.16	2.60	407	519	12.3	60.4	-	-	0.797	0.175	2.97	2.34	0.646
SM2 (241°C)	J2-209-IGT4+	26.6	2.69	400	478	7.07	31.0	9.40	12.1	0.715	0.215	0.705	1.11	0.311
	J2-209-M2	16.9	2.37	374	455	5.87	38.6	-	-	0.691	0.287	1.12	1.68	0.441
SM3 (288°C)	J2-214-IGT8	9.73	2.50	403	510	13.1	58.1	12.3	2.49	0.763	0.197	0.982	1.82	0.601
	J2-214-IGT5	9.81	2.48	402	510	13.1	56.4	12.2	2.35	0.772	0.203	0.958	1.82	0.587
	J2-214-M4	9.72	-	403	511	13.1	57.0	-	-	0.787	0.207	1.04	1.99	0.600
Snowcap:														
SC1 (152°C)	J2-210-IGT8	30.8	4.61	419	499	6.38	24.6	6.78	10.8	0.756	0.128	0.029	0.993	0.298
	J2-210-IGT5+	48.5	5.00	450	532	9.71	12.9	1.69	24.1	0.809	0.078	-	0.212	0.089
	J2-210-M2	31.5	4.69	420	501	6.57	24.8	-	-	0.749	0.126	0.032	1.07	0.313
SC2 (180°C)	J2-211-IGT4	24.2	3.40	440	532	6.80	34.7	9.45	5.18	0.816	0.170	0.141	1.63	0.486
	J2-211-IGT3	24.8	3.74	437	536	6.79	34.0	9.28	5.73	0.825	0.160	0.169	1.55	0.476
	J2-211-M4	24.5	3.44	435	530	6.59	34.4	-	-	0.820	0.173	0.129	1.64	0.503
Tsukushi:														
TK1 (62°C)	J2-211-IGT7	44.4	5.90	477	572	12.5	20.7	3.55	18.2	0.883	0.077	0.124	0.570	0.219
	J2-214-IGT2	45.2	5.80	477	570	12.3	19.8	3.24	22.6	0.869	0.077	-	0.558	0.209
	J2-214-M2	44.8	5.71	473	570	12.5	20.0	-	-	0.874	0.077	0.117	0.574	0.219
Fenway:														
F1 (329°C)	J2-210-IGT1	5.97	2.53	347	463	14.3	53.8	12.7	0.93	0.717	0.279	7.37	2.31	0.637
	J2-210-M4	5.84	2.62	340	465	14.3	53.8	-	-	0.714	0.291	7.56	2.56	0.654
	J2-214-IGT1+	39.8	4.51	422	520	11.3	21.2	3.69	20.3	0.796	0.121	2.03	0.658	0.198
F2 (343°C)	J2-212-IGT8	4.90	2.68	485	683	25.2	86.4	13.8	0.55	1.08	0.168	13.3	4.22	1.03
	J2-212-IGT5	5.26	2.70	485	685	25.2	85.8	13.8	0.74	1.07	0.169	13.1	4.16	1.03
	J2-212-M4	4.66	2.70	483	685	25.7	86.8	-	-	1.08	0.173	13.4	4.54	1.07
F3* (358°C)	J2-212-IGT2	4.52	2.74	417	589	22.2	73.9	11.9	0.97	0.919	0.165	11.5	3.60	0.904
	J2-212-IGT1	4.74	2.78	377	517	20.3	64.9	10.4	2.45	0.796	0.154	9.83	3.09	0.748
	J2-212-M2	8.89	2.79	425	573	20.4	66.8	-	-	0.910	0.160	9.97	3.42	0.793
F4 (284°C)	J2-216-IGT7	8.95	2.55	395	527	17.7	60.2	10.9	2.46	0.826	0.158	6.85	2.95	0.713
	J2-216-IGT6	8.69	2.53	392	524	17.7	60.7	11.3	2.17	0.834	0.155	6.65	2.94	0.685
	J2-216-M2	10.2	2.36	394	527	17.4	58.2	-	-	0.816	0.158	6.88	3.05	0.688
F5 (80°C)	J2-216-IGT4	45.0	4.98	437	517	13.3	14.1	1.72	27.6	0.792	0.082	0.868	0.325	0.109
	J2-216-IGT3	44.0	4.86	436	517	14.1	15.3	1.90	27.4	0.797	0.082	0.572	0.368	0.119
	J2-216-M4	48.8	5.77	453	535	11.8	11.7	-	-	0.822	0.069	0.172	0.157	0.065
NE Pual														
NP1 (35°C)	J2-218-IGT3	50.6	6.94	466	536	12.9	10.5	0.926	30.0	0.807	0.071	0.105	0.199	0.044
	J2-218-IGT4	49.9	6.88	461	535	14.1	10.8	1.19	29.5	0.795	0.071	0.062	0.135	0.046
	J2-218-M4	50.3	6.89	454	535	13.5	10.7	-	-	0.797	0.069	0.174	0.210	0.049
Bottom SW (3°C)		52.4	7.90	471	540	10.5	9.87	0.13[c]	28.2	0.808	0.064	0.0	0.0	0.028

mM = mmol/L fluid, mm = mmol/kg fluid, µm = µmol/kg fluid, µM = µmol/L fluid. "-" = not determined. *Vigorous 2-phase venting. +Substantial SW entrainment suspected based on temperature monitoring. a. Each vent represents an individual orifice from which multiple samples were taken (T_{max} = max. observed vent temperature). b. Samples named by Jason (J2) dive number and gas-tight (-IGT) or major (-M) sampler number. c. Sarmiento and Gruber (2006) d. Spencer et al. (1970) e. Craig (1970) f. Redfield and Friedman (1965) g. Craig and Gordon (1965). h. Rees et al.(1978).

Table 5.1. (cont'd)

Measured compositions of vent fluid samples from the Vienna Woods, PACMANUS and NE Pual vent fields, Manus Basin

Vent Field	B	Sr	Rb	Cs	Al	ΣH_2S	H_2	CH_4	CO	ΣCO_2	$\delta^{13}C_{CO2}$	$\delta^{13}C_{CH4}$	δD_{H2O}	$\delta^{18}O_{H2O}$	$\delta^{34}S_{SO4}$	$\delta^{34}S_{H2S}$	$^{87}Sr/^{86}Sr$
Area: **VENT**[a] (T_{max})	mm	µm	µm	µm	µm	mM	µM	µM	µM	mm	‰	‰	‰	‰	‰	‰	
Vienna Woods																	
VW1 (282°C)	0.240	232	15.8	0.267	5.5	1.3	42	65	-	4.36	-5.7	-20.8	2.1	0.50	-	-	-
	0.250	240	17.5	0.283	6.2	1.5	39	61	-	4.21	-4.8	-20.7	2.6	0.55	-	-	0.70440
	-	236	19.4	0.288	7.2	-	-	-	-	-	-	-	-	-	-	-	-
VW2 (273°C)	0.250	244	18.1	0.281	7.3	1.6	55	70	-	4.39	-5.1	-20.7	2.5	-	-	-	-
VW3 (285°C)	0.240	224	16.6	0.256	6.7	1.5	43	62	-	4.47	-5.6	-20.8	0.28	0.40	-	-	-
	0.185	183	13.0	0.188	5.1	1.0	32	46	-	3.80	-	-	2.3	0.41	20.6	-	-
PACMANUS																	
Roman Ruins:																	
RMR1 (314°C)	1.85	78.4	63.8	2.23	8.9	6.4	65	27	0.043	15.3	-3.3	-13.4	-	-	-	0.87	-
	1.82	80.1	62.6	2.24	7.1	6.5	66	27	0.047	15.3	-	-	-0.38	1.0	-	1.9	-
	-	76.9	67.2	2.42	-	-	-	-	-	-	-	-	-	-	-	-	-
RMR2 (272°C)	1.34	62.0	42.3	1.57	5.6	2.7	29	36	-	19.1	-3.0	-13.3	-3.1	0.94	20.6	-	-
	1.34	61.0	41.2	1.50	4.7	2.9	29	35	0.023	19.2	-	-	-1.5	1.1	20.6	2.8	-
	-	71.3	33.9	1.16	4.1	-	-	-	-	-	-	-	-	-	-	-	-
RMR3 (278°C)	1.42	85.1	48.8	1.69	4.6	2.5	72	8.2	0.023	6.72	-	-	-2.6	0.82	20.7	2.1	-
	-	85.7	80.9	2.85	15	-	-	-	-	-	-	-	-	-	-	-	-
RMR4 (341°C)	1.62	88.0	74.5	2.23	6.5	6.3	53	22	-	9.54	-4.0	-	-2.5	1.0	-	0.0	0.70460
	1.57	86.5	71.5	2.26	5.1	-	-	-	-	-	-	-	-	-	-	-	-
Roger's Ruins:																	
RGR1 (320°C)	1.20	111	68.6	1.93	6.1	3.3	18	30	-	7.03	-	-	-	-	21.3	4.7	0.70468
	1.15	107	65.2	1.79	5.3	3.1	17	27	0.0050	6.36	-	-	-2.7	0.74	-	4.1	-
	-	111	73.8	2.04	-	-	-	-	-	-	-	-	-	-	-	-	-
RGR2 (274°C)	0.814	91.8	42.3	1.19	3.4	1.5	26	16	-	4.80	-3.1	-12.8	-1.2	0.70	-	1.7	-
	1.12	102	66.7	1.71	5.1	2.5	42	22	-	6.37	-3.7	-13.0	-2.0	0.77	-	4.2	-
	1.13	98.9	65.5	1.88	-	-	-	-	-	-	-	-	-	-	-	-	-
Satanic Mills:																	
SM1 (295°C)	1.14	62.6	57.9	1.77	9.5	7.4	23	14	-	168	-3.1	-9.1	-0.2	0.90	-	-2.7	-
	1.17	61.7	57.2	1.80	7.0	8.1	26	15	0.098	181	-	-	-3.0	0.63	20.9	-	-
	-	62.6	61.0	1.93	-	-	-	-	-	-	-	-	-	-	-	-	0.70497
SM2 (241°C)	0.768	48.6	24.8	0.844	4.5	3.3	4.3	15	0.0042	79.6	-	-	-0.27	0.55	21.4	-1.3	-
	-	34.5	36.3	1.23	-	-	-	-	-	-	-	-	-	-	-	-	-
SM3 (288°C)	1.01	69.7	56.0	1.71	5.2	8.3	6.7	26	0.034	216	-2.4	-7.4	-2.2	1.2	21.5	-0.48	-
	0.990	70.4	56.2	1.72	5.9	8.3	7.0	28	0.030	230	-	-	-1.8	0.83	21.8	-0.52	0.70512
	-	71.1	57.9	1.81	-	-	-	-	-	-	-	-	-	-	-	-	-
Snowcap:																	
SC1 (152°C)	0.592	43.6	18.2	0.654	0.91	2.9	7.7	35	0.033	112	-3.1	-14.4	-1.1	0.36	20.1	-1.8	-
	0.222	82.3	6.02	0.141	0.15	0.54	6.5	6.1	-	-	-	-	-2.1	0.16	-	-	-
	-	45.6	19.0	0.683	-	-	-	-	-	-	-	-	-	-	-	-	-
SC2 (180°C)	0.851	55.6	27.4	1.10	1.7	-	18	36	0.045	102	-2.9	-15.2	-4.2	0.63	20.6	-	0.70635
	0.823	55.9	27.2	1.09	2.4	1.0	17	34	-	-	-	-	-2.3	1.1	20.5	-	-
	-	55.8	28.9	1.16	2.3	-	-	-	-	-	-	-	-	-	-	-	-
Tsukushi:																	
TK1 (62°C)	0.370	93.0	12.2	0.422	-	-	0.16	7.1	0.040	5.74	-	-	-1.2	0.40	21.0	-	-
	0.351	93.0	11.3	0.401	-	-	0.57	6.5	0.0012	5.13	-	-	-1.2	0.24	21.0	-	-
	-	92.7	12.8	0.422	-	-	-	-	-	-	-	-	-	-	-	-	-
Fenway:																	
F1 (329°C)	1.36	95.3	53.2	1.85	7.9	18.5	24	29	0.033	61.3	-2.7	-10.2	-4.3	1.2	20.8	-0.73	-
	-	95.6	55.9	1.96	6.4	-	-	-	-	-	-	-	-	-	-	-	-
	0.453	90.9	15.5	0.484	1.9	4.6	6.4	7.0	0.0031	17.7	0.0	-	-2.4	0.43	-	-0.71	-
F2 (343°C)	1.83	121	87.2	2.92	8.2	9.2	95	13	0.054	23.6	-3.5	-10.6	-0.9	1.4	-	1.2	-
	1.84	117	82.2	2.93	6.9	9.0	93	12	0.049	23.3	-2.9	-11.7	-1.5	1.4	20.4	-1.0	-
	-	118	87.7	3.18	-	-	-	-	-	-	-	-	-	-	-	-	-
F3* (358°C)	1.60	103	73.5	2.49	6.1	15.0	233	32	0.14	44.0	-	-	-1.6	1.4	20.9	-1.2	0.70428
	1.42	89.7	60.0	2.17	5.8	19.3	325	44	0.16	58.6	-2.6	-8.6	-0.3	1.1	20.8	-0.20	0.70447
	-	92.9	65.0	2.38	-	-	-	-	-	-	-	-	-	-	-	-	0.70482
F4 (284°C)	1.31	86.8	57.5	2.07	7.5	11.6	25	39	0.036	51.8	-3.1	-8.8	-1.2	1.1	21.7	-0.17	-
	1.32	85.8	57.3	2.08	8.4	11.6	26	38	0.037	54.7	-	-	-4.0	1.4	21.5	5.4	0.70461
	-	83.3	55.6	2.05	-	-	-	-	-	-	-	-	-	-	-	-	-
F5 (80°C)	0.268	104	9.33	0.218	0.66	2.5	2.8	7.7	-	14.4	-	-	-	-	-	-	-
	0.287	104	9.35	0.256	1.2	2.7	2.7	11	-	15.5	-	-	-2.5	0.39	21.1	-0.28	-
	-	97.0	3.64	0.108	-	-	-	-	-	-	-	-	-	-	-	-	-
NE Pual																	
NP1 (35°C)	0.166	98.6	2.49	0.051	3.4	-	0.18	1.0	-	3.04	-	-	-0.13	0.38	20.9	-	-
	0.176	105	2.34	0.075	2.6	-	0.21	1.7	-	2.51	-	-	-2.4	0.31	20.8	-	-
	-	100	2.53	0.066	-	-	-	-	-	-	-	-	-	-	-	-	-
Bottom SW (3°C)	0.426	91.0	1.3[d]	0.0023[d]	0.0	0.0	0.0	0.0	0.0	2.3	0.3[e]	-	- 0.14f	-0.17g	20.99h	-	0.70916

mM = mmol/L fluid, mm = mmol/kg fluid, µm = µmol/kg fluid, µM = µmol/L fluid. "-" = not determined. *Vigorous 2-phase venting. +Substantial SW entrainment suspected based on temperature monitoring. a. Each vent represents an individual orifice from which multiple samples were taken (T_{max} = max. observed vent temperature). b. Samples named by Jason (J2) dive number and gas-tight (-IGT) or major (-M) sampler number. c. Sarmiento and Gruber (2006) d. Spencer et al. (1970) e. Craig (1970) f. Redfield and Friedman (1965) g. Craig and Gordon (1965). h. Rees et al.(1978).

Table 5.2.
Summary of vent fluid compositions extrapolated to zero Mg concentration from the Vienna Woods, PACMANUS and NE Pual vent fields, Manus Basin

Vent Field	T_{max}	Mg_{min}	pH_{min}	Na	Cl	Ca	K	SiO_2	Br	F	Fe	Mn	Li	B	Sr	Rb	Cs	Al	ΣH_2S	H_2	CH_4	CO	ΣCO_2	$\delta^{13}C_{CO2}$	$\delta^{13}C_{CH4}$	δD_{H2O}	$\delta^{18}O_{H2O}$	$\delta^{34}S_{H2S}$	$^{87}Sr/^{86}Sr$
***Area*: VENT**	**°C**	**mm**	**(25°C)**	mm	mm	mm	mm	mm	mm	mm	mm	mm	mm	mm	µm	µm	µm	µm	mM	µM	µM	µM	mm	‰	‰	‰	‰	‰	
Vienna Woods																													
VW1	282	1.44	4.41	513	691	80.1	21.2	15.3	1.06	0.019	0.15	0.35	1.08	0.236	242	18.3	0.291	6.6	1.4	43	66	-	4.38	-5.4	-20.7	2.4	0.56	-	0.70435
VW2	273	1.02	4.22	509	690	80.9	21.2	15.0	1.06	0.021	0.17	0.37	1.16	0.246	247	18.4	0.286	7.5	1.6	56	71	-	4.43	-5.2	-20.7	2.6		-	-
VW3	285	1.11	4.71	504	672	70.7	20.1	14.6	1.02	0.019	0.12	0.21	1.07	0.186	225	17.2	0.261	7.0	1.5	44	64	-	4.48	-5.7	-20.8	1.3	0.49	-	-
PACMANUS																													
Roman Ruins:																													
RMR1	314	7.26	2.32	477	632	19.8	81.7	15.7	0.947	0.135	6.5	4.0	1.13	2.07	76.3	75.4	2.69	9.3	7.5	76	31	0.052	17.5	-3.4	-13.4	-0.42	1.2	1.4	-
RMR2	272	15.9	2.34	417	551	10.5	68.5	23.9	0.802	0.113	1.4	3.3	0.895	1.74	48.9	61.2	2.24	7.6	4.0	41	51	0.033	26.5	-3.1	-13.3	-3.2	1.6	2.8	-
RMR3	278	6.39	2.45	541	731	25.5	96.8	20.5	1.13	0.167	7.8	4.8	1.32	2.17	83.7	90.0	3.17	14.6	4.4	127	14	0.041	10.1	-	-	-4.5	1.6	2.1	-
RMR4	341	3.63	2.62	497	658	23.1	82.1	19.0	1.04	0.126	6.9	3.0	1.09	1.70	86.9	79.2	2.44	6.3	6.8	57	23	-	10.1	-4.1	-	-2.7	1.1	0.0	0.70425
Roger's Ruins:																													
RGR1	320	4.24	2.69	488	648	27.1	81.1	18.8	1.00	0.158	4.6	2.8	0.888	1.28	112	77.4	2.15	6.5	3.6	20	32	0.006	7.31	-	-	-3.1	0.90	4.4	0.70429
RGR2	274	8.61	2.56	485	650	24.7	80.4	19.0	1.00	0.148	3.88	2.6	0.901	1.23	101	78.0	2.14	6.1	2.8	49	27	-	7.04	-3.9	-12.9	-2.3	1.1	2.9	-
Satanic Mills:																													
SM1	295	8.16	2.60	397	517	12.8	69.6	14.5	0.799	0.187	3.4	2.6	0.769	1.31	56.4	70.6	2.21	10.1	9.4	30	17	0.12	212	-3.1	-9.1	-2.0	0.97	-2.7	0.70374
SM2	241	16.9	2.37	328	414	3.59	52.4	19.0	0.630	0.386	1.6	2.4	0.627	1.12	6.68	51.6	1.78	9.2	6.8	8.7	31	0.009	160	-	-	-0.40	1.3	-1.3	-
SM3	288	9.72	2.48	387	503	13.7	68.0	15.1	0.766	0.234	1.2	2.3	0.726	1.13	65.7	69.4	2.15	6.8	10.2	8.4	33	0.039	274	-2.3	-7.4	-2.4	1.3	-0.50	0.70383
Snowcap:																													
SC1	152	30.8	4.61	343	441	0.508	46.4	16.4	0.672	0.220	0.076	2.5	0.714	0.779	-23.4	44.0	1.65	2.2	7.0	20	85	0.079	268	-3.3	-14.4	-2.8	1.2	-1.8	-
SC2	180	24.2	3.40	408	526	3.38	55.9	17.5	0.831	0.259	0.27	3.0	0.893	1.20	24.9	51.1	2.10	3.9	1.9	32	66	0.084	187	-3.0	-15.2	-6.0	1.8	-	0.69768
Tsukushi:																													
TK1	62	44.4	5.71	505	749	23.7	81.3	22.8	1.28	0.154	0.81	3.9	1.33	-0.021	104	75.9	2.86	n/d	-	2.4	47	0.15	24.1	-	-			-	-
Fenway:																													
F1	329	5.84	2.62	326	454	14.8	59.3	14.3	0.705	0.313	8.4	2.7	0.724	1.42	95.8	61.3	2.14	8.1	20.8	27	32	0.036	68.7	-2.7	-10.2	-5.2	1.4	-0.72	-
F2	343	4.66	2.70	486	699	26.9	94.3	15.2	1.10	0.181	14.6	4.8	1.15	1.99	122	94.5	3.32	8.4	10.1	104	14	0.057	25.7	-3.3	-11.1	-1.4	1.6	0.10	-
F3	358	4.52	2.74	397	562	22.3	76.1	12.2	0.882	0.172	11.8	3.8	0.917	1.61	95.9	74.6	2.65	6.5	18.8	306	42	0.17	56.1	-3.0	-8.6	-1.0	1.4	-0.72	0.70394
F4	284	8.69	2.53	377	523	19.1	70.5	13.3	0.829	0.177	8.3	3.6	0.839	1.50	84.2	68.7	2.51	9.6	14.0	31	46	0.044	63.6	-3.0	-8.8	-3.1	1.5	2.6	0.70364
F5	80	44.0	4.86	240	388	31.8	42.1	11.3	0.738	0.181	4.6	2.3	0.599	-0.55	176	53.6	1.57	6.3	17.2	18	62	-	86.4	-	-	-	-	-0.28	-
NE Pual																													
NP1	35	49.9	6.88	205	410	84.8	29.6	22.8	0.586	0.220	2.6	4.2	0.475	-5.6	352	28.8	1.55	69	-	4.7	35	-	12.0	-	-	-	-	-	-
Bottom SW	3	52.4	7.9	471	540	10.5	9.9	0.13[a]	0.808	0.064	0.0	0.0	0.028	0.426	91.0	1.3[b]	0.0023	0.0	0.0	0.0	0.0	0.0	2.3	0.3[c]	-	-0.14d	-0.17e	-	0.70916

mM = mmol/L fluid, mm = mmol/kg fluid, µm = µmol/kg fluid, µM = µmol/L fluid. T_{max} = max. measured temperature at vent. Mg_{min} = lowest measured Mg concentration for vent fluid. pH_{min} = lowest measured (25°C) pH for vent fluid. "-" = not determined. a. Sarmiento and Gruber (2006) b. Spencer et al.(1970). c. Craig (1970) d. Redfield and Friedman (1965). e. Craig and Gordon (1965).

Table 5.3.
Selected elemental ratios at zero Mg concentration from the Vienna Woods, PACMANUS and NE Pual vent fields, Manus Basin

Vent Field *Area*: Vent	T_{max} °C	Mg_{min} mm	pH_{min} (25°C)	Na/Cl	Ca/Cl	K/Cl	Sr/Cl x 10^{-3}	Li/Cl x 10^{-3}	Rb/Cl x 10^{-3}	Cs/Cl x 10^{-6}	Br/Cl x 10^{-3}	B/Cl x 10^{-3}	Fe/Cl x 10^{-3}	Mn/Cl x 10^{-3}	Fe/Mn
Vienna Woods															
VW1	282	1.44	4.41	0.74	0.12	0.031	0.35	1.6	0.026	0.42	1.5	0.34	0.22	0.51	0.44
VW2	273	1.02	4.22	0.74	0.12	0.031	0.36	1.7	0.027	0.41	1.5	0.36	0.24	0.53	0.45
VW3	285	1.11	4.71	0.75	0.11	0.030	0.33	1.6	0.026	0.39	1.5	0.28	0.19	0.31	0.59
PACMANUS															
Roman Ruins:															
RMR1	314	7.26	2.32	0.75	0.031	0.13	0.12	1.8	0.12	4.3	1.5	3.3	10	6.3	1.6
RMR2	272	15.9	2.34	0.76	0.019	0.12	0.089	1.6	0.11	4.1	1.5	3.2	2.6	6.0	0.43
RMR3	278	6.39	2.45	0.74	0.035	0.13	0.11	1.8	0.12	4.3	1.5	3.0	11	6.5	1.6
RMR4	341	3.63	2.62	0.76	0.035	0.12	0.13	1.7	0.12	3.7	1.6	2.6	10	4.6	2.3
Roger's Ruins:															
RGR1	320	4.24	2.69	0.75	0.042	0.13	0.17	1.4	0.12	3.3	1.5	2.0	7.2	4.3	1.7
RGR2	274	8.61	2.56	0.75	0.038	0.12	0.15	1.4	0.12	3.3	1.5	1.9	6.0	4.0	1.505
Satanic Mills:															
SM1	295	8.16	2.60	0.77	0.025	0.13	0.11	1.5	0.14	4.3	1.5	2.5	6.6	5.1	1.3
SM2	241	16.9	2.37	0.79	0.0087	0.13	0.016	1.5	0.12	4.3	1.5	2.7	3.8	5.8	0.66
SM3	288	9.72	2.48	0.77	0.027	0.14	0.13	1.4	0.14	4.3	1.5	2.2	2.4	4.6	0.53
Snowcap:															
SC1	152	30.8	4.61	0.78	0.0012	0.11	-0.053	1.6	0.10	3.7	1.5	1.8	0.17	5.8	0.030
SC2	180	24.2	3.40	0.78	0.0064	0.11	0.047	1.7	0.097	4.0	1.6	2.3	0.52	5.7	0.091
Tsukushi:															
TK1	62	44.4	5.71	0.67	0.032	0.11	0.14	1.8	0.10	3.8	1.7	-0.028	1.1	5.2	0.21
Fenway:															
F1	329	5.84	2.62	0.72	0.032	0.13	0.21	1.6	0.13	4.7	1.6	3.1	19	6.0	3.1
F2	343	4.66	2.70	0.69	0.039	0.13	0.17	1.6	0.14	4.8	1.6	2.8	21	6.8	3.1
F3	358	4.52	2.74	0.71	0.040	0.14	0.17	1.6	0.13	4.7	1.6	2.9	21	6.8	3.1
F4	284	8.69	2.53	0.72	0.037	0.13	0.16	1.6	0.13	4.8	1.6	2.9	16	6.9	2.3
F5	80	44.0	4.86	0.62	0.082	0.11	0.45	1.5	0.14	4.0	1.9	-1.4	12	6.0	2.0
NE Pual															
NP1	35	49.9	6.88	0.50	0.21	0.072	0.86	1.2	0.070	3.8	1.4	-14	6.4	10	0.62
Bottom SW	3	52.4	7.9	0.87	0.019	0.018	0.17	0.052	0.0024	0.0043	1.5	0.79	<0.001	<0.001	-

All ratios are on a molar basis. T_{max} = max. measured temperature at vent. Mg_{min} = lowest measured Mg concentration for vent fluid. pH_{min} = lowest measured (25°C) pH for vent fluid.

Figure 5.1.

(a) Regional map showing the Manus Basin (eastern Bismarck Sea) and the locations (in light gray) of the Manus Spreading Center (MSC), Eastern Manus Volcanic Zone (EMVZ), major transform faults (TF) and known sites of hydrothermal activity. The Vienna Woods and PACMANUS sites are shown as stars (adapted from Craddock, 2008). The inactive Manus Trench is to the northeast. **(b)** SeaBeam bathymetric map of Pual Ridge and nearby Marmin Knolls neovolcanic edifices showing locations of the PACMANUS and Northeast (NE) Pual vent fields. Individual areas of venting are shown as circles (adapted from Tivey et al., 2006).

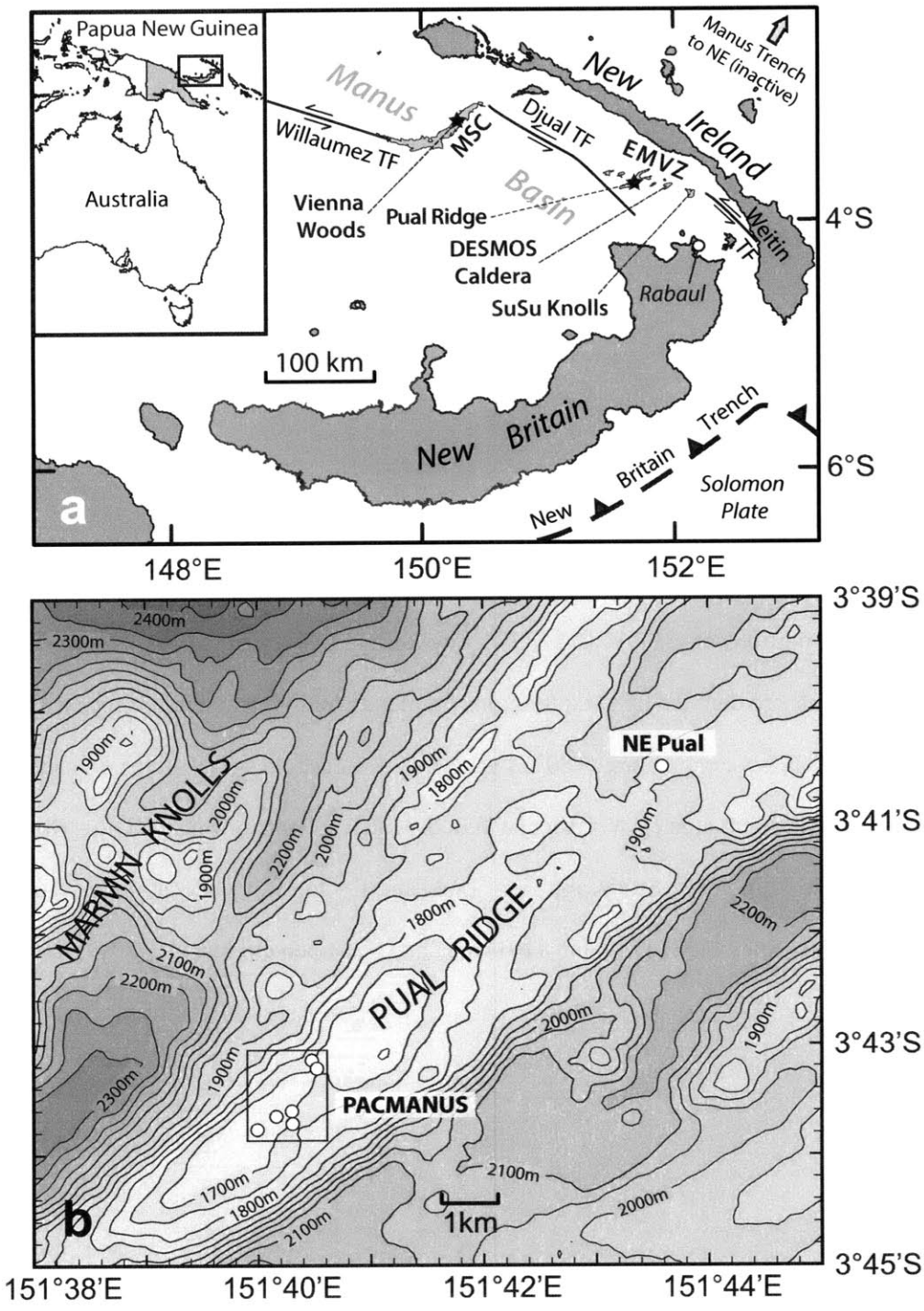
Papua New Guinea
Australia
Manus
Willaumez TF
MSC
Djual TF
EMVZ
New Ireland
Manus Trench to NE (inactive)
Basin
Vienna Woods
Pual Ridge
DESMOS Caldera
SuSu Knolls
Rabaul
Weitin TF
100 km
New Britain
New Britain Trench
Solomon Plate
a
4°S
6°S
148°E
150°E
152°E
b
NE Pual
MARWIN KNOLLS
PUAL RIDGE
PACMANUS
1km
3°39'S
3°41'S
3°43'S
3°45'S
151°38'E
151°40'E
151°42'E
151°44'E

Figure 5.1.

Figure 5.2.

SM2000 bathymetry of the Vienna Woods hydrothermal field **(a)** and the northern **(b)** and southern **(c)** portions of the PACMANUS hydrothermal field (adapted from Tivey et al., 2006). Sampled vents are denoted by solid triangles (moderate to high temperature focused flow), or open triangles (low temperature (<80°C) vents). Each discrete vent is given an identifier abbreviating the vent area (VW = Vienna Woods; RMR = Roman Ruins; RGR = Roger's Ruins; SM = Satanic Mills; SC = Snowcap; TK = Tsukushi; F = Fenway). Locations of the ODP Leg 193 drillholes (Sites 1188, 1189 and 1191) are shown as open circles.

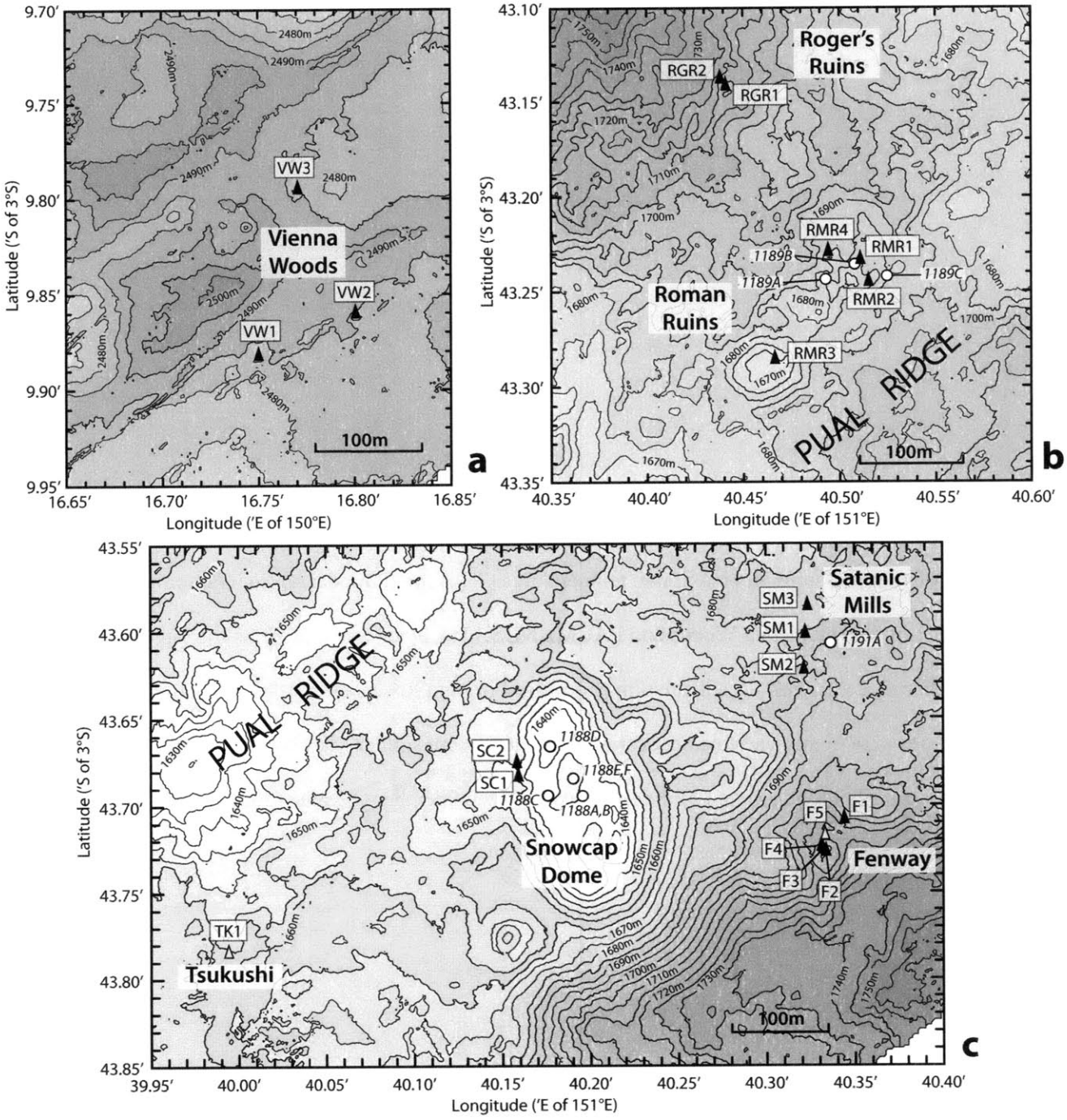
Vienna Woods
VW1
VW2
VW3
100m
a
Roger's Ruins
RGR1
RGR2
Roman Ruins
RMR1
RMR2
RMR3
RMR4
1189A
1189B
1189C
PUAL RIDGE
100m
b
Latitude ('S of 3°S)
Longitude ('E of 150°E)
Longitude ('E of 151°E)
Satanic Mills
SM1
SM2
SM3
1191A
PUAL RIDGE
Snowcap Dome
SC1
SC2
1188A,B
1188C
1188D
1188E,F
Fenway
F1
F2
F3
F4
F5
Tsukushi
TK1
100m
c

Figure 5.2.

Figure 5.3.

Plot of vent pressures and maximum temperatures (T_{max}) for all moderate- to high-temperature fluids sampled at Vienna Woods and PACMANUS. The black line represents the 2-phase boundary for a 3.2wt.% NaCl solution (from Bischoff and Rosenbauer, 1985). Though Cl contents were highly variable between samples at F3 with similar Mg (517 – 589mmol/kg) due to the vigorously boiling nature of the fluid, using the endmember Cl value (562mmol/kg) the fluid approximates a ~3.3 wt.% NaCl equivalent solution.

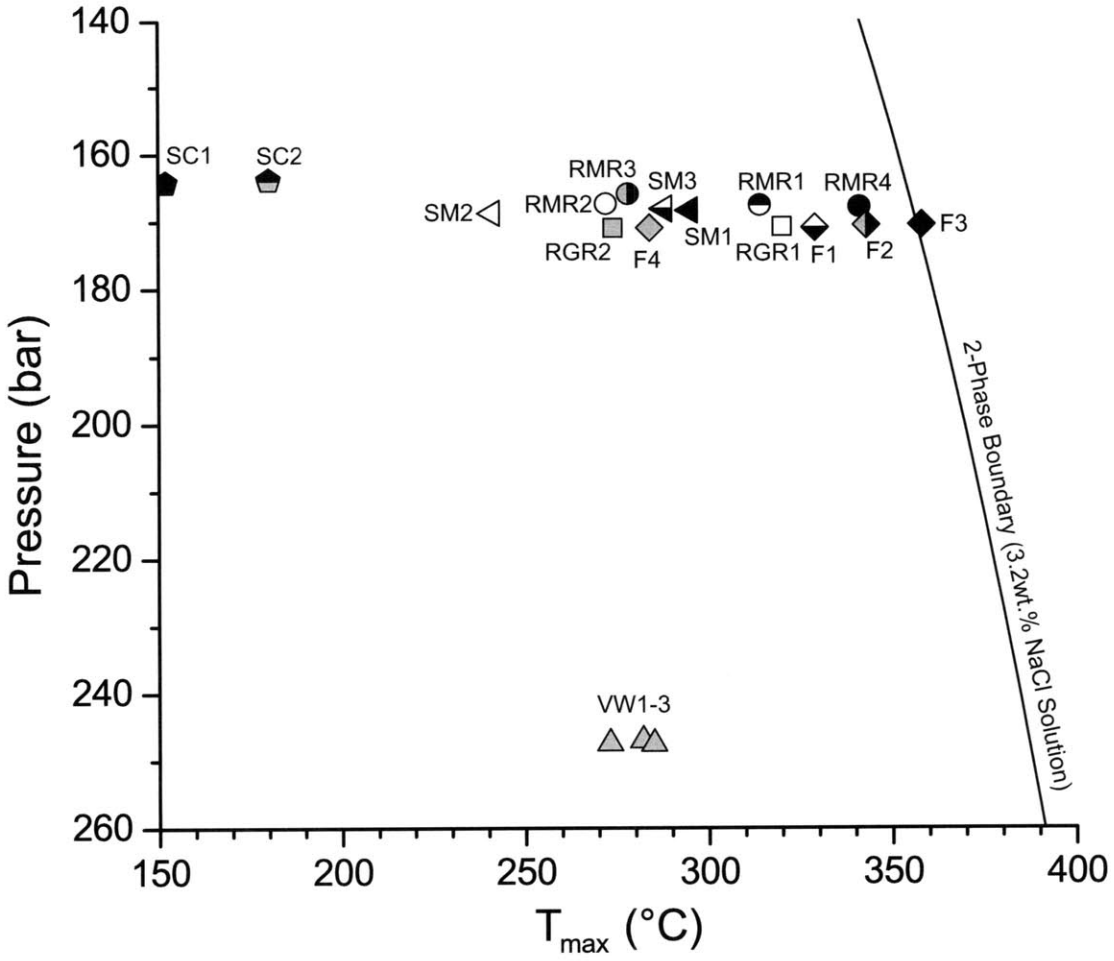
140
160
180
200
220
240
260
Pressure (bar)
150
200
250
300
350
400
T_{max} (°C)
SC1
SC2
SM2
RMR3
RMR2
SM3
SM1
RGR2
F4
RMR1
RGR1
F1
RMR4
F2
F3
VW1-3
2-Phase Boundary (3.2wt.% NaCl Solution)

Figure 5.3.

Figure 5.4.

Measured SO_4 concentrations *vs.* measured Mg for all vent fluid samples from the Vienna Woods, PACMANUS and NE Pual fields. BSW is bottom seawater (denoted by star).

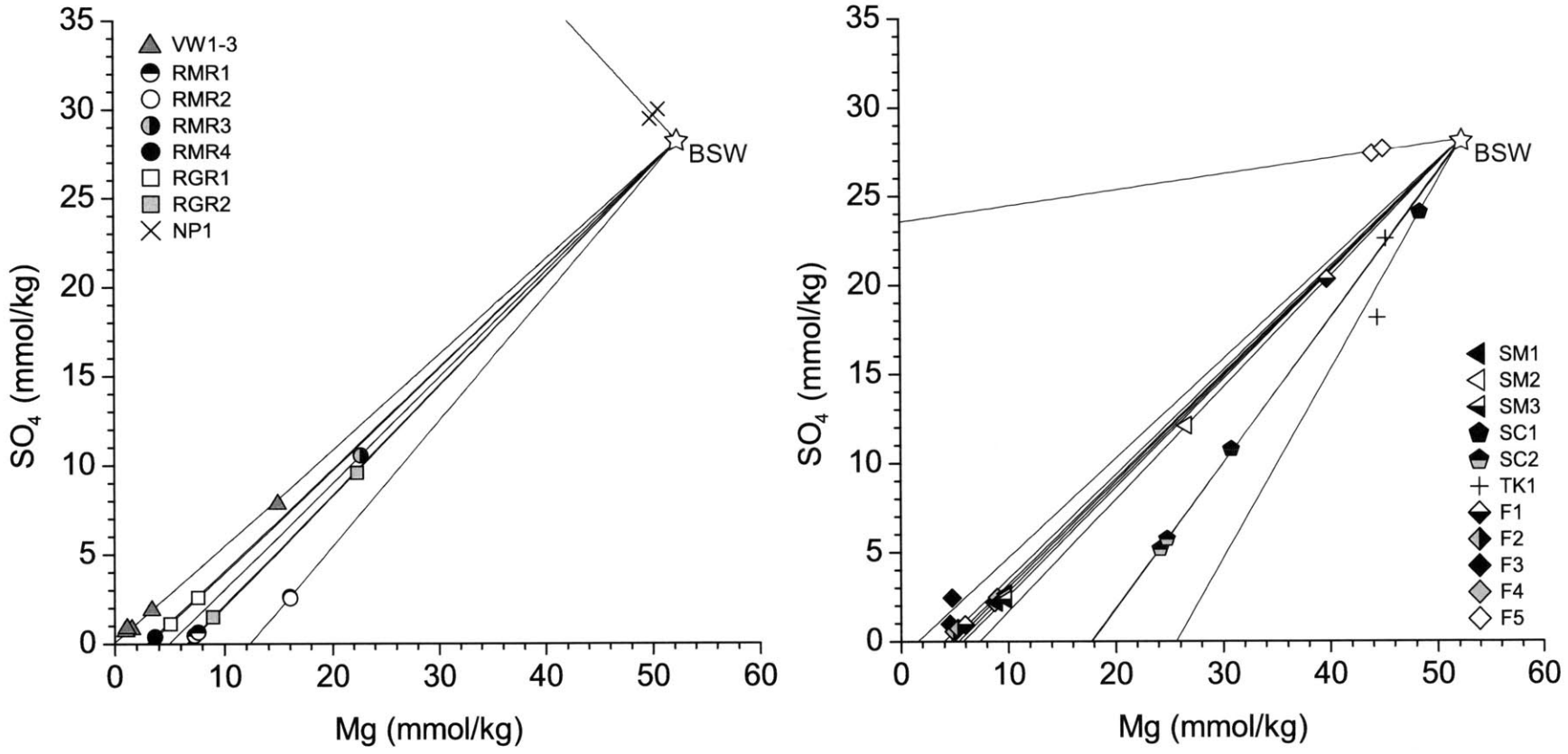
VW1-3
RMR1
RMR2
RMR3
RMR4
RGR1
RGR2
NP1
BSW
SO4 (mmol/kg)
Mg (mmol/kg)
SM1
SM2
SM3
SC1
SC2
TK1
F1
F2
F3
F4
F5

Figure 5.4.

Figure 5.5. Endmember H_2 **(a)**, ΣCO_2 **(b)**, H_2S **(c)** and CH_4 **(d)** concentrations *vs.* endmember Cl concentrations for all PACMANUS, NE Pual and Vienna Woods fluids. Dashed lines are drawn between closely co-located vents at Fenway, Snowcap, Roman Ruins and Roger's Ruins (cf. Fig. 2). BSW = Bottom Seawater.

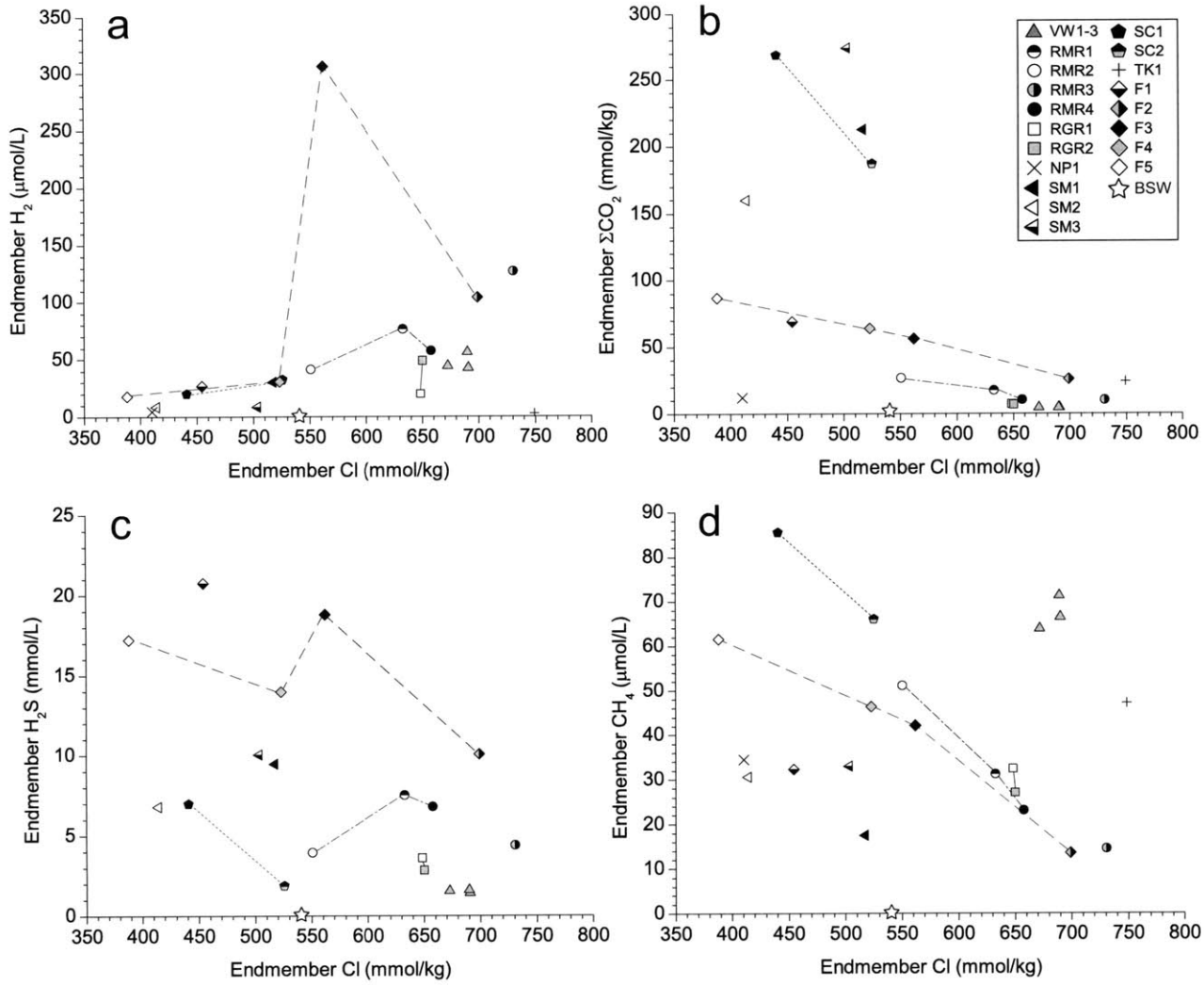
a
b
c
d
Endmember H2 (µmol/L)
Endmember ΣCO2 (mmol/kg)
Endmember H2S (mmol/L)
Endmember CH4 (µmol/L)
Endmember Cl (mmol/kg)
VW1-3
RMR1
RMR2
RMR3
RMR4
RGR1
RGR2
NP1
SM1
SM2
SM3
SC1
SC2
TK1
F1
F2
F3
F4
F5
BSW

Figure 5.5.

Figure 5.6.

Endmember ΣCO_2 concentrations *vs*. endmember F concentration for all PACMANUS, NE Pual and Vienna Woods fluids. BSW = Bottom Seawater.

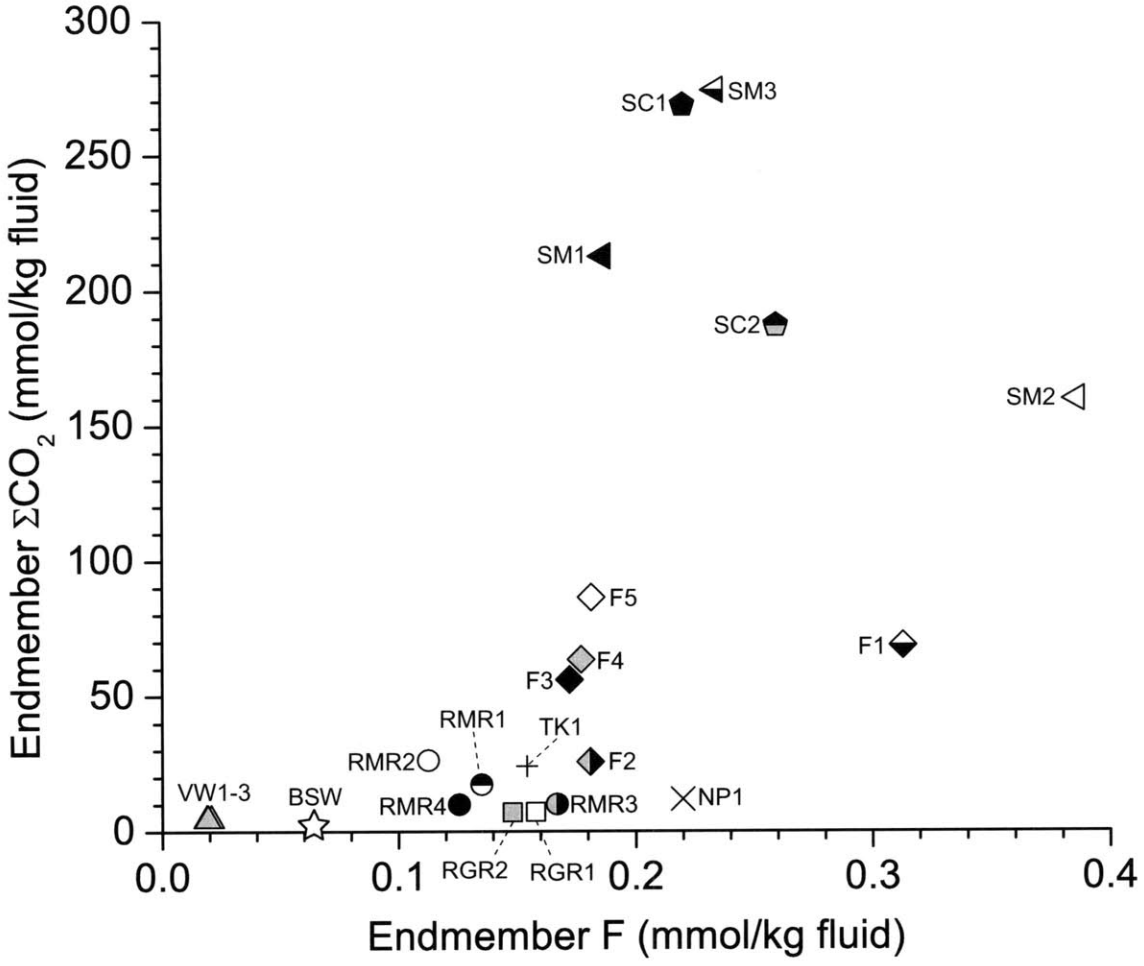
300
250
200
150
100
50
0
Endmember ΣCO2 (mmol/kg fluid)
0.0
0.1
0.2
0.3
0.4
Endmember F (mmol/kg fluid)
SC1
SM3
SM1
SC2
SM2
F5
F1
F4
F3
RMR1
TK1
RMR2
F2
VW1-3
BSW
RMR4
RMR3
NP1
RGR2
RGR1

Figure 5.6.

Figure 5.7.

Endmember δD_{H2O} and $\delta^{18}O_{H2O}$ values from Vienna Woods and PACMANUS vent fields, with axes expanded to show compositions of mantle-derived water (MDW; Taylor, 1979b; Ohmoto, 1986) and subduction-related volcanic vapors (SRVV; Giggenbach, 1992; Hedenquist and Lowenstern, 1994). For clarity, the inset shows the data at a larger scale and 1s analytical errors. The isotopic composition of Pacific bottom seawater (SW) is shown by a star (Craig and Gordon, 1965; Redfield and Friedman, 1965). Fluids with near-SW Mg concentrations (F5, TK1 and NP1) are not plotted due to the large uncertainty associated with extrapolation of δD_{H2O} values to zero Mg. The solid black line represents a least squares regression of all PACMANUS and Vienna Woods isotopic compositions (excluding SW). This extrapolated trend strongly suggests a mixing scenario between SRVV compositions and an evolved SW-derived hydrothermal fluid (see text).

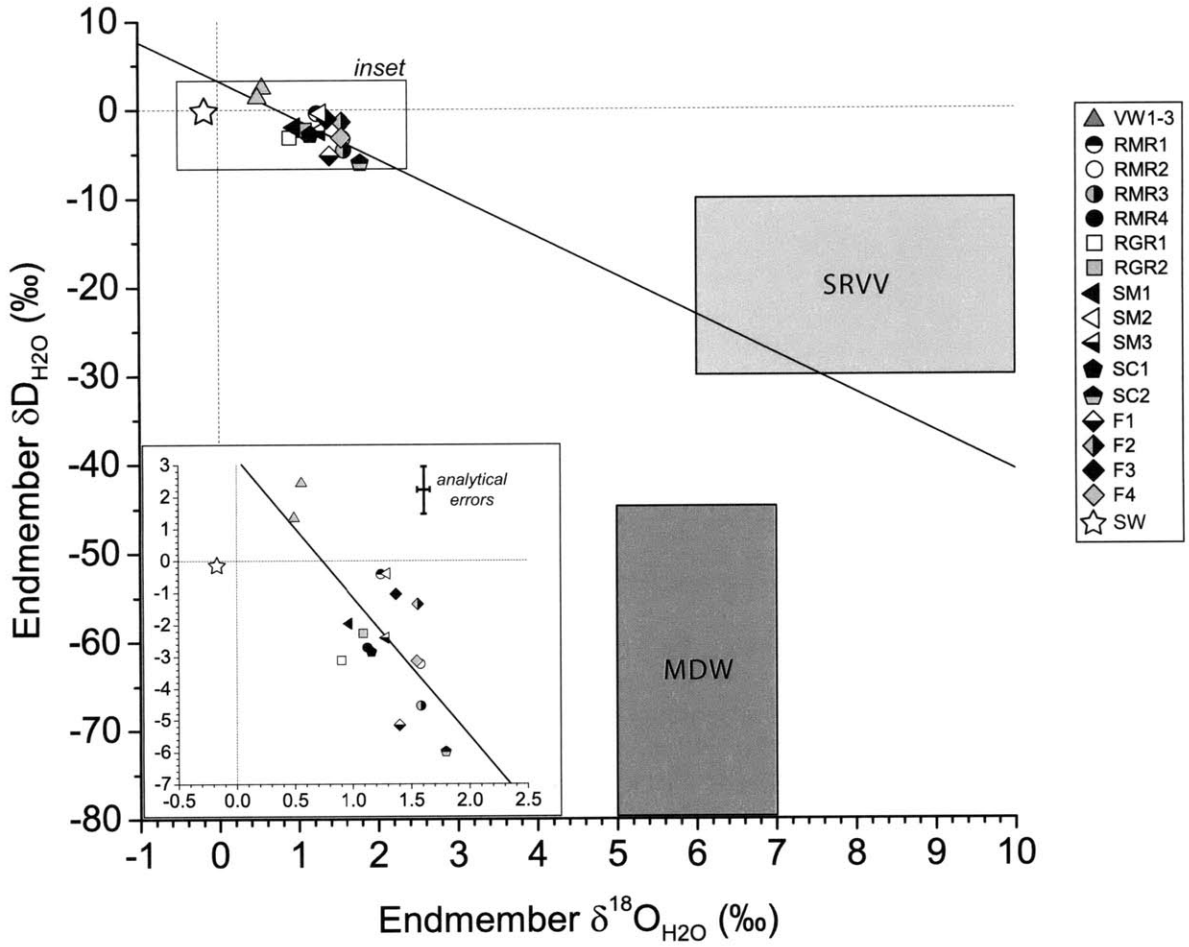
inset
SRVV
MDW
analytical errors
VW1-3
RMR1
RMR2
RMR3
RMR4
RGR1
RGR2
SM1
SM2
SM3
SC1
SC2
F1
F2
F3
F4
SW
Endmember δD$_{H2O}$ (‰)
Endmember δ^{18}O$_{H2O}$ (‰)

Figure 5.7.

Figure 5.8.

Measured $^{87}Sr/^{86}Sr$ ratios versus measured Mg/Sr ratios for select Vienna Woods and PACMANUS fluids. Lines of extrapolation from bottom seawater (BSW) to zero Mg/Sr endmember ratios are shown (Albarède et al., 1981). The range of $^{87}Sr/^{86}Sr$ ratios for Pual Ridge/ EMVZ lavas (0.703446–0.703690, Kamenetsky et al., 2001; Marty et al., 2001) are shown by arrows, with Manus Spreading Center (MSC) basalt (0.703275, Sinton et al. 2003) lying just below this range. The SC1 vent fluid extrapolates to a ratio below that possible for modern terrestrial materials (Banner, 2004) – an artifact of high measured Mg/Sr ratio. Sr loss due to co-precipitation in anhydrite is non-fractionating (Michard et al., 1984), and would increase measured Mg/Sr without changing measured $^{87}Sr/^{86}Sr$.

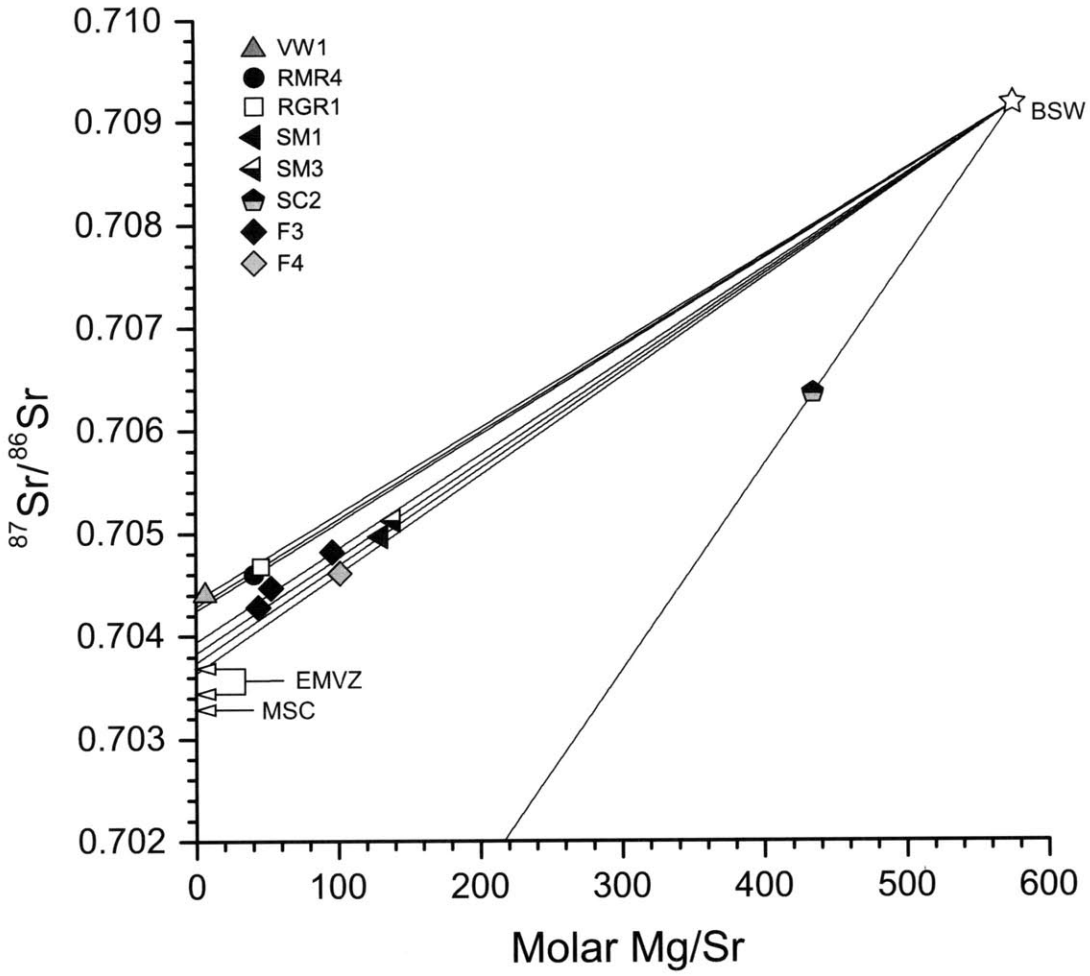
0.710
0.709
0.708
0.707
0.706
0.705
0.704
0.703
0.702
$^{87}Sr/^{86}Sr$
VW1
RMR4
RGR1
SM1
SM3
SC2
F3
F4
BSW
EMVZ
MSC
0
100
200
300
400
500
600
Molar Mg/Sr

Figure 5.8.

Figure 5.9.

Endmember K **(A)**, Li **(B)** and Cs **(C)** concentrations *vs.* endmember Rb concentration for Vienna Woods, PACMANUS and NE Pual fluids. Light gray triangles refer to ranges of alkali/Rb ratios found in Manus Spreading Center (MSC) lavas (basalts and basaltic andesites), (Sinton et al., 2003). Dark gray triangles represent corresponding ranges for EMVZ (Sinton et al., 2003) and Pual Ridge (Kamenetsky et al., 2001) lavas.

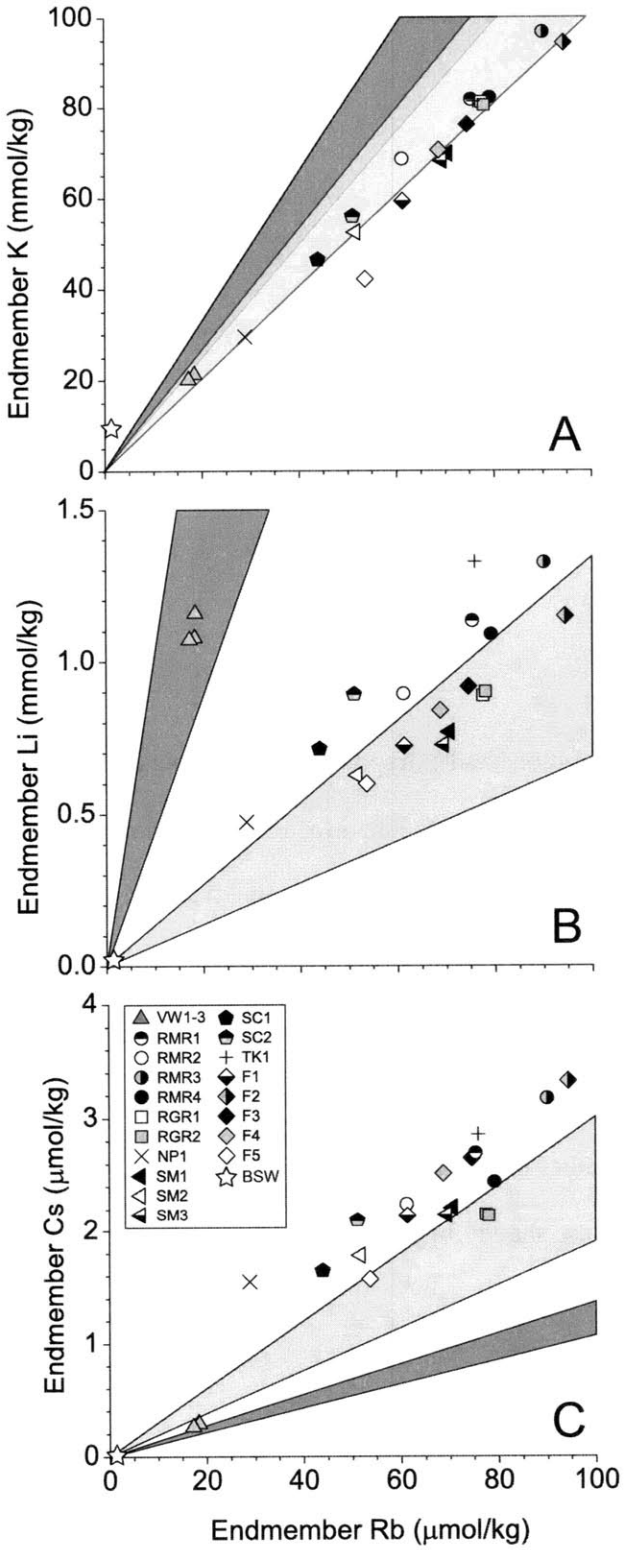
Endmember K (mmol/kg)
100
80
60
40
20
0
A
Endmember Li (mmol/kg)
1.5
1.0
0.5
0.0
B
Endmember Cs (µmol/kg)
4
3
2
1
0
C
VW1-3
RMR1
RMR2
RMR3
RMR4
RGR1
RGR2
NP1
SM1
SM2
SM3
SC1
SC2
TK1
F1
F2
F3
F4
F5
BSW
0
20
40
60
80
100
Endmember Rb (µmol/kg)

Figure 5.9.

Figure 5.10.

Endmember SiO_2 concentrations and extrapolated vent temperatures for Vienna Woods and PACMANUS fluids. The latter are calculated for vent fluids hotter than ~270°C where consistent temperatures (within 10°C as measured by IGT samplers) and Mg concentrations were obtained in repeat samples of a given vent fluid. Temperatures were extrapolated (neglecting changes in heat capacity) to the estimated sampler dead volume contribution by linear regression forced through seawater. These calculations assume no conductive cooling occurred during mixing with seawater and neglect changes in heat capacity over the temperature range of extrapolation. Quartz saturation curves are shown for pressures of 100 to 1000 bar as a function of temperature (Von Damm et al., 1991).

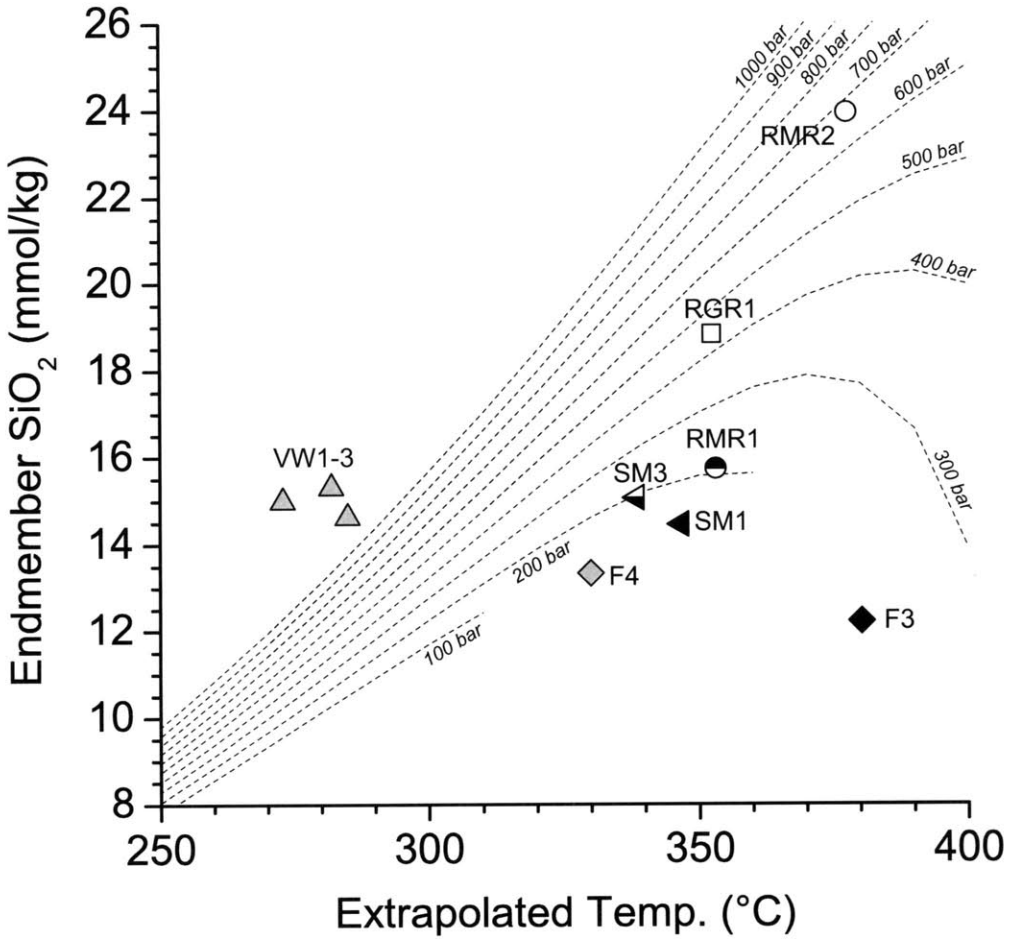
Endmember SiO2 (mmol/kg)
Extrapolated Temp. (°C)
26
24
22
20
18
16
14
12
10
8
250
300
350
400
1000 bar
900 bar
800 bar
700 bar
600 bar
500 bar
400 bar
300 bar
200 bar
100 bar
RMR2
RGR1
RMR1
SM3
SM1
F4
F3
VW1-3

Figure 5.10.

Figure 5.11.

Endmember Li **(a)**, Rb **(b)**, K **(c)** and Cs **(d)** concentrations *vs.* corresponding endmember Cl concentration for Vienna Woods, PACMANUS and NE Pual vent fluids. Solid (Satanic Mills), dashed (Fenway), dot-dashed (Roman Ruins) and dotted (Snowcap) lines represent unweighted linear least squared regressions of endmember fluid compositions within each respective vent area (limited to co-located vent fluids with largest degrees of intra-vent Cl variability). Co-located vent fluids (cf. Fig. 2) exhibit strong correlations with Cl which trend toward the origin, indicative of phase separation control and unmixing of high and low salinity fluid phases (Butterfield et al., 1994). BSW = bottom seawater.

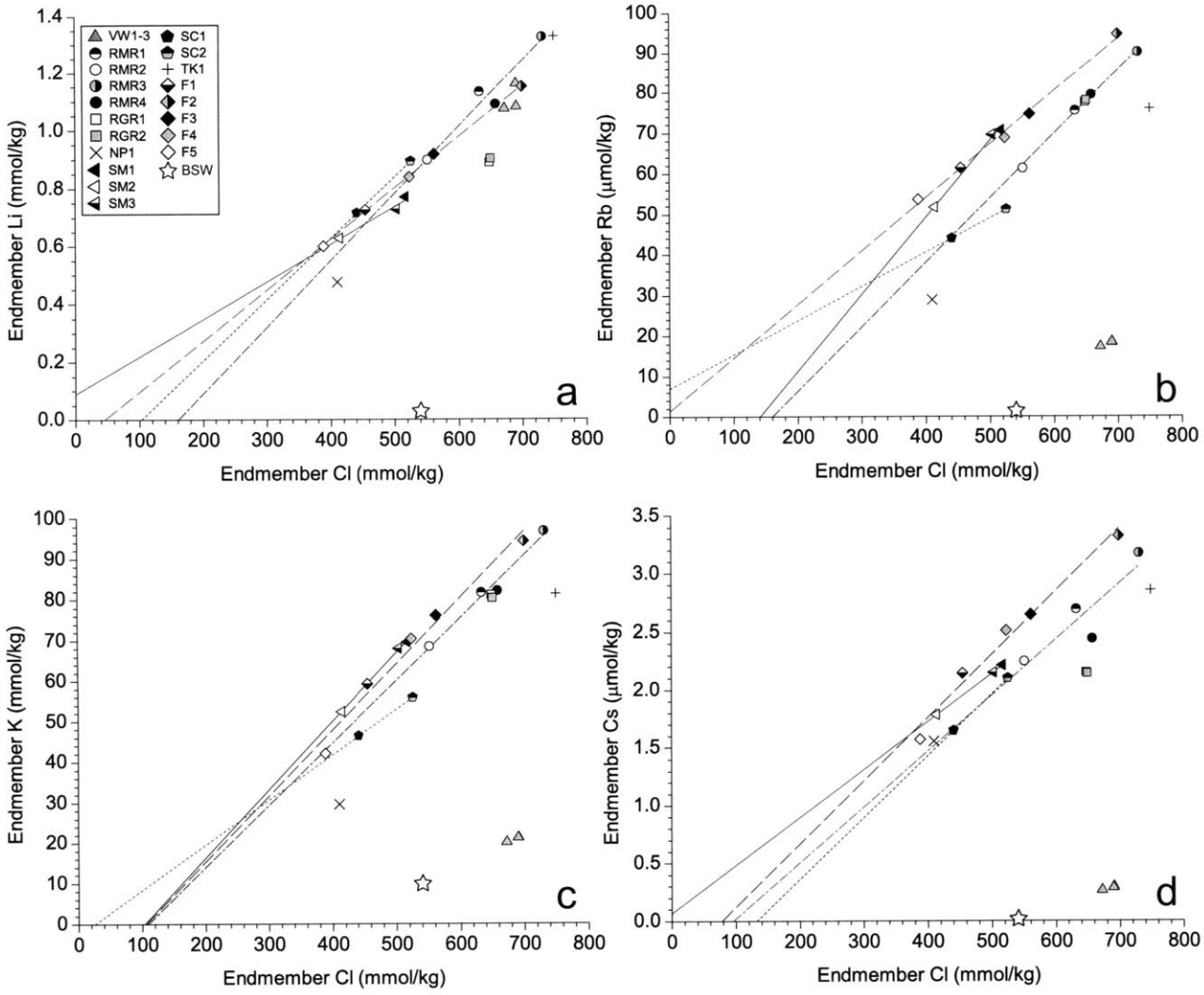
VW1-3
RMR1
RMR2
RMR3
RMR4
RGR1
RGR2
NP1
SM1
SM2
SM3
SC1
SC2
TK1
F1
F2
F3
F4
F5
BSW
Endmember Li (mmol/kg)
Endmember Cl (mmol/kg)
a
Endmember Rb (µmol/kg)
Endmember Cl (mmol/kg)
b
Endmember K (mmol/kg)
Endmember Cl (mmol/kg)
c
Endmember Cs (µmol/kg)
Endmember Cl (mmol/kg)
d

Figure 5.11.

Figure 5.12.

$\delta^{34}S$ values for dissolved H_2S ($\delta^{34}S_{H2S}$) versus endmember ΣCO_2 concentrations. The range of $\delta^{34}S_{H2S}$ values for unsedimented hydrothermal systems in MOR settings is +1.4‰ to +8.6‰ (Shanks, 2001). Values from Pual Ridge fluids below this range are associated with higher CO_2 concentrations of magmatic origin.

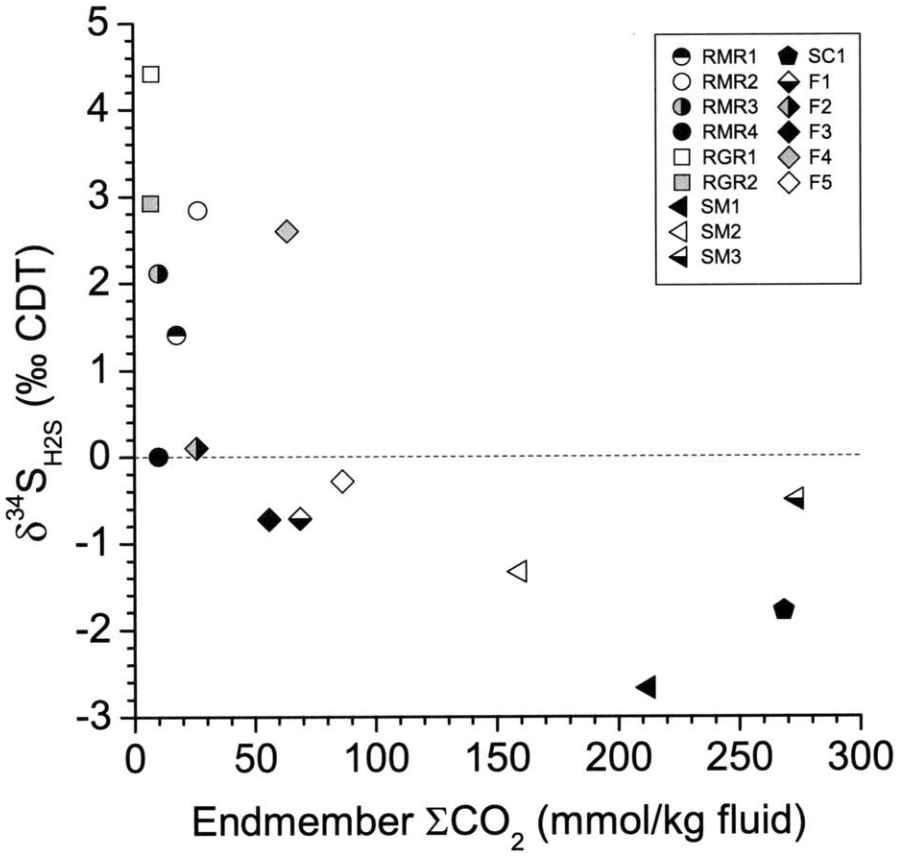
RMR1
RMR2
RMR3
RMR4
RGR1
RGR2
SM1
SM2
SM3
SC1
F1
F2
F3
F4
F5
δ34SH2S (‰ CDT)
Endmember ΣCO2 (mmol/kg fluid)
5
4
3
2
1
0
-1
-2
-3
0
50
100
150
200
250
300

Figure 5.12.

Figure 5.13.

Maximum measured vent temperatures (T_{max}) for co-located vent fluids at Roman Ruins and Fenway versus their lowest measured Mg concentrations (Mg_{min}). Only fluids where multiple samples yielded consistently high Mg concentrations and temperatures (within 10°C as measured by IGT samplers) are plotted (cf. Table 5.1). Mixing lines expected for conservative isenthalpic mixing between the vent fluids F3 (solid lines) and seawater, and RMR4 (dashed lines) and seawater are shown. Temperatures depicted by these mixing lines were calculated using the specific enthalpy data for a 3.2wt.% NaCl solution at 200bar (Bischoff and Rosenbauer, 1985) and Mg concentrations are used as a conservative metric of mixing fraction between the hottest hydrothermal fluid and seawater compositions. The mixing lines assume a constant heat capacity for seawater below 200°C of 4.1 J/gK (the actual change in heat capacity below 200°C is <5%).

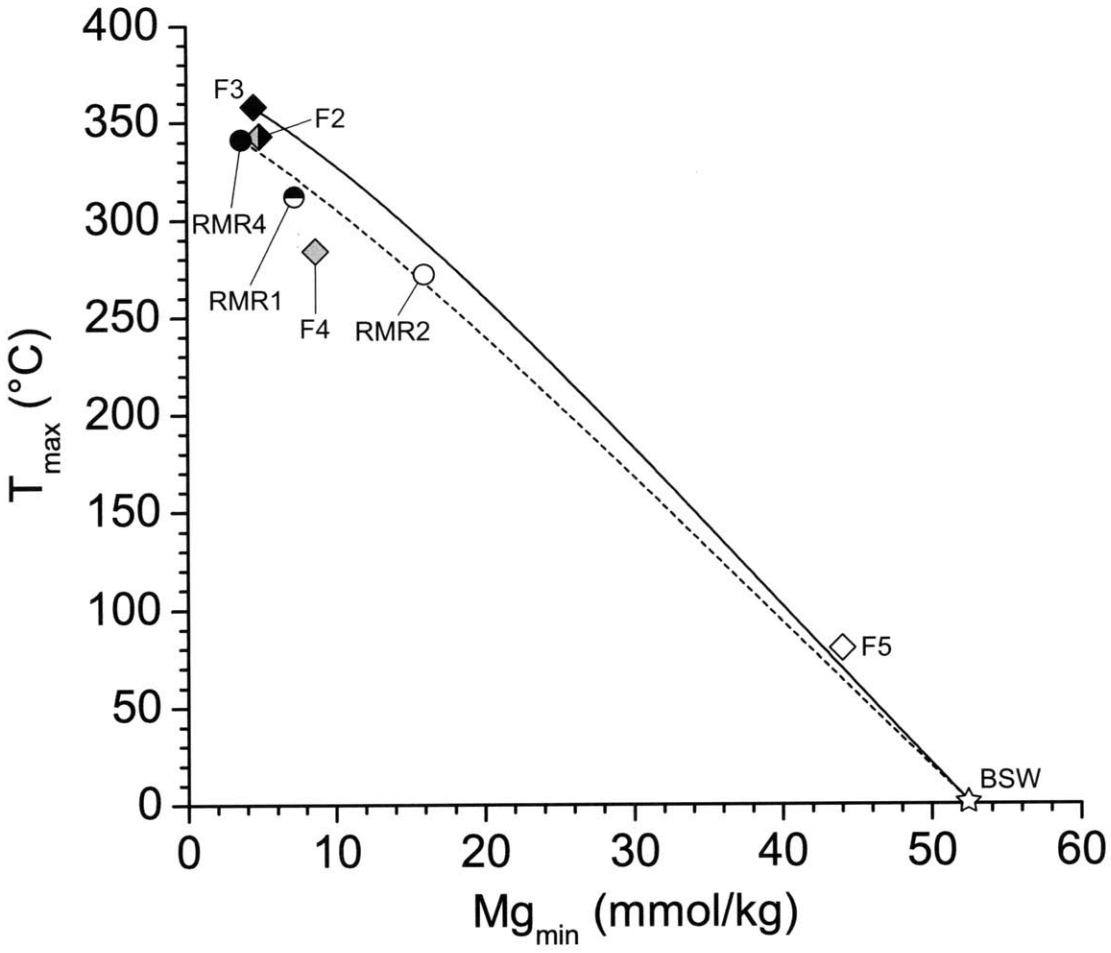
400
350
300
250
200
150
100
50
0
0
10
20
30
40
50
60
T max (°C)
Mg min (mmol/kg)
F3
F2
RMR4
RMR1
F4
RMR2
F5
BSW

Figure 5.13.

Figure 5.14.

Plots of **(a)** endmember Ca/Cl ratios, **(b)** endmember Sr/Cl ratios, **(c)** lowest measured fluid pH(25°C) and **(d)** endmember Fe/Mn ratios from Vienna Woods and Pual Ridge vent fluids *vs.* the lowest measured Mg concentration (Mg_{min}) for each fluid. While these plots are unconventional, they are intended to show that at Pual Ridge, calculated endmember Ca/Cl, Sr/Cl and Fe/Mn ratios appear to decrease with increasing extents of seawater entrainment (accompanied by decreases in measured pH) consistent with non-conservative behavior of Ca, Sr and Fe. NP1, F5 and TK1 are anomalous in that they have high endmember Ca/Cl and Sr/Cl ratios. BSW = bottom seawater.

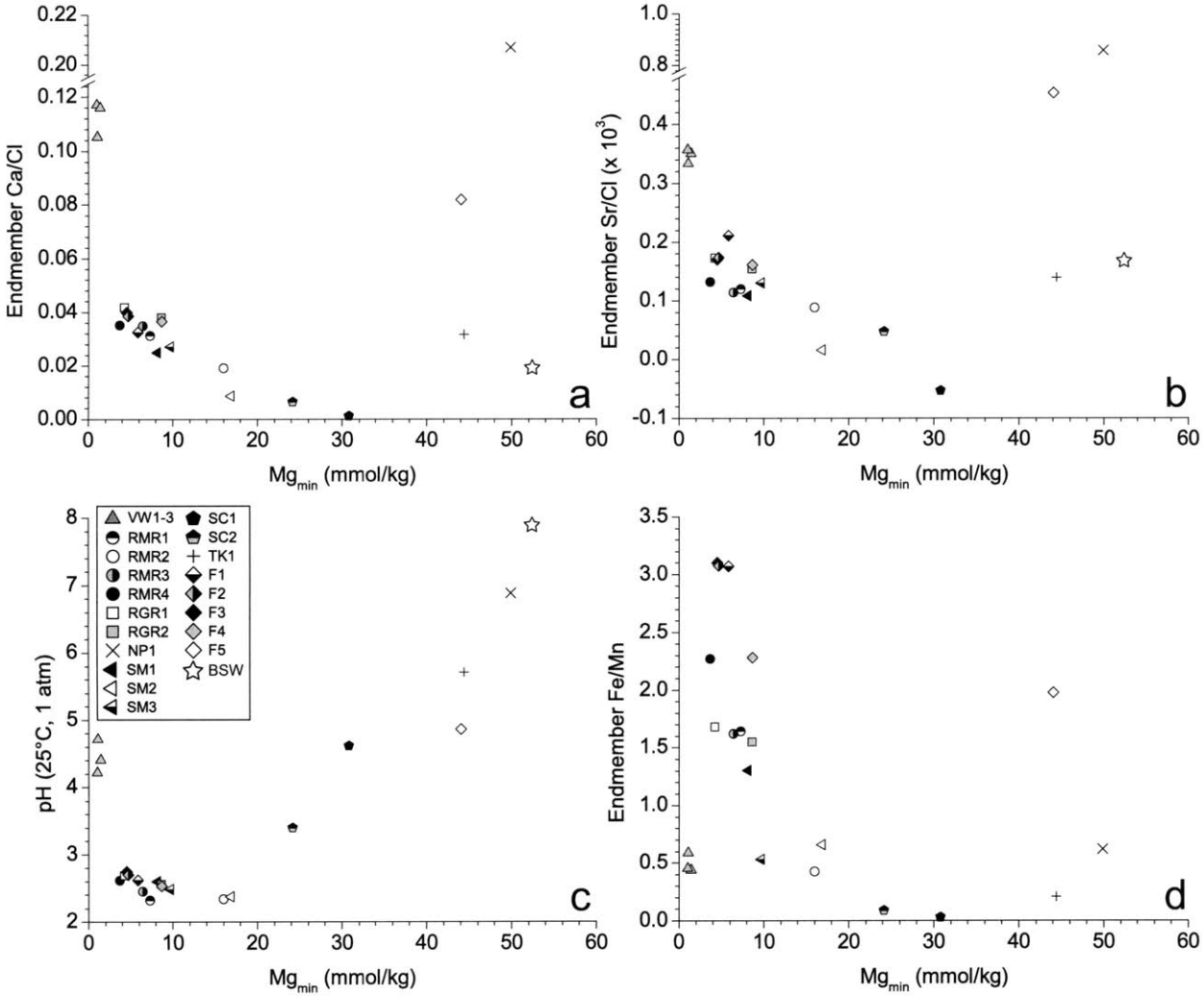
Endmember Ca/Cl
Endmember Sr/Cl (x 10^3)
pH (25°C, 1 atm)
Endmember Fe/Mn
Mg$_{min}$ (mmol/kg)
a
b
c
d
VW1-3
RMR1
RMR2
RMR3
RMR4
RGR1
RGR2
NP1
SM1
SM2
SM3
SC1
SC2
TK1
F1
F2
F3
F4
F5
BSW

Figure 5.14.

Figure 5.15.

Plot of measured molar Ca/Cl ratios ("*in situ*") and corresponding "*corrected*" values (adjusted for anhydrite precipitation) versus lowest measured Mg concentrations (Mg_{min}) for closely co-located PACMANUS vent fluids. The "*in situ*" symbols denote the Ca/Cl of each fluid calculated at Mg_{min} from regressions of measured Ca and Cl concentrations. Deviations in the "*in situ*" SO_4 concentration of these fluids (also calculated from measured SO_4^{2-} regressions at Mg_{min}) from conservative mixing of a hypothetical zero Mg, zero SO_4^{2-} fluid are calculated and used to the correct the Ca/Cl ratios for molar equivalent Ca loss (vertical arrows). Regression lines for each group of anhydrite "*corrected*" compositions (grouped by vent area) are shown. BSW = bottom seawater.

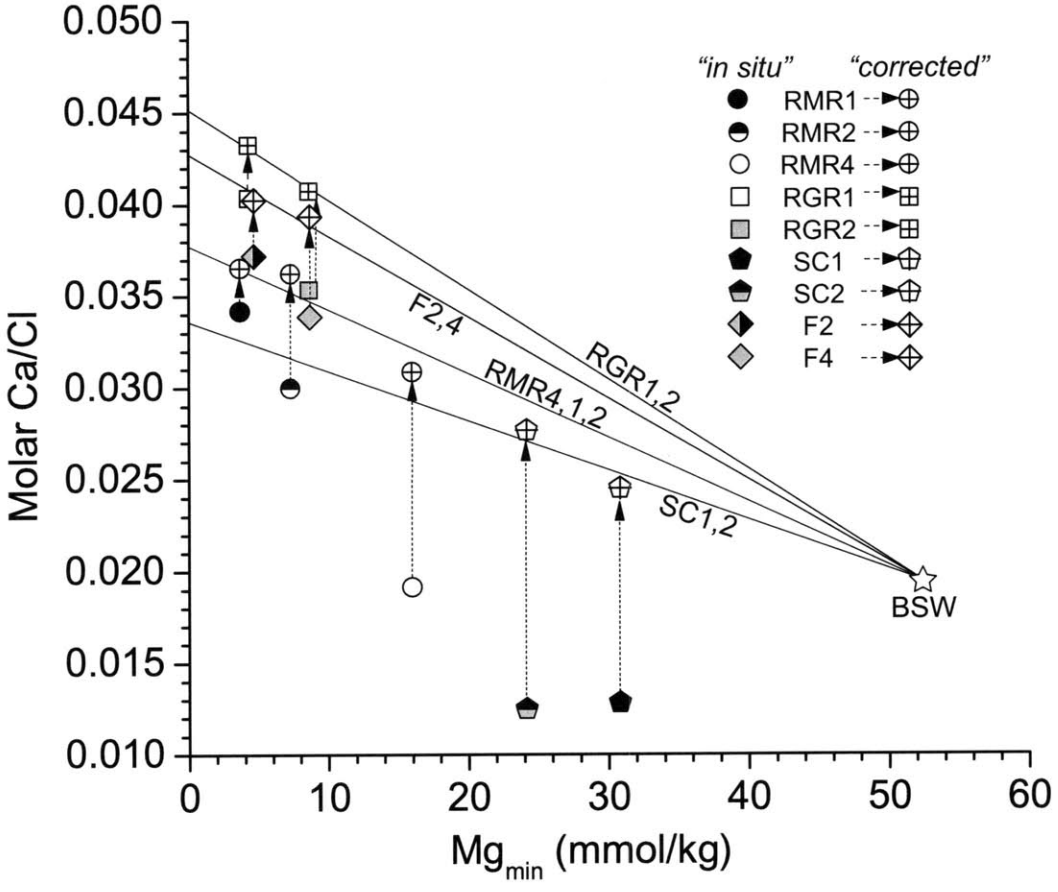
0.050
0.045
0.040
0.035
0.030
0.025
0.020
0.015
0.010
Molar Ca/Cl
0
10
20
30
40
50
60
Mg$_{min}$ (mmol/kg)
"in situ"
"corrected"
RMR1
RMR2
RMR4
RGR1
RGR2
SC1
SC2
F2
F4
F2,4
RMR4,1,2
RGR1,2
SC1,2
BSW

Figure 5.15.

REFERENCES

Aiuppa, A., D. R. Baker, and J. D. Webster (2009) Halogens in volcanic systems. *Chemical Geology* **263**(1-4), 1-18.

Albarède, F., A. Michard, J. F. Minster, and G. Michard (1981) $^{87}Sr/^{86}Sr$ ratios in hydrothermal waters and deposits from the East Pacific Rise at 21°N. *Earth and Planetary Science Letters* **55**, 229-236.

Alt, J. C. (1995) Subseafloor processes in mid-ocean ridge hydrothermal systems. In: *Seafloor Hydrothermal Systems: Physical, Chemical, Biological, and Geological Interactions, AGU Monograph*, (*Ed:* S. E. Humphris, R. A. Zierenberg, L. S. Mullineaux, and R. E. Thomson), AGU Mongraph, **91**, American Geophysical Union. pp. 85-114.

Alt, J. and W. Bach (2003) Alteration of Ocean Crust. In: *Dahlem Workshop Report: Energy and Mass Transfer in Marine Hydrothermal Systems*, (*Ed:* P. E. Halbach, V. Tunnicliffe, and J. R. Hein), **89**, Dahlem University Press. pp. 7-27.

Alt, J. C. and D. A. H. Teagle (1999) The uptake of carbon during alteration of ocean crust. *Geochimica et Cosmochimica Acta* **63**(10), 1527-1535.

Arnorsson, S. and A. Andresdottir (1995) Processes controlling the distribution of boron and chlorine in natural waters in Iceland. *Geochimica et Cosmochimica Acta* **59**(20), 4125-4146.

Arnorsson, S., K. Gronvold, and S. Sigurdsson (1978) Aquifer chemistry of four high-temperature geothermal systems in Iceland. *Geochimica et Cosmochimica Acta* **42**(5), 523-536.

Audetat, A., D. Gunther, and C. A. Heinrich (1998) Formation of a magmatic-hydrothermal ore deposit: Insights with LA-ICP-MS analysis of fluid inclusions. *Science* **279**(5359), 2091-2094.

Auzende, J. M., T. Urabe, E. Ruellan, D. Chabroux, J. L. Charlou, K. Gena, T. Gamo, K. Henry, O. Matsubayashi, T. Matsumoto et al. (1996) "Shinkai 6500" Dives in the Manus Basin: New STARMER Japanese-French Program. *JAMSTEC Journal of Deep Sea Research* **12**, 323-334.

Bach, W., S. Roberts, D. A. Vanko, R. A. Binns, C. J. Yeats, P. R. Craddock, and S. E. Humphris (2003) Controls of fluid chemistry and complexation on rare-earth element contents of anhydrite from the PACMANUS subseafloor hydrothermal system, Manus Basin, Papua New Guinea. *Mineralium Deposita* **38**(8), 916-935.

Banner, J. L. (2004) Radiogenic isotopes: systematics and applications to earth surface processes and chemical stratigraphy. *Earth-Science Reviews* **65**(3-4), 141-194.

Berndt, M. E. and W. E. Seyfried (1990) Boron, bromine, and other trace elements as clues to the fate of chlorine in mid-ocean ridge vent fluids. *Geochimica et Cosmochimica Acta* **54**, 2235-2245.

Berndt, M. E. and W. E. Seyfried (1993) Calcium and sodium exchange during hydrothermal alteration of calcic plagioclase at 400°C and 400 bars. *Geochimica et Cosmochimica Acta* **57**(18), 4445-4451.

Berndt, M. E., W. E. Seyfried, and J. W. Beck (1988) Hydrothermal alteration processes at midocean ridges: experimental and theoretical constraints from Ca and Sr exchange reactions and Sr isotopic ratios. *Journal of Geophysical Research* **93**(B5), 4573-4583.

Berndt, M. E., W. E. Seyfried, and D. R. Janecky (1989) Plagioclase and epidote buffering of cation ratios in mid-ocean ridge hydrothermal fluids - experimental results in and near the supercritical region. *Geochimica et Cosmochimica Acta* **53**(9), 2283-2300.

Berndt, M. E., R. R. Seal, W. C. Shanks, and W. E. Seyfried (1996) Hydrogen isotope systematics of phase separation in submarine hydrothermal systems: Experimental calibration and theoretical models. *Geochimica et Cosmochimica Acta* **60**(9), 1595-1604.

Binns, R. A. and S. D. Scott (1993) Actively forming polymetallic sulfide deposits associated with felsic volcanic-rocks in the Eastern Manus Back-Arc Basin, Papua New Guinea. *Economic Geology* **88**(8), 2226-2236.

Binns, R. A., S. D. Scott, J. B. Gemmell, K. Crook, and S. S. Party (1997) The SuSu Knolls Hydrothermal Field, Eastern Manus Basin, Papua New Guinea. *EOS Trans. AGU,* **78**(722), Fall Meet. Suppl. V22E-02 (abstr.).

Binns, R. A., F. J. A. S. Barriga, and D. J. Miller (2007) Leg 193 Synthesis: Anatomy of an active felsic-hosted hydrothermal system, Eastern Manus Basin, Papua New Guinea. In: *Proceedings of the Ocean Drilling Program, Scientific Results*, (*Ed:* F. J. A. S. Barriga, R. A. Binns, D. J. Miller, and P. M. Herzig), **193**, pp. 1-71.

Bischoff, J. L. and F. W. Dickson (1975) Seawater-basalt interaction at 200°C and 500 bars: Implications for origin of sea-floor heavy-metal deposits and regulation of seawater chemistry. *Earth and Planetary Science Letters* **25**, 385-397.

Bischoff, J. L. and K. S. Pitzer (1985) Phase relations and adiabats in boiling seafloor geothermal systems. *Earth and Planetary Science Letters* **75**(4), 327-338.

Bischoff, J. L. and R. J. Rosenbauer (1985) An empirical equation of state for hydrothermal seawater (3.2 percent NaCl). *American Journal of Science* **285**(8), 725-763.

Bischoff, J. L. and W. E. Seyfried (1978) Hydrothermal chemistry of seawater from 25 to 350°C. *American Journal of Science* **278**, 838-860.

Both, R., K. Crook, B. Taylor, S. Brogan, B. Chappell, E. Frankel, L. Liu, J. Sinton, and D. Tiffin (1986) Hydrothermal chimneys and associated fauna in the Manus back-arc basin, Papua New Guinea. *EOS Trans. AGU* **67**, 489-491.

Bowers, T. S. (1989) Stable isotope signatures of water-rock interaction in mid-ocean ridge hydrothermal systems: sulfur, oxygen and hydrogen. *Journal of Geophysical Research* **94**(B5), 5775-5786.

Bowers, T. S. and H. P. Taylor (1985) An integrated chemical and stable-isotope model of the origin of midocean ridge hot spring systems. *Journal of Geophysical Research* **90**(B14), 12583-12606.

Brimhall, G. H. and M. S. Ghiorso (1983) Origin and ore-forming consequences of the advanced argillic ateration process in hypogene environments by magmatic gas contamination of meteoric fluids. *Economic Geology* **78**(1), 73-90.

Burnham, C. W. (1979) Magmas and hydrothermal fluids. In: *Geochemistry of Hydrothermal Ore Deposits*, (*Ed:* H. L. Barnes), Wiley. pp. 71-136.

Butterfield, D. A. and G. J. Massoth (1994) Geochemistry of North Cleft Segment vent fluids - temporal changes in chlorinity and their possible relation to recent volcanism. *Journal of Geophysical Research-Solid Earth* **99**(B3), 4951-4968.

Butterfield, D. A., G. J. Massoth, R. E. Mcduff, J. E. Lupton, and M. D. Lilley (1990) Geochemistry of hydrothermal fluids from Axial Seamount Hydrothermal Emissions Study vent field, Juan De Fuca Ridge: Subseafloor boiling and subsequent fluid-rock interaction. *Journal of Geophysical Research-Solid Earth and Planets* **95**(B8), 12895-12921.

Butterfield, D. A., R. E. Mcduff, M. J. Mottl, M. D. Lilley, J. E. Lupton, and G. J. Massoth (1994) Gradients in the composition of hydrothermal fluids from the Endeavor Segment

vent field: Phase separation and brine loss. *Journal of Geophysical Research-Solid Earth* **99**(B5), 9561-9583.

Butterfield, D. A., I. R. Jonasson, G. J. Massoth, R. A. Feely, K. K. Roe, R. E. Embley, J. F. Holden, R. E. Mcduff, M. D. Lilley, and J. R. Delaney (1997) Seafloor eruptions and evolution of hydrothermal fluid chemistry. *Philosophical Transactions of the Royal Society of London Series A-Mathematical Physical and Engineering Sciences* **355**(1723), 369-386.

Butterfield, D., W. E. Seyfried, and M. Lilley (2003) Composition and evolution of hydrothermal fluids. In: *Dahlem Workshop Report: Energy and Mass Transfer in Marine Hydrothermal Systems*, (*Ed:* P. E. Halbach, V. Tunnicliffe, and J. R. Hein), **89**, Dahlem University Press. pp. 123-161.

Carroll, M. R. and M. J. Rutherford (1988) Sulfur speciation in hydrous experimental glasses of varying oxidation-state: Results from measured wavelength shifts of sulfur x-rays. *American Mineralogist* **73**(7-8), 845-849.

Carroll, M. R. and J. D. Webster (1994) Solubilities of sulfur, noble gases, nitrogen, chlorine, and fluorine in magmas. In: *Volatiles in magmas*, (*Ed:* M. R. Carroll and J. R. Holloway), Reviews in Mineralogy, **30**, Mineralogical Society of America. pp. 231-279.

Cartigny, P., N. Jendrzejewski, F. Pineau, E. Petit, and M. Javoy (2001) Volatile (C, N, Ar) variability in MORB and the respective roles of mantle source heterogeneity and degassing: the case of the Southwest Indian Ridge. *Earth and Planetary Science Letters* **194**(1-2), 241-257.

Charlou, J. L., J. P. Donval, P. Jean-Baptiste, and A. Dapoigny (1996) Gases and helium isotopes in high temperature solutions sampled before and after ODP Leg 158 drilling at TAG hydrothermal field (26°N, MAR). *Geophysical Research Letters* **23**(23), 3491-3494.

Charlou, J. L., J. P. Donval, Y. Fouquet, P. Jean-Baptiste, and N. Holm (2002) Geochemistry of high H_2 and CH_4 vent fluids issuing from ultramafic rocks at the Rainbow hydrothermal field (36°14'N, MAR). *Chemical Geology* **191**(4), 345-359.

Cheminée, J. L., P. Stoffers, G. McMurtry, H. Richnow, D. Puteanus, and P. Sedwick (1991) Gas-rich submarine exhalations during the 1989 eruption of Macdonald Seamount. *Earth and Planetary Science Letters* **107**(2), 318-327.

Cline, J. S. and R. J. Bodnar (1991) Can economic porphyry copper mineralization be generated by a typical calc-alkaline melt? *Journal of Geophysical Research-Solid Earth and Planets* **96**(B5), 8113-8126.

Coltice, N., L. Simon, and C. Lecuyer (2004) Carbon isotope cycle and mantle structure. *Geophysical Research Letters* **31**(5).

Corliss, J. B., J. Dymond, L. I. Gordon, J. M. Edmond, R. P. Von Herzen, R. D. Ballard, K. Green, D. Williams, A. Bainbridge, K. Crane et al. (1979) Submarine thermal springs on the Galapagos Rift. *Science* **203**, 1073-1083.

Craddock, P. R. (2008) Geochemical Tracers of Processes Affecting the Formation of Seafloor Hydrothermal Fluids and Deposits in the Manus Back-arc Basin. Ph.D. Thesis. MIT-WHOI Joint Program in Oceanography, MIT.

Craig, H. (1970) Abyssal Carbon-13 in the South Pacific. *Journal of Geophysical Research* **75**(3), 691-695.

Craig, H. and L. I. Gordon (1965) Deuterium and oxygen 18 variations in the ocean and marine atmosphere. In: *Stable Isotopes in Oceanographic Studies and Paleotemperatures*, (*Ed:* E. Tongiogi), Consiglio Nazionale Delle Ricerche, Laboratorio Di Geologia Nucleare, Pisa. pp. 9-130.

Cruse, A. M. and J. S. Seewald (2006) Geochemistry of low-molecular weight hydrocarbons in hydrothermal fluids from Middle Valley, northern Juan de Fuca Ridge. *Geochimica et Cosmochimica Acta* **70**(8), 2073-2092.

de Ronde, C. E. J. (1995) Fluid chemistry and isotopic characteristics of seafloor hydrothermal systems and associated VMS deposits: potential for magmatic contributions. In: *Magmas, fluids, and ore deposits: MAC Short Course Series Vol. 23*, (*Ed:* J. F. H. Thompson), Mineralogical Association of Canada. pp. 479-509.

de Ronde, C. E. J., M. D. Hannington, P. Stoffers, I. C. Wright, R. G. Ditchburn, A. G. Reyes, E. T. Baker, G. J. Massoth, J. E. Lupton, S. L. Walker et al. (2005) Evolution of a submarine magmatic-hydrothermal system: Brothers volcano, southern Kermadec arc, New Zealand. *Economic Geology* **100**(6), 1097-1133.

Douville, E., P. Bienvenu, J. L. Charlou, J. P. Donval, Y. Fouquet, P. Appriou, and T. Gamo (1999) Yttrium and rare earth elements in fluids from various deep-sea hydrothermal systems. *Geochimica et Cosmochimica Acta* **63**(5), 627-643.

Drummond, S. E. (1981) Boiling and mixing of hydrothermal fluids: Chemical effects on mineral precipitation, Ph.D. Dissertation, Penn. State University.

Edmond, J. M., C. Measures, R. E. Mcduff, L. H. Chan, R. Collier, B. Grant, L. I. Gordon, and J. B. Corliss (1979a) Ridge crest hydrothermal activity and the balances of the major and minor elements in the ocean: the Galapagos data. *Earth and Planetary Science Letters* **46**(1), 1-18.

Edmond, J. M., C. Measures, B. Mangum, B. Grant, F. R. Sclater, R. Collier, A. Hudson, L. I. Gordon, and J. B. Corliss (1979b) Formation of Metal-Rich Deposits At Ridge Crests. *Earth and Planetary Science Letters* **46**(1), 19-30.

Edmond, J. M., A. C. Campbell, M. R. Palmer, G. Klinkhammer, C. German, H. N. Edmonds, H. Elderfield, G. Thompson, and P. Rona (1995) Time series studies of vent fluids from the TAG and MARK sites (1986, 1990) Mid-Atlantic Ridge: a new solution chemistry model and a mechanism for Cu/Zn zonation in massive sulphide ore-bodies. In: *Hydrothermal Vents and Processes*, (*Ed:* L. Parson and J. R. Dixon), Geological Society Special Publication No. 87. pp. 77-86.

Eickmann, B., W. Bach, M. Rosner, and J. Peckmann (2009) Geochemical constraints on the modes of carbonate precipitation in peridotites from the Logatchev Hydrothermal Vent Field and Gakkel Ridge. *Chemical Geology* **268**(1-2), 97-106.

Embley, R. W., W. W. Chadwick, E. T. Baker, D. A. Butterfield, J. A. Resing, C. E. J. de Ronde, V. Tunnicliffe, J. E. Lupton, S. K. Juniper, K. H. Rubin et al. (2006) Long-term eruptive activity at a submarine arc volcano. *Nature* **441**(7092), 494-497.

Fouquet, Y., U. Vonstackelberg, J. L. Charlou, J. P. Donval, J. Erzinger, J. P. Foucher, P. Herzig, R. Muhe, S. Soakai, M. Wiedicke et al. (1991a) Hydrothermal activity and metallogenesis in the Lau Back-Arc Basin. *Nature* **349**(6312), 778-781.

Fouquet, Y., U. Vonstackelberg, J. L. Charlou, J. P. Donval, J. P. Foucher, J. Erzinger, P. Herzig, R. Muhe, M. Wiedicke, S. Soakai et al. (1991b) Hydrothermal activity in the Lau Back-Arc Basin - Sulfides and water chemistry. *Geology* **19**(4), 303-306.

Fouquet, Y., U. Vonstackelberg, J. L. Charlou, J. Erzinger, P. M. Herzig, R. Muhe, and M. Wiedicke (1993) Metallogenesis in back-arc environments - The Lau Basin example. *Economic Geology* **88**(8), 2154-2181.

Fournier, R. O. (1983) A method of calculating quartz solubilities in aqueous sodium-chloride solutions. *Geochimica et Cosmochimica Acta* **47**(3), 579-586.

Fourre, E., P. Jean-Baptiste, J. L. Charlou, J. P. Donval, and J. I. Ishibashi (2006) Helium isotopic composition of hydrothermal fluids from the Manus back-arc Basin, Papua New Guinea. *Geochemical Journal* **40**(3), 245-252.

Foustoukos, D. I. and W. E. Seyfried (2007a) Quartz solubility in the two-phase and critical region of the NaCl-KCl-H_2O system: Implications for submarine hydrothermal vent systems at 9 degrees 50 ' N East Pacific Rise. *Geochimica et Cosmochimica Acta* **71**(1), 186-201.

Foustoukos, D. I. and W. E. Seyfried (2007b) Fluid phase separation processes in submarine hydrothermal systems. In: *Fluid-Fluid Interactions*, (*Ed:* A. Liebsher and C. A. Heinrich), Reviews In Mineralogy & Geochemistry, **65**, Mineralogical Society of America. pp. 213-239.

Foustoukos, D. I. and W. E. Seyfried (2007c) Trace element partitioning between vapor, brine and halite under extreme phase separation conditions. *Geochimica et Cosmochimica Acta* **71**(8), 2056-2071.

Franklin, J., J. W. Lyndon, and D. F. Sangster (1981) Volcanic-associated massive sulfide deposits. *Economic Geology* **75**, 485-627.

Gallant, R. M. and K. L. Von Damm (2006) Geochemical controls on hydrothermal fluids from the Kairei and Edmond Vent Fields, 23°-25°S, Central Indian Ridge. *Geochemistry Geophysics Geosystems* **7**(6), Q06018, doi:10.1029/2005GC001067.

Galluccio, J., J. Maclean, S. Mcfadyen, J. Moore, P. Saccocia, and J. Seewald (2009) The Mobility of Fluoride in Back-Arc Hydrothermal Systems. *Eos Trans. AGU,* **90**(52), Fall Meet. Suppl. OS13A-1182 (abstr.).

Gamo, T., H. Sakai, J. Ishibashi, E. Nakayama, K. Isshiki, H. Matsuura, K. Shitashima, K. Takeuchi, and S. Ohta (1993) Hydrothermal plumes in the Eastern Manus Basin, Bismarck Sea - CH_4, Mn, Al and pH anomalies. *Deep-Sea Research Part I-Oceanographic Research Papers* **40**(11-12), 2335-2349.

Gamo, T., K. Okamura, T. Kodama, J. L. Charlou, T. Urabe, J. M. Auzende, J. Ishibashi, and A. T. S. S. Party (1996a) Chemical characteristics of hydrothermal fluids from the Manus back-arc basin, Papua New Guinea, I. Major Chemical Components. *EOS Trans. AGU* **77**(W116), WPGM Suppl. T32A-5 (abstr.).

Gamo, T., H. Chiba, H. Masuda, H. N. Edmonds, K. Fujioka, Y. Kodama, H. Nanba, and Y. Sano (1996b) Chemical characteristics of hydrothermal fluids from the TAG mound of the Mid-Atlantic Ridge in August 1994: Implications for spatial and temporal variability of hydrothermal activity. *Geophysical Research Letters* **23**(23), 3483-3486.

Gamo, T., K. Okamura, J. L. Charlou, T. Urabe, J. M. Auzende, J. Ishibashi, K. Shitashima, and H. Chiba (1997) Acidic and sulfate-rich hydrothermal fluids from the Manus back-arc basin, Papua New Guinea. *Geology* **25**(2), 139-142.

Gamo, T., J. Ishibashi, U. Tsunogai, K. Okamura, and H. Chiba (2006) Unique geochemistry of submarine hydrothermal fluids from arc-back-arc settings of the Western Pacific. In: *Back-Arc Spreading Systems: Geological, Biological, Chemical, and Physical Interactions,* (*Ed:* D. M. Christie, C. R. Fisher, S.-M. Lee, and S. Givens), AGU Mongraph, **166**, American Geophysical Union. pp. 147-161.

Gena, K., T. Mizuta, D. Ishiyama, and T. Urabe (2001) Acid-sulphate type alteration and mineralization in the Desmos caldera, Manus back-arc basin, Papua New Guinea. *Resource Geology* **51**(1), 31-44.

German, C. and K. L. Von Damm (2003) Hydrothermal Processes. In: *The Treatise on Geochemistry*, (*Ed:* K. K. Turekian and H. D. Holland), **6.07**, Elsevier. pp. 181-222.

Giggenbach, W. F. (1992) Isotopic shifts in waters from geothermal and volcanic systems along convergent plate boundaries and their origin. *Earth and Planetary Science Letters* **113**(4), 495-510.

Goff, F. and G. M. McMurtry (2000) Tritium and stable isotopes of magmatic waters. *Journal of Volcanology and Geothermal Research* **97**(1-4), 347-396.

Goldfarb, M. S., D.R. Converse, H.D. Holland and J.M. Edmond (1983) The genesis of hot spring deposits on the East Pacific Rise, 21°N. *Economic Geology* **Monograph 5**, 184-197.

Hajash, A. and G. W. Chandler (1982) An experimental investigation of high-temperature interactions between seawater and rhyolite, andesite, basalt and peridotite. *Contributions to Mineralogy and Petrology* **78**(3), 240-254.

Hannington, M., P. Herzig, P. Stoffers, J. Scholten, R. Botz, D. Garbe-Schonberg, I. R. Jonasson, and W. Roest (2001) First observations of high-temperature submarine hydrothermal vents and massive anhydrite deposits off the north coast of Iceland. *Marine Geology* **177**(3-4), 199-220.

Haymon, R. M. and M. Kastner (1981) Hot-spring deposits on the East Pacific Rise at 21°N - preliminary description of mineralogy and genesis. *Earth and Planetary Science Letters* **53**(3), 363-381.

Hedenquist, J. W. and J. B. Lowenstern (1994) The role of magmas in the formation of hydrothermal ore deposits. *Nature* **370**(6490), 519-527.

Herzig, P. M. and M. D. Hannington (1995) Polymetallic massive sulfides at the modern seafloor - a review. *Ore Geology Reviews* **10**(2), 95-115.

Holland, H. D. (1965) Some applications of thermochemical data to problems in ore deposits II. Mineral assemblages and the composition of ore-forming fluids. *Economic Geology* **60**(6), 1101-1166.

Horita, J., D. R. Cole, and D. J. Wesolowski (1995) The activity-composition relationship of oxygen and hydrogen isotopes in aqueous salt solutions: III. Vapor-liquid water equilibration of NaCl solutions to 350°C. *Geochimica et Cosmochimica Acta* **59**(6), 1139-1151.

Hrischeva, E., S. D. Scott, and R. Weston (2007) Metalliferous sediments associated with presently forming volcanogenic massive sulfides: The SuSu knolls hydrothermal field, eastern manus basin, Papua New Guinea. *Economic Geology* **102**(1), 55-73.

Humphris, S. E. and M. K. Tivey (2000) A synthesis of geological and geochemical investigations of the TAG hydrothermal field: Insights into fluid flow and mixing processes in a hydrothermal system. In: *Ophiolites and Oceanic Crust: New Insights from Field Studies and the Ocean Drilling Program*, (*Ed:* Y. Dilek, Moores, E.M., Elthon, D. and Nicholas, A.), Special Paper 349, Geological Society of America. pp. 213-235.

Humphris, S. E., P. M. Herzig, D. J. Miller, J. C. Alt, K. Becker, D. Brown, G. Brugmann, H. Chiba, Y. Fouquet, J. B. Gemmell et al. (1995) The internal structure of an active sea-floor massive sulfide deposit. *Nature* **377**(6551), 713-716.

Ishibashi, J. and T. Urabe (1995) Hydrothermal activity related to arc-backarc magmatism in the Western Pacific. In: *Backarc Basins: Tectonics and Magmatism*, (*Ed:* B. Taylor), Plenum Press. pp. 451-495.

Ishibashi, J. I., H. Wakita, Y. Nojiri, D. Grimaud, P. Jeanbaptiste, T. Gamo, J. M. Auzende, and T. Urabe (1994) Helium and carbon geochemistry of hydrothermal fluids from the North

Fiji Basin spreading ridge (Southwest Pacific). *Earth and Planetary Science Letters* **128**(3-4), 183-197.

Iwasaki, I. and O. Takejiro (1960) Genesis of sulfate in acid hot spring. *Bulletin of the Chemical Society of Japan* **33**(7), 1018-1019.

Javoy, M., F. Pineau, and J. T. Iiyama (1978) Experimental determination of the isotopic fractionation between gaseous CO_2 and carbon dissolved in the tholeiitic magma: a preliminary study. *Contributions to Mineralogy and Petrology* **67**, 35-39.

Kamenetsky, V. S., R. A. Binns, J. B. Gemmell, A. J. Crawford, T. P. Mernagh, R. Maas, and D. Steele (2001) Parental basaltic melts and fluids in eastern Manus backarc Basin: implications for hydrothermal mineralisation. *Earth and Planetary Science Letters* **184**(3-4), 685-702.

Kamenetsky, V. S., P. Davidson, T. P. Mernagh, A. J. Crawford, J. B. Gemmell, M. V. Portnyagin, and R. Shinjo (2002) Fluid bubbles in melt inclusions and pillow-rim glasses: high-temperature precursors to hydrothermal fluids? *Chemical Geology* **183**(1-4), 349-364.

Karl, D. M., G. M. McMurtry, A. Malahoff, and M. O. Garcia (1988) Loihi-Seamount, Hawaii: a mid-plate volcano with a distinctive hydrothermal system. *Nature* **335**(6190), 532-535.

Kelley, D. S. and G. Früh-Green (2000) Volatiles in mid-ocean ridge environments. In: *Ophiolites and Ocean Crust: Insights from Field Studies and the Ocean Drilling Program.*, (*Ed:* Y. Dilek, E. M. Moores, D. Elthon, and A. Nicholas), Geological Society of America Special Paper 349. pp. 237-260.

Kelley, D. S., M. D. Lilley, and G. L. Früh-Green (2004) Volatiles in submarine environments: food for life. In: *The Subseafloor Biosphere at Mid-Ocean Ridges*, (*Ed:* W. S. D. Wilcock,

E. F. DeLong, D. S. Kelley, J. A. Baross, and S. C. Cary), AGU Monograph, **144**, American Geophysical Union. pp. 167-189.

Kendall, C. and T. B. Coplen (1985) Multisample conversion of water to hydrogen by zinc for stable isotope determination. *Analytical Chemistry* **57**(7), 1437-1440.

Kusakabe, M., Y. Komoda, B. Takano, and T. Abiko (2000) Sulfur isotopic effects in the disproportionation reaction of sulfur dioxide in hydrothermal fluids: implications for the $\delta^{34}S$ variations of dissolved bisulfate and elemental sulfur from active crater lakes. *Journal of Volcanology and Geothermal Research* **97**(1-4), 287-307.

Lackschewitz, K. S., C. W. Devey, P. Stoffers, R. Botz, A. Eisenhauer, M. Kummetz, M. Schmidt, and A. Singer (2004) Mineralogical, geochemical and isotopic characteristics of hydrothermal alteration processes in the active, submarine, felsic-hosted PACMANUS field, Manus Basin, Papua New Guinea. *Geochimica et Cosmochimica Acta* **68**(21), 4405-4427.

Lee, S. M. (2003) Multidisciplinary investigation of the Western Pacific I (2000-2001). *Ocean Polar Res.* **24**(3), 131-135.

Lee, S. M. and E. Ruellan (2006) Tectonic and magmatic evolution of the Bismarck Sea, Papua New Guinea: Review and New Synthesis. In: *Back-Arc Spreading Systems: Geological, Biological, Chemical, and Physical Interactions*, (*Ed:* D. M. Christie, C. R. Fisher, S.-M. Lee, and S. Givens), AGU Monograph, **166**, American Geophysical Union. pp. 263-286.

Lilley, M. D., D. A. Butterfield, J. E. Lupton, and E. J. Olson (2003) Magmatic events can produce rapid changes in hydrothermal vent chemistry. *Nature* **422**(6934), 878-881.

Lisitsyn, A. P., K. Crook, Y. A. Bogdanov, L. P. Zonenshain, K. G. Murav'yev, W. Tufar, Y. G. Gurvich, V. V. Gordeyev, and G. V. Ivanov (1993) A hydrothermal field in the rift zone of the Manus Basin, Bismarck Sea. *International Geology Review* **35**(2), 105-126.

Lowenstern, J. B. (2000) A review of the contrasting behavior of two magmatic volatiles: chlorine and carbon dioxide. *Journal of Geochemical Exploration* **69**, 287-290.

Lupton, J., D. Butterfield, M. Lilley, L. Evans, K. I. Nakamura, W. Chadwick, J. Resing, R. Embley, E. Olson, G. Proskurowski et al. (2006) Submarine venting of liquid carbon dioxide on a Mariana Arc volcano. *Geochemistry Geophysics Geosystems* **7**(8), 1-20.

Lupton, J., M. Lilley, D. Butterfield, L. Evans, R. Embley, G. Massoth, B. Christenson, K. Nakamura, and M. Schmidt (2008) Venting of a separate CO_2-rich gas phase from submarine arc volcanoes: Examples from the Mariana and Tonga-Kermadec arcs. *Journal of Geophysical Research-Solid Earth* **113**(B8).

Maris, C. R. P., M. L. Bender, P. N. Froelich, R. Barnes, and N. A. Luedtke (1984) Chemical evidence for advection of hydrothermal solutions in the sediments of the galapagos mounds hydrothermal field. *Geochimica et Cosmochimica Acta* **48**(11), 2331-2346.

Martinez, F. and B. Taylor (1996) Backarc spreading, rifting, and microplate rotation, between transform faults in the Manus basin. *Marine Geophysical Researches* **18**(2-4), 203-224.

Marty, B., Y. Sano, and C. France-Lanord (2001) Water-saturated oceanic lavas from the Manus Basin: volatile behaviour during assimilation-fractional crystallisation-degassing (AFCD). *Journal of Volcanology and Geothermal Research* **108**(1-4), 1-10.

Massoth, G. J., D. A. Butterfield, J. E. Lupton, R. E. Mcduff, M. D. Lilley, and I. R. Jonasson (1989) Submarine venting of phase-separated hydrothermal fluids at Axial Volcano, Juan De Fuca Ridge. *Nature* **340**(6236), 702-705.

Mattey, D. P. (1991) Carbon-dioxide solubility and carbon isotope fractionation in basaltic melt. *Geochimica et Cosmochimica Acta* **55**(11), 3467-3473.

McCollom, T. M. and J. S. Seewald (2007) Abiotic synthesis of organic compounds in deep-sea hydrothermal environments. *Chemical Reviews* **107**, 382-401.

McDermott, J. M and Von Damm, K. L. (2008) On the re-dissolution of subsurface hydrothermal deposits at 9°50'N East Pacific Rise: Implications from geochemical studies of high- and low-temperature fluids. *EOS Trans. AGU* **89**(53), Fall Meet. Suppl. B51D-0402 (abstr.).

McMurtry, G. M., P. N. Sedwick, P. Fryer, D. L. Vonderhaar, and H. W. Yeh (1993) Unusual geochemistry of hydrothermal vents on submarine arc volcanos - Kasuga Seamounts, Northern Mariana Arc. *Earth and Planetary Science Letters* **114**(4), 517-528.

Michael, P. J. and W. C. Cornell (1998) Influence of spreading rate and magma supply on crystallization and assimilation beneath mid-ocean ridges: Evidence from chlorine and major element chemistry of mid-ocean ridge basalts. *Journal of Geophysical Research-Solid Earth* **103**(B8), 18325-18356.

Michael, P. J. and J. G. Schilling (1989) Chlorine in mid-ocean ridge magmas: Evidence for assimilation of seawater-influenced components. *Geochimica et Cosmochimica Acta* **53**(12), 3131-3143.

Michard, G., F. Albarède, A. Michard, J. F. Minster, J. L. Charlou, and N. Tan (1984) Chemistry of solutions from the 13°N East Pacific Rise hydrothermal site. *Earth and Planetary Science Letters* **67**(3), 297-307.

Mills, R. A. and M. Tivey (1999) Seawater entrainment and fluid evolution within the TAG hydrothermal mound: evidence from analyses of anhydrite. In: *Mid-Ocean Ridges: Dynamics of processes associated with creation of new ocean crust*, (*Ed:* J. R. Cann, H. Elderfield, and A. Laughton), Cambridge University Press. pp. 225-248.

Monecke, T., G. Giorgetti, O. Scholtysek, R. Kleeberg, J. Gotze, M. D. Hannington, and S. Petersen (2007) Textural and mineralogical changes associated with the incipient hydrothermal alteration of glassy dacite at the submarine PACMANUS hydrothermal

system, eastern Manus Basin. *Journal of Volcanology and Geothermal Research* **160**(1-2), 23-41.

Moss, R. and S. D. Scott (2001) Geochemistry and mineralogy of gold-rich hydrothermal precipitates from the eastern Manus Basin, Papua New Guinea. *Canadian Mineralogist* **39**, 957-978.

Mottl, M. J. and H. D. Holland (1978) Chemical exchange during hydrothermal alteration of basalt by seawater-I. Experimental results for major and minor components of seawater. *Geochimica et Cosmochimica Acta* **42**(8), 1103-1115.

Mottl, M. J., H. D. Holland, and R. F. Corr (1979) Chemical exchange during hydrothermal alteration of basalt by seawater-II. Experimental results for Fe, Mn, and sulfur species. *Geochimica et Cosmochimica Acta* **43**(6), 869-884.

Nakagawa, T., K. Takai, Y. Suzuki, H. Hirayama, U. Konno, U. Tsunogai, and K. Horikoshi (2006) Geomicrobiological exploration and characterization of a novel deep-sea hydrothermal system at the TOTO caldera in the Mariana Volcanic Arc. *Environmental Microbiology* **8**(1), 37-49.

Nilsson, K. and C. L. Peach (1993) Sulfur speciation, oxidation state, and sulfur concentration in backarc magmas. *Geochimica et Cosmochimica Acta* **57**(15), 3807-3813.

Ogawa, Y., N. Shikazono, D. Ishiyama, H. Sato, and T. Mizuta (2005) An experimental study on felsic rock-artificial seawater interaction: implications for hydrothermal alteration and sulfate formation in the Kuroko mining area of Japan. *Mineralium Deposita* **39**(8), 813-821.

Ohmoto, H. (1986) Stable isotope geochemistry of ore deposits. In: *Stable Isotopes in High Temperature Geological Processes*, (*Ed:* J. W. Valley, H. P. Taylor, and J. R. O'Neil), Reviews in Mineralogy, **16**, Mineralogical Society of America. pp. 491-559.

Ohmoto, H. and M. B. Goldhaber (1997) Sulfur and carbon isotopes. In: *Geochemistry of Hydrothermal Ore Deposits*, (*Ed:* H. L. Barnes), Wiley. pp. 517-612.

Ohmoto, H. and A. C. Lasaga (1982) Kinetics of reactions between aqueous sulfates and sulfides in hydrothermal systems. *Geochimica et Cosmochimica Acta* **46**(10), 1727-1745.

Ohmoto, H. and R. Rye (1979) Isotopes of Sulfur and Carbon. In: *Geochemistry of Hydrothermal Ore Deposits*, (*Ed:* H. L. Barnes), Wiley. pp. 509-567.

Park, S. H., S.-M. Lee, G. D. Kamenov, S.-T. Kwon, and K.-Y. Lee (in press) Tracing the origin of subduction components beneath the South East rift in the Manus Basin, Papua New Guinea. *Chemical Geology* (doi:10.1016/j.chemgeo.2009.10.008).

Paulick, H. and W. Bach (2006) Phyllosilicate alteration mineral assemblages in the active subsea-floor Pacmanus hydrothermal system, Papua New Guinea, ODP Leg 193. *Economic Geology* **101**(3), 633-650.

Paulick, H., D. A. Vanko, and C. J. Yeats (2004) Drill core-based facies reconstruction of a deep-marine felsic volcano hosting an active hydrothermal system (Pual Ridge, Papau New Guinea, ODP Leg 193). *Journal of Volcanology and Geothermal Research* **130**(1-2), 31-50.

Pearce, J. A. and R. J. Stern (2006) Origin of back-arc basin magmas: trace element and isotope perspectives. In: *Back-Arc Spreading Systems: Geological, Biological, Chemical, and Physical Interactions*, (*Ed:* D. M. Christie, C. R. Fisher, S.-M. Lee, and S. Givens), AGU Monograph, **166**, American Geophysical Union. pp. 63-86.

Pineau, F., M. Javoy, and Y. Bottinga (1976) $^{13}C/^{12}C$ ratios of rocks and inclusions in popping rocks of the mid-atlantic ridge and their bearing on the problem of isotopic composition of deep-seated carbon. *Earth and Planetary Science Letters* **29**, 413-421.

Pineau, F., S. Shilobreeva, A. Kadik, and M. Javoy (1998) Water solubility and D/H fractionation in the system basaltic andesite-H_2O at 1250°C and between 0.5 and 3 kbars. *Chemical Geology* **147**(1-2), 173-184.

Proskurowski, G., J. S. Seewald, E. Reeves, M. McCollom Thomas, J. Lupton, S. P. Sylva, and M. K. Tivey (2007) Volatile chemistry at Lau Basin hydrothermal sites: Basin-wide trends of slab carbonate influence and suggestions of abiotic methane oxidation at the Mariner vent site. *EOS Trans. AGU* **88**(52), Fall Meet. Suppl. V34B-04 (abstr.).

Redfield, A. C. and I. Friedman (1965) Factors affecting the distribution of deuterium in the ocean. In: *Symposium on Marine Geochemistry*, (*Ed:* D. R. Schink and J. T. Corless), Occasional Publication no. 3, Narragansett Marine Laboratory, University of Rhode Island. pp. 149-168.

Rees, C. E., W. J. Jenkins, and J. Monster (1978) Sulfur isotopic composition of ocean water sulfate. *Geochimica et Cosmochimica Acta* **42**(4), 377-381.

Resing, J. A., G. Lebon, E. T. Baker, J. E. Lupton, R. W. Embley, G. J. Massoth, W. W. Chadwick, and C. E. J. de Ronde (2007) Venting of acid-sulfate fluids in a high-sulfidation setting at NW Rota-1 submarine volcano on the Mariana Arc. *Economic Geology* **102**(6), 1047-1061.

Roberts, S., W. Bach, R. A. Binns, D. A. Vanko, C. J. Yeats, D. A. H. Teagle, K. Blacklock, J. S. Blusztajn, A. J. Boyce, M. J. Cooper et al. (2003) Contrasting evolution of hydrothermal fluids in the PACMANUS system, Manus Basin: The Sr and S isotope evidence. *Geology* **31**(9), 805-808.

Rosenbauer, R. J. and J. L. Bischoff (1983) Uptake and transport of heavy metals by heated seawater: a summary of experimental results. In: *Hydrothermal Processes at Seafloor*

Spreading Centers, NATO Conference Series, (*Ed:* P. Rona, K. Bostrom, L. Laubier, and K. Smith), **IV:12**, Plenum Press.

Ryan, J. G. and C. H. Langmuir (1993) The systematics of boron abundances in young volcanic rocks. *Geochimica et Cosmochimica Acta* **57**(7), 1489-1498.

Sakai, H., T. Gamo, E. S. Kim, K. Shitashima, F. Yanagisawa, M. Tsutsumi, J. Ishibashi, Y. Sano, H. Wakita, T. Tanaka et al. (1990a) Unique chemistry of the hydrothermal solution in the Mid-Okinawa Trough Backarc Basin. *Geophysical Research Letters* **17**(12), 2133-2136.

Sakai, H., T. Gamo, E. S. Kim, M. Tsutsumi, T. Tanaka, J. Ishibashi, H. Wakita, M. Yamano, and T. Oomori (1990b) Venting of carbon dioxide-rich fluid and hydrate formation in Mid-Okinawa Trough Backarc Basin. *Science* **248**(4959), 1093-1096.

Sarmiento, J. L. and N. Gruber (2006) *Ocean Biogeochemical Dynamics*. Princeton University Press.

Scaillet, B. and M. Pichavant (2003) Experimental constraints on volatile abundances in arc magmas and their implications for degassing processes. *Geological Society, London, Special Publications* **213**, 23-52.

Schoofs, S. and U. Hansen (2000) Depletion of a brine layer at the base of ridge-crest hydrothermal systems. *Earth and Planetary Science Letters* **180**(3-4), 341-353.

Sedwick, P. N., G. M. McMurtry, and J. D. Macdougall (1992) Chemistry of hydrothermal solutions from Pele Vents, Loihi Seamount, Hawaii. *Geochimica et Cosmochimica Acta* **56**(10), 3643-3667.

Seewald, J. S. and W. E. Seyfried (1990) The effect of temperature on metal mobility in subseafloor hydrothermal systems: constraints from basalt alteration experiments. *Earth and Planetary Science Letters* **101**(2-4), 388-403.

Seewald, J., A. Cruse, and P. Saccocia (2003) Aqueous volatiles in hydrothermal fluids from the Main Endeavour Field, northern Juan de Fuca Ridge: temporal variability following earthquake activity. *Earth and Planetary Science Letters* **216**(4), 575-590.

Seewald, J. S., K. W. Doherty, T. R. Hammar, and S. P. Liberatore (2002) A new gas-tight isobaric sampler for hydrothermal fluids. *Deep-Sea Research Part I-Oceanographic Research Papers* **49**(1), 189-196.

Seewald, J., T. Mccollum, G. Proskurowski, E. Reeves, M. Mottl, J. Sharkey, G. Wheat, and M. K. Tivey (2005) Aqueous volatiles in Lau Basin hydrothermal fluids. *EOS Trans. AGU* **86**(52), Fall Meet. Suppl. T31A-0478 (abstr.).

Seyfried, W. E. (1987) Experimental and theoretical constraints on hydrothermal alteration processes at mid-ocean ridges. *Annual Review of Earth and Planetary Sciences* **15**, 317-335.

Seyfried, W. E. and J. L. Bischoff (1981) Experimental seawater-basalt interaction at 300°C, 500 bars, chemical exchange, secondary mineral formation and implications for the transport of heavy-metals. *Geochimica et Cosmochimica Acta* **45**(2), 135-147.

Seyfried, W. E. and K. Ding (1995a) The hydrothermal chemistry of fluoride in seawater. *Geochimica et Cosmochimica Acta* **59**(6), 1063-1071.

Seyfried, W. E. and K. Ding (1995b) Phase equilibria in subseafloor hydrothermal systems: a review of the role of redox, temperature, pH and dissolved Cl on the chemistry of hot spring fluids at mid-ocean ridges. In: *Seafloor Hydrothermal Systems: Physical, Chemical, Biological, and Geological Interactions, (Ed:* S. E. Humphris, R. A. Zierenberg, L. S. Mullineaux, and R. E. Thomson), AGU Monograph, **91**, American Geophysical Union. pp. 248-272.

Seyfried, W. E. and D. R. Janecky (1985) Heavy metal and sulfur transport during subcritical and supercritical hydrothermal alteration of basalt: Influence of fluid pressure and basalt composition and crystallinity. *Geochimica et Cosmochimica Acta* **49**(12), 2545-2560.

Seyfried, W. E. and M. J. Mottl (1982) Hydrothermal alteration of basalt by seawater under seawater-dominated conditions. *Geochimica et Cosmochimica Acta* **46**(6), 985-1002.

Seyfried, W. E., D. R. Janecky, and M. J. Mottl (1984) Alteration of the oceanic crust: Implications for geochemical cycles of lithium and boron. *Geochimica et Cosmochimica Acta* **48**(3), 557-569.

Shanks, W. C. (2001) Stable isotopes in seafloor hydrothermal systems: Vent fluids, hydrothermal deposits, hydrothermal alteration, and microbial processes. In: *Stable Isotope Geochemistry*, (*Ed:* J. W. Valley and D. R. Cole), Reviews in Mineralogy & Geochemistry, **43**, Mineralogical Society of America. pp. 469-525.

Shanks, W. C. and W. E. Seyfried (1987) Stable isotope studies of vent fluids and chimney minerals, Southern Juan De Fuca Ridge: Sodium metasomatism and seawater sulfate reduction. *Journal of Geophysical Research-Solid Earth and Planets* **92**(B11), 11387-11399.

Shanks, W. C., J. K. Böhlke, and R. R. Seal (1995) Stable isotopes in mid-ocean ridge hydrothermal systems: interactions between fluids, minerals, and organisms. In: *Seafloor Hydrothermal Systems: Physical, Chemical, Biological, and Geological Interactions*, (*Ed:* S. E. Humphris, R. A. Zierenberg, L. S. Mullineaux, and R. E. Thomson), AGU Monograph, **91**, American Geophysical Union. pp. 194-221.

Shaw, A. M., D. R. Hilton, C. G. Macpherson, and J. M. Sinton (2004) The CO_2-He-Ar-H_2O systematics of the Manus back-arc basin: Resolving source composition from degassing and contamination effects. *Geochimica et Cosmochimica Acta* **68**(8), 1837-1856.

Shaw, A. M., E. H. Hauri, T. P. Fischer, D. R. Hilton, and K. A. Kelley (2008) Hydrogen isotopes in Mariana arc melt inclusions: Implications for subduction dehydration and the deep-Earth water cycle. *Earth and Planetary Science Letters* **275**(1-2), 138-145.

Shikazono, N. and H. D. Holland (1983) The partitioning of Sr between anhydrite and aqueous solutions from 150 to 250°C, The Kuroko and Related Volcanogenic Massive Sulfide Deposits. *Economic Geology* Monograph **5**, 320-328.

Shinohara, H. (1994) Exsolution of immiscible vapor and liquid phases from a crystallizing silicate melt: Implications for chlorine and metal transport. *Geochimica et Cosmochimica Acta* **58**(23), 5215-5221.

Shiraki, R., H. Sakai, M. Endoh, and N. Kishima (1987) Experimental studies on rhyolite-seawater and andesite-seawater interactions at 300°C and 1000 bars. *Geochemical Journal* **21**(4), 139-148.

Shmulovich, K. I., D. Landwehr, K. Simon, and W. Heinrich (1999) Stable isotope fractionation between liquid and vapour in water-salt systems up to 600°C. *Chemical Geology* **157**(3-4), 343-354.

Simmons, S. F. and K. L. Brown (2006) Gold in magmatic hydrothermal solutions and the rapid formation of a giant ore deposit. *Science* **314**(5797), 288-291.

Sinton, J. M., L. L. Ford, B. Chappell, and M. T. Mcculloch (2003) Magma genesis and mantle heterogeneity in the Manus back-arc basin, Papua New Guinea. *Journal of Petrology* **44**(1), 159-195.

Snyder, G. T., U. Fehn, and R. Goff (2002) Iodine isotope ratios and halide concentrations in fluids of the Satsuma-Iwojima volcano, Japan. *Earth Planets and Space* **54**(3), 265-273.

Spencer, D. W., D. E. Robertson, K. K. Turekian, and T. R. Folsom (1970) Trace element calibrations and profiles at the GEOSECS test station in the Northeast Pacific Ocean. *Journal of Geophysical Research* **75**(36), 7688-7696.

Spivack, A. J. and J. M. Edmond (1987) Boron isotope exchange between seawater and the oceanic crust. *Geochimica et Cosmochimica Acta* **51**(5), 1033-1043.

Stoffers, P., T. J. Worthington, U. Schwarz-Schampera, M. D. Hannington, G. J. Massoth, R. Hekinian, M. Schmidt, L. J. Lundsten, L. J. Evans, R. Vaiomo'unga et al. (2006) Submarine volcanoes and high-temperature hydrothermal venting on the Tonga arc, southwest Pacific. *Geology* **34**(6), 453-456.

Sun, W. D., R. J. Arculus, V. S. Kamenetsky, and R. A. Binns (2004) Release of gold-bearing fluids in convergent margin magmas prompted by magnetite crystallization. *Nature* **431**(7011), 975-978.

Sun, W. D., R. A. Binns, A. C. Fan, V. S. Kamenetsky, R. Wysoczanski, G. J. Wei, Y. H. Hu, and R. J. Arculus (2007) Chlorine in submarine volcanic glasses from the eastern Manus basin. *Geochimica et Cosmochimica Acta* **71**(6), 1542-1552.

Takai, K., T. Nunoura, J. I. Ishibashi, J. Lupton, R. Suzuki, H. Hamasaki, Y. Ueno, S. Kawagucci, T. Gamo, Y. Suzuki et al. (2008) Variability in the microbial communities and hydrothermal fluid chemistry at the newly discovered Mariner hydrothermal field, southern Lau Basin. *Journal of Geophysical Research-Biogeosciences* **113**(G02031), doi:10.1029/2007JG000636.

Taylor, B. (1979a) Bismarck Sea: evolution of a back-arc basin. *Geology* **7**(171-174).

Taylor, B. E. (1986) Magmatic volatiles: isotopic variation of C, H, and S. In: *Stable isotopes in high temperature geological processes*, (*Ed:* J. W. Valley, H. P. Taylor, and J. R. O'Neil), Reviews in Mineralogy, **16**, Mineralogical Society of America. pp. 185-225.

Taylor, H. P. (1979b) Oxygen and hydrogen isotope relationships in hydrothermal mineral deposits. In: *Geochemistry of Hydrothermal Ore Deposits*, (*Ed:* H. L. Barnes), Wiley. pp. 236-277.

Taylor, B., K. Crook, and J. Sinton (1994) Extensional transform zones and oblique spreading centers. *Journal of Geophysical Research-Solid Earth* **99**(B10), 19707-19718.

Taylor, H. P. (1997) Oxygen and hydrogen isotope relationships in hydrothermal mineral deposits. In: *Geochemistry of Hydrothermal Ore Deposits*, (*Ed:* H. L. Barnes), Wiley. pp. 229-302.

Tivey, M., W. Bach, J. Seewald, M. K. Tivey, D. A. Vanko and the Shipboard Science Party (2006) *Cruise Report for R/V Melville cruise MGLN06MV - Hydrothermal systems in the Eastern Manus Basin: Fluid Chemistry and Magnetic Structure as Guides to Subseafloor Processes*. Woods Hole Oceanographic Institution (available upon request to authors).

Tivey, M. K., S. E. Humphris, G. Thompson, M. D. Hannington, and P. A. Rona (1995) Deducing patterns of fluid flow and mixing within the TAG active hydrothermal mound using mineralogical and geochemical data. *Journal of Geophysical Research-Solid Earth* **100**(B7), 12527-12555.

Trefry, J. H., D. B. Butterfield, S. Metz, G. J. Massoth, R. P. Trocine, and R. A. Feely (1994) Trace metals in hydrothermal solutions from cleft segment on the southern Juan De Fuca Ridge. *Journal of Geophysical Research-Solid Earth* **99**(B3), 4925-4935.

Tregoning, P. (2002) Plate kinematics in the western Pacific derived from geodetic observations. *Journal of Geophysical Research-Solid Earth* **107**(B1).

Tsunogai, U., J. Ishibashi, H. Wakita, T. Gamo, K. Watanabe, T. Kajimura, S. Kanayama, and H. Sakai (1994) Peculiar features of Suiyo Seamount hydrothermal fluids, Izu-Bonin Arc: differences from subaerial volcanism. *Earth and Planetary Science Letters* **126**(4), 289-301.

Tufar, W. (1990) Modern hydrothermal activity, formation of complex massive sulfide deposits and associated vent communities in the Manus Back-arc Basin (Bismarck Sea, Papua New Guinea). *Mitteilung der Osterreichen Geologischen Gesellshaft* **82**, 183-210.

Von Damm, K. L. (1988) Systematics of and postulated controls on submarine hydrothermal solution chemistry. *Journal of Geophysical Research-Solid Earth and Planets* **93**(B5), 4551-4561.

Von Damm, K. L. (1990) Seafloor Hydrothermal Activity - Black Smoker Chemistry and Chimneys. *Annual Review of Earth and Planetary Sciences* **18**, 173-204.

Von Damm, K. L. (1995) Controls on the chemistry and temporal variability of seafloor hydrothermal systems. In: *Seafloor Hydrothermal Systems: Physical, Chemical, Biological, and Geological Interactions*, (*Ed:* S. E. Humphris, R. A. Zierenberg, L. S. Mullineaux, and R. E. Thomson), AGU Monograph, **91**, American Geophysical Union. pp. 222-247.

Von Damm, K. L. and J. L. Bischoff (1987) Chemistry of hydrothermal solutions from the Southern Juan De Fuca Ridge. *Journal of Geophysical Research-Solid Earth and Planets* **92**(B11), 11334-11346.

Von Damm, K. L., J. M. Edmond, B. Grant, and C. I. Measures (1985) Chemistry of submarine hydrothermal solutions at 21°N, East Pacific Rise. *Geochimica et Cosmochimica Acta* **49**(11), 2197-2220.

Von Damm, K. L., J. L. Bischoff, and R. J. Rosenbauer (1991) Quartz solubility in hydrothermal seawater: an experimental study and equation describing quartz solubility for up to 0.5-M NaCl solutions. *American Journal of Science* **291**(10), 977-1007.

Von Damm, K. L., A. M. Bray, L. G. Buttermore, and S. E. Oosting (1998) The geochemical controls on vent fluids from the Lucky Strike vent field, Mid-Atlantic Ridge. *Earth and Planetary Science Letters* **160**(3-4), 521-536.

Von Damm, K. L., C. M. Parker, R. A. Zierenberg, M. D. Lilley, E. J. Olson, D. A. Clague, and J. S. Mcclain (2005) The Escanaba Trough, Gorda Ridge hydrothermal system: Temporal stability and subseafloor complexity. *Geochimica et Cosmochimica Acta* **69**(21), 4971-4984.

Wallace, P. J. (2005) Volatiles in subduction zone magmas: concentrations and fluxes based on melt inclusion and volcanic gas data. *Journal of Volcanology and Geothermal Research* **140**(1-3), 217-240.

Webster, J. D. (2004) The exsolution of magmatic hydrosaline chloride liquids. *Chemical Geology* **210**(1-4), 33-48.

Welhan, J. A. (1988) Origins of methane in hydrothermal systems. *Chemical Geology* **71**(1-3), 183-198.

Yang, K. H. and S. D. Scott (1996) Possible contribution of a metal-rich magmatic fluid to a sea-floor hydrothermal system. *Nature* **383**(6599), 420-423.

Yang, K. H. and S. D. Scott (2002) Magmatic degassing of volatiles and ore metals into a hydrothermal system on the modern sea floor of the eastern Manus back-arc basin, western Pacific. *Economic Geology* **97**(5), 1079-1100.

Yang, K. H. and S. D. Scott (2005) Vigorous exsolution of volatiles in the magma chamber beneath a hydrothermal system on the modern sea floor of the eastern Manus back-arc basin, western Pacific: Evidence from melt inclusions. *Economic Geology* **100**(6), 1085-1096.

Yang, K. and S. D. Scott (2006) Magmatic fluids as a source of metals in seafloor hydrothermal systems. In: *Back-Arc Spreading Systems: Geological, Biological, Chemical, and Physical Interactions,* (*Ed:* D. M. Christie, C. R. Fisher, S.-M. Lee, and S. Givens), AGU Mongraph, **166**, American Geophysical Union. pp. 163-184.

Zengqian, H., K. Zaw, L. Yahne, Z. Qiling, Z. Zhignag, and T. Urabe (2005) Contribution of magmatic fluid to the active hydrothermal system in the JADE Field, Okinawa Trough: Evidence from fluid inclusions, oxygen and helium isotopes. *International Geology Review* **47**, 420-437.

CHAPTER 6

Comments and future research directions

This section briefly outlines any criticisms of the previous four chapters as well as highlighting future directions of research each respective area should progress toward.

CHAPTER 2 demonstrates that CO_2 reduction in the absence of mineral catalysis does proceed on timescales relevant to estimated fluid residence times in seafloor hydrothermal systems. Our understanding of the likelihood of CH_4 formation *via* CH_3OH in hydrothermal systems will be greatly improved if the distribution of the latter is characterized in vent fluids as a function of temperature and redox. A correlation of CH_3OH abundance with aqueous H_2 across the spectrum of redox states between basalt-hosted and ultramafic-hosted hydrothermal systems would provide compelling evidence of formation of CH_3OH by a reductive process. Measured concentrations could be evaluated in a thermodynamic context and may provide an insight into subsurface conditions if temperatures of equilibration are higher than measured vent temperatures. Furthermore, additional experimental work aimed at constraining the carbon isotopic fractionations associated with CH_4 formation *via* CH_3OH may aid in understanding in the isotopic composition of CH_4 in unsedimented hydrothermal systems.

By characterizing the distribution of CH_3SH in present day vent fluids, CHAPTER 3 represents a first step in testing the assumptions inherent in the 'metabolism-first' model for the origin of chemoautotrophic life. However, further work is needed to constrain the origin of CH_3SH observed in vent fluids. In particular, the possibility of CH_3SH production by pyrolysis of biological materials in unsedimented hydrothermal systems must be thoroughly examined, both through experimental work and further characterization of CH_3SH in low to moderate

temperature fluids where this process may occur. The possibility of organic compound production via biomass pyrolysis is still in infancy as a research direction and no major studies have been conducted to examine this process. PROSKUROWSKI *et al.* (2008) speculated on the significance of this process for CH_4 production but key questions still remain. Specifically, what is the lower temperature limit at which thermogenic alteration of vent biomass ceases to occur, and what is the temporal extent of biomass available for alteration? If biomass alteration is simply a transient process related to shifts in the hydrologic regime (e.g. passage of hotter fluids through conduits that previously experienced much cooler temperatures and more active biomass production), then temporal variations should be evident in the organic composition of low temperature/diffuse fluids. Clear demonstration of biomass pyrolysis as a source of organic compounds such as CH_3SH to fluids will significantly complicate the identification of truly abiotic organic processes in bare rock systems. Isotopic analyses could provide useful information on the origin of CH_3SH, but will likely face analytically challenges given the trace quantities present and the labile nature of CH_3SH with respect to oxidation in storage. Analysis of the radiocarbon content of CH_3SH in vent fluids could provide definitive evidence for abiotic *vs.* thermogenic origins (PROSKUROWSKI *et al.*, 2008) but this is simply not possible at the present time. The advent of compound-specific sulfur isotope analysis may provide some insight into the origin of CH_3SH if issues of sample storage are addressed.

CHAPTER 4 presents compelling evidence for hydrogen isotope exchange between *n*-alkanes and water under hydrothermal conditions. Unfortunately, the experiments in CHAPTER 4 cannot be used to derive accurate estimates of alkane-water hydrogen isotope fractionation factors or rate constants for exchange at the conditions of the experiments. Both k and F_{eq} in equation (7), CHAPTER 4, are unknown and because of the nature of these experiments it is difficult to derive their magnitudes accurately. The time series isotopic compositions in Experiments 1 and 2

cannot be viewed as partial exchange scenarios (*e.g.* SUZUOKI and EPSTEIN, 1976; SACCOCIA *et al.*, 2009) in order to derive F_{eq} because the fundamental assumption of this technique (that equivalent fractions of exchange occur per unit time between parallel experiments) is likely to be invalid. This is due to differing hydrocarbon concentrations and concomitant effects on the observed rate of exchange which simply arise from the difficulties in loading the reaction cell contents accurately. Furthermore, differing H_2 and alkene abundances between experiments will also likely influence the validity of that assumption. Alternatively, the use of non-linear least squares regression techniques (*e.g.* a Levenberg-Marquardt Method, BEVINGTON and ROBINSON, 2003) to fit equation (7) to the observed trends yields highly erratic values of F_{eq} and k_{obs} between the experiments due to excessive degrees of extrapolation and estimated values of k_{obs} would therefore have very weak predictive capabilities. Finally, because exchange occurred in the bulk molecule and not at specific carbon positions, it would not be possible to derive carbon-specific fractionation factors for alkane H and water based on such results.

While these drawbacks do not compromise the contribution of CHAPTER 4, estimates of fractionation factors above the 100°C limit of WANG *et al.* (2009a,b) to temperatures encountered by dissolved hydrocarbons in hydrothermal systems (~400°C) would be useful in confirming the extents of exchange occurring in seafloor hydrothermal systems. The lack of substantial temperature dependency of $\alpha_{o/w}$ values below 100°C (CHAPTER 4, Figure 4.9; WANG *et al.*, 2009b) could reasonably be extended to slightly higher temperatures, but it would be unwise to assume such insensitivity holds to ~400°C. Unfortunately, there are likely to be significant challenges in experimentally determining these values at such high temperatures. WANG *et al.* (2009a,b) used a keto-enol tautomerization reaction mechanism to equilibrate water with H bound to individual carbon positions adjacent to carbonyl groups in a suite of aliphatic, branched and aromatic ketones. However, it is highly unlikely such a mechanism could be used to achieve the

same result under hydrothermal conditions given the demonstrated potential for aqueous ketone oxidation at elevated temperatures (SEEWALD, 2001). An approach similar to HORIBE and CRAIG (1995), whereby gaseous mixtures of CH_4 and H_2 were isotopically equilibrated over a Ni-Thoria catalyst, might be possible for low molecular weight alkanes and water, but this is speculative and would not allow for carbon-specific H equilibration.

CHAPTER 5 illustrates that magmatic fluids and subsurface mixing processes can influence the chemistry of convectively circulating hydrothermal fluids in backarc environments. Figure 6.1 shows a cartoon of the proposed evolution of circulating fluids in a PACMANUS-type hydrothermal system. A key question arising from this study is on what temporal scales magmatic fluid inputs occur. YANG and SCOTT (2005) argue that the exsolution of magmatic volatiles from differentiating silicic magmas could proceed for extended periods of time (on the order of years to decades), thereby having the potential to influence hydrothermal fluid compositions for much of the typical lifetime of sites of hydrothermal activity. This remains to be demonstrated, but is important given the hypothesized role of magmatic fluids in contributing substantial quantities of economic metals to seafloor massive sulfide deposits in backarc hydrothermal systems (YANG and SCOTT, 1996, 2002, 2005, 2006). However, the data presented in CHAPTER 5 only represent a snapshot in time and considerable time series studies must be conducted before such hypotheses can be validated. Future expeditions to the Manus Basin, within the next few years will shed valuable light on the temporal evolution of magmatic inputs and mixing processes. Another potential avenue of research related to CHAPTER 5 involves an examination of the role of water/rock reactions in buffering pH to very low values. In some of the vent fluids at PACMANUS which lack substantial magmatic CO_2 contents (*e.g.* Roman Ruins and Roger's Ruins), pH values are similar to fluids with substantial magmatic inputs (*e.g.* Satanic Mills and Snowcap). This strongly suggests some component of water/rock reaction in regulating

fluid pH. Whether this occurs by incomplete titration of magma-derived acidity following magmatic fluid input or by buffering induced by pre-existing acid-sulfate alteration assemblages could be examined both experimentally with water/rock reaction experiments and theoretically using reaction-path modeling.

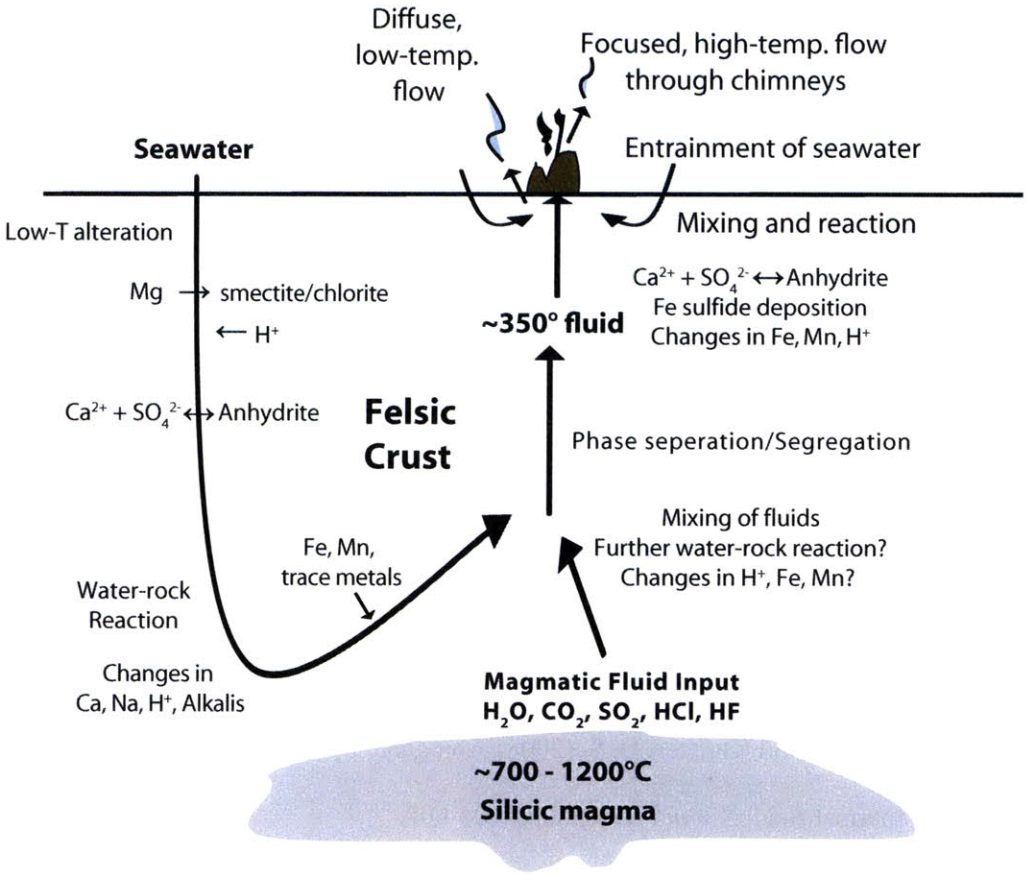

Figure 6.1. Cartoon showing the postulated evolution of fluids in a backarc hydrothermal system influenced by magmatic fluid inputs. The typical sequences of reactions taking place during 'recharge' in mid-ocean ridge systems occur, such as Mg-fixation and anhydrite deposition (ALT, 1995). Water/rock interactions in the 'reaction' zone will occur regardless of the presence of a magmatic fluid exsolved from silicic magma chambers. However, admixing of this fluid with evolved seawater-derived hydrothermal fluids complicates the history of fluid evolution if further water/rock interaction occurs. Phase separation can occur wherever the 2-phase boundary is intersected, either as a result of decompression during upflow or elsewhere in the system. Entrainment and admixing of seawater prior to venting of fluids at the seafloor further alters fluid compositions, leading to deposition of Fe sulfide minerals and admixed seawater-derived anhydrite.

REFERENCES

ALT, J. C. (1995) Subseafloor processes in mid-ocean ridge hydrothermal systems. In: *Seafloor Hydrothermal Systems: Physical, Chemical, Biological, and Geological Interactions, AGU Monograph*, (*Ed:* S. E. Humphris, R. A. Zierenberg, L. S. Mullineaux, and R. E. Thomson), AGU Mongraph, **91**, American Geophysical Union. pp. 85-114.

BEVINGTON, P. R. and ROBINSON, D. K. (2003) *Data Reduction and Error Analysis for the Physical Sciences*. 3rd Ed. McGraw Hill.

HORIBE, Y. and CRAIG, H. (1995) D/H fractionation in the system methane-hydrogen-water. *Geochimica Et Cosmochimica Acta* **59**(24), 5209-5217.

PROSKUROWSKI, G., LILLEY, M. D., and OLSON, E. J. (2008) Stable isotopic evidence in support of active microbial methane cycling in low-temperature diffuse flow vents at 9°50'N East Pacific Rise. *Geochimica et Cosmochimica Acta* **72**(8), 2005-2023.

PROSKUROWSKI, G., LILLEY, M. D., SEEWALD, J. S., FRUH-GREEN, G. L., OLSON, E. J., LUPTON, J. E., SYLVA, S. P., and KELLEY, D. S. (2008) Abiogenic hydrocarbon production at Lost City hydrothermal field. *Science* **319**(5863), 604-607.

SACCOCIA, P. J., SEEWALD, J. S., and SHANKS, W. C. (2009) Oxygen and hydrogen isotope fractionation in serpentine-water and talc-water systems from 250 to 450°C, 50 MPa. *Geochimica et Cosmochimica Acta* **73**(22), 6789-6804.

SEEWALD, J. S. (2001) Aqueous geochemistry of low molecular weight hydrocarbons at elevated temperatures and pressures: Constraints from mineral buffered laboratory experiments. *Geochimica Et Cosmochimica Acta* **65**(10), 1641-1664.

SUZUOKI, T. and EPSTEIN, S. (1976) Hydrogen isotope fractionation between OH-bearing minerals and water. *Geochimica et Cosmochimica Acta* **40**, 1229-1240.

WANG, Y., SESSIONS, A., NIELSEN, R. J., and GODDARD, W. A., III (2009a) Equilibrium $^{2}H/^{1}H$ fractionations in organic molecules: I. Experimental calibration of ab initio calculations. *Geochimica et Cosmochimica Acta* **73**(23), 7060-7075.

WANG, Y., SESSIONS, A., NIELSEN, R. J., and GODDARD, W. A., III (2009b) Equilibrium $^{2}H/^{1}H$ fractionations in organic molecules. II: Linear alkanes, alkenes, ketones, carboxylic acids, esters, alcohols and ethers. *Geochimica et Cosmochimica Acta* **73**(23), 7076-7086.

YANG, K. and SCOTT, S. D. (2006) Magmatic fluids as a source of metals in seafloor hydrothermal systems. In: *Back-Arc Spreading Systems: Geological, Biological, Chemical, and Physical Interactions*, (*Ed:* D. M. Christie, C. R. Fisher, S.-M. Lee, and S. Givens), AGU Monograph, **166**, American Geophysical Union. pp. 163-184.

YANG, K. H. and SCOTT, S. D. (1996) Possible contribution of a metal-rich magmatic fluid to a sea-floor hydrothermal system. *Nature* **383**(6599), 420-423.

YANG, K. H. and SCOTT, S. D. (2002) Magmatic degassing of volatiles and ore metals into a hydrothermal system on the modern sea floor of the eastern Manus back-arc basin, western Pacific. *Economic Geology* **97**(5), 1079-1100.

YANG, K. H. and SCOTT, S. D. (2005) Vigorous exsolution of volatiles in the magma chamber beneath a hydrothermal system on the modern sea floor of the eastern Manus back-arc basin, western Pacific: Evidence from melt inclusions. *Economic Geology* **100**(6), 1085-1096.